ECMWF COPERNICUS REPORT

Copernicus Atmosphere Monitoring Service

Validation report of the CAMS near-real time global atmospheric composition service

Period December 2019 – February 2020

Issued by: KNMI

Date: 10 June 2020

Ref: CAMS84_2018SC2_D1.1.1_DJF2020

Validation report of the CAMS near-real-time global atmospheric composition service: Period December 2019 – February 2020

EDITORS:
M. Schulz (MetNo), Y. Christophe (BIRA-IASB), M. Ramonet (LSCE), A. Wagner (MPG), H.J. Eskes (KNMI)

AUTHORS:
S. Basart (BSC), A. Benedictow (MetNo), Y. Bennouna (CNRS-LA), A.-M. Blechschmidt (IUP-UB), S. Chabrillat (BIRA-IASB), E. Cuevas (AEMET), A. El-Yazidi (LSCE), H. Flentje (DWD), P. Fritzsche (DWD), K. M. Hansen (AU), U. Im (AU), J. Kapsomenakis (AA), B. Langerock (BIRA-IASB), A. Richter (IUP-UB), N. Sudarchikova (MPG), V. Thouret (CNRS-LA), T. Warneke (UBC), C. Zerefos (AA)

REPORT OF THE COPERNICUS ATMOSPHERE MONITORING SERVICE, VALIDATION SUBPROJECT.

AVAILABLE AT:
http://atmosphere.copernicus.eu/quarterly_validation_reports

CITATION:
M. Schulz, Y. Christophe, M. Ramonet, Wagner, A., H. J. Eskes, S. Basart, A. Benedictow, Y. Bennouna, A.-M. Blechschmidt, S. Chabrillat, E. Cuevas, A. El-Yazidi, H. Flentje, P. Fritzsche, K.M. Hansen, U. Im, J. Kapsomenakis, B. Langerock, A. Richter, N. Sudarchikova, V. Thouret, T. Warneke, C. Zerefos, Validation report of the CAMS near-real-time global atmospheric composition service: Period December 2019 – February 2020, Copernicus Atmosphere Monitoring Service (CAMS) report, CAMS84_2018SC2_D1.1.1_DJF2020.pdf, June 2020, doi:10.24380/322n-jn39.

STATUS:
Version 1, final

DATE:
10 June 2020

Executive Summary

The Copernicus Atmosphere Monitoring Service (http://atmosphere.copernicus.eu, CAMS) is a component of the European Earth Observation programme Copernicus. The CAMS global near-real time (NRT) service provides daily analyses and forecasts of reactive trace gases, greenhouse gases and aerosol concentrations. This document presents the validation statistics and system evolution of the CAMS NRT service for the period up to 1 March 2020, with a focus on December 2019 to February 2020 (DJF-2020). Updates of this document appear every 3 months, e.g. Wagner et al. (2020). A detailed description of the measurement datasets used is provided in Eskes et al. (2019). Automated verification plots are made available through the CAMS global evaluation server, https://global-evaluation.atmosphere.copernicus.eu.

This summary is split according to service themes as introduced on the CAMS website: air quality & atmospheric composition, climate forcing, ozone layer and UV. Specific attention is given to the ability of the CAMS system to capture recent events. We focus on the 'o-suite' composition fields, which are the daily analyses and forecasts produced by the IFS (Integrated Forecast System) modelling system at ECMWF, using the available meteorological and atmospheric composition observations which are ingested in the ECMWF 4D-Var assimilation system. The model and assimilation configurations are summarised in section 2. We furthermore assess the impact of the composition observations by comparing the validation results from the 'o-suite' to a 'control' configuration without atmospheric composition data assimilation. Also, the pre-operational delayed-mode analyses and high-resolution forecasts of CO_2 and CH_4 are assessed in this report.

On 9 July 2019, a major upgrade of the CAMS system to version 46R1 took place. Among other things this involved a change from 60 vertical levels to 137 vertical levels. The upgrade is described in more detail in section 2, and special attention is given in this validation report to changes in performance linked to this upgrade.

The o-suite data delivery for the period DJF-2020 was very good, with an on-time percentage of 99.4%.

Air quality and atmospheric composition

Tropospheric ozone (O_3)

CAMS o-suite ozone is validated with surface and free tropospheric ozone observations from the GAW and ESRL networks, IAGOS airborne data, ozone sondes and IASI tropospheric ozone retrievals. For free tropospheric ozone against ozone sondes the o-suite modified normalized mean biases (MNMBs) are on average small, ±10% over the Northern Hemisphere (NH), between ±30% for stations in the Tropics, and ±20% for the Arctic in more recent years (Fig. S.1). Over Antarctica o-suite biases are observed between 0% and +30% for recent years, whereas the control run shows negative biases. For DJF 2019/2020 good agreement is found over the NH mid latitudes, Arctic and Antarctica in the free troposphere.

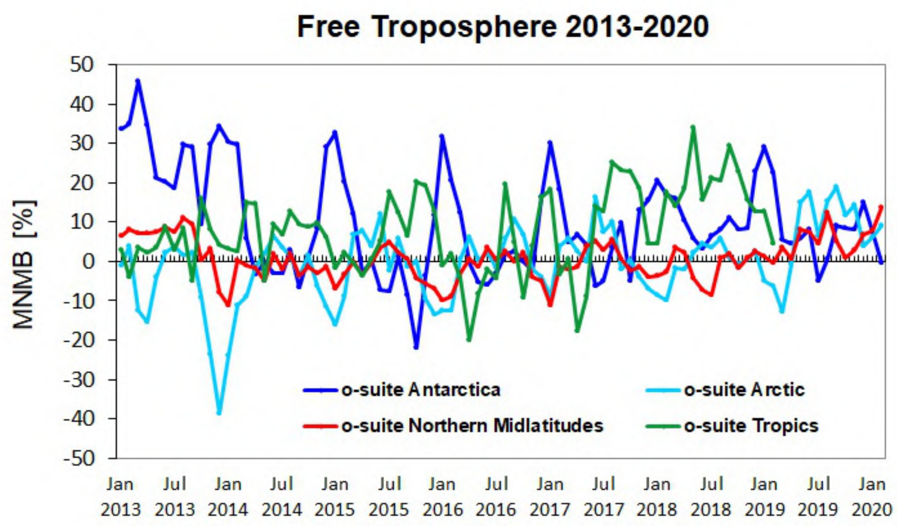

Figure S.1: Time series of MNMB of ozone in the o-suite, compared against ozone sondes, averaged over different latitude bands. The free troposphere is defined here as the layer between 750 and 300 hPa.

Good agreement with IAGOS is found over Frankfurt from the surface to the free troposphere with mostly small overestimations in the lowest layers from both, o-suite and control run. Smallest biases are found in the free troposphere. In the UTLS region, the bias is larger and the results from the models differ. Ozone is mostly overestimated by the o-suite, whereas the control run often shows underestimations. Good agreement with the IAGOS free troposphere ozone profiles is also found over the other regions of the world, with sometimes large differences in the UTLS region.

The validation with IASI satellite data shows that the o-suite run captures both, high and low O_3 values relatively well and is in good agreement with the observations, showing MNMBs within 5%. The control run is mainly positively biased (up to 30% over the high northern latitudes).

In comparison with surface observations we find a steady improvement of the o-suite over the past 5 years over European GAW stations. Biases are within 20% (the Arctic is discussed below). The o-suite has positive biases mostly smaller than 20% for surface ozone for Europe and Asia during December to February 2019/2020. Small underestimations appear for stations in the southern hemisphere.

Tropospheric Nitrogen dioxide (NO_2)

Model validation with respect to GOME-2/MetOp-A and Sentinel-5P TROPOMI NO_2 data shows that tropospheric NO_2 columns are well reproduced by the NRT model runs, indicating that emission patterns and NO_x photochemistry are generally well represented, although modelled shipping signals are more pronounced than in the satellite retrievals. Tropospheric NO_2 columns over some local emission hotspots (e.g. Moscow, and Red Basin in China) are overestimated, while wintertime and springtime values over Europe around Benelux are underestimated. The long-term development over East-Asia (and Europe) for previous years (Fig. S.2), associated with the development of emissions, is not in agreement with the observations. Between spring and autumn, the models regularly show an overestimation over several regions with boreal forest fire activity (Canada, Alaska, Siberia).

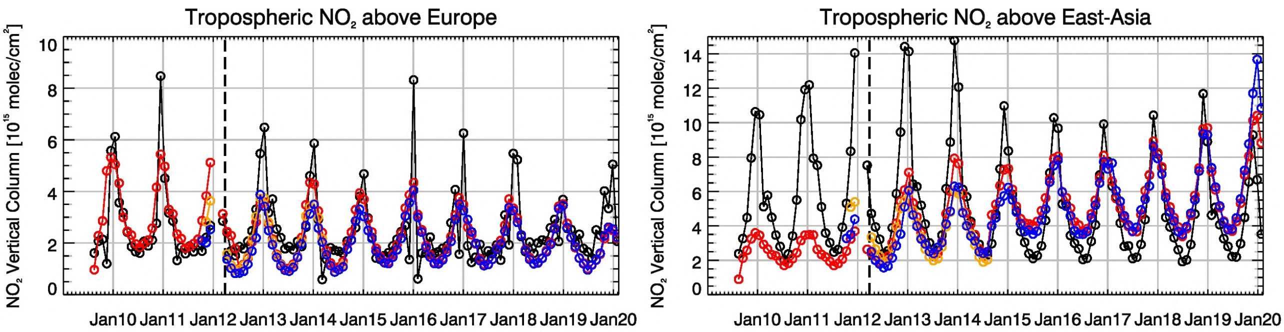

Figure S.2: Time series of tropospheric NO_2 columns from SCIAMACHY (up to March 2012) and GOME-2 (from April 2012 onwards) compared to model results for Europe and East-Asia. Black lines show the observations, red shows the o-suite, blue lines show CAMS control results including older configurations from the MACC projects before September 2014, orange shows the forecast from the MACC project, based on the Mozart-IFS model.

Tropospheric Carbon Monoxide (CO)

Model validation with respect to GAW network surface observations, IAGOS airborne data, FTIR observations (NDACC and TCCON) and MOPITT / IASI satellite retrievals reveals that the absolute values, latitude dependence and seasonality, as well as day-to-day variability of CO can be reproduced well by the CAMS-global analyses and forecasts. Biases are within -10% for European and Asian GAW stations and likewise for stations located in the Southern Hemisphere.

The comparison with NDACC data shows, that the model upgrade (60 to 137 levels) implemented in July 2019 changes the overall biases in both the troposphere and stratosphere. The bias for the tropospheric columns becomes -8.5% in DJF (-7% in SON) and is larger than the reported measurement uncertainty. The bias in the stratosphere is reduced to -12% and just exceeds the measurement's uncertainty.

For TCCON data, sites with available data are Nicosia, Orleans and Reunion. The comparisons show that all models capture the seasonality well and the agreement is within 5-10 ppb.

According to IAGOS observations, CO is mostly underestimated over Frankfurt by both, the o-suite and the control run, largest biases appearing in the lowest layers. The performance of the two runs is similar in the lowest layers, while in the free troposphere, the performance of the o-suite is slightly better than that of the control run. For most other regions of the world, the results are similar to those of Europe.

The relative difference between the model runs and MOPITT shows that the o-suite performs better than the control run without data assimilation. The o-suite generally underestimates the satellite data by about 10% with some regional exceptions where the negative bias reaches 20% (mostly over land).

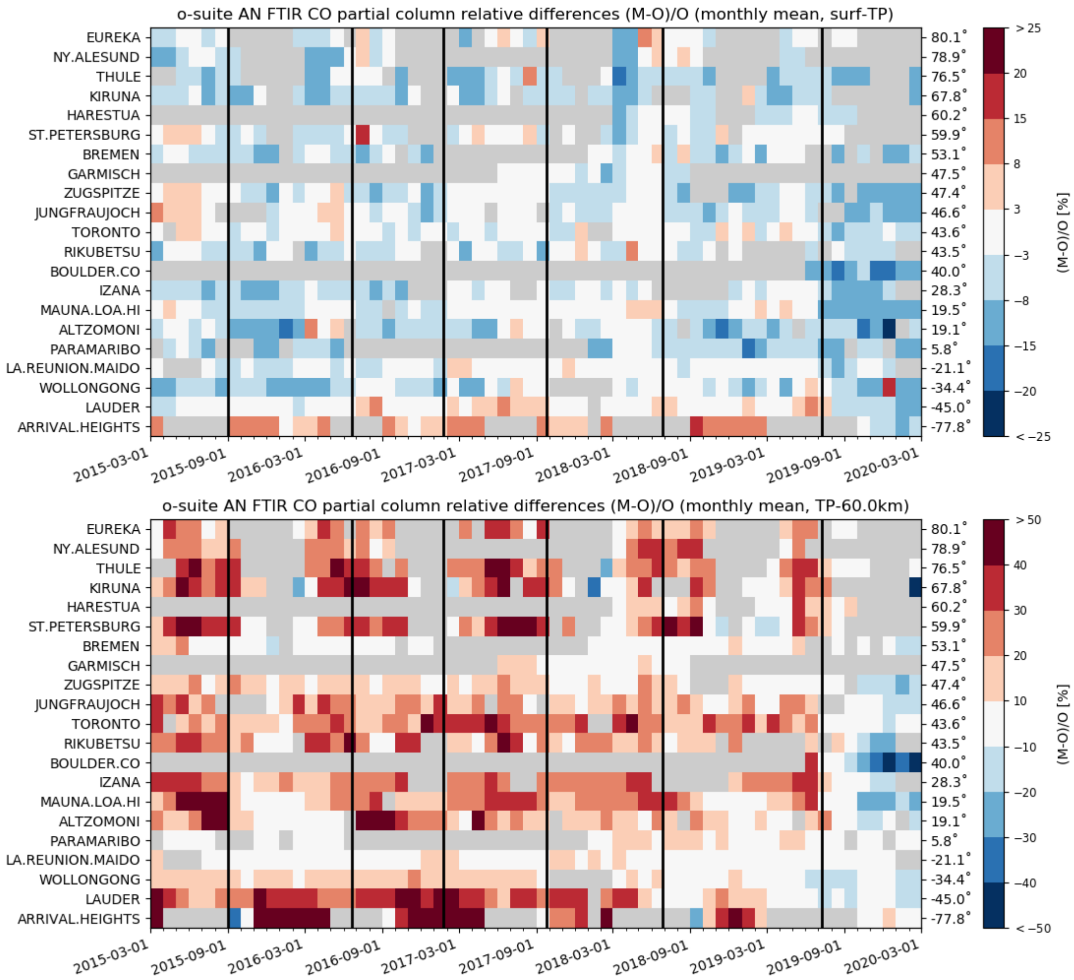

Figure S.3: Monthly relative mean bias from the NDACC FTIR comparisons for tropospheric (top) and stratospheric (bottom) CO columns (%) for the considered period up to 1 March 2020. Model upgrades are indicated in black vertical lines. The overall uncertainty for the CO measurements is approximately 3% on the tropospheric columns and 10% for the stratospheric columns. The o-suite analysis averaged bias in tropospheric columns increased to -8.5% for DJF 2019/2020. The bias in the stratosphere reduced to +2% and lies within the measurement's uncertainty. Stations are sorted with decreasing latitude (northern to southern hemisphere).

After the update from 60 to 137 levels in the second half of the year 2019, we see the following changes:

- Enhanced negative biases over the US and Europe in the o-suite run and more pronounced underestimations in the control run.
- Improvement of the o-suite results over East and South Asia (bias is almost zero).
- General change of bias sign in the control run from positive to negative over the Siberian fire region and enhanced negative biases in the o-suite run.
- Strong increase of negative bias for the control run over the Alaskan region.
- Stronger underestimation over South Africa in both, the o-suite and control run and stronger underestimation over North Africa for the o-suite.

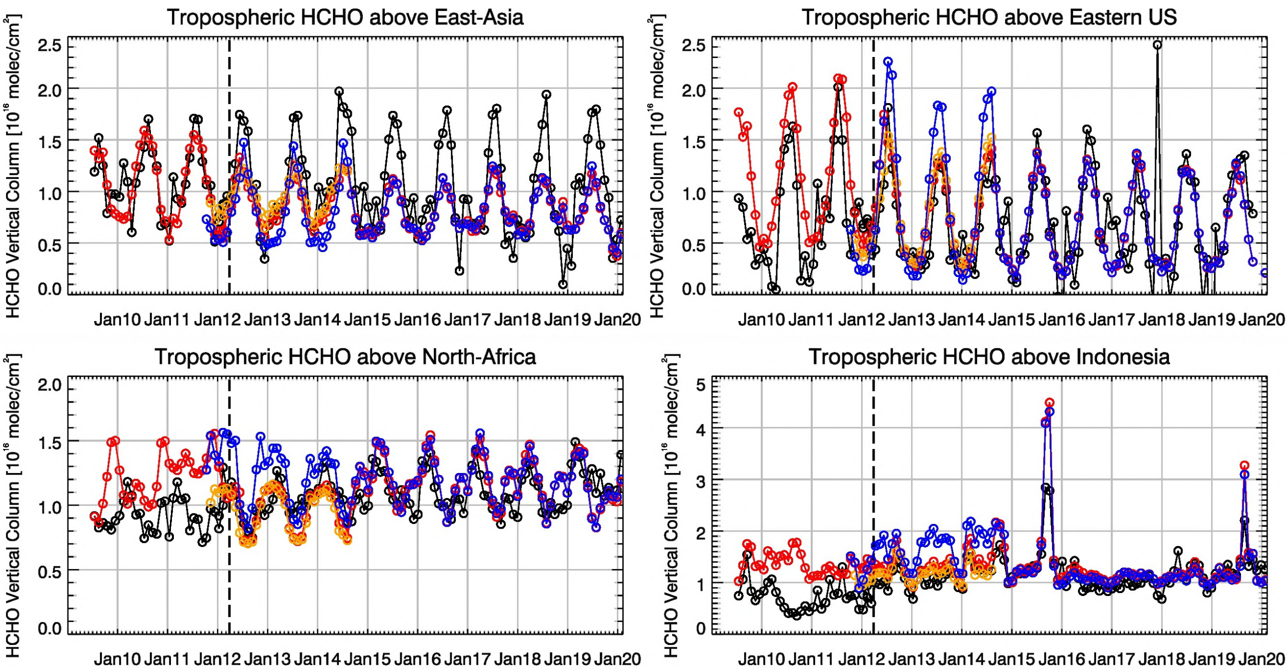

Figure S.4: Time series of average tropospheric HCHO columns [10^{16} molec cm-2] from SCIAMACHY (up to March 2012) and GOME-2 (from April 2012 onwards) compared to model results for different regions. Black lines show the observations, red shows the o-suite, blue lines show CAMS control results including older configurations from the MACC projects before September 2014, orange shows forecasts from the MACC projects. The regions are: East-Asia (25-40°N, 110-125°E), Eastern US (30-40°N, 75-90°W), Northern Africa (0-15°N, 15°W-25°E) and Indonesia (5°S-5°N, 100-120°E). Vertical dashed black lines mark the change from SCIAMACHY to GOME-2 based comparisons in April 2012.

Formaldehyde

Model validation, with respect to SCIAMACHY/Envisat HCHO data (before April 2012), GOME-2/MetOp-A and Sentinel-5P TROPOMI HCHO data, shows that modelled monthly HCHO columns represent well the magnitude of oceanic and continental background values and the overall spatial distribution in comparison with mean satellite HCHO columns (Fig. S.4). Compared to GOME-2 satellite retrievals, an overestimation of values regularly occurs over Australia and Central Africa, which could be both related to biogenic emissions and fire emissions. For time series over East-Asia and the Eastern US, both regions where HCHO columns are probably dominated by biogenic emissions, models and retrievals agree rather well, but the yearly cycle over East-Asia is underestimated by the models.

Tropospheric Water Vapour (H_2O)

The first quarterly evaluation for water vapour in comparison with IAGOS is provided in this report. The results from CAMS global and the control run are very similar at all levels over Frankfurt. Overall, water vapour values and variability are well represented by the two runs in the low troposphere with small positive biases and high correlation values. Large biases are obtained for the free troposphere and UTLS, with both negative and positive signs, while correlation values remain high in the free troposphere. A similar behaviour is found for the results in other regions of the world.

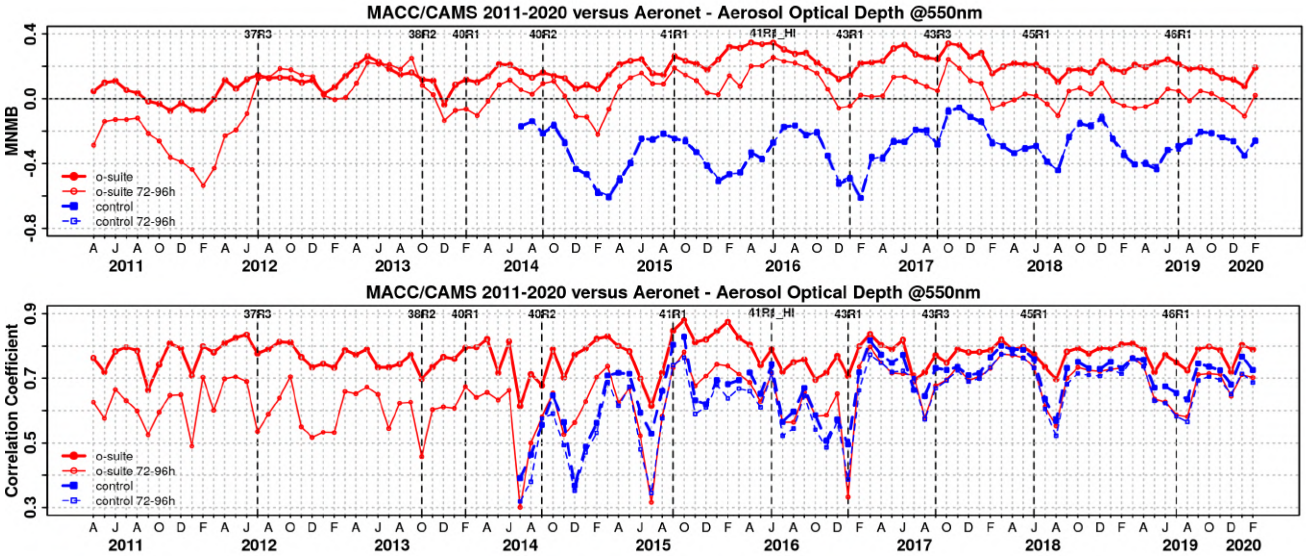

Figure S.5. Aerosol optical depth at 550nm in IFS 00Z model simulations for April 2011 – February 2020 against daily matching Aeronet Version3 level 1.5 data. a) Modified normalized mean bias (MNMB); o-suite (thick red curve); o-suite at last forecast day (light red curve); Control (blue dashed); Control at last forecast day (light blue dashed); b) Corresponding correlation coefficient. Model version changes are marked as vertical bars.

Aerosol

We estimate that the o-suite aerosol optical depth showed an average positive bias in the latest three months of +16%, measured as modified normalized mean bias against daily Aeronet (V3 level 1.5) sun photometer data. The 3-day forecasted aerosol distribution shows 14% less aerosol optical depth (AOD) than that from the initial forecast day, as shown in Fig. S.5-a. Spatiotemporal correlation, shown in Fig. S.5-b, shows month-to-month variation in DJF 2019/20 similar to winter 2018/19, indicating the simulation reproduces approximately 63% of the day to day AOD variability across all Aeronet stations. The o-suite forecast at +3 days shows slightly lower correlation, as a consequence of imperfect forecasted meteorology and fading impact of the initial assimilation of MODIS AOD and MODIS fire info on model performance. The o-suite forecast running each day at 12UTC shows almost identical performance as the forecast starting at 00UTC.

The AOD performance of the o-suite with respect to the AERONET data exhibits no pronounced seasonal cycle but somewhat less correlation in late summer. Since the latest upgrade, the largest contributions to global AOD come from organics, sulphate and sea salt. All species AOD decreased due to the model upgrade in July 2019 with nitrate now contributing to AOD. With the coupling of chemistry and aerosol schemes for sulphur in the latest upgrade in July 2019, first there was an increase of SO4 especially in the northern hemisphere, but then in the beginning of 2020, an increase is seen in the southern hemisphere.

The aerosol Ångström exponent (AE) contains information about the size distribution of the aerosol, and implicitly about composition. The o-suite AE became more positive indicating a change to slightly more fine particles since the model upgrade to version 45R1 in June 2018.

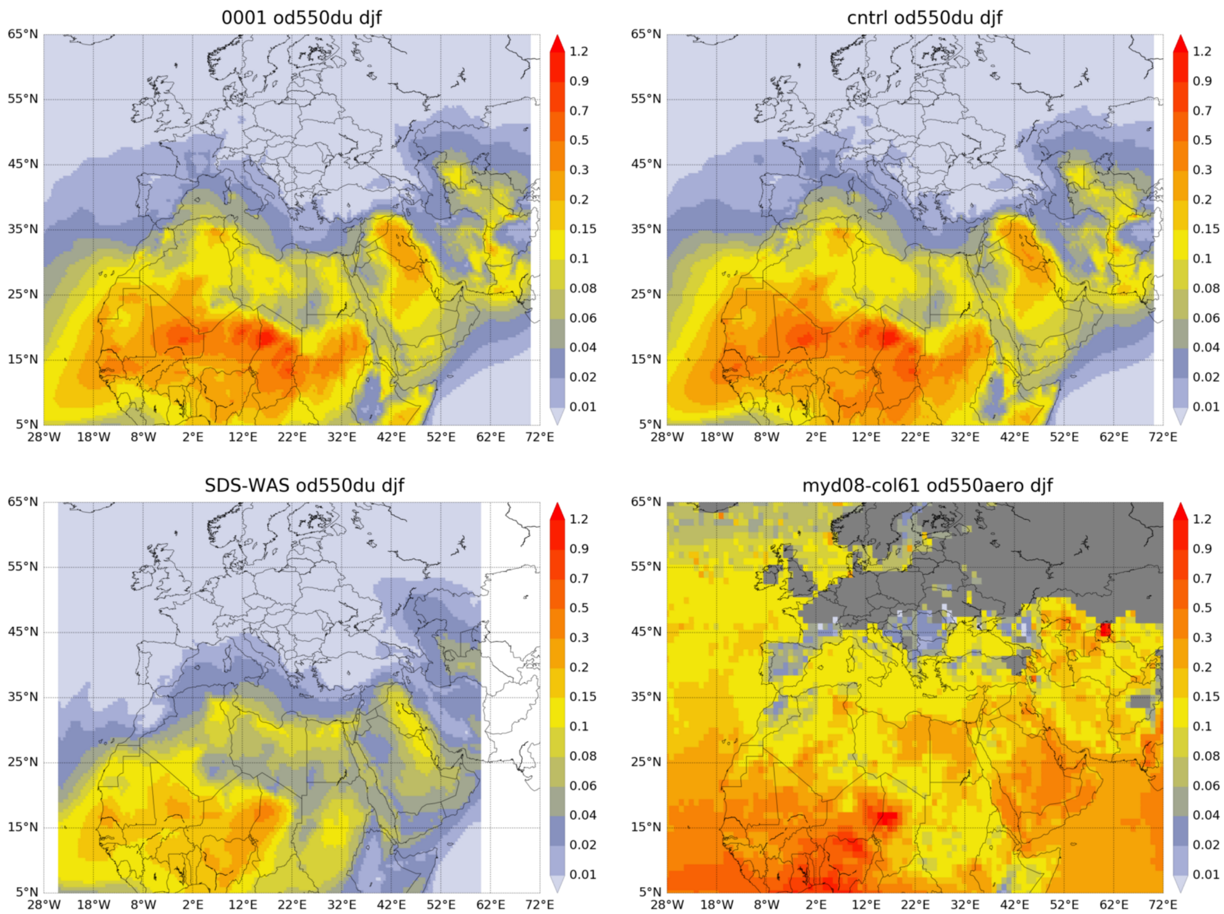

Figure S.6: Averaged DOD 24h forecast from o-suite (top left) and control (top right), DOD of the multi-model SDS-WAS Median product (bottom left) as well as AOD from MODIS/Aqua Collection 6.1 Level 3 combined Dark Target and Deep Blue product (bottom right) for the study period.

PM10 and PM25, as defined by the IFS aerosol model, are evaluated against an average from rural and background site data in the period 2000-2009 at 160 sites in North America and Europe. This indicates that PM10 concentrations exhibit on average in the latest period an underestimation with MNMB bias of -53% in Europe and an overestimation of 5% in North America. PM25 concentrations are underestimated with -60% in Europe and overestimated with 24% in North America. Consistent with this finding a higher positive bias is also found for AOD in North America than in Europe. The fraction of PM simulated data within a factor 2 of observed values stayed similar since September 2017 for both PM10 and PM25. PM25 seems to have deteriorated compared to periods before mid-2017, while PM10 shows an improvement. However, with the latest model version upgrade in July 2019, the PM25 has improved significantly.

Over Northern Africa, the Middle East and Europe, the dust component of the CAMS o-suite shows lower season values than the control run, which is in general higher than the SDS-WAS multi-median product. The CAMS o-suite can reproduce the dust transport over the North Atlantic region. However, the maximum dust activity is shifted to Chad, Mali, Niger and Algeria border and Sudan as shown in MODIS. Also, DOD over Iraq and in the Mediterranean Basin appears overestimated in comparison with the SDS-WAS multi-model ensemble. These changes in dust activity in the main source regions are linked to the new dust module implemented in the operational CAMS model since early-July 2019.

From December to February, the o-suite and control experiments reproduce the daily variability of AERONET SDA observations with a correlation coefficient of 0.59 for o-suite and 0.52 for control averaged over all AERONET sites, which is lower than the SDS-WAS multi-model product which has a correlation coefficient of 0.82. Regarding mean bias (MB), the CAMS o-suite tends to underestimate the AERONET observations with a MB of -0.04 for o-suite and -0.03 for the control experiment. The SDS-WAS multi-model underestimates (MB of -0.04) the AERONET dust-filtered observations.

The comparison of 1 to 3-day forecasts shows that the prediction is stable during the 3-days forecasts in comparison with AERONET direct-sun observations with correlation coefficients of 0.59 (0.52), 0.60 (0.60), and 0.57 (0.58) respectively for 24, 48 and 72h forecasts for all the sites for o-suite (control).

The vertical profiles of backscatter are evaluated in Germany. The changes due to the model upgrades in July 2019 and the unusual warm Winter 2019/2020 have an impact on model performance. Notable is the low positive bias of the model backscatter with better correlation. The step at the top of the PBL is captured notably better with 137 levels than with 60 levels (51L instead of 27L <8 km altitude), same for o-suite and control. The amplitude of the model vertical profile is now very close to the observation (reference). Foehn situations over the alps have been observed including some transport of Saharan dust into Germany, leading to slightly higher bias in mean profiles. Based on three-hourly data Pearson's correlation coefficients in Dec/Jan (run g7h4) have improved and cluster around r= 0.2-0.8 for the 137L model in contrast to r=0.0-0.6 for the 60L version (Winter 2018/19) before.

System performance in the Arctic

The CAMS model runs are validated using surface ozone measurements from the ESRL-GMD and the IASOA networks (5 sites) and ozone concentrations in the free troposphere and UTLS are evaluated using balloon sonde measurement data.

From December 2019 to February 2020 the simulations of the surface ozone concentrations are on average in good agreement with the observations with positive MNMB between 5% and 23%.

During DJF-2020 there is an overestimation of ozone concentrations in the Arctic free troposphere for the o-suite (MNMB = 5% – 10%) and for the control run (MNMB = 0% – 3%) as well as in the UTLS (MNMB up to 30% for the o-suite).

The coverage over the Arctic of the IASI Metop-A version v20191122 daytime only satellite observations, which is used to compare total column ozone with the o-suite and control run is low for the winter months. High O_3 concentrations are seen over the northern high-latitudes, especially over the east of Russia and Canada, which is underestimated by the o-suite and control runs. The IASI sensitivity is the lowest over the cold surfaces such as the Greenland ice sheet where IASI O_3 values are positively biased by up to 20%.

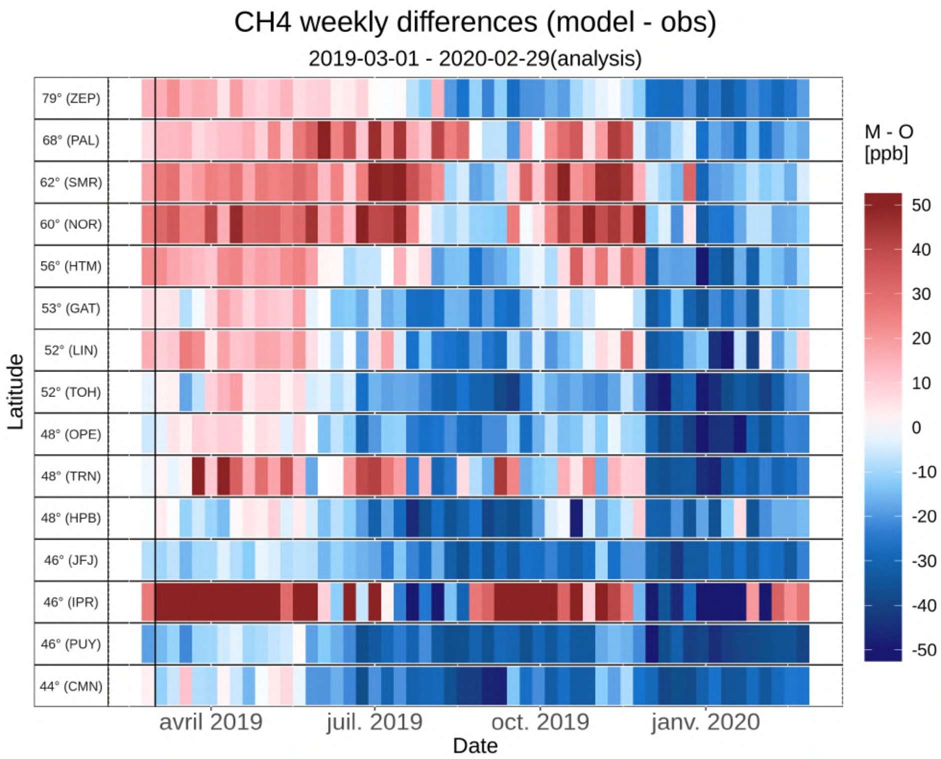

Figure S.7: Mosaic plot of CH_4 biases (in ppb) of the CAMS analysis, compared to surface station observations. Each vertical coloured line represents a weekly mean.

System performance in the Mediterranean

The CAMS o-suite reproduces the daily variability of AERONET direct-sun observations. In the Western, Central and Eastern Mediterranean, the correlation coefficient of the o-suite (0.49, 0.67 and 0.56) is improved by the assimilation compared to the control run (0.51, 0.66 and 0.46) during winter. In general, both CAMS experiments overestimated the AERONET observations in the Mediterranean basin in control (MB of 0.02, 0.05 and 0.07 for Western, Central and Eastern Mediterranean regions respectively) and o-suite (MB of 0.06, 0.06 and 0.11 for Western, Central and Eastern Mediterranean regions respectively). The highest peaks on CAMS AOD simulations are linked to desert dust intrusions occurring during the whole season in the entire Mediterranean basin. In February 2020, high AOD values are observed in Eastern Mediterranean (up to 0.5) that are not associated with natural aerosols (i.e. dust or sea-salt). This can be associated with the latest model upgrade with the improved description of the sulphur cycle.

The PM10 and PM2.5 results of the CAMS o-suite and control run show very similar skill scores in comparison with EIONET-Airbase observations. The CAMS experiments tend to underestimate the surface concentration EIONET-Airbase observations (with MB of -3.46 and -3.92 µg/m^3, respectively PM10 and PM2.5). However, overestimations are observed in Central and Southern European sites.

The model is compared to surface O_3 observations from the AirBase network. Our analysis shows that model MNMBs are mostly within ±30% depending on the station. Temporal correlation coefficients between simulated and observed surface ozone for both the o-suite and control runs are highly significant over the entire Mediterranean from Gibraltar to Cyprus.

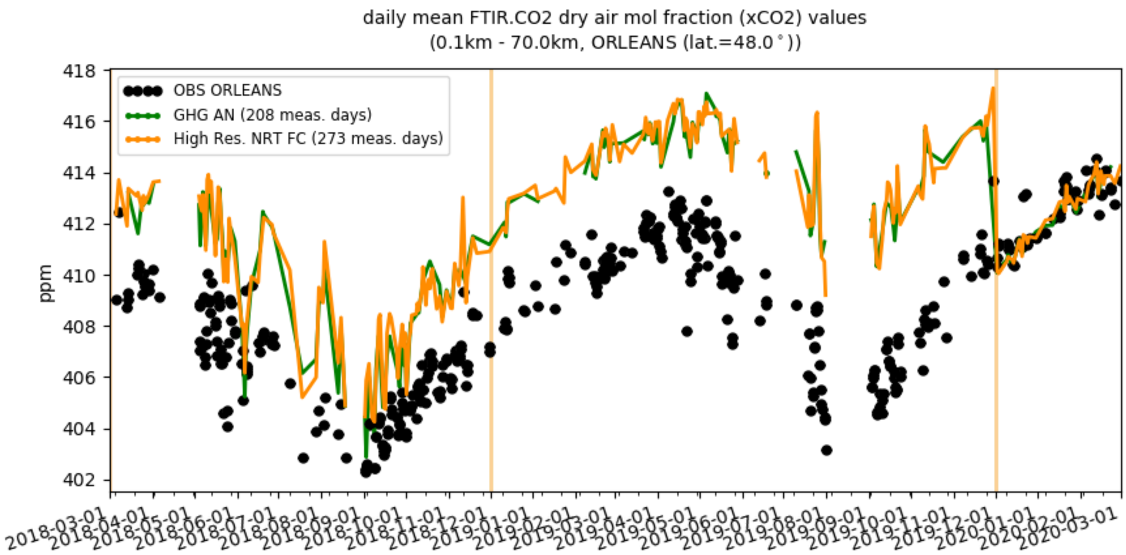

Figure S.8: Comparison of the CO_2 model data with TCCON CO_2 at Orleans.

Climate forcing

Greenhouse gases

CO_2 and CH_4 surface concentrations from ICOS network, and total or partial columns from TCCON and NDACC stations have been used to validate the CAMS greenhouse gas analysis and high-resolution forecast.

Since December 2019 both ICOS (surface) and TCCON (total columns) observations display negative biases ranging from -10 to -50 ppb (Figure S.7). NDACC partial columns indicate also negative biases in the troposphere, but slight positive biases in the stratosphere.

The surface and total column measurements were showing with the previous experiments an overestimation of the amplitude of the CO_2 seasonal cycle in the northern hemisphere by ±1%. The upgrade to Cy46R1, started on December 2019, shows a step change with a clear improvement in the CO_2 concentrations at the surface and in total columns, as illustrated at the TCCON site of Orléans (Figure S.8).

Ozone layer and UV

Ozone partial columns and vertical profiles

Ozone columns and profiles have been compared with the following observations: vertical profiles from balloon-borne ozonesondes; ground-based remote-sensing observations from the NDACC (Network for the Detection of Atmospheric Composition Change, http://www.ndacc.org); and satellite observations by 3 instruments (OMPS-LP, ACE-FTS and SAGE-III). Furthermore, the o-suite analyses are compared with those delivered by the independent assimilation system BASCOE.

Compared to ozone sondes (Fig. S.9) the model O_3 partial pressures are slightly overestimated in all latitude bands (MNMB between -1 and +14%) except above the Antarctic.

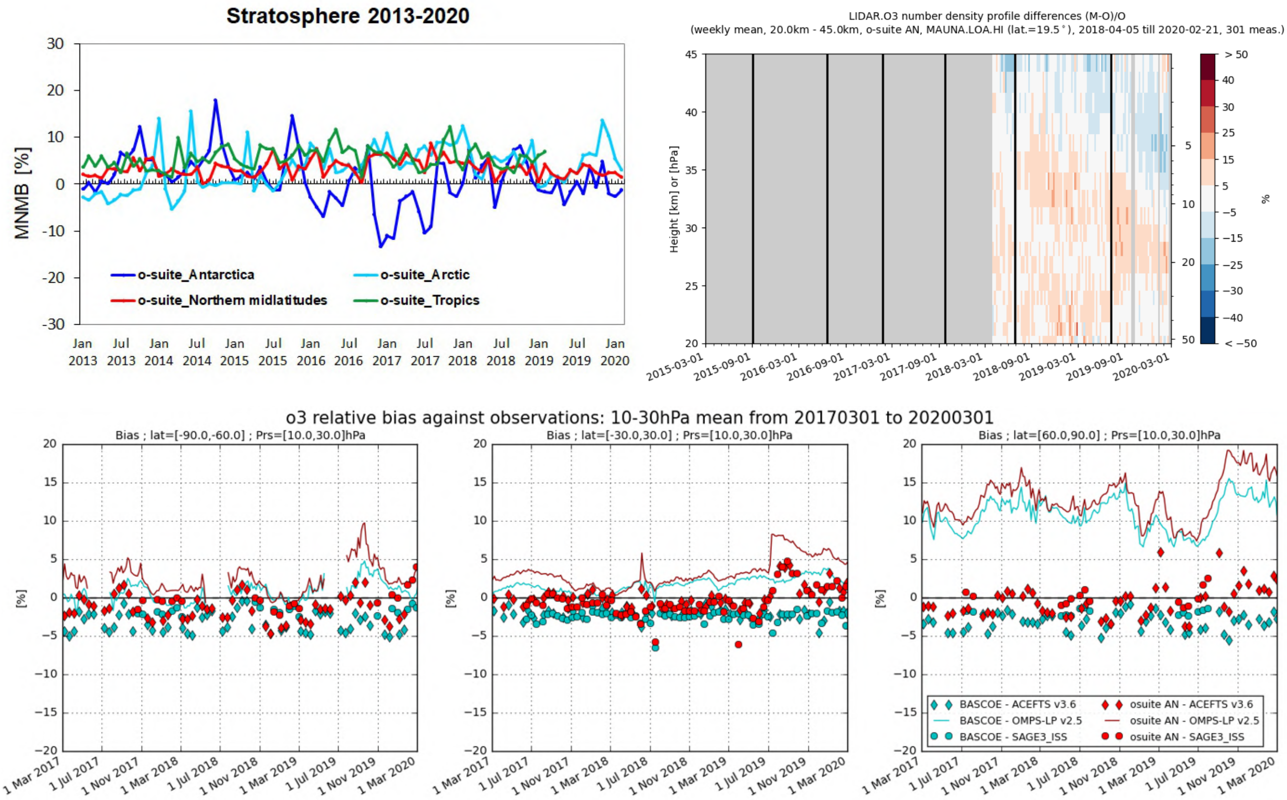

Figure S.9: Top-left: MNMBs (%) of ozone in the stratosphere from the o-suite against aggregated ozonesonde data in the Arctic (light blue), Antarctic (dark blue) northern midlatitudes (red) and tropics (green) from 2013 to February 2020. The stratosphere is defined as the altitude region between 60 and 10 hPa in the tropics and between 90 and 10 hPa elsewhere. Top-right: Comparison of the weekly mean profile bias between the O_3 density profile of the o-suite and the NDACC LIDAR at Mauna Loa. Bottom: Time series comparing models to observations for the period 2017-03-01 to 2020-03-01 in the upper stratosphere (10-30hPa averages): o-suite analyses (red) and BASCOE (cyan) vs OMPS-LP (solid), ACE-FTS (diamonds) and SAGE-III (bullets). Shown is the normalized mean bias (model-observation)/observation (%).

Comparisons with the NDACC network include 19 stations for FTIR, 16 stations for UVVIS stratospheric columns, microwave profiles for Ny Alesund (78.9°N) and Bern (47°N) and LIDAR profiles at Hohenpeissenberg (47.8°N) and Observatoire Haute Provence (OHP), France (43°N) and Mauna Loa (Fig. S.9), Hawai (19.5°N). The comparisons show a general good agreement with the o-suite, with small performance differences between AN and 1d forecasts. At the tropical sites the 1d FC performs significantly worse since the June 2016 update of the o-suite. This is confirmed by FTIR and the Mauna Loa LIDAR measurements.

The comparison with independent satellite observations (Fig. S.9) is generally in good agreement for the considered period: for ACE-FTS, the NMB is mainly within 10% between 5km and 40km, and mostly within 5% between 15km and 35km except in the tropics; for SAGE-III, the NMB is mainly within 10% between 15km and 40km. OMPS-LP has less regular profiles, but the NMB still remain within 15% for most parts of the 20-40 km range. Since the upgrade to cycle 46R1 and the new vertical grid of 137 levels on July 9th, a systematic overestimation of up to 10% around 30km (20hPa) is present in the NMB profiles.

Other stratospheric trace gases

Due to the lack of stratospheric chemistry in the C-IFS-CB05 scheme, the only useful product in the stratosphere is ozone. Other species, like NO_2, have also been evaluated but the results are only indicative.

Events

Australia: The heatwaves in Australia with temperatures exceeding 40°C in the time period from December to February 2020 led to many fire events. IASI satellite data indicate several plumes of CO near the south-east of Australia. The model run does not show the plume observed on 16 December, but it captures well the location of the plume during other days, but with smaller CO values. The transportation pathways are captured by the CAMS runs, but are not as extended as in IASI. Enhancements in CO were observed locally south of Sydney at Wollongong (Fig. 11.1.2) with FTIR. The peak early January was well captured by the CAMS o-suite and control run.

Exceptional dust event over Canary Islands in late-February 2020: In late-February 2020, strong Saharan winds picked up dust from Africa and carried it over the Canary Islands, achieving surface concentrations over 3000µg/m3 and reducing visibility to less than 10m. The event is originating in Mauritania on 22nd February in the early morning. Dust was transported towards the West achieving Canary Islands few hours later. MODIS satellite detected an intense outbreak of dust over Canary Islands achieving maximum AOD values up to 5. The comparison with the MODIS AOD product show that The CAMS o-suite AOD reproduces the spatial distribution and timing of the dust plume. However, the comparison shows that CAMS o-suite underestimates the aerosol concentrations during this event, reaching AOD values up to 1.5 and PM10 up to 300 $\mu g/m^3$ in over Canary Islands.

Table of Contents

1. Introduction

The Copernicus Atmosphere Monitoring Service (CAMS, http://atmosphere.copernicus.eu/) is a component of the European Earth Observation programme Copernicus. The CAMS global near-real time (NRT) service provides daily analyses and forecasts of trace gas and aerosol concentrations. The CAMS near-real time services consist of daily analysis and forecasts with the ECMWF IFS system with data assimilation of trace gas concentrations and aerosol properties. This document presents the system evolution and the validation statistics of the CAMS NRT global atmospheric composition analyses and forecasts. The validation methodology and measurement datasets are discussed in Eskes et al. (2015).

In this report the performance of the system is assessed in two ways: both the longer-term mean performance (seasonality) as well as its ability to capture recent events are documented. Table 1.1 provides an overview of the trace gas species and aerosol aspects discussed in this CAMS near-real time validation report. This document is updated every 3 months to report the recent status of the near-real time service. The report covers results for a period of at least one year to document the seasonality of the biases. Sometimes reference is made to other model versions or the reanalysis to highlight aspects of the near-real time products.

This validation report is accompanied by the "Observations characterization and validation methods" report, Eskes et al. (2019), which describes the observations used in the comparisons, and the validation methodology. This report can also be found on the global validation page, http://atmosphere.copernicus.eu/user-support/validation/verification-global-services.

Key CAMS NRT products and their users are: Boundary conditions for regional air quality models (e.g. AQMEII, air quality models not participating in CAMS); Long range transport of air pollution (e.g. LRTAP); Stratospheric ozone column and UV (e.g. WMO, DWD); 3D ozone fields (e.g. SPARC). As outlined in the MACC-II Atmospheric Service Validation Protocol (2013) and MACC O-INT document (2011), relevant user requirements are quick looks of validation scores, and quality flags and uncertainty information along with the actual data. This is further stimulated by QA4EO (Quality Assurance Framework for Earth Observation, http://www.qa4eo.org) who write that “all earth observation data and derived products is associated with it a documented and fully traceable quality indicator (QI)”. It is our long-term aim to provide such background information. The user is seen as the driver for any specific quality requirements and should assess if any supplied information, as characterised by its associated QI, are "fit for purpose" (QA4EO task team, 2010).

CAMS data are made available to users as data products (grib or netcdf files) and graphical products from ECMWF, accessible through the catalogue on http://atmosphere.copernicus.eu/.

A summary of the system and its recent changes is given in section 2. Subsequent sections give an overview of the performance of the system for various species, and during recent events. Routine validation results can be found online via regularly updated verification pages,
http://atmosphere.copernicus.eu/user-support/validation/verification-global-services.
Table 1.2 lists all specific validation websites that can also be found through this link.

Table 1.1: Overview of the trace gas species and aerosol aspects discussed in this CAMS near-real time validation report. Shown are the datasets assimilated in the CAMS analysis (second column) and the datasets used for validation, as shown in this report (third column). Green colours indicate that substantial data is available to either constrain the species in the analysis, or substantial data is available to assess the quality of the analysis. Yellow boxes indicate that measurements are available, but that the impact on the analysis is not very strong or indirect (second column), or that only certain aspects are validated (third column).

Species, vertical range	Assimilation	Validation
Aerosol, optical properties	MODIS Aqua/Terra AOD PMAp AOD	AOD, Ångström: AERONET, GAW, Skynet, MISR, OMI, lidar, ceilometer
Aerosol mass (PM10, PM2.5)	MODIS Aqua/Terra	European AirBase stations
O_3, stratosphere	MLS, GOME-2, OMI, SBUV-2, TROPOMI	Sonde, lidar, MWR, FTIR, OMPS, ACE-FTS, OSIRIS, BASCOE and MSR analyses
O_3, UT/LS	MLS	IAGOS, ozone sonde
O_3, free troposphere	Indirectly constrained by limb and nadir sounders	IAGOS, ozone sonde, IASI
O_3, PBL / surface		Surface ozone: WMO/GAW, NOAA/ESRL-GMD, AIRBASE
CO, UT/LS	IASI, MOPITT	IAGOS
CO, free troposphere	IASI, MOPITT	IAGOS, MOPITT, IASI, TCCON
CO, PBL / surface	IASI, MOPITT	Surface CO: WMO/GAW, NOAA/ESRL
NO_2, troposphere	OMI, GOME-2, partially constrained due to short lifetime	TROPOMI, SCIAMACHY, GOME-2, MAX-DOAS
HCHO		TROPOMI, GOME-2, MAX-DOAS
SO_2	GOME-2 (Volcanic eruptions)	
Stratosphere, other than O_3		NO_2 column only: SCIAMACHY, GOME-2
CO_2, surface, PBL		ICOS
CO_2, column	GOSAT	TCCON
CH_4, surface, PBL		ICOS
CH_4, column	GOSAT, IASI	TCCON

Table 1.2: Overview of quick-look validation websites of the CAMS system.

The CAMS global evaluation server
https://global-evaluation.atmosphere.copernicus.eu
Reactive gases – Troposphere
IAGOS tropospheric ozone and carbon monoxide: http://www.iagos.fr/cams/ Surface ozone from EMEP (Europe) and NOAA-ESRL (USA): http://www.academyofathens.gr/cams Tropospheric nitrogen dioxide and formaldehyde columns against satellite retrievals: http://www.doas-bremen.de/macc/macc_veri_iup_home.html Tropospheric CO columns against satellite retrievals: http://www.mpimet-cams.de GAW surface ozone and carbon monoxide: https://atmosphere.copernicus.eu/charts/cams_gaw_ver/v0d_gaw_oper_operfc_nrt_sites?facets=undefined&time=2018060100,0,2018060100&fieldpair=CO&site=cmn644n00
Reactive gases - Stratosphere
Stratospheric composition: http://www.copernicus-stratosphere.eu NDACC evaluation in stratosphere and troposphere (the NORS server) http://nors-server.aeronomie.be
Aerosol
Evaluation against Aeronet stations: http://aerocom.met.no/cams-aerocom-evaluation/ More in-depth evaluations are available from the Aerocom website. WMO Sand and Dust Storm Warning Advisory and Assessment System (SDS-WAS) model intercomparison and evaluation: http://sds-was.aemet.es/forecast-products/models Aeronet verification of CAMS NRT forecasts: https://atmosphere.copernicus.eu/charts/cams_aeronet_ver/?facets=undefined&time=2019020100,0,2019020100&site=ARM_Graciosa
Satellite data monitoring
Monitoring of satellite data usage in the Near-Real-Time production: https://atmosphere.copernicus.eu/charts/cams/cams_satmon?facets=undefined&time=2016071800&Parameter=AURA_MLS_profile_Ozone_1_GLOBE

The CAMS global evaluation server, https://global-evaluation.atmosphere.copernicus.eu, became available in Summer 2019. This server combines many of the individual verification results shown on the other CAMS web pages listed in Table 1.2, and presents the comparisons through a uniform interface.

Naming and color-coding conventions in this report follow the scheme as given in Table 1.3.

Table 1.3. Naming and colour conventions as adopted in this report.

Name in figs	experiment	Colour
{obs name}	{obs}	black
o-suite D+0 FC	0001	red
control	gsyg	blue
GHG high-resolution run	gqpe / ghqy	orange
GHG global analysis	gqiq	green

2. System summary and model background information

The specifics of the different CAMS model versions are given below (section 2.1) including an overview of model changes. Other systems used in CAMS are listed in section 2.2. An overview of products derived from this system is given in section 2.3. Timeliness and availability of the CAMS products is given in section 2.4.

2.1 System based on the ECMWF IFS model (the o-suite and control run)

Key model information is given on the CAMS data-assimilation and forecast run o-suite and its control experiment, used to assess the performance of the assimilation. The forecast products are listed in Table 2.1. Table 2.2 provides information on the satellite data used in the o-suite. Further details on the different model runs and their data usage can be found at http://atmosphere.copernicus.eu/documentation-global-systems.

Table 2.1: Overview of model runs assessed in this validation report.

Forecast system	Exp. ID	Brief description	Upgrades (e-suite ID)	Cycle
O-suite	0001	Operational CAMS DA/FC run	20190709-present 20180626-20190708 20170926-20180625 20170124-20170926 20160621-20170124 20150903-20160620 20140918-20150902	46R1 45R1 43R3 43R1 41R1 41R1 40R2
Control	h7c4 gzhy gsyg gnhb gjjh geuh g4o2	control FC run without DA	20190709-present 20180626-20190708 20170926-20180625 20170124-20170926 20160621-20170124 20150901-20160620 20140701-20150902	46R1 45R1 43R3 43R1 41R1 41R1 40R2
GHG run	h72g	Tco399L137 NRT CO_2, CH_4 analyses (~25km)	20191201-present	46R1
	h9sp	High resolution Tco1279 (~9km) NRT CO_2, CH_4 forecast	20191201-present	46R1
	gwx3 gqiq	GHG analysis Tco399 (~25km)	20181201-20191130 20170101-20181130	45R1 43R1
	gznv gqpe	High resolution Tco1279 (~9km) NRT CO_2, CH_4 forecast	20181201-20191130 20170101-20181130	45R1 43R1
	ghqy gf39	High resolution T1279, NRT CO_2 and CH_4 without DA	20160301-20170621 20150101-20160229	

Table 2.2: Satellite retrievals of reactive gases and aerosol optical depth that are actively assimilated in the o-suite.

Instrument	Satellite	Provider	Version	Type	Status
MLS	AURA	NASA	V4	O3 Profiles	20130107 -
OMI	AURA	NASA	V883	O3 Total column	20090901 -
GOME-2A	Metop-A	Eumetsat	GDP 4.8	O3 Total column	20131007 - 20181231
GOME-2B	Metop-B	Eumetsat	GDP 4.8	O3 Total column	20140512 -
SBUV-2	NOAA-19	NOAA	V8	O3 21 layer profiles	20121007 -
OMPS	Suomi-NPP	NOAA / EUMETSAT		O3 Profiles	20170124 - 20190409
TROPOMI	Sentinel-5P	ESA		O3 column	20181204-
IASI	MetOp-A	LATMOS/ULB Eumetsat	-	CO Total column	20090901 - 20180621 20180622 - 20191118
IASI	MetOp-B	LATMOS/ULB Eumetsat	-	CO Total column	20140918 - 20180621 20180622 -
IASI	MetOp-C	Eumetsat		CO total column	20191119 -
MOPITT	TERRA	NCAR	V5-TIR V7-TIR V7-TIR Lance V8-TIR	CO Total column	20130129 - 20160124 - 20180626 20180626 20190702
OMI	AURA	KNMI	DOMINO V2.0	NO2 Tropospheric column	20120705 -
GOME-2A/2B	METOP A/B	Eumetsat	GDP 4.8	NO2 Tropospheric column	20180626 -
OMI	AURA	NASA	v003	SO2 Tropospheric column	20120705-20150901
GOME-2A/2B	METOP A/B	Eumetsat	GDP 4.8	SO2 Tropospheric column	20150902 -
MODIS	AQUA / TERRA	NASA	Col. 5 Deep Blue Col. 6, 6.1	Aerosol total optical depth, fire radiative power	20090901 - 20150902 - 20170124 -
PMAp	METOP-A METOP-B	EUMETSAT		AOD	20170124 - 20170926 -

2.1.1 The CAMS o-suite

The o-suite consists of the IFS-CB05 chemistry combined with the CAMS bulk aerosol model. The chemistry is described in Flemming et al. (2015) and Flemming et al. (2017), aerosol is described in Morcrette et al. (2009). The forecast length is 120 h. The o-suite data is stored under **expver '0001'** of **class 'MC'**. On 21 June 2016 the model resolution has seen an upgrade from T255 to T511, and forecasts are produced twice per day.

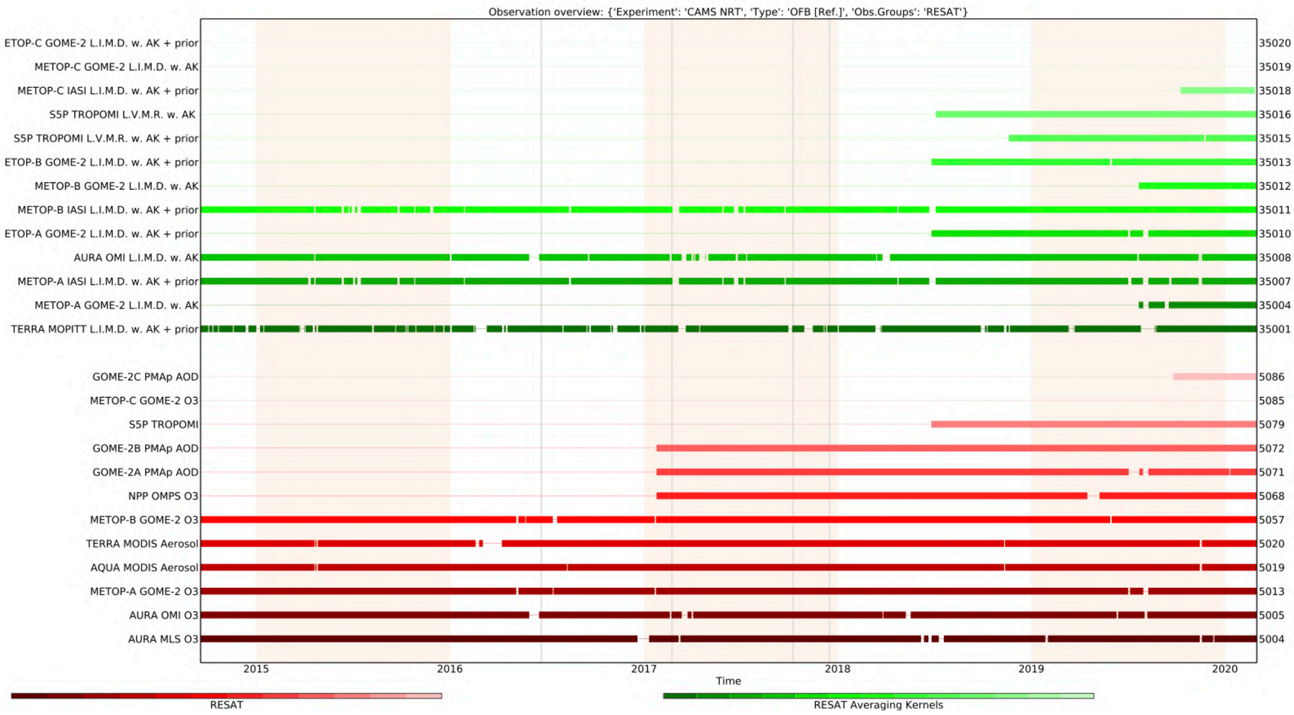

Figure 2.1: Satellite observation usage in the real-time analysis, for ozone, CO, aerosol AOD and NO2, from October 2014 onwards. Top rows (in green): products assimilated using averaging kernels. New assimilated products are the PMaP AOD including GOME-2B , GOME-2C and OMPS ozone profile observations and METOP-C GOME-2 data. Sentinel-5P TROPOMI ozone is assimilated since Dec. 2018 (5079=O3) and other products are monitored (35016=NO2, 35015=CO, 5081=SO2).

A short summary of the main model specifications:

- The modified CB05 tropospheric chemistry is used (Williams et al., 2013), originally taken from the TM5 chemistry transport model (Huijnen et al., 2010)
- Stratospheric ozone during the forecast is computed from the Cariolle scheme (Cariolle and Teyssèdre, 2007) as already available in IFS, while stratospheric NOx is constrained through a climatological ratio of HNO_3/O_3 at 10 hPa.
- Monthly mean dry deposition velocities are based on the SUMO model provided by the MOCAGE team.
- Data assimilation is described in Inness et al. (2015) and Benedetti et al. (2009) for chemical trace gases and aerosol, respectively. Satellite data assimilated is listed in Table 2.2 and Fig. 2.1.
- Anthropogenic and biogenic emissions are based on MACCity (Granier et al., 2011) and a climatology of the MEGAN-MACC emission inventories (Sindelarova et al., 2014)
- NRT fire emissions are taken from GFASv1.2 (Kaiser et al. 2012).

The aerosol model includes 14 prognostic variables (Remy et al., 2019).

- 3 size bins each for sea-salt and desert dust
- 2 bins (hydrophibic and hydrophobic) each for organic matter and black carbon
- 1 bin for sulphate

- 2 bins (fine and coarse) for nitrate (New since 46R1)
- 1 bin for ammonium (New since 46R1)

The SO_2 precursor for sulphate aerosol no longer exists as a separate prognostic in the aerosol scheme, which since 46R1 couples directly to the SO_2 in the chemistry scheme instead. Likewise, the precursors for the new nitrate and ammonium aerosol (nitric acid and ammonia) are also part of the chemistry scheme rather than the aerosol scheme.

Aerosol total mass is constrained by the assimilation of MODIS and PMAp AOD (Benedetti et al. 2009). A variational bias correction is currently applied for the PMAp AOD based on the approach used also elsewhere in the IFS (Dee and Uppala, 2009).

A history of updates of the o-suite is given in Table 2.3, and is documented in earlier MACC-VAL and CAMS reports: https://atmosphere.copernicus.eu/node/326. This includes a list with changes concerning the assimilation system.

The CAMS o-suite system is upgraded regularly, following updates to the ECMWF meteorological model as well as CAMS-specific updates such as changes in chemical data assimilation. These changes are documented in e-suite validation reports, as can be found from the link above. Essential model upgrades are also documented in Table 2.3.

The penultimate upgrade of the system (45r1) took place on 26 June 2018. This upgrade is also relevant for this report (for the period up to 8 July), and the validation for this upgrade is described in Eskes et al., 2018b/2018c.

2.1.2 Short description of the latest CAMS upgrade (46r1)

The latest upgrade of the system took place on 9 July 2019 and is based on IFS version cy46r1_CAMS and involves the move from 60 to 137 vertical levels, see https://atmosphere.copernicus.eu/cycle-46r1 or https://confluence.ecmwf.int/display/COPSRV/Current+global+production+suites.

The validation for this 46r1 upgrade is described in Basart et al. 2019: https://atmosphere.copernicus.eu/sites/default/files/2019-07/CAMS84_2018SC1_D3.2.1-201907_esuite_v1.pdf

The meteorological changes can be found on the ECMWF-IFS CY46R1 page, https://confluence.ecmwf.int/display/FCST/Implementation+of+IFS+cycle+46R1.

The atmospheric composition content of the new cycle includes the following aspects:

Assimilation:

- New model-error covariance matrices for aerosol and chemistry at 137 levels.

Observations:

- No new atmospheric composition observations compared to Cycle 45r1.

Table 2.3: Long-term o-suite system updates.

Date	o-suite update
2009.08.01	Start of first NRT experiment f7kn with coupled MOZART chemistry, without aerosol. Also without data assimilation.
2009.09.01	Start of first MACC NRT experiment f93i, based on meteo cy36r1, MOZART v3.0 chemistry, MACC aerosol model, RETRO/REAS and GFEDv2 climatological emissions, T159L60 (IFS) and 1.875°×1.875° (MOZART) resolution.
2012.07.05	Update to experiment fnyp: based on meteo cy37r3, MOZART v3.5 chemistry, where changes mostly affect the stratosphere, MACCity (gas-phase), GFASv1 emissions (gas phase and aerosol), T255L60 (IFS) and 1.125°×1.125° (MOZART) resolution. Rebalancing aerosol model, affecting dust.
2013.10.07	Update of experiment fnyp from e-suite experiment fwu0: based on meteo cy38r2, no changes to chemistry, but significant rebalancing aerosol model. Assimilation of 21 layer SBUV/2 ozone product
2014.02.24	Update of experiment fnyp from e-suite experiment fzpr: based on meteo cy40r1. No significant changes to chemistry and aerosol models.
2014.09.18	Update to experiment g4e2: based on meteo cy40r2. In this model version IFS-CB05 is introduced to model atmospheric chemistry.
2015.09.03	Update to experiment g9rr: based on meteo cy41r1.
2016.06.21	Update to experiment 0067: based on meteo cy41r1, but a resolution increase from T255 to T511, and two production runs per day
2017.01.24	Update to cycle 43R1_CAMS, T511L60
2017.09.26	Update to cycle 43R3_CAMS, T511L60
2018.06.26	Update to cycle 45R1_CAMS, T511L60
2019-07-09	Update to cycle 46R1_CAMS, T511L137

Emissions:

- New emissions inventories: CAMS_GLOB_ANT v2.1 (anthropogenic) and CAMS_GLOB_BIO v1.1 (biogenic), in place of previous MACCity and MEGAN_MACC inventories.
- Biomass-burning injection heights from GFAS and updated diurnal cycle. In particular, this reduces the overestimation of near-surface PM2.5 during fire events.
- Anthropogenic SOA production was updated with a diurnal cycle and a regionally-varying ratio to CO emissions. This has a small impact on AOD, but significantly reduces night-time near-surface PM2.5 in polluted regions.
- New online dust emission scheme (Nabat et al., 2012). This increases total dust emissions and shifts them towards larger particle sizes, in line with recent literature. An updated dust source function improves the selection of source regions, reducing "gaps" in dust emissions.

- Sea-salt production over freshwater lakes eliminated. This corrects an issue that was particularly noticeable over the Great Lakes.

Other model changes:

- Vertical resolution increased from 60 levels to 137 levels, matching that used at ECMWF for NWP. This includes moving the model top from 0.1 hPa to 0.01 hPa.
- New nitrate and ammonium aerosol species are included and are coupled to the gas-phase nitrogen chemistry. This is a major expansion of the aerosol species represented in the model, giving a more complete representation of the species which contribute to e.g. PM2.5 over Europe.
- Sulphur species (SO_2 and SO_4) coupled between chemistry and aerosol schemes. See discontinued parameters below. This brings a greater consistency between the chemistry and aerosol products related to the sulphur cycle.
- Online calculation of dry deposition velocities for trace gases. This was already in place for aerosols in 45r1 and allows the deposition scheme to better account for variations in surface properties.
- Updates to wet deposition parameterisations. This brings improvements in the distinction between scavenging by liquid and ice and harmonises the treatment for aerosols and trace gases.
- Updates to chemical reaction rates following latest recommendations by JPL/IUPAC.

2.1.3 Control

The control run (relevant expver = **gzhy,** since 26/06/2018; expver = **h7c4** since 09/07/2019) applies the same settings as the respective o-suites, based on the coupled IFS-CB05 system with CAMS aerosol for cy54r1, except that data assimilation is not switched on. The meteorology in the control run is initialized with the meteorological fields from the o-suite.

2.1.4 High-resolution CO_2 and CH_4 forecasts and delayed-mode analyses

The pre-operational forecasts of CO_2 and CH_4 use an independent setup of the IFS at a resolution of TL1279, i.e. ~16 km horizontal, and with 137 levels. This system runs in real time and does not apply data assimilation for the greenhouse gases.

The land vegetation fluxes for CO_2 are modelled on-line by the CTESSEL carbon module (Boussetta et al., 2013). A biogenic flux adjustment scheme is used in order to reduce large-scale biases in the net ecosystem fluxes (Agusti-Panareda, 2015). The anthropogenic fluxes are based on the annual mean EDGARv4.2 inventory using the most recent year available (i.e. 2008) with estimated and climatological trends to extrapolate to the current year. The fire fluxes are from GFAS (Kaiser et al., 2012). Methane fluxes are prescribed in the IFS using inventory and climatological data sets, consistent with those used as prior information in the CH_4 flux inversions from Bergamaschi et al. (2009). The anthropogenic fluxes are from the EDGAR 4.2 database (Janssens-Maenhout et al, 2012) valid for the year 2008. The biomass burning emissions are from GFAS v1.2 (Kaiser et al., 2012). The high-resolution forecast experiments also included a linear CO scheme (Massart et al., 2015).

The experiments analysed in this report are:

- "**h72g**" NRT CO_2, CH_4 analyses from 1 December 2019, with a resolution Tco399 (~25km) and 137 vertical levels. Cycle 46R1.
- "**h9sp**" NRT CO_2, CH_4 forecasts from 1 December 2019, with high resolution Tco1279 (~9km) and 137 vertical levels. Cycle 46R1.
- "**gqpe**" (43R1) from January 2017, and "**gznv**" (45R1) from 1 December 2018 to present. It runs with a TCO1279 Gaussian cubic octahedral grid (equivalent to approximately 9km horizontal resolution). Note that the CO_2, CH_4 and linear CO tracers are initialized with the GHG analysis (gqiq) for CO_2 and CH_4 and the CAMS operational analysis for CO.
- The greenhouse gas analysis experiment runs on a TCO399 grid (equivalent to around 25km) and 137 vertical levels and is available from January 2017 ("**gqiq**", 43R1) and 1 December 2018 ("**gwx3**", 45R1). This experiment runs in delayed mode (4 days behind real time) and makes use of observations from TANSO-GOSAT (methane and CO_2) and MetOp-IASI (methane).
- "**ghqy**" from March 2016. The initial conditions used in ghqy on 1st of March 2016 are from the GHG analysis (experiment gg5m). Furthermore, the meteorological analysis used to initialize the ghqy forecast changed resolution and model grid in March 2016. Note that the CO_2, CH_4 and linear CO tracers are free-running.

2.2 Other systems

2.2.1 BASCOE

The NRT analyses and forecasts of ozone and related species for the stratosphere, as delivered by the Belgian Assimilation System for Chemical ObsErvations (BASCOE) of BIRA-IASB (Lefever et al., 2014; Errera et al., 2008), are used as an independent model evaluation of the CAMS products. The NRT BASCOE product is the ozone analysis of Aura/MLS-SCI level 2 standard products, run in the following configuration (version 05.07):

- The following species are assimilated: O_3, H_2O, HNO_3, HCl, HOCl, N_2O and ClO.
- It lags by typically 4 days, due to latency time of 4 days for arrival of non-ozone data from Aura/MLS-SCI (i.e. the scientific offline Aura/MLS dataset).
- Global horizontal grid with a 3.75° longitude by 2.5° latitude resolution.
- Vertical grid is hybrid-pressure and consists in 86 levels extending from 0.01 hPa to the surface.
- Winds, temperature and surface pressure are interpolated in the ECMWF operational 6-hourly analyses.
- Time steps of 20 minutes, output every 3 hours

See the stratospheric ozone service at http://www.copernicus-stratosphere.eu/. It delivers graphical products dedicated to stratospheric composition and allows easy comparison between the results of o-suite, BASCOE and TM3DAM. The BASCOE data products (HDF4 files) are also distributed from this webpage. Other details and bibliographic references on BASCOE can be found at http://bascoe.oma.be/. A detailed change log for BASCOE can be found at http://www.copernicus-stratosphere.eu/4_NRT_products/3_Models_changelogs/BASCOE.php.

2.2.2 TM3DAM and the multi-sensor reanalysis

One of the products CAMS is compared with is are multi-decadal reanalyses, near-real time analysis and 10-day forecast of ozone column amounts performed with the KNMI TM3DAM data assimilation system, and the Multi-Sensor Reanalysis (MSR) system (van der A et al., 2010, 2013), http://www.temis.nl/macc/index.php?link=o3_msr_intro.html.
The corresponding validation report can be found at
http://www.copernicus-atmosphere.eu/services/gac/global_verification/validation_reports/.

An update of the MSR (MSR-2) was presented in van der A et al. (2015), which extended the record to 43 years based on ERA-interim reanalysis meteo and with an improved resolution of 1x1 degree.

2.2.3 SDS-WAS multimodel ensemble

The World Meteorological Organization's Sand and Dust Storm Warning Advisory and Assessment System (WMO SDS-WAS) for Northern Africa, Middle East and Europe (NAMEE) Regional Center (http://sds-was.aemet.es/) has established a protocol to routinely exchange products from dust forecast models as the basis for both near-real-time and delayed common model evaluation. Currently, twelve regional and global models (see the complete list in the following link https://sds-was.aemet.es/forecast-products/forecast-evaluation/model-inter-comparison-and-forecast-evaluation/at_download/file) provides daily operational dust forecasts (i.e. dust optical depth, DOD, and dust surface concentration).

Different multi-model products are generated from the different prediction models. Two products describing centrality (multi-model median and mean) and two products describing spread (standard deviation and range of variation) are daily computed. In order to generate them, the model outputs are bi-linearly interpolated to a common grid mesh of 0.5º x 0.5º. The multimodel DOD (at 550 nm) Median from nine dust prediction models participating in the SDS-WAS Regional Center is used for the validation of the CAMS NRT streams.

2.3 CAMS products

An extended list of output products from the NRT stream o-suite are available as 3-hourly instantaneous values up to five forecast days. These are available from ECMWF (through ftp in grib2 and netcdf format, https://atmosphere.copernicus.eu/data).

2.4 Availability and timing of CAMS products

The availability statistics provided in Table 2.6 are computed for the end of the 5-day forecast run. The CAMS production KPI is defined as the percentage of cycles in which all the general data dissemination tasks are completed before the deadlines: 10 UTC for the 00:00 and 22 UTC for the 12:00 UTC run. This was in part based on requirements from the regional models. We note that at present most regional models can still provide their forecasts even if the global forecast is available a bit later. Note that since 21 June 2016 two CAMS forecasts are produced each day.

The o-suite data delivery for the period December 2019 – February 2020 (DJF-2020) was good, with an on-time percentage of 99.4 %. There was one small delay in December.

See table 2.6 for detailed statistics from 2014 to DJF-2020.

Table 2.6: Timeliness of the o-suite from December 2014. From June 2016 onwards CAMS has produced two forecasts per day.

Months	On time, 10 & 22 utc	80th perc	90th perc	95th perc
Dec-Feb '14-'15	97%	D+0, 19:43	D+0, 20:28	D+0, 21:13
Mar-May 2015	96%	D+0, 19:38	D+0, 21:03	D+0, 21:40
Jun-Aug 2015	95%	D+0, 20:24	D+0, 20:53	D+0, 21:54
Sept-Nov 2015	95%	D+0, 19:44	D+0, 20:55	D+0, 21:51
Dec-Feb '15-'16	100%	D+0, 18:39	D+0, 18:57	D+0, 19:43
Mar-May 2016	98%	D+0, 19:32	D+0, 19:47	D+0, 20:00
Jun-Aug 2016 (00 and 12 cycle)	100%	D+0, 08:53 D+0, 20:55	D+0, 09:04 D+0, 21:01	D+0, 09:18 D+0, 21:18
Sep-Nov 2016	98.9%	D+0, 08:44 D+0, 20:44	D+0, 08:51 D+0, 20:48	D+0, 08:52 D+0, 20:51
Dec 2016 - Feb 2017	99.4%	D+0, 09:02 D+0, 21:01	D+0, 09:11 D+0, 21:02	D+0, 09:18 D+0, 21:04
Mar-May 2017	100%	D+0, 09:08 D+0, 21:07	D+0, 09:14 D+0, 21:09	D+0, 09:19 D+0, 21:11
Jun-Aug 2017	100%	D+0, 09:05 D+0, 21:05	D+0, 09:07 D+0, 21:08	D+0, 9:09 D+0, 21:10
Sep-Nov 2017	100%	D+0, 09:02 D+0, 21:00	D+0, 09:05 D+0, 21:04	D+0, 9:09 D+0, 21:07
Dec 2017 - Feb 2018	98.33%	D+0, 08:55 D+0, 20:54	D+0, 08:59 D+0, 20:59	D+0, 09:01 D+0, 21:02
Mar-May 2018	98.9%	D+0, 09:00 D+0, 21:00	D+0, 09:06 D+0, 21:03	D+0, 09:08 D+0, 21:06
Jun-Aug 2018	100%	D+0, 09:11 D+0, 21:07	D+0, 09:14 D+0, 21:09	D+0, 09:20 D+0, 21:11
Sep-Nov 2018	100%	D+0, 09:05 D+0, 21:03	D+0, 09:09 D+0, 21:07	D+0, 09:13 D+0, 21:10
Dec 2018 - Feb 2019	98.9%	D+0, 09:03 D+0, 21:04	D+0, 09:06 D+0, 21:06	D+0, 09:08 D+0, 21:10
Mar-May 2019	100%	D+0, 09:07 D+0, 21:05	D+0, 09:10 D+0, 21:09	D+0, 09:12 D+0, 21:11
Jun-Aug 2019	99.5%	D+0, 09:19 D+0, 21:14	D+0, 09:22 D+0, 21:17	D+0, 09:27 D+0, 21:19
Sep-Nov 2019	98.9%	D+0, 09:14 D+0, 21:07	D+0, 09:23 D+0, 21:20	D+0, 09:26 D+0, 21:24
Dec 2019 - Feb 2020	99.4%	D+0, 09:00 D+0, 20:58	D+0, 09:03 D+0, 21:02	D+0, 09:12 D+0, 21:08

3. Tropospheric Ozone

3.1 Validation with sonde data in the free troposphere

Model profiles of the CAMS runs were compared to free tropospheric balloon sonde measurement data of 38 stations taken from the NDACC, WOUDC, NILU and SHADOZ databases for January 2013 to February 2020 (see Fig. 3.1.1 - 3.1.2). Towards the end of the period, the number of available soundings decreases, which implies that the evaluation results may become less representative. The figures contain the number of profiles in each month that are available for the evaluation. The methodology for model comparison against the observations is described in Douros et al., 2017. The free troposphere is defined as the altitude range between 750 and 200hPa in the tropics and between 750 and 300hPa elsewhere.

Please note that recent scientific findings (https://tropo.gsfc.nasa.gov/shadoz/Archive.html, Thompson et al., 2017; Witte et al., 2017; 2018, Stauffer, et al. in preparation 2020) show a drop-off in Total Ozone at various global ozone stations in comparison with satellite instruments. This drop-off amounts between 5-10% for stratospheric ozone. Changes in the ECC ozone instrument are associated with the drop-off, but no single factor has been identified as cause yet. For tropospheric ozone (<50 hPa) no alternations are reported, but cannot be ruled out. Data availability is thus recently limited.

MNMBs for the o-suite are mostly within the range ±20%, for all months, in all zonal bands, except for the Tropics and Antarctica, where larger positive MNMBs up to ±45% appear, see Fig. 3.1.4. During the last year (February 2019 to February 2020) MNMBs are within ±20% over the Arctic, ±14% over the Northern Midlatitudes and up to 23% for Antarctica, see Fig. 3.1.1.-3.1.4.

Over the Arctic, the o-suite mostly shows slightly negative MNMBs during winter and spring season 2019 (MNMBs up to -13%) and positive biases during the rest of the period (MNMBs up to 20%) see, Fig. 3.1.1.

Over the NH mid-latitudes MNMBs for the o-suite are on average close to zero and only during the summer season maxima up to 14% appear.

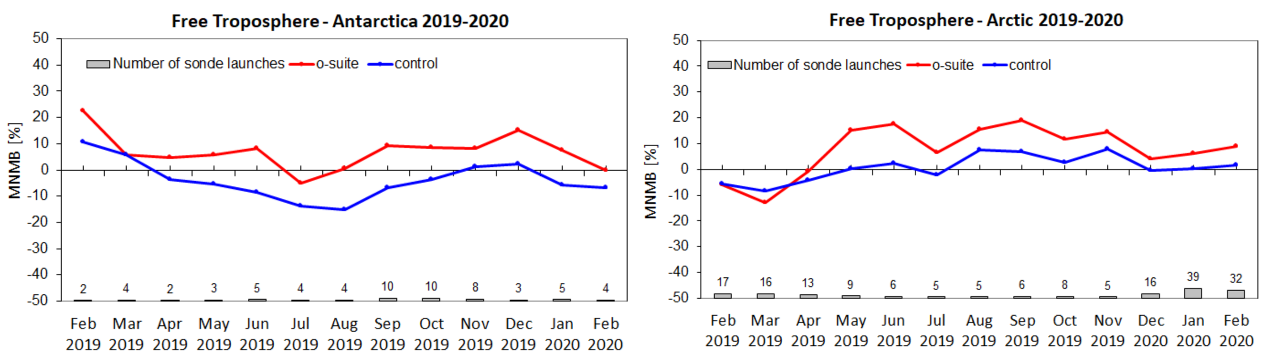

Figure 3.1.1: MNMBs (%) of ozone in the free troposphere (between 750 and 300 hPa) from the IFS model runs against aggregated sonde data over the Arctic (left) and the Northern mid latitudes (right). The numbers indicate the amount of individual number of sondes.

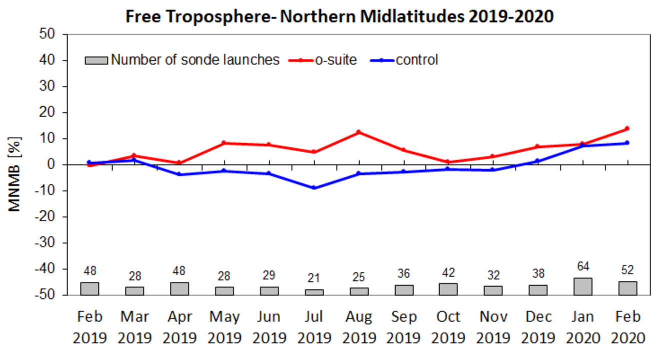

Figure 3.1.2: MNMBs (%) of ozone in the free troposphere (between 750 and 200hPa (Tropics) / 300hPa) from the IFS model runs against aggregated sonde data over the Tropics (left) and Antarctica (right). The numbers indicate the amount of individual number of sondes.

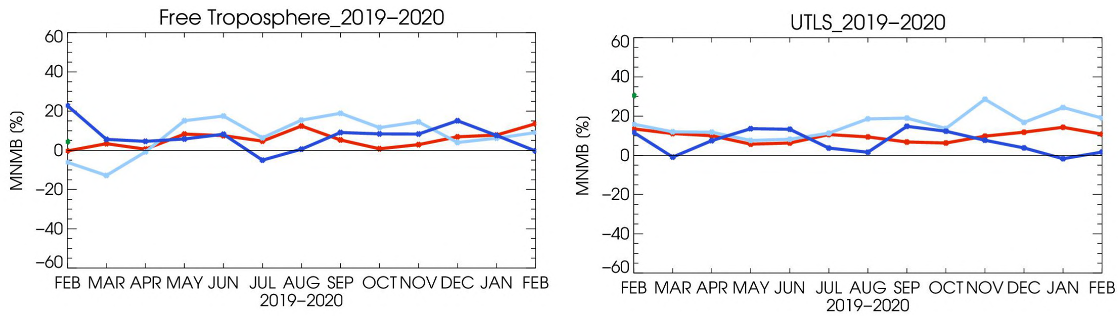

Figure 3.1.3: MNMBs (%) of ozone in the free troposphere (left, between 750 and 200hPa (Tropics) / 300hPa) and UTLS (right, between 300 and 100hPa (Tropics) / 60hPa) from the IFS model runs against aggregated sonde data over Antarctica (blue), Arctic (light blue) and Northern Midlatitudes (red).

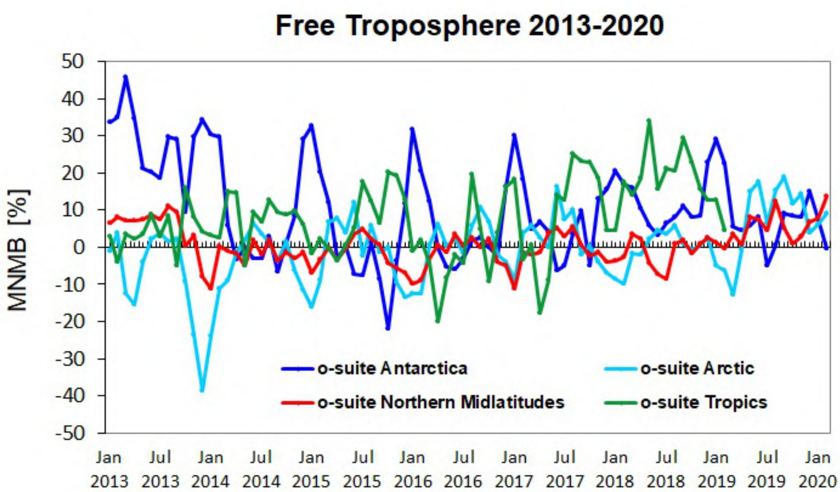

Figure 3.1.4: Time series of MNMB of ozone in the o-suite, compared against ozone sondes, averaged over different latitude bands. The free troposphere is defined here as the layer between 750 and 300 hPa.

The control run shows comparable results, with generally lower ozone mixing ratios that partly lead to lower positive MNMBs (Arctic) or larger negative MNMBs (Antarctica).

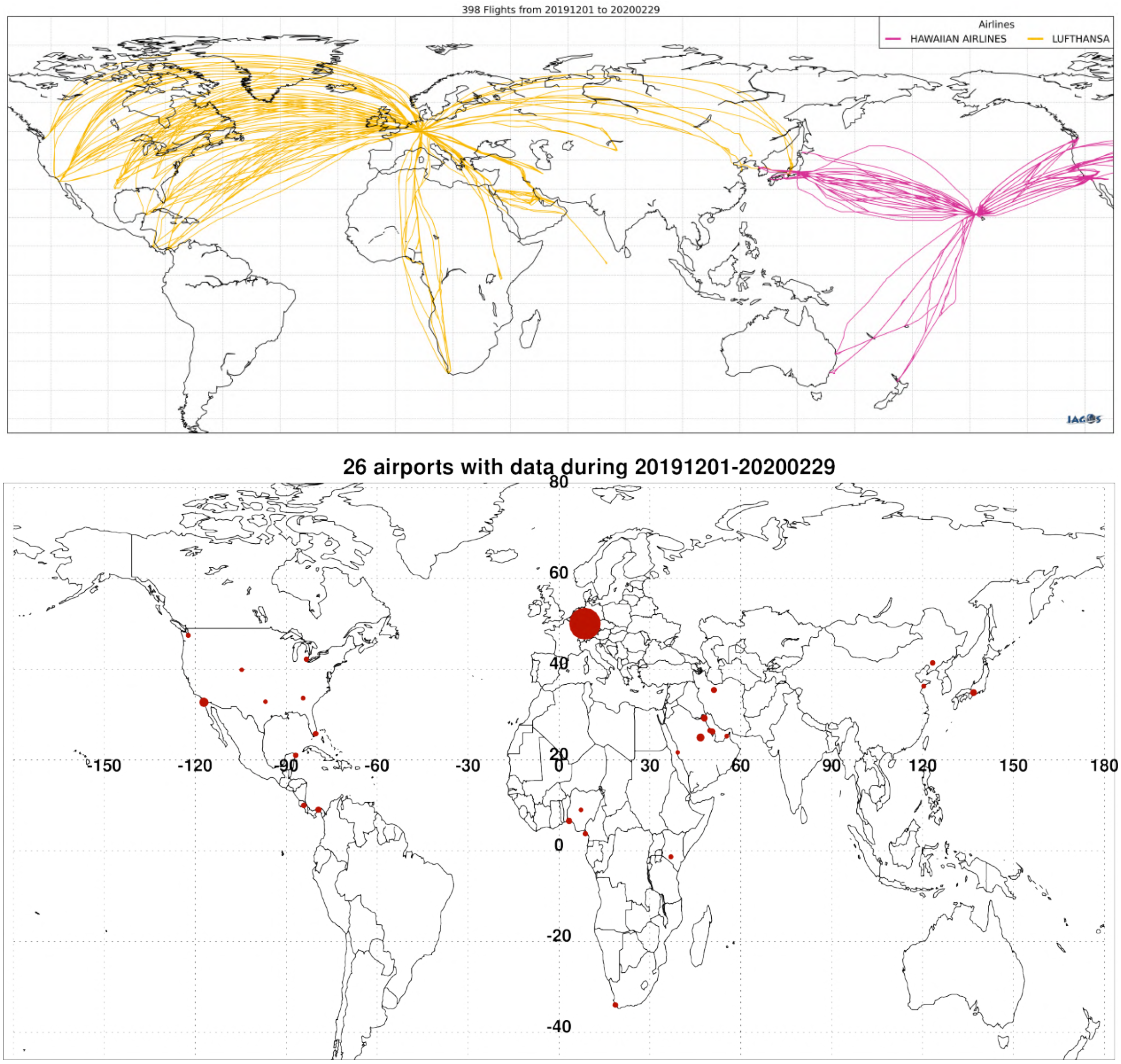

Figure 3.2.1: Map of the flights (top) and the visited airports (bottom) during the period December 2019 - February 2020, by the IAGOS-equipped aircraft. The size of the plotting circle represents the number of profiles available. In the UTLS, ozone is overestimated by the o-suite over all regions. MNMBs range within ±20% over the NH mod-latitudes and Antarctica and up to ±30% over the Arctic.

3.2 Ozone validation with IAGOS data

The daily profiles of ozone measured at airports around the world are shown on the CAMS website at http://www.iagos-data.fr/cams/nrt_profiles.php. For the period from December-February 2019/2020, the data displayed on the web pages and in this report include only the data as validated by the instrument PI. The available flights and available airports are shown in Fig. 3.2.1 top and bottom respectively. Performance indicators have been calculated for different parts of the IAGOS operations.

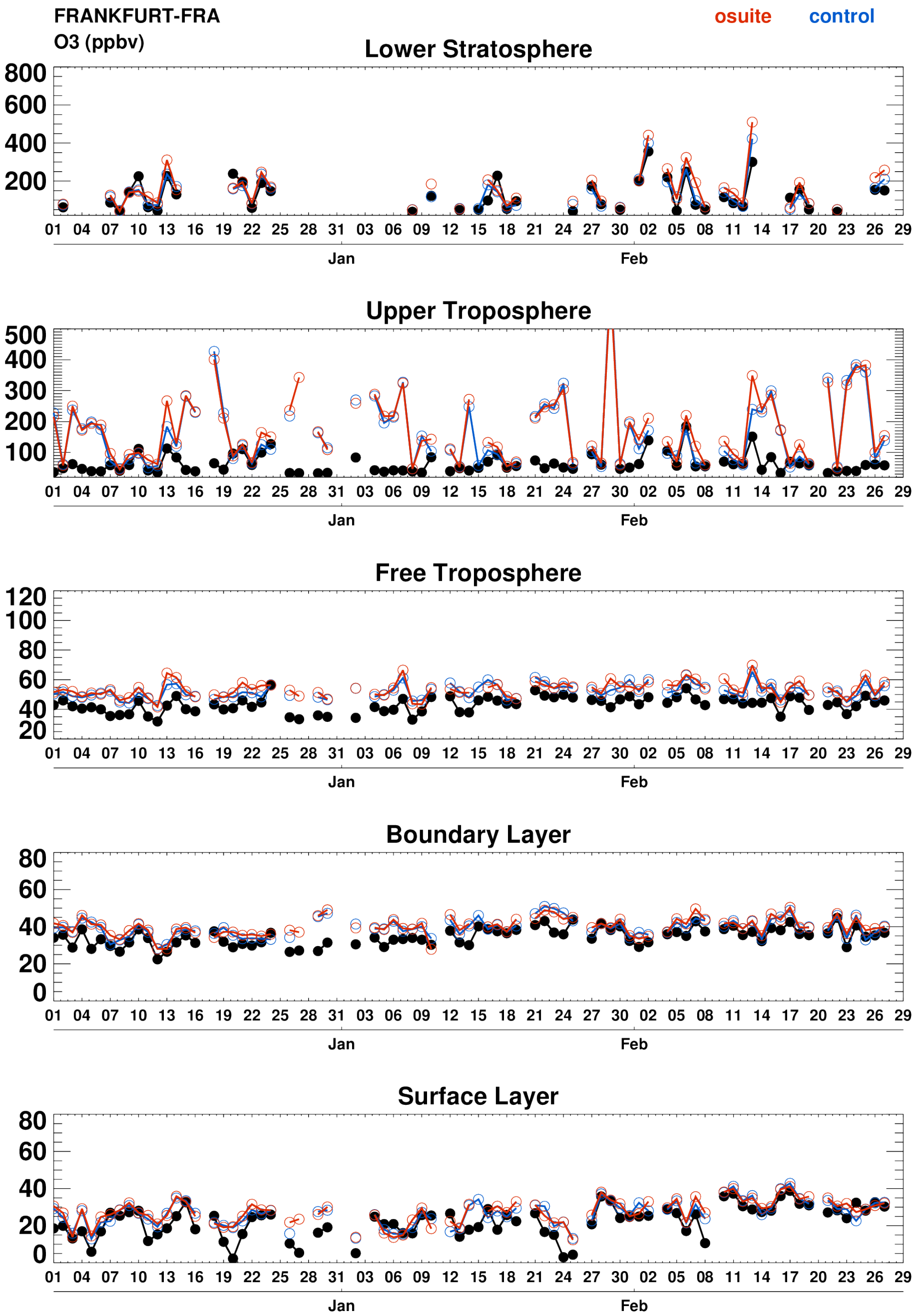

Figure 3.2.2: Time series of daily mean ozone over Frankfurt during DJF 2020 for 5 layers: Surface Layer, Boundary Layer, Free Troposphere, Upper Troposphere and Lower Stratosphere. The o-suite is shown in red and associated control run in blue. Units: ppbv.

Six aircraft were operating during this period. With these aircrafts, operating fully over the three-month period, we can expect a total of about 1260 flights. The actual number of flights within the period was 398 (796 profiles) giving a performance of 32%. These flights are shown in Fig. 3.2.1 (top). Eighty percent (80%) of the operational flights had usable measurements of ozone and 45% of the flights had usable CO. Delivering these O_3 and CO data is only one aircraft from Lufthansa operating from Frankfurt. Fig. 3.2.1 (bottom) shows the available airports, with a plotting circle scaled to the highest number of flights at an airport. Fig. 3.2.1 (bottom) shows the available airports, with a plotting circle scaled to the highest number of flights at an airport.

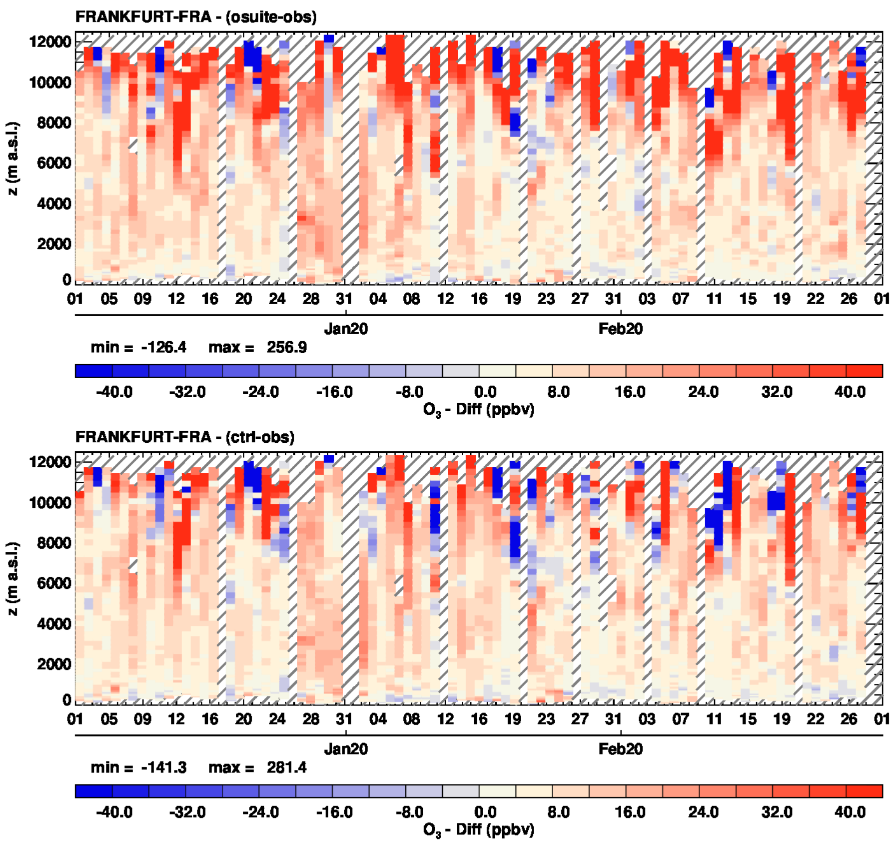

Figure 3.2.3: Time series of the absolute differences (model - observations) in daily profiles for ozone over Frankfurt during DJF 2020. The top panel corresponds to o-suite the bottom panel to control run. Units: ppbv.

Europe

Figure 3.2.2 presents ozone time series at Frankfurt during the full period December 2019 – February 2020 for 5 atmospheric layers. Time series of the profile differences (in ppbv) are also presented in Fig. 3.2.3. In the low to mid-troposphere the two runs behave similarly. Ozone is well represented by both runs in the low troposphere with mostly small overestimations, and the best agreement is obtained in the free troposphere. In the UTLS region the bias is larger and the results from the two runs differ, ozone is mostly overestimated by the o-suite whereas control run does not present a systematic behaviour with frequent underestimations.

Some examples of individual profiles at Frankfurt are also presented in Fig. 3.2.4.a-b. As shown on the time series, no major episode of ozone is observed during this period as ozone values remain below 50 ppbv in the surface and boundary layer (Fig. 3.2.2). In the profiles shown, these observed ozone values are in general well represented by the two CAMS runs and are sometimes slightly overestimated(Fig. 3.2.4).

On several of the profiles presented in Fig. 3.2.4.a-b it can be seen that the model generally reproduces the low tropopause events (i.e. days 1209, 1210, 1223, 0119, 0128, 0209, 0211). However, when model and observations differ in the tropopause this leads to large positive biases like those observed in the time-series of the bias like on 11 December and 20 February (Fig. 3.2.3).

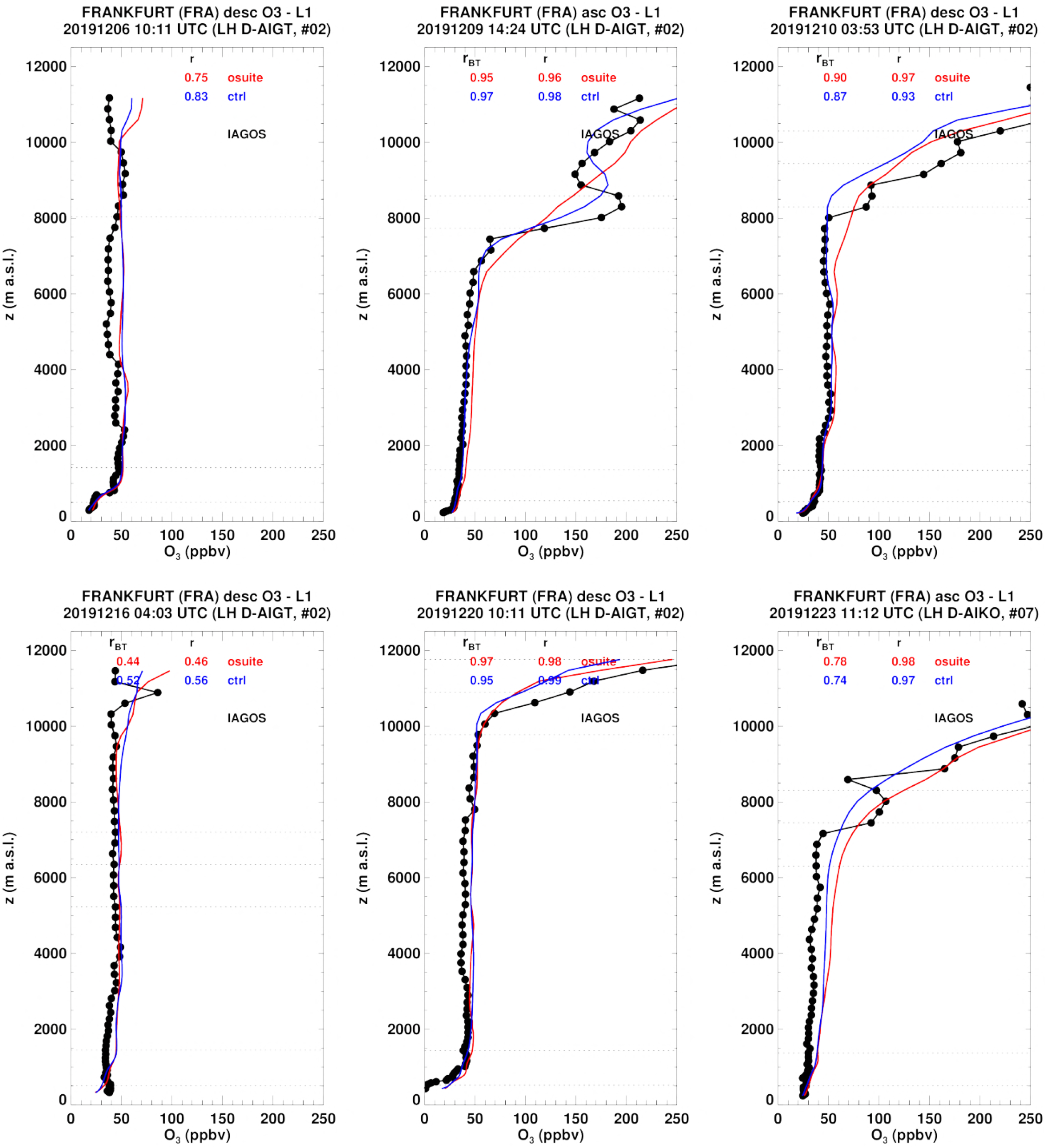

Figure 3.2.4.a: Daily profiles for ozone from IAGOS (black) and the two NRT runs (o-suite: red, control: blue) over Europe during DJF 2020.

Middle East

Profiles are available over several airports across the Middle East, at the airports of Bahrain, Dubai, Jeddah, Kuwait City and Riyadh (Fig. 3.2.5.a-b). For these profiles, values in the lowest layers are well reproduced with in general small overestimations and often a slightly smaller bias from the o-suite compared to control run. In the free troposphere, many of these profiles show a nearly

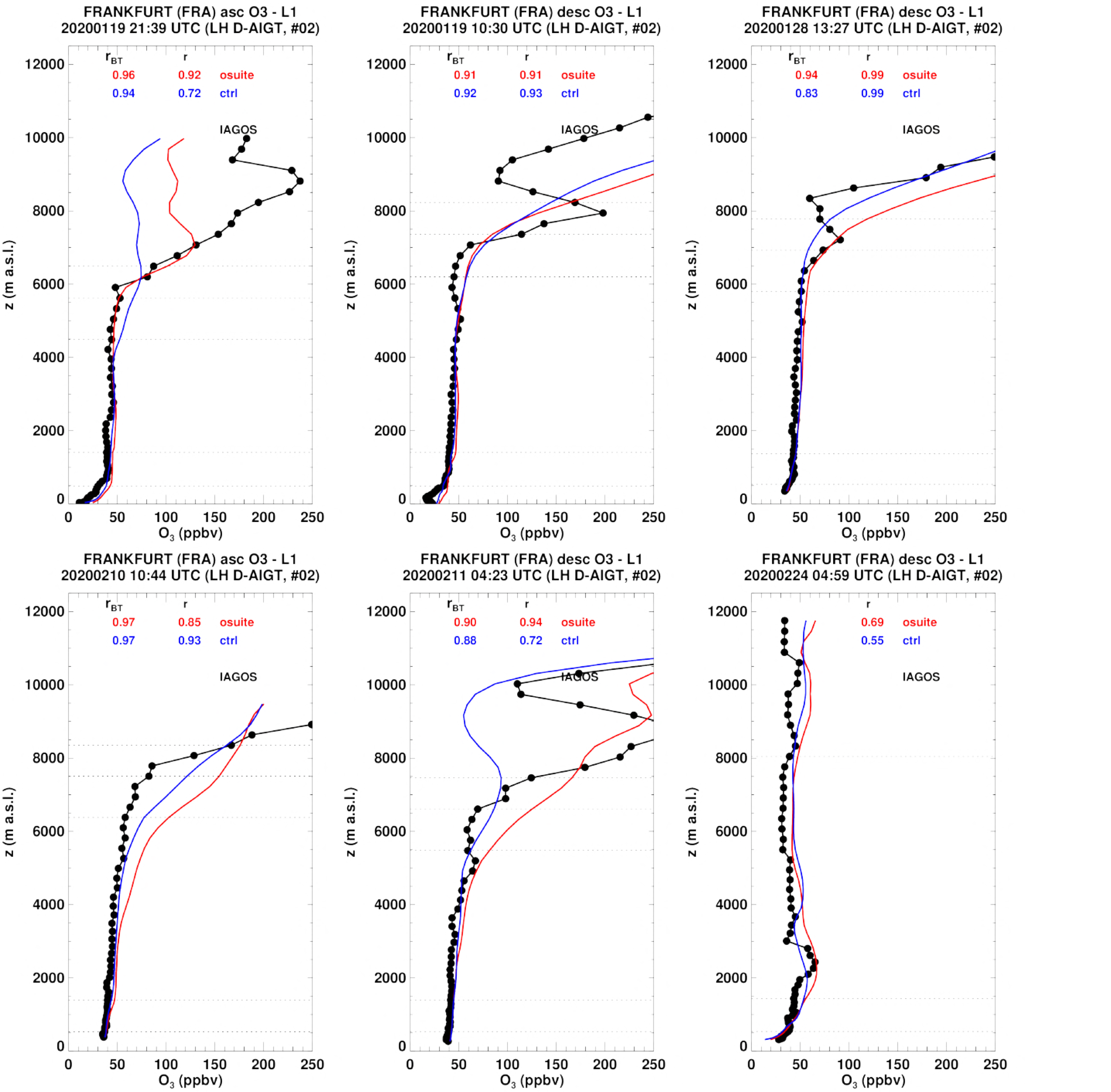

Figure 3.2.4.b: Daily profiles for ozone from IAGOS (black) and the two NRT runs (o-suite: red, control: blue) over Europe during DJF 2020.

constant concentration with ozone values of about 50 ppbv. For these profiles, the CAMS runs agree well with observations. However, some profiles present maxima in the free troposphere, like in Bahrain on 14 January at 18:33 (100 ppbv at 3000 m) and Riyadh on 6 January at 00:01 and 14 January at 16:35 (70 ppbv at 3500 and 2000 m respectively), which are not well reproduced by the models in both magnitude and shape. In these cases, large overestimations of the o-suite are found (Bahrain 0114 18:33 and Riyadh 0106 00:01). In the free troposphere and UTLS, ozone is often overestimated by the two runs, with an overall similar performance.

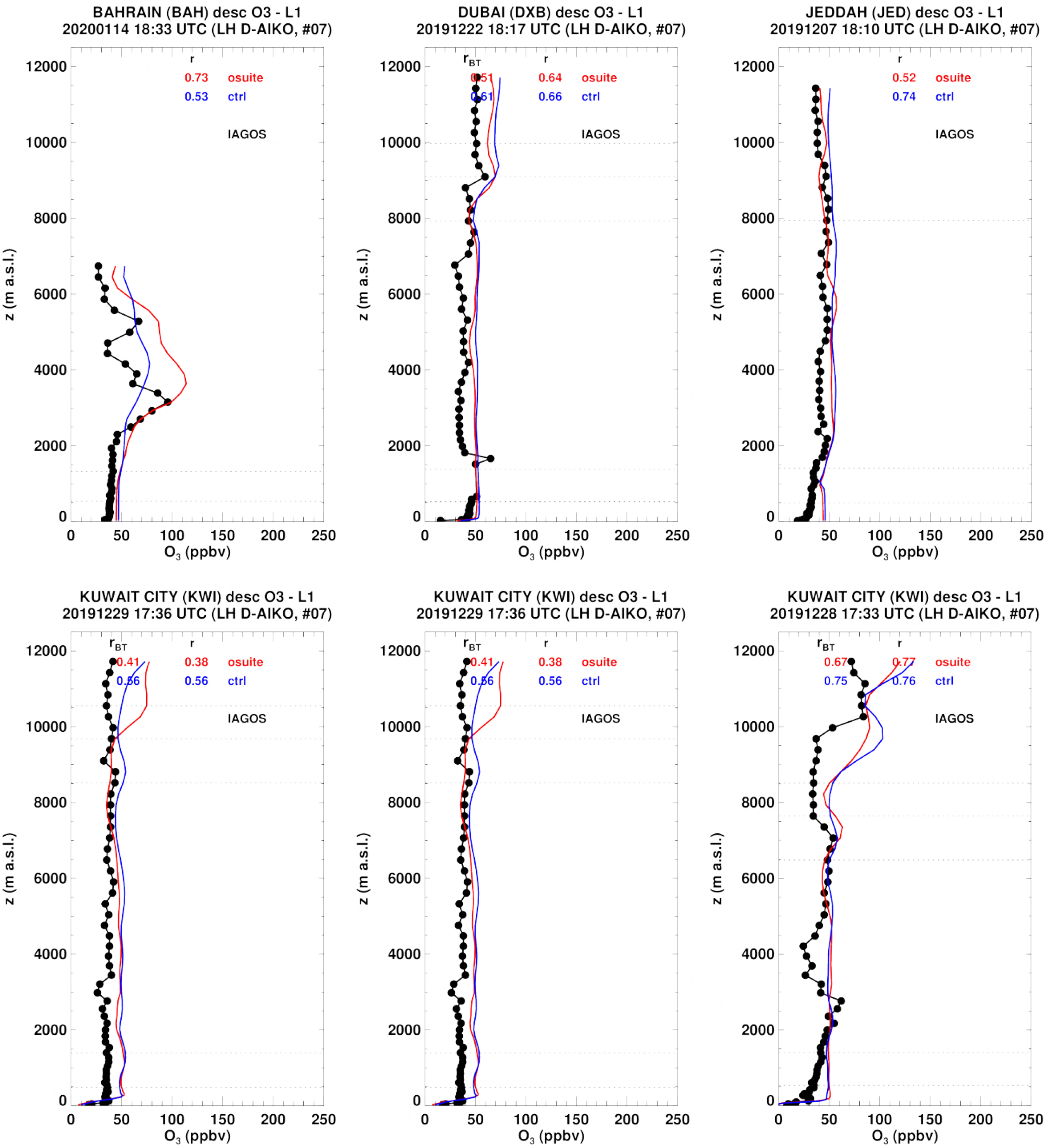

Figure 3.2.5.a: Daily profile for ozone from IAGOS (black) and the two NRT runs (o-suite: red, control: blue) over the Middle East during DJF 2020.

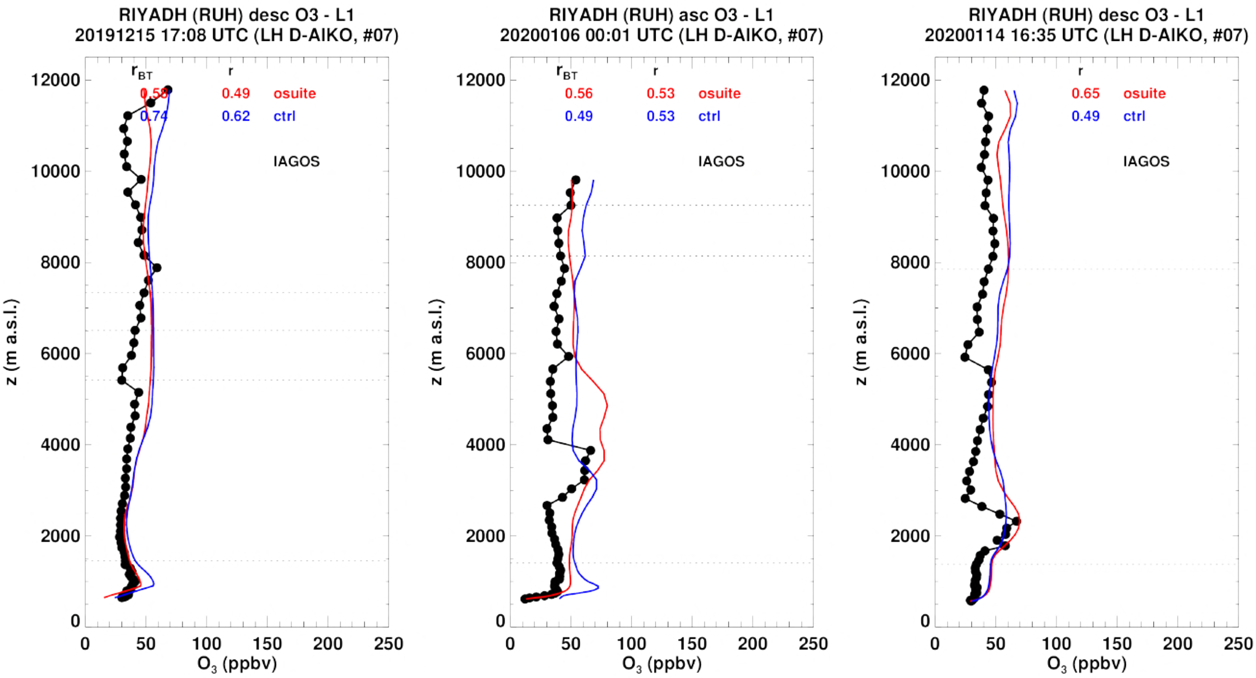

Figure 3.2.5.b: Daily profile for ozone from IAGOS (black) and the two NRT runs (o-suite: red, control: blue) over the Middle East during DJF 2020.

West and East Africa

IAGOS profiles are available at airports in the Gulf of Guinea at Lagos and Malabo, at the Nigerian airport of Abuja, as well as at the Kenyan airport of Nairobi (Fig. 3.2.6.a-b). In most of these profiles, surface and boundary layer values are below 50 ppbv and both runs agree well with observations from the surface to the free troposphere, except at Lagos where large positive biases are found in the surface and boundary layer. The agreement is best in the free troposphere for both runs, however, for some of these profiles, which present sharp maxima of about 80 ppbv in the lower part of the free troposphere (Abuja 1202 16:41, Malabo 1208 1942, Lagos 1204 16:51, 0113 20:55), these features are not well reproduced by the models, which show a much smoother profile shape. In the upper layer, the bias is often large at most airports with some differences between the two runs, except in Abuja where CAMS show similar results and smaller bias in the available profiles.

South Africa

Several ozone profiles are available at the airport of Cape Town (Fig. 3.2.7). The results from the two models are similar in all layers. The models agree well with observations from the surface to the free troposphere, while in the UTLS large positive biases are found for both models.

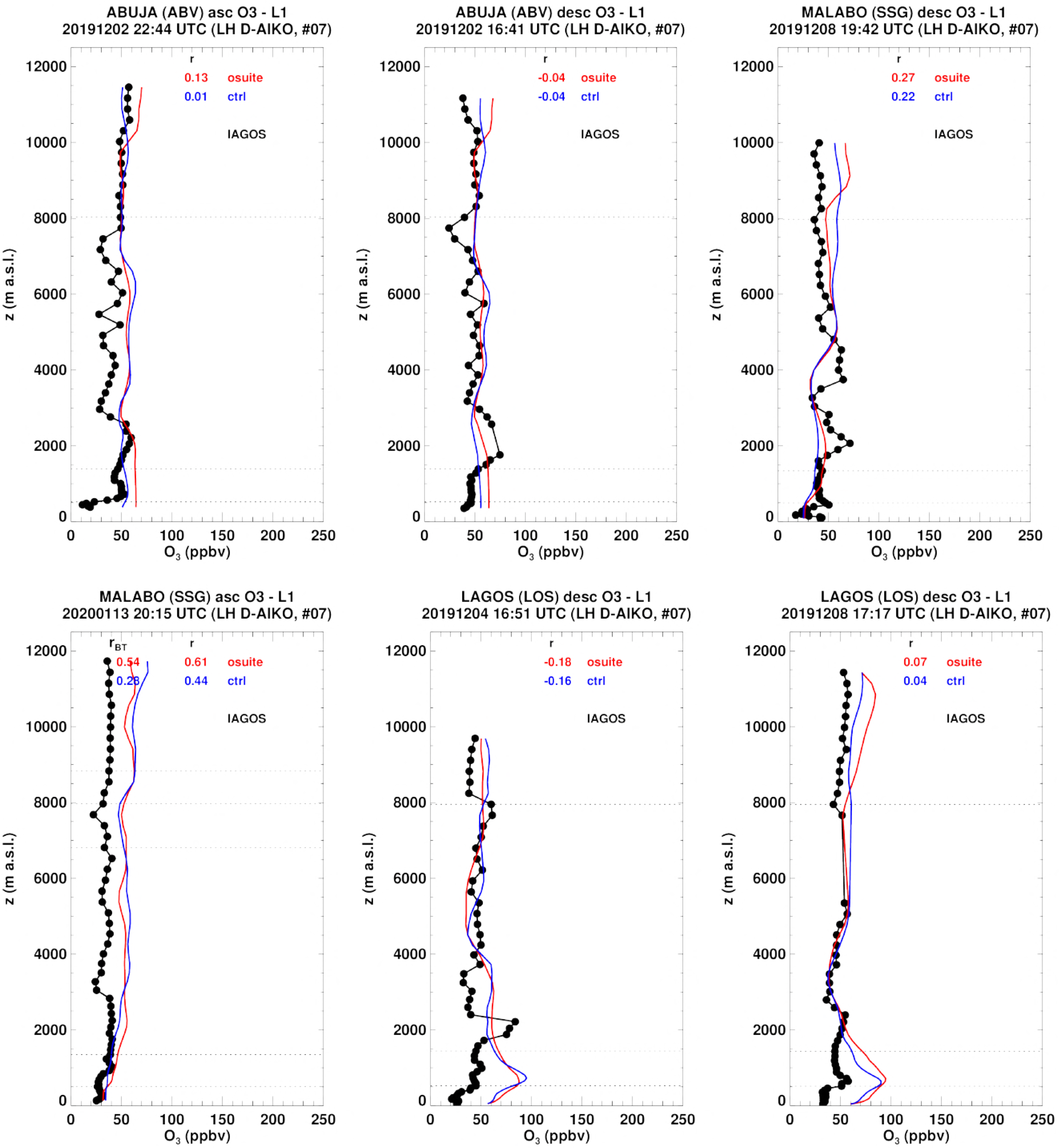

Figure 3.2.6.a: Daily profiles for ozone from IAGOS (black) and the two NRT runs (o-suite: red, control: blue) over West Africa during DJF 2020.

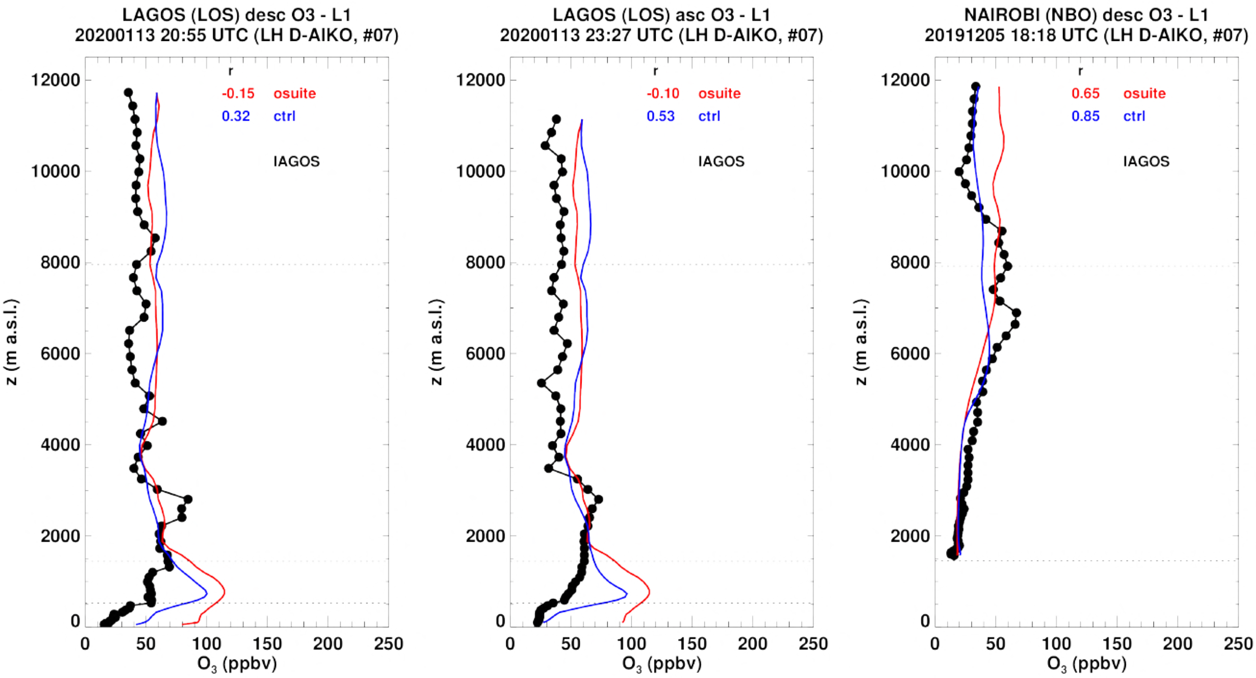

Figure 3.2.6.b: Daily profiles for ozone from IAGOS (black) and the two NRT runs (o-suite: red, control: blue) over West and East Africa during DJF 2020.

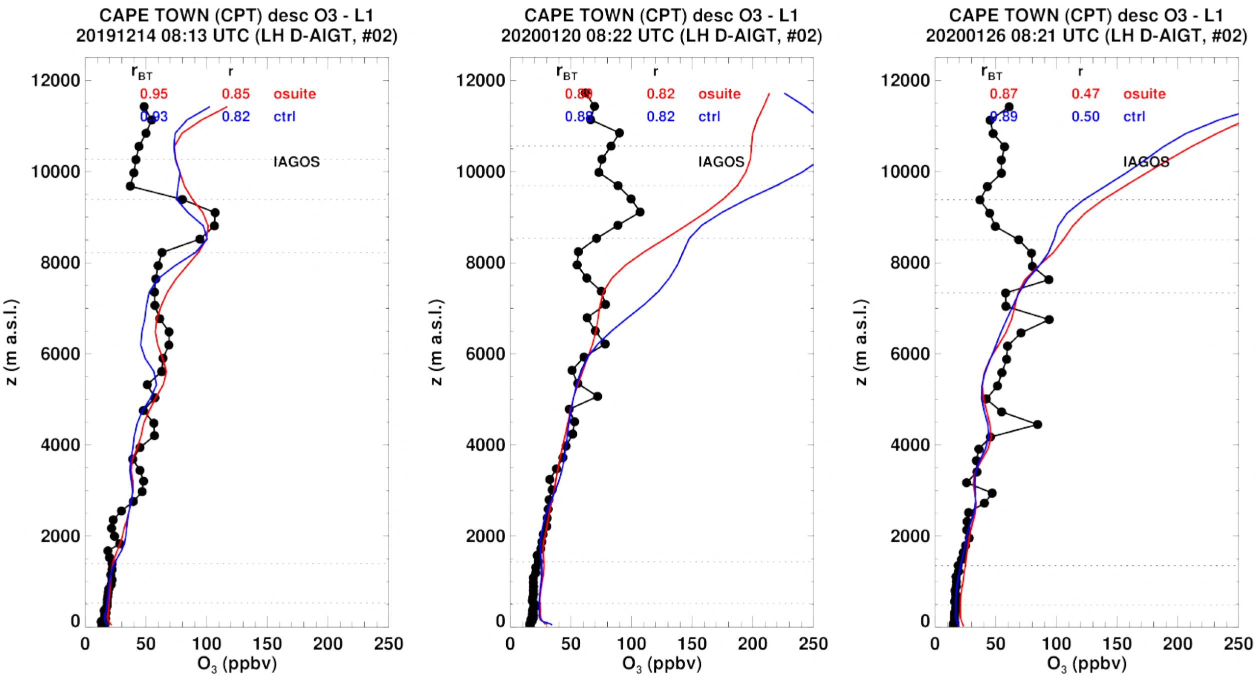

Figure 3.2.7: Daily profiles for ozone from IAGOS (black) and the two NRT runs (o-suite: red, control: blue) over South Africa during DJF 2020.

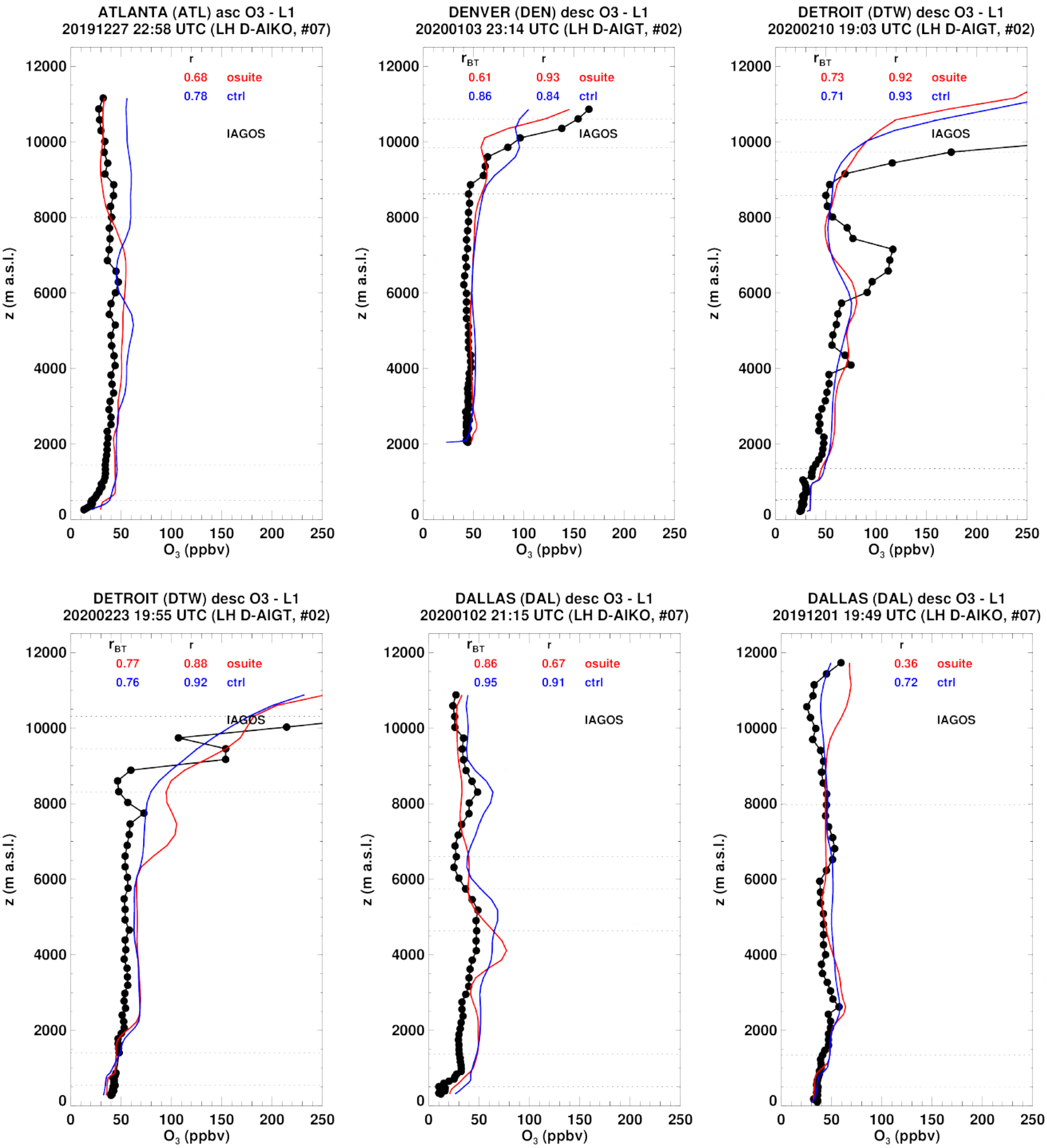

Figure 3.2.8.a: Daily profiles for ozone from IAGOS (black) and the two NRT runs (o-suite: red, control: blue) over North America during DJF 2020.

North America

In North America, IAGOS observations during DJF 2020 are available at: Detroit, Denver, Miami, Dallas, San Diego and Seattle. For all profiles, ozone values are generally close to or below 50 ppbv in the low troposphere and often with a nearly constant shape up to the mid-troposphere (Fig. 3.2.8.a-b). In these layers, the results from both runs are very similar with a rather good agreement,

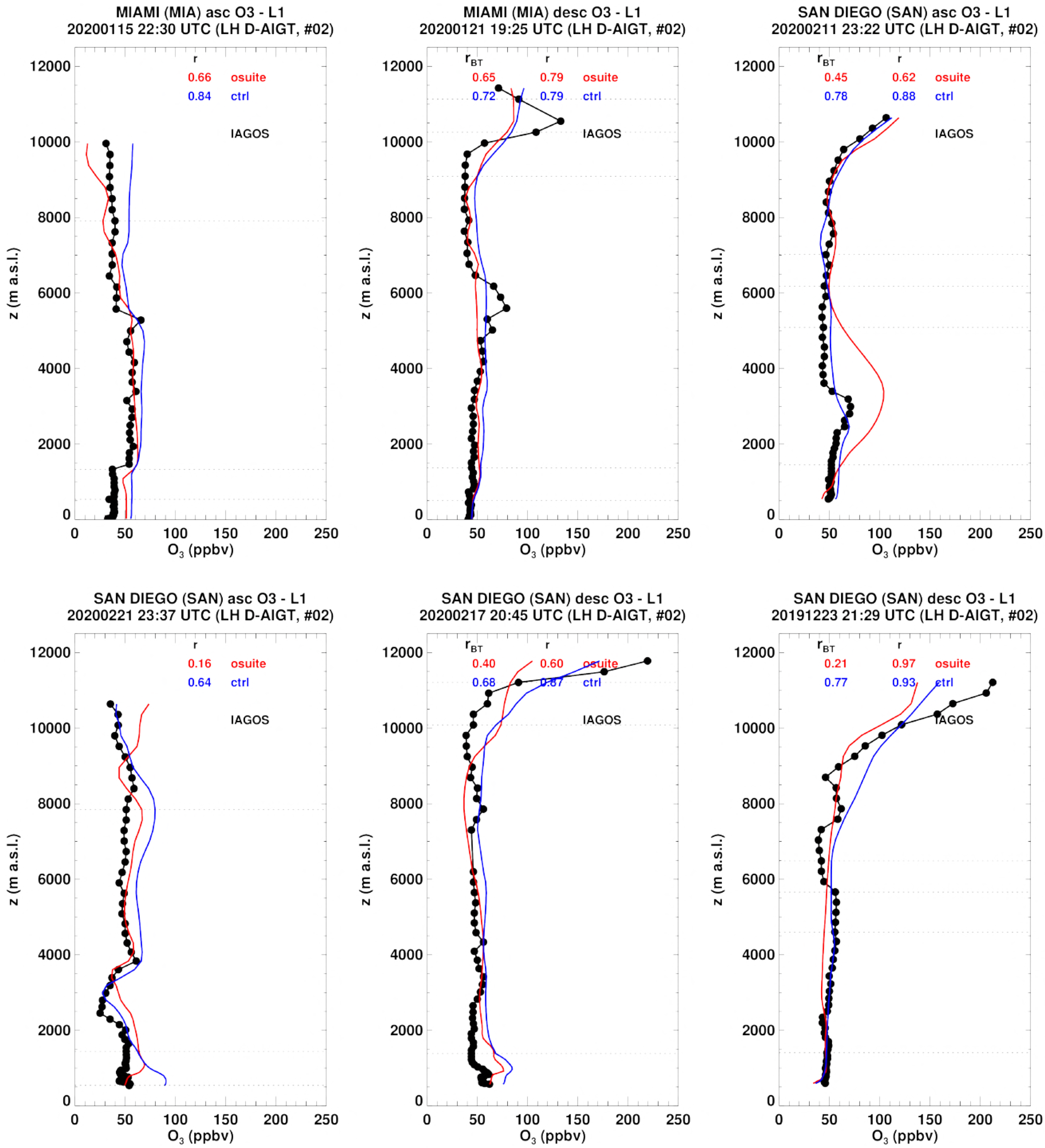

Figure 3.2.8.b: Daily profiles for ozone from IAGOS (black) and the two NRT runs (o-suite: red, control: blue) over North America during DJF 2020.

except in San Diego, where larger overestimations are found in the surface and boundary layer. When maxima of ozone are observed in the free troposphere, the results of the two runs sometimes differ (i.e. Detroit 0210 19:03, Dallas 0102 21:15, Miami 0121 19:25, San Diego 0211 23:22, 0221 23:37). These maxima are detected by the models but are not always well reproduced in terms of magnitude and altitude, with large biases in some cases (i.e. San Diego 0211 23:22). When the observed tropopause is low (i.e. Denver 0103 23:14, Detroit 0210 19:03, 0223 19:55, San-

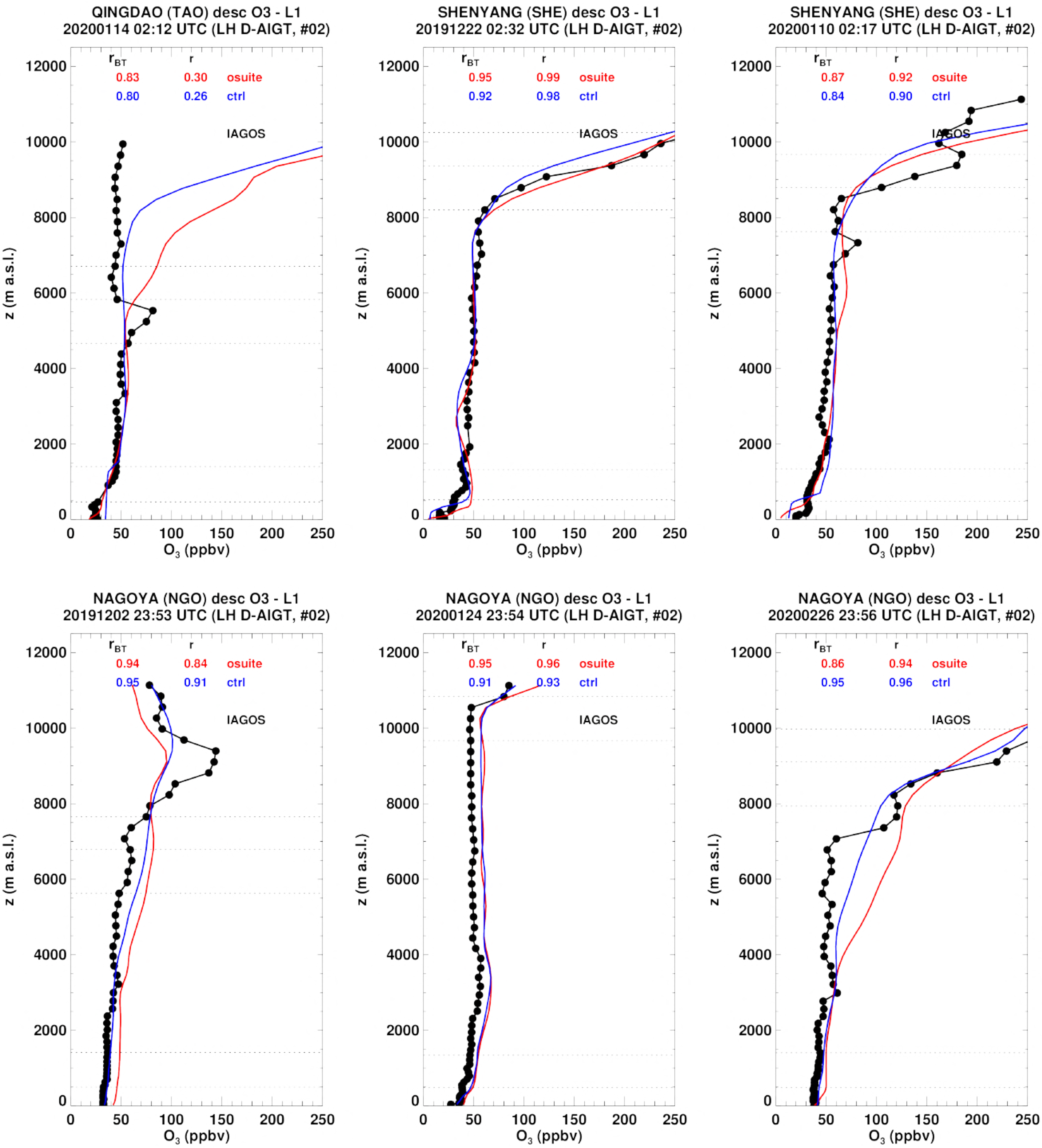

Figure 3.2.9: Daily profiles for ozone from IAGOS (black) and the two NRT runs (o-suite: red, control: blue) over East Asia during DJF 2020.

Diego 1223 21:29) the two runs usually reproduce well the ozone values and the related ozone increases with a similar performance for the two runs. In the UTLS, the bias is large for both runs and the behaviour sometimes differs.

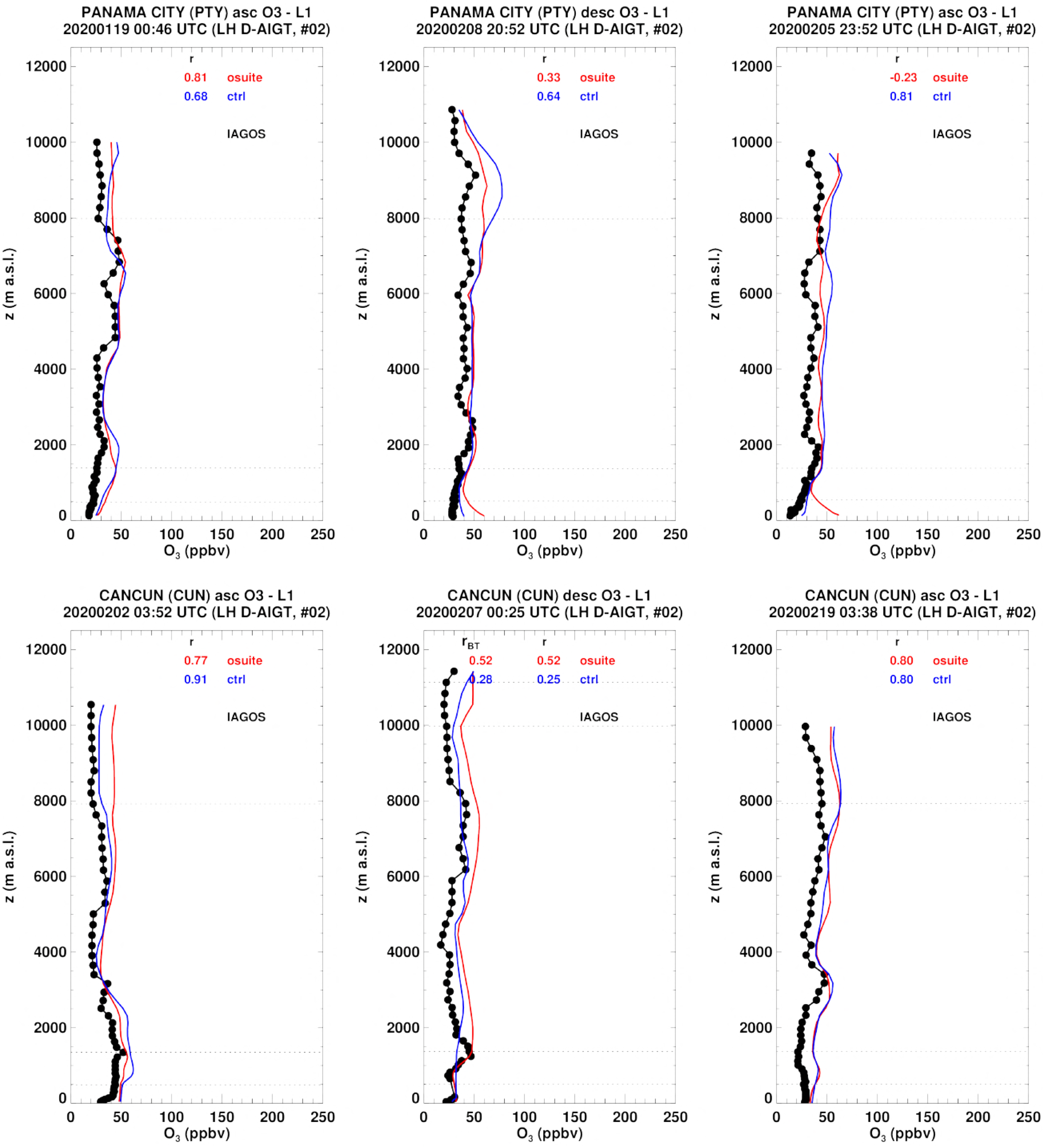

Figure 3.2.10: Daily profile for ozone from IAGOS (black) and the two NRT runs (o-suite: red, control: blue) over Central America during DJF 2020.

East Asia

Over East Asia, ozone profiles are available at Qingdao (China), Shenyang (China) and Nagoya (Japan). Most profiles show a nearly constant concentration from the surface to the free troposphere with ozone values around 50 ppbv, well represented by the two CAMS runs (Fig. 3.2.9). The cases with a low tropopause are in general well represented as shown in the examples of Shenyang and Nagoya.

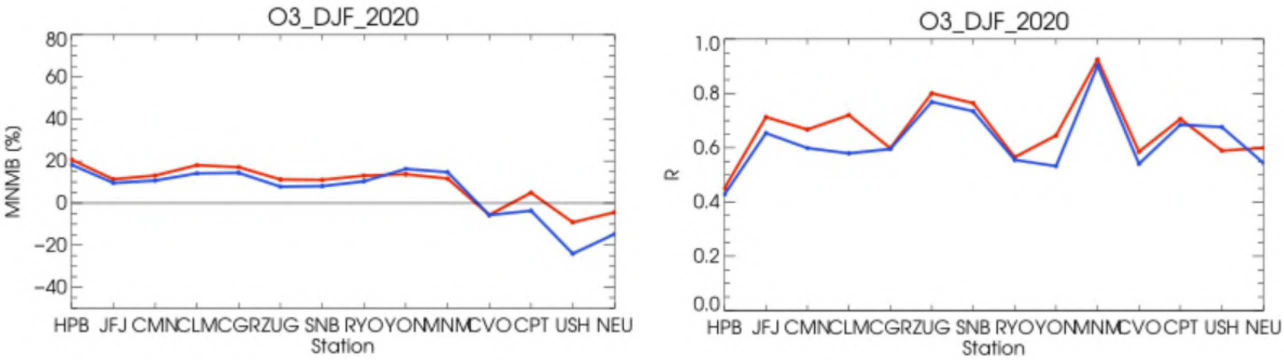

Figure 3.3.1: Modified normalized mean bias in % (left) and correlation coefficient (right) of the NRT forecast runs compared to observational GAW data in the period December-February 2019/2020 (o-suite: red, control: blue).

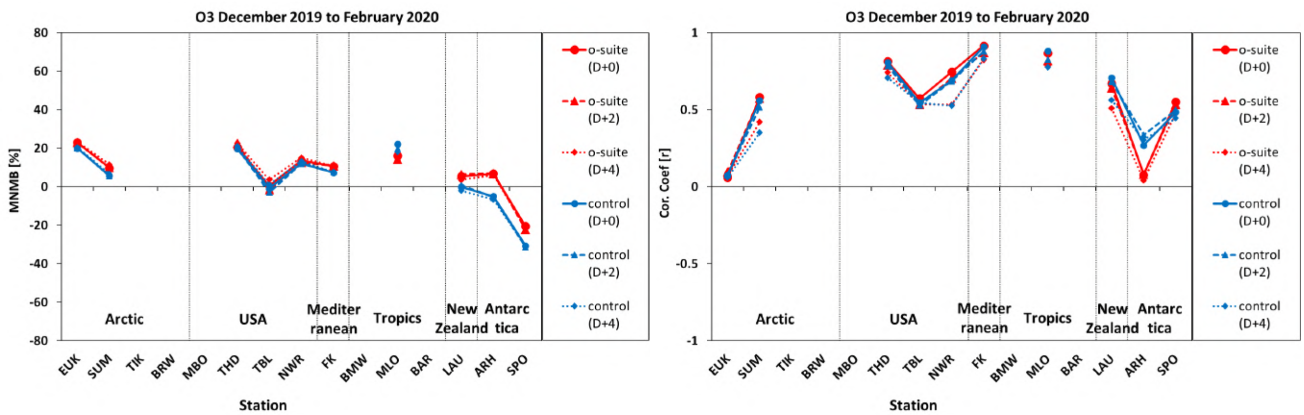

Figure 3.3.2: Modified normalized mean bias in % (left) and correlation coefficient (right) of the NRT forecast runs compared to observational ESRL data in the period December-February 2019/2020. Circles correspond to D+0, triangles to D+2 and rhombs to D+4 metrics respectively.

Central America

Over Central America, a few ozone profiles are available at airports of Panama City (Panama) and Cancun (Mexico) as shown in Fig. 3.2.10. In the lowest to mid-troposphere the results from both runs are very similar at Cancun with small overestimations. At Panama, the same results are found except near the surface where the bias from the o-suite is larger than that of the control run. In the upper part of the free troposphere and UTLS the bias is often larger than in the lowest layers for both runs, with in general a slightly better performance from control run at Cancun.

3.3 Validation with GAW and ESRL-GMD surface observations

For the Near Real Time (NRT) validation, 13 GAW stations and 14 ESRL stations are currently delivering O_3 surface concentrations in NRT, and the data are compared to model results. In the following, a seasonal evaluation of model performance for the 2 NRT runs (o-suite and control) has been carried out for the period from December to February 2019/2020. The latest validation results based on GAW stations and based on ESRL observations can be found on the CAMS website, see section 1, Table 1.2.

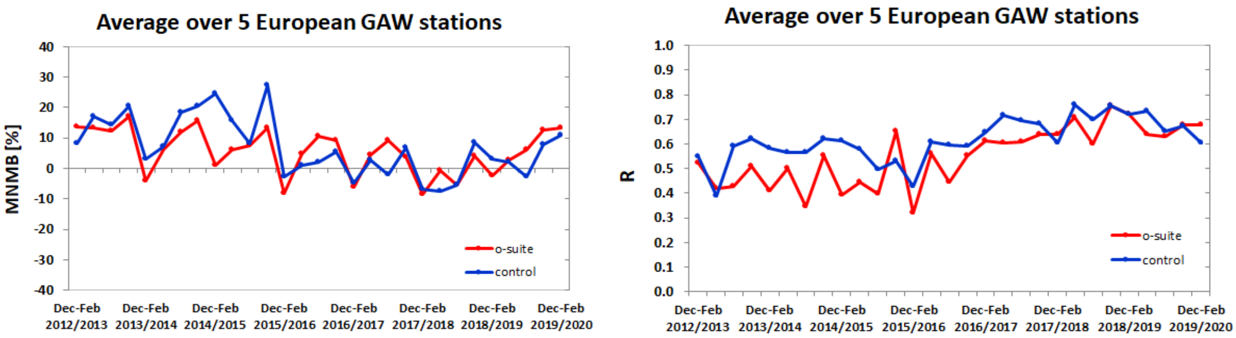

Figure 3.3.3: Long term (Dec. 2012 – February 2020) evolution of seasonal mean MNMB (left) and correlation (right), as averaged over 5 GAW stations in Europe, for o-suite (red) and control (blue).

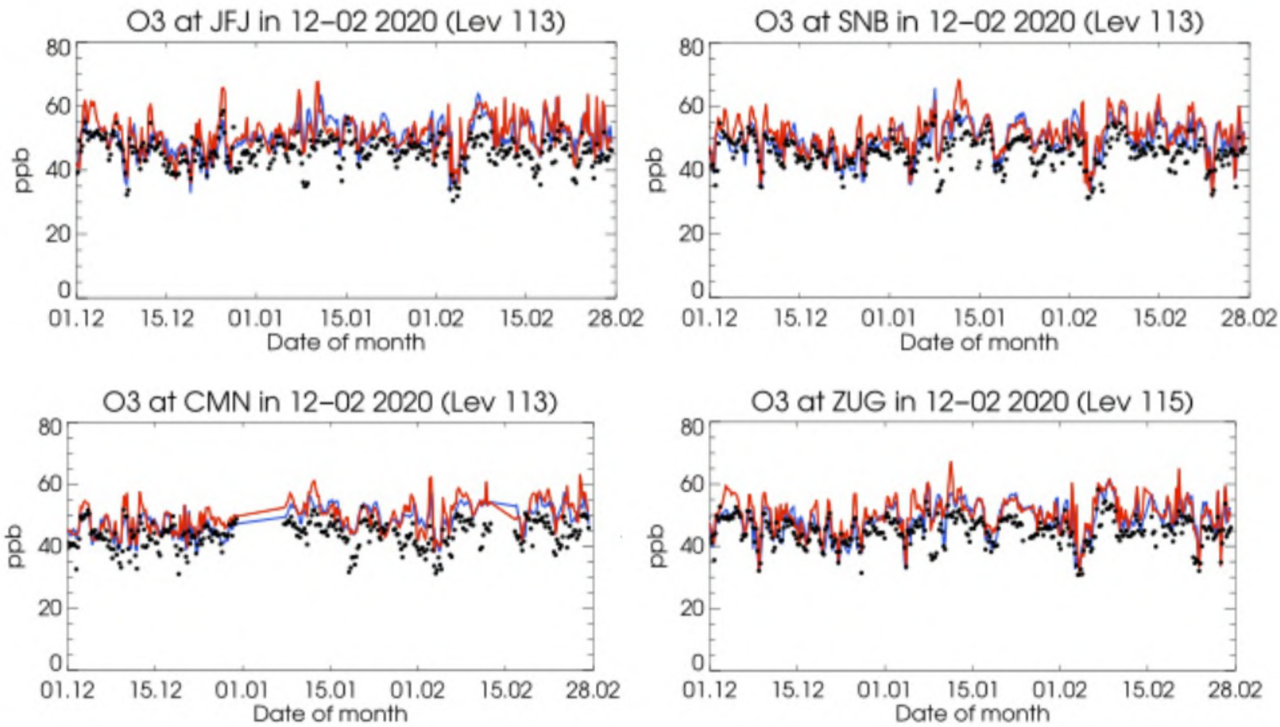

Figure 3.3.4: Time series for the o-suite (red) and control (blue) compared to GAW observations for Jungfraujoch (46.55°N, 7.99°E) and Sonnblick (47.05°N, 12.96°E) (upper panel), Cimone (44.18°N, 10.70°E) and Zugspitze (47.4°N, 10.9°E) (lower panel).

Modified normalized mean biases in % (left panel) and correlation coefficients (right panel) for different forecasts days (D+2, red-dashed and D+4, red- pointed) with respect to GAW and ESRL observations are shown in Figs. 3.3.1 and 3.3.2. It indicates that MNMBs for both o-suite and control run mostly remain stable up to D+4 (forecast run from 96h to 120h). Correlations between simulated and observed surface ozone values remain almost stable up to D+2 (forecast run from 48h to 72h), but then drop (correlations for D+4 are lower than correlations for D+2 and D+0), see Fig. 3.3.1 and 3.3.2, right graph).

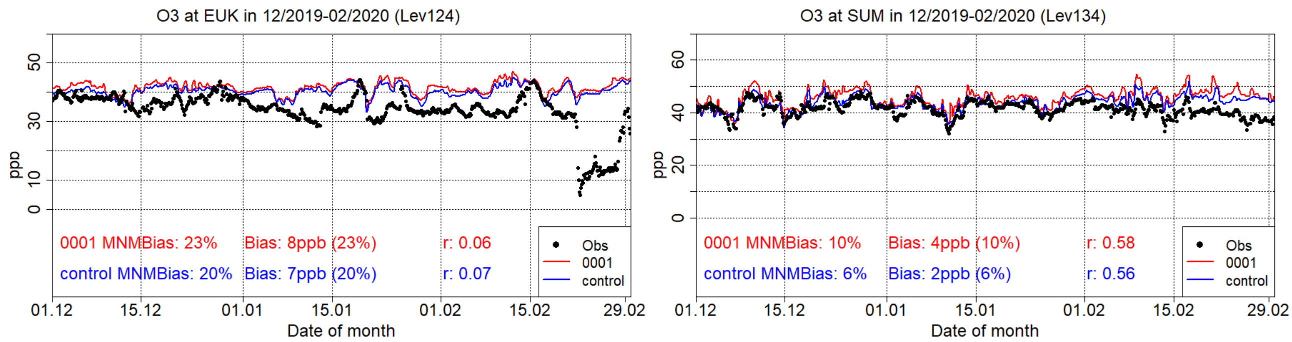

Figure 3.3.5: Time series for the o-suite (red) and control (blue) compared to ESRL observations at Eureka Canada station (80.05°N, 86.42°W, left) and at Summit, Greenland station (72.57°N, 38.48°W, right)

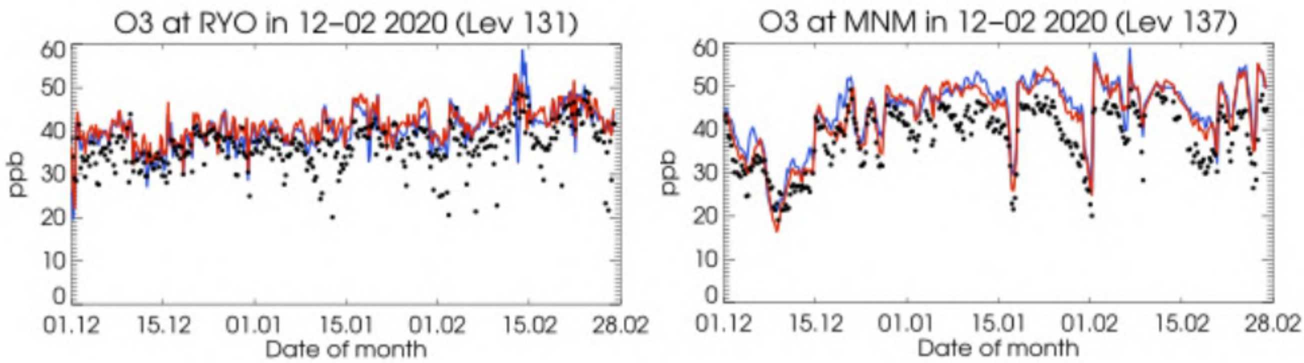

Figure 3.3.6: Time series for the o-suite (red) and control (blue) compared to GAW observations for Ryori (39.03°N, 141.82°E, left panel) and Minamitorishima (24.29°N, 153.98°E, right panel).

A comparison of the seasonal-mean MNMB over Europe (Fig. 3.3.3) from December 2012 to present shows minimal MNMBs during the winter season and larger biases in other months. Also, on average the MNMB for the o-suite and control shows an improvement over the years. The temporal correlation is consistently better for the control run than for the o-suite, but the o-suite shows strong improvements recently. The GAW results are summarized in Figs 3.3.1 and 3.3.3.

Looking at different regions, for European stations (HPB, JFJ, ZUG, SNB, CMN, CLM, CGR), observed O_3 surface mixing ratios are overestimated with MNMBs within 20% for the o-suite and within 18% for the control run (Fig. 3.3.4). Correlations for European stations are between 0.45 and 0.8 for the o-suite and between 0.42 and 0.76 for the control run, see Fig. 3.3.1.

Over Arctic stations (EUK and SUM), the o-suite overestimates surface ozone values by 23% at Eureka and by 10% at Summit. On the other hand, the control run's O_3 surface mixing ratios are closer to the observations (MNMBs 20% at EUK and 6% at SUM). Correlations between modelled and observed ozone values for both runs are 0.6 for SUM station while for EUK are almost zero mainly because both runs cannot reproduce the ozone depletion event during the last 10 part of February, see Fig. 3.3.2.

For THD, TBL and NWR USA stations, the observed ozone mixing ratios are overestimated by both the o-suite and the control run by 20% and 14% while in the TBL station both models MNMBs is almost zero. Correlations between o-suite and observations are between 0.57 (at NWR) and 0.81 (at THD) for the o-suite and between 0.54 (at NWR) and 0.81 (at THD) for the control run.

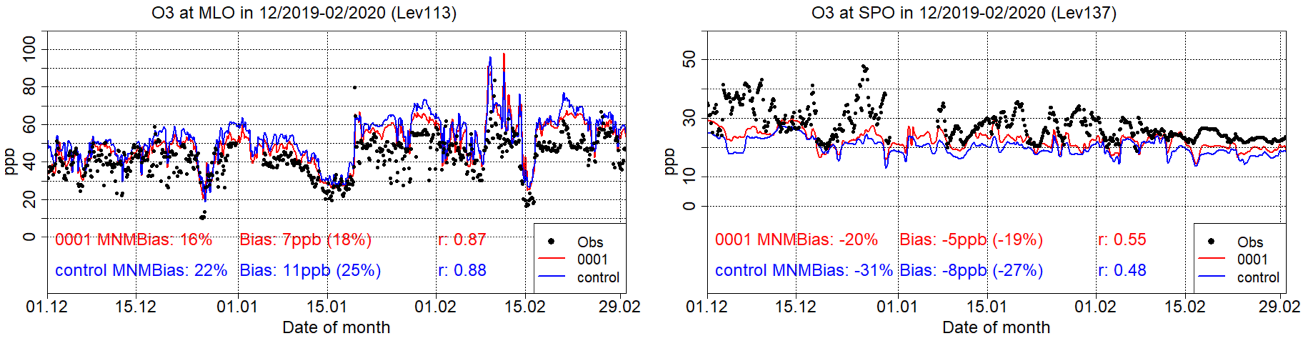

Figure 3.3.7: Time series for the o-suite (red) and control (blue) compared to ESRL observations (black dots) at Mauna Loa, Hawaii station (19.54°N, 155.58°W) and at South Pole, Antarctica station (90.00°S, 24.80°W).

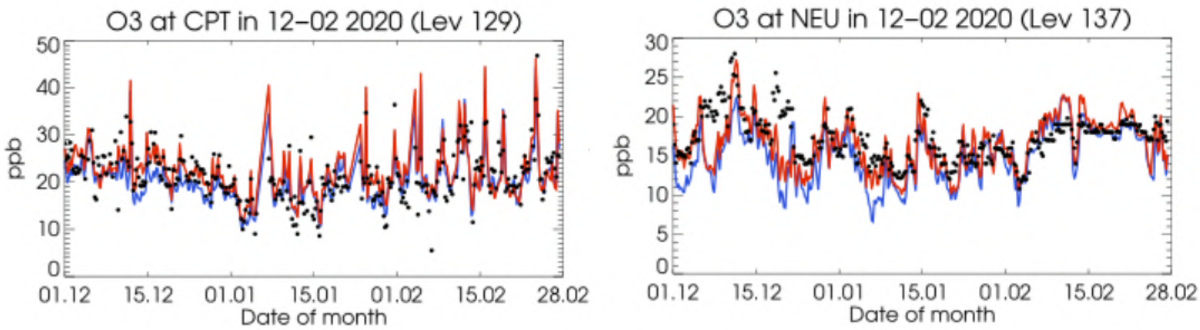

Figure 3.3.8: Time series for the o-suite (red) and control (blue) compared to GAW observations (black dots) at Cape Point (34.55°S, 18.48°W) and GAW observations at Neumayer (70.65°S, 8.25°W).

Ozone mixing ratios for Asian stations (RYO, MNM, YON) are slightly overestimated by around 13% by both runs. Correlation coefficients range between 0.56 and 0.92, with higher correlation for the o-suite.

At CVO station, the model corresponds very well to the observations with MNMB of -5% for both runs and correlation of 0.58 (control: 0.54).

The O_3 mixing ratios of the southern hemispheric stations (CPT, USH) show MNMBs between 4 and -9% for the o-suite. The control run shows larger underestimations for USH up to -24%, see Fig 3.3.8. At Lauder (LDR) station in New Zealand the o-suite overestimates O_3 mixing ratios by 5% while the control run has 0 bias. Correlations between simulated and observed surface ozone values for the o-suite and the control run are 0.67 and 0.70, respectively.

At Arrival Height (ARH) station in Antarctica, the MNMB is 6% for the o-suite and -5% for the control run. Correlation coefficients are very poor for both runs (r≈0). Finally, for South Pole station in Antarctica (SPO), the MNMB is -20% for the o-suite and -33% for the control run. Correlation coefficients 0.55 for the o-suite and 0.48 for the control run.

For Neumayer station (NEU) the MNMB is -4% for the o-suite and -14% for the control run. Correlation coefficients are 0.59 for the o-suite and 0.54 for the control run, Fig. 3.3.8.

Table 3.4.1: Coordinates, elevation, corresponding model level (level 137 is the surface level), as well as validation scores (MNMBs and correlations for the period DJF 2019-2020) obtained with the 2 forecast runs (o-suite and control), for each one of the selected Mediterranean stations. MNMBs and correlations with blue denote stations where control run performs better while with red are denoted stations where o-suite performs better.

						Distance from the	MNMB		Cor. Coef	
Station Name	Stat_ID	Lon	Lat	Alt (m)	Level	shore (km)	o-suite	control	o-suite	control
Al Cornocales	ES1648A	-5.66	36.23	189	133	16	31.6	29.9	0.48	0.47
Caravaka	ES1882A	-1.87	38.12	1	137	73	42.5	42.0	0.56	0.57
Zarra	ES0012R	-1.10	39.08	885	130	70	21.0	20.0	0.53	0.47
VIillar Del Arzobispo	ES1671A	-0.83	39.71	430	137	48	-6.3	-6.9	0.86	0.85
Cirat	ES1689A	-0.47	40.05	466	137	37	41.1	40.5	0.83	0.85
Bujaraloz	ES1400A	-0.15	41.51	327	137	60	21.9	19.9	0.79	0.79
Morella	ES1441A	-0.09	40.64	1150	128	51				
Bc-La Senia	ES1754A	0.29	40.64	428	137	21	-35.9	-36.4	0.67	0.67
Ay-Gandesa	ES1379A	0.44	41.06	368	136	15	35.5	34.9	0.59	0.55
Ak-Pardines	ES1310A	2.21	42.31	1226	135	81	34.6	32.1	0.39	0.30
Hospital Joan March	ES1827A	2.69	39.68	172	133	3	14.1	12.0	0.74	0.67
Al-Agullana	ES1201A	2.84	42.39	214	137	25	-2.7	-3.7	0.61	0.58
Av-Begur	ES1311A	3.21	41.96	200	132	9	29.3	27.2	0.70	0.63
Plan Aups/Ste Baume	FR03027	5.73	43.34	675	124	21	24.0	21.4	0.50	0.52
Montemonaco	IT1842A	13.34	42.90	1000	127	46	20.8	18.1	0.87	0.84
Gharb	MT00007	14.20	36.07	114	132	31	4.7	1.6	0.74	0.73
Aliartos	GR0001R	23.11	38.37	110	59	18				
NEO	-	21.67	37.00	50	60	2				
Finokalia	GR0002R	25.67	35.32	250	57	4	10.7	7.4	0.91	0.91
Agia Marina	CY0002R	33.06	35.04	532	55	14	8.9	6.6	0.77	0.76

3.4 Validation with AirBase observations in Mediterranean

The surface ozone validation analysis over the Mediterranean is based on an evaluation against station observations from the Airbase Network (http://acm.eionet.europa.eu/databases/airbase/). In addition, 1 station from the Department of Labour Inspection - Ministry of Labour and Social Insurance, of Cyprus (http://www.airquality.dli.mlsi.gov.cy/) is used in the validation analysis. For the validation analysis, stations in the Mediterranean located within about 100 km from the shoreline of the Mediterranean shore are used. Table 3.4.1 shows the names, coordinates, elevation and the MNMBs and correlations obtained with the 2 forecast runs (o-suite and control). It indicates that the variance explained by each station of both the o-suite and control is high and correlations are highly significant over Western, Central and Eastern Mediterranean. It should be noted that the o-suite run reproduces slightly better than the control run the surface ozone day to day variability over most of the Mediterranean stations (see Table 3.4.1). In terms of biases, the o-suite mostly overestimates surface ozone values and its MNMBs vary between -35% and +42% depending on the stations over the Mediterranean shore of Spain (average MNMB for the 13 Spain Mediterranean station is 19%). For the Control run, MNMBs are on average 1.5% lower than for the o-suite. Over the stations Plan Aups/Ste Baume in France and Montemonaco in Italy, the o-suite overestimates surface ozone concentrations by 24% and 20% respectively. Again, the Control run's MNMBs are lower by 2.5%. Over Gharb station in Malta, the o-suite overestimates surface ozone values by 4.7% and the control run by 1.6%. Over Finokalia station in Crete and Agia Marina in Cyprus, the o-suite overestimates surface ozone by 10.7% and 8.9. Again, the Control run's MNMBs are lower by 3.5%.

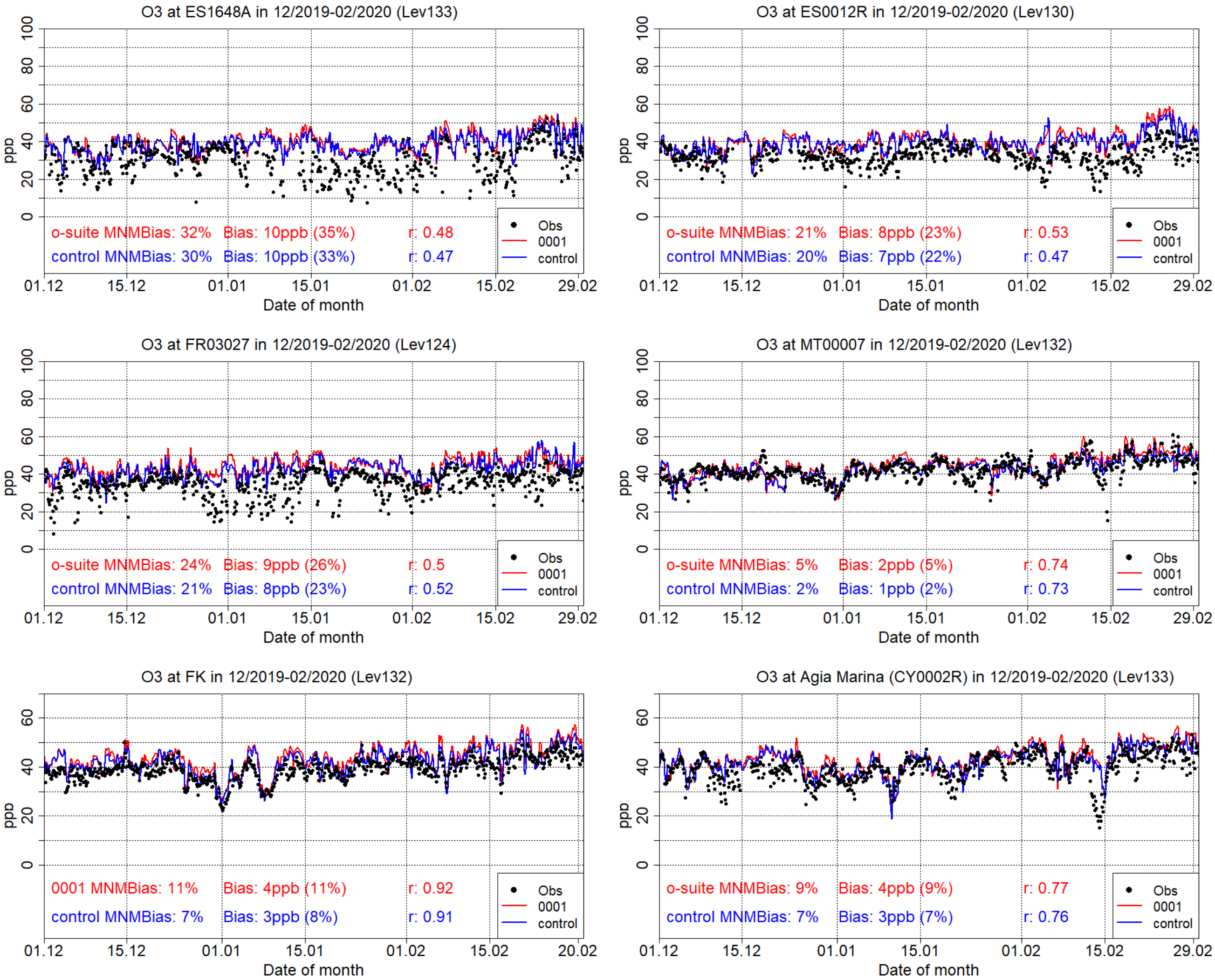

Figure 3.4.1: Time series for the o-suite (red) and Control (blue) compared to Airbase observations at Al Cornocales, Spain station (36.23°N, 5.66 °W, top left), at Zarra, Spain station (39.08°N, 1.10°W, top right), at Plan Aups/Ste Baume, France station (43.34°N, 5.73°E, center left), at Gharb, Malta station (36.07°N, 14.20°E, center right at Finokalia, Crete Greece station (35.32°N, 25.67°E, bottom left) and compared to observations provided by the Department of Labour Inspection - Ministry of Labour and Social Insurance of Cyprus) at Agia Marina, Cyprus station (35.04°N, 33.06 °E, low right).

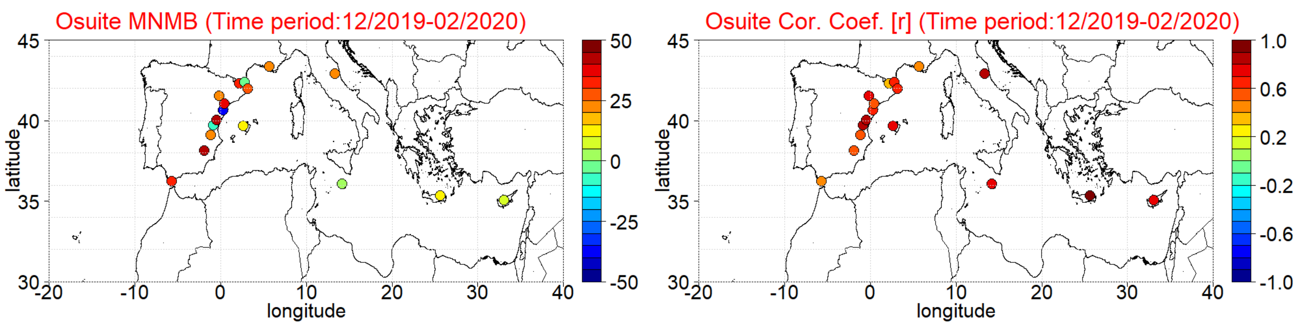

Figure 3.4.2: Spatial distribution of MNMB in % (left) and correlation coefficient (right) of the o-suite run compared to observational data during the period from 1 December 2019 to 29 February 2020.

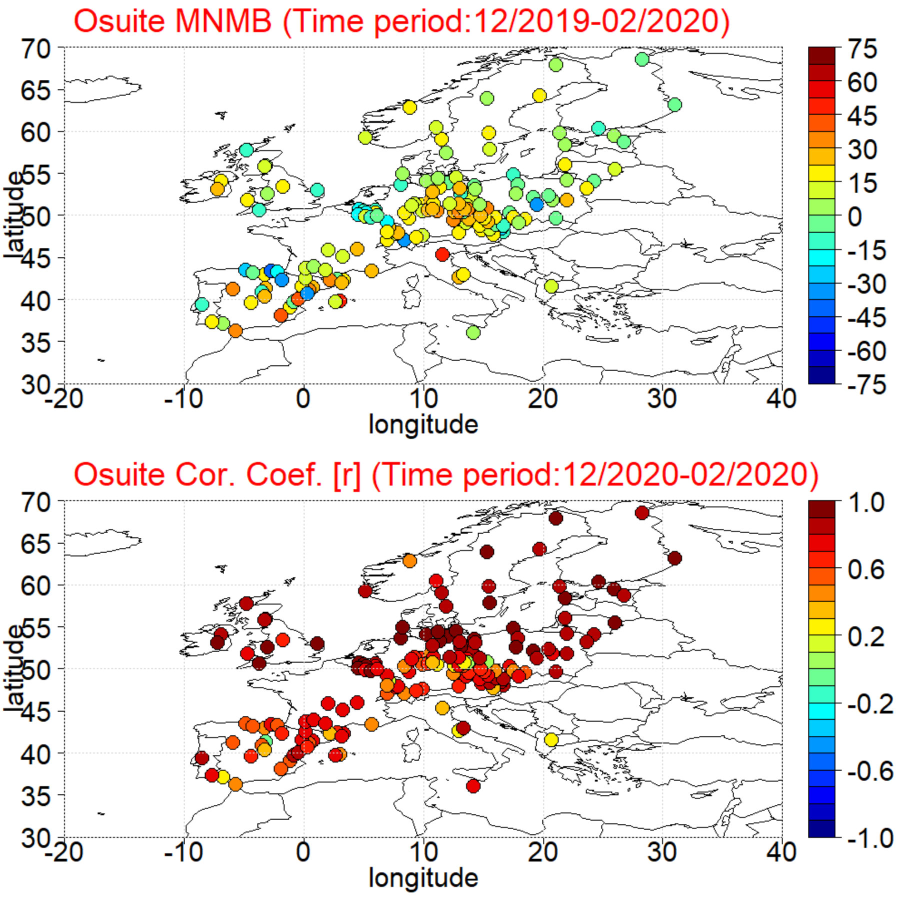

Figure 3.5.1: Spatial distribution of MNMB in % (left) and correlation coefficient (right) of the o-suite run compared to observational data during the period from 1 December 2019 to 29 February 2019.

The spatial distribution of MNMBs and the correlation coefficients of the o-suite over the Mediterranean are shown in 3.4.2, where it is evident that correlations over the entire Mediterranean from Gibraltar to Cyprus are highly significant. It is also evident that the CAMS NRT runs have a better performance over Central and Eastern Mediterranean compared to the Mediterranean shore of Spain in terms of biases.

3.5 Validation with AirBase observations over Europe

The surface ozone validation analysis over Europe is based on an evaluation against Background Rural Classes 1-2 O_3 July-Peuch classification station observations from Airbase Network (http://acm.eionet.europa.eu/databases/airbase/). The spatial distribution of MNMBs and the correlation coefficients of the o-suite over Europe are shown in 3.5.1, where it is evident that correlations over most European AirBase stations (with a very few exceptions) are highly significant (0.5<r<0.95). It is also evident that the CAMS NRT runs reproduce well the surface ozone mean concentrations over Belgium, Poland the Baltics, and Finland (depending on the station MNMBs vary from -10% to +10%). Likewise, over the rest of Central and Northern Europe the o-suite mostly overestimates surface ozone values up to 35% and the higher positive offsets are prevailing over Germany and the Czech Republic. It should be noted, that over the Iberian Peninsula the MNMBs

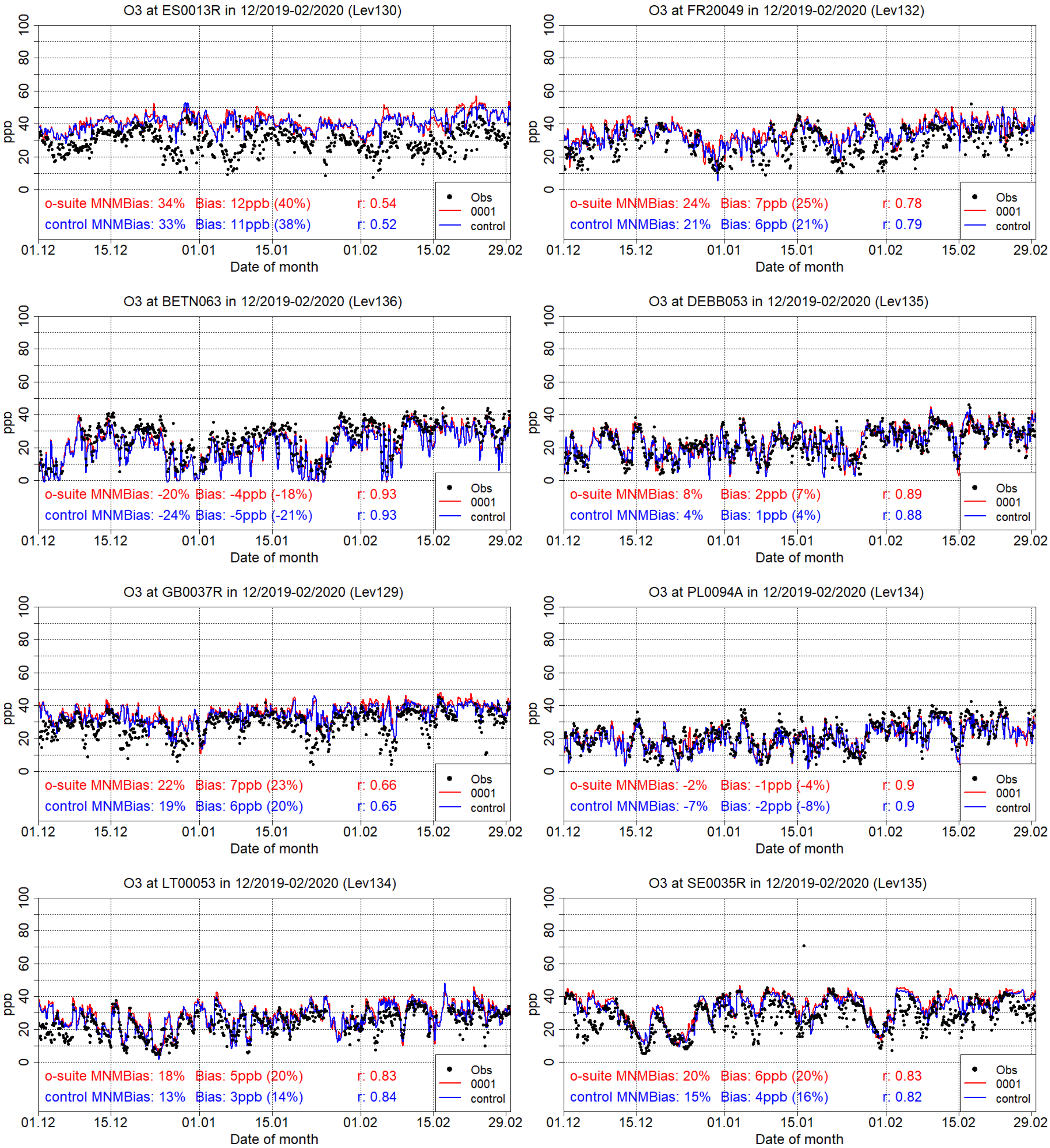

Figure 3.5.2: Time series for the o-suite (red) and Control (blue) compared to Airbase observations at Al Penausende, Spain station (41.24°N, 5.90 °W, 1st row left), at Haut Beaujolais, France station (45.96°N, 4.47°E, 1st row right), at Corroy L.G., Belgium Station (50.67°N, 4.67°E, 2nd row left), at Hasenholz, Germany (52.56°N, 14.02°E, 2nd row rigth), at Ladybower, Great Britain station (53.40°N, 1.75°W, 3nd row left), at LdGajewWIOSAGajew, Poland station (52.14°N, 19.23°E 3nd row rigth), at Zemaitija, Lithuania station (56.01°N, 21.89°E, 4nd row left) and at Vindeln, Sweden station (64.25°N, 19.77°E, 4nd row right).

has a strong spatial variability and the MNMBs vary from -50% to +50%. The above-mentioned findings concerning CAMS NRT runs biases and correlations are also observed in individual time series at selected stations plotted in Figure 3.5.2. From this time series and the plotted validation metrics it is also evident that the control run surface ozone concentrations are 1-2 ppb (1%-7%) lower than the o-suite values resulting in most cases a closer to zero bias.

3.6 Validation with IASOA surface observations

Model results were compared to surface O3 observations from the Villum Research Station, Station Nord in north Greenland (81.6°N 16.7°W), Alert Nunavut, Canada (82.5°N 62.5°W), and Zeppelin Mountain, Svalbard (78.9°N 11.9°E) from the IASOA network, Fig. 3.6.1.

The data from Svalbard and VRS cover the period from December 2014 to February 2020 and Data from Alert covers the period January 2016 – February 2020. Ozone depletion events in March – June in 2015 – 2019 are not captured by the model simulations during spring at any of the sites. These events are related to halogen chemistry reactions that are not represented in the model simulations. The simulations are on average in good agreement with the observations apart from the spring depletion events.

For the period December 2019 – February 2020 the measurements are not quality controlled. The bias is low with a tendency for overestimation at the three stations for both the o-suite (5% - 10%) and the control run (2% - 7%) (Table 3.6.1). The performance of the model has improved compared to previous winter seasons where the bias has been consistently negative in the winter period (Fig. 3.6.1). The two model runs performs equally well in terms of the correlation; r = 0.62 – 0.71 for the o-suite compared to r = 0.60 – 0.72 for the control run.

Table 3.6.1. Modified Normalised Mean Bias (MNMB) and correlation coefficient (r) of the Control and the O-suite simulations for the sites Alert, Svalbard, and Villum Research Station (VRS) for the period December 2019 – February 2020.

		MNMB	R
Alert	o-suite	0.10	0.65
	control	0.07	0.60
Svalbard	o-suite	0.06	0.71
	control	0.03	0.72
VRS	o-suite	0.05	0.62
	control	0.02	0.58

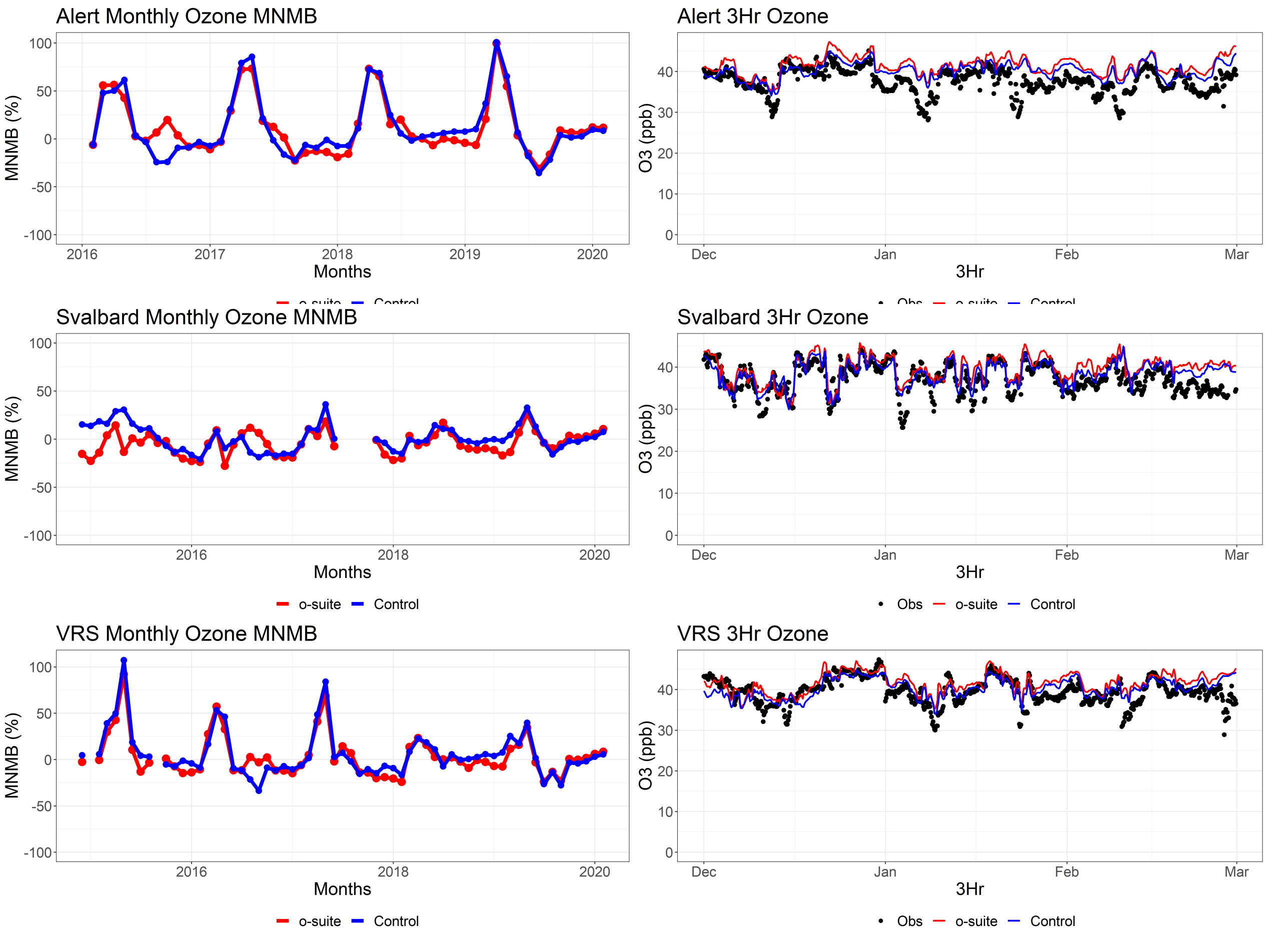

Figure 3.6.1: Time series for o-suite (red) and Control (blue) compared to observations (black dots) at Alert, Nunavut, Canada (Top row) Svalbard (second row), and the Villum Research Station, Greenland (bottom row), MNMB for the full period (left) and concentrations for December 2019 – February 2020 (right).

3.7 Validation with IASI data

Ozone total columns from the o-suite and control run are compared with IASI Metop-A version v20191122 daytime only satellite observations (Clerbaux et al., 2009). For the comparison with the IASI data, the vertically integrated model O_3 data were transformed using IASI averaging kernels (Rodgers, 2000).

The global distribution of the O_3 total column obtained from IASI, as well as the relative difference between the model runs and IASI, are shown in Fig. 3.7.1 for January 2020. Satellite data shows high O_3 over the northern mid- and high latitudes, especially over the east of Russia, Canada and Pacific Ocean and low values over the equatorial region. The o-suite run captures both, high and low O_3 values relatively well and is in good agreement with the observations, showing MNMBs within 5%. The underestimation over the high O_3 concentration land regions mentioned above is most likely due to the low IASI sensitivity over the cold surfaces. The control run is positively biased over the northern mid- and high latitudes up to 30%. Some underestimated spots can be seen over the east of Russia and north of Canada (within 20%). The forecast day 4 is almost similar to the forecast day 0. Note, that the IASI sensitivity is lowest over the cold surfaces of Antarctica and Greenland

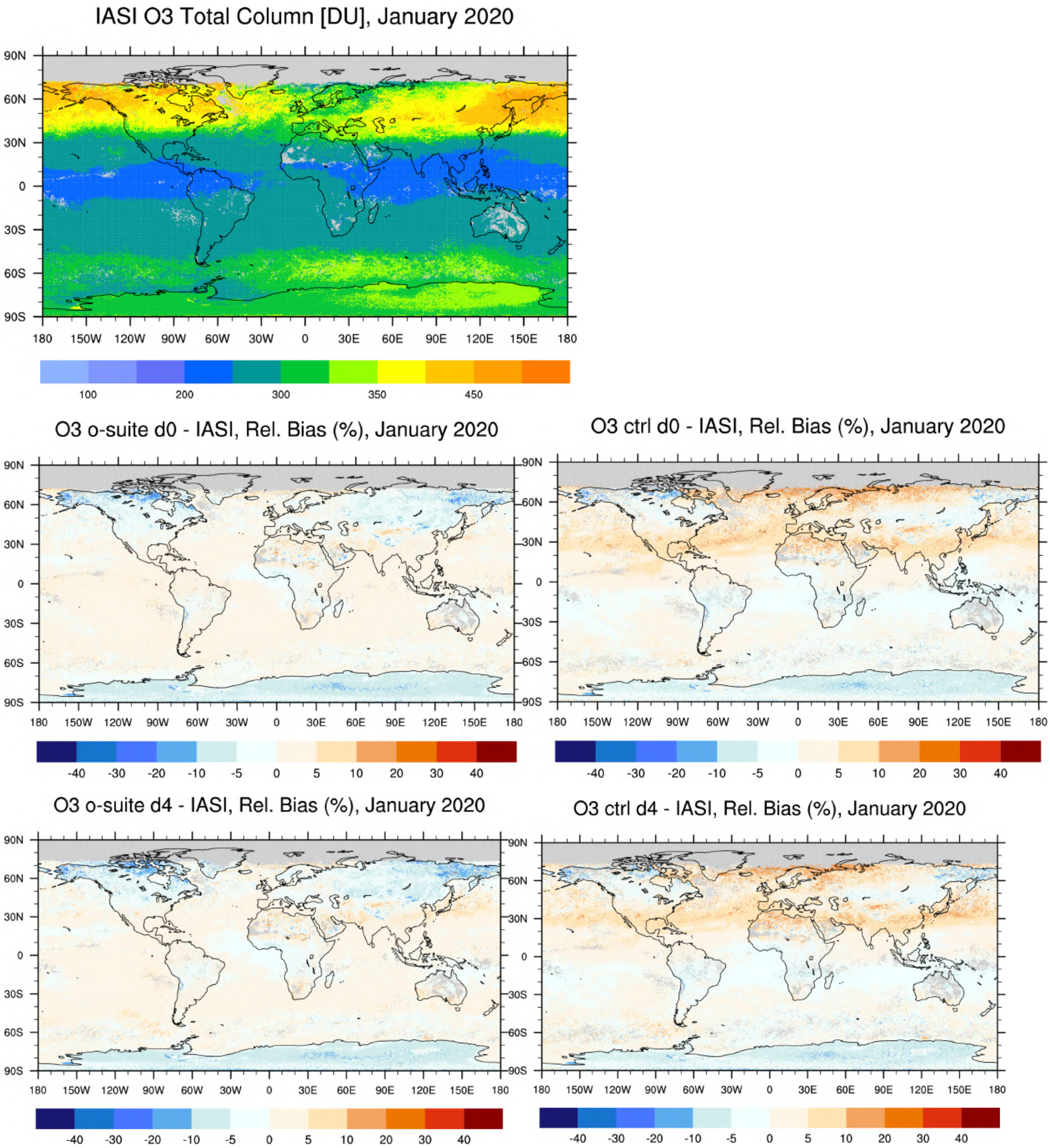

Figure 3.7.1: O_3 total column for IASI satellite observations (top) and relative difference between the model runs and IASI for January 2020: o-suite day 0 and day 4 (left), control run day 0 and day 4 (right). Grey colour indicates missing values.

(especially during March-April-May season) where IASI O_3 values are positively biased by up to 20%. Figure 3.7.2 shows data as a function of latitude and time from January 2019 till February 2020. The o-suite shows good agreement with the observations with a slight bias within 5 %. The control run has distinct differences in the data before the model upgrade in July 2019, showing mostly negative biases and after July 2019, when the bias changes sign especially over the Northern Hemisphere.

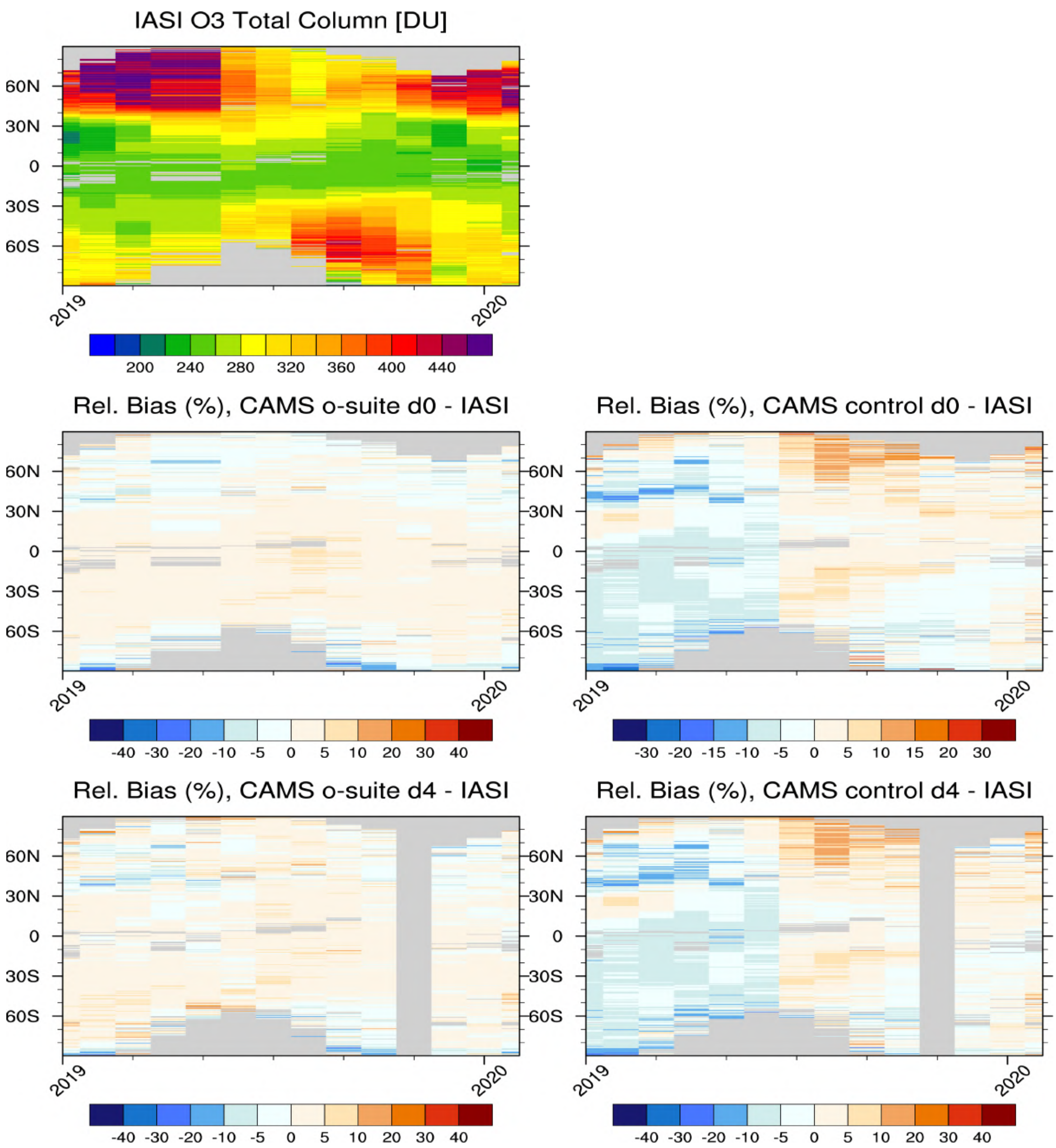

Figure 3.7.2: IASI Metop-A O_3 total column (top) as function of latitude and time from January 2019 to February 2020. Relative difference between the model runs and IASI: o-suite day 0 and day 4 (left), control run day 0 and day 4 (right). Grey colour indicates missing values.

4. Carbon monoxide

4.1 Validation with Global Atmosphere Watch (GAW) Surface Observations

For the Near-Real-Time (NRT) validation, 10 GAW stations have delivered CO surface mixing ratios in NRT and data is compared to model results as described in Eskes et al. (2019) and is used for CAMS model evaluation for December 2019 to February 2020. The latest validation results can be found on the CAMS website, see section 1.

For stations in the Northern Hemisphere, both runs mostly show slightly negative MNMBs for stations in Europe (Fig. 4.1.1).

A comparison of the seasonal-mean MNMB over Europe (Fig. 4.1.2) from December 2012 to present shows a slowly improving MNMB from about -20% in 2013 to about -10% for more recent periods. Temporal correlation remains relatively constant at r=0.6 on average, except for the quarter JJA in 2018, where the correlation of the control run drops to 0.24.

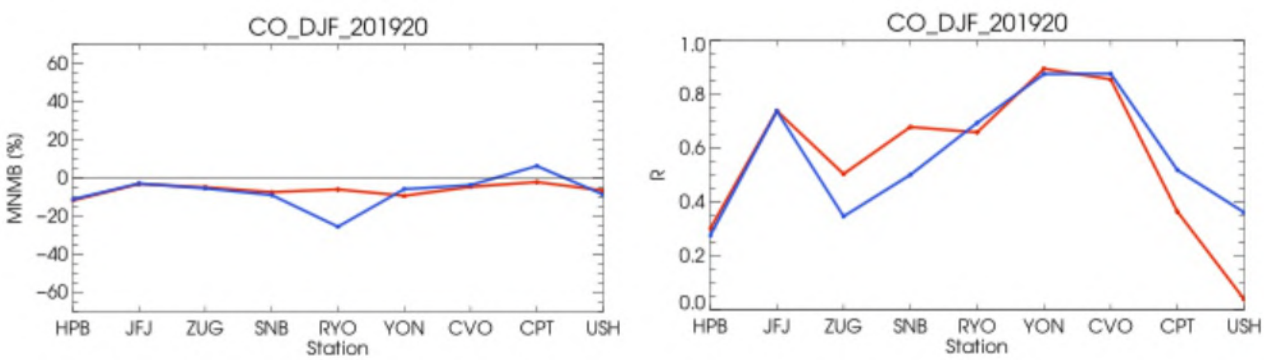

Figure 4.1.1: Modified normalized mean bias in % (left) and correlation coefficient (bottom right) of the NRT model runs compared to observational GAW data in the period December 2019 to February 2020 (o-suite: solid red, and control: blue).

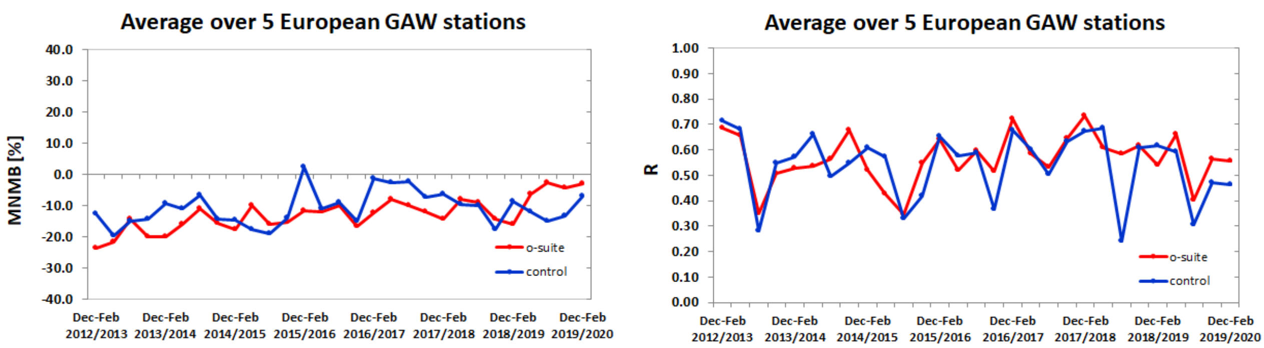

Figure 4.1.2: Long term (Dec. 2012 – February 2020) evolution of seasonal mean MNMB (left) and correlation (right), as averaged over 5 GAW stations in Europe, for o-suite (red) and control (blue).

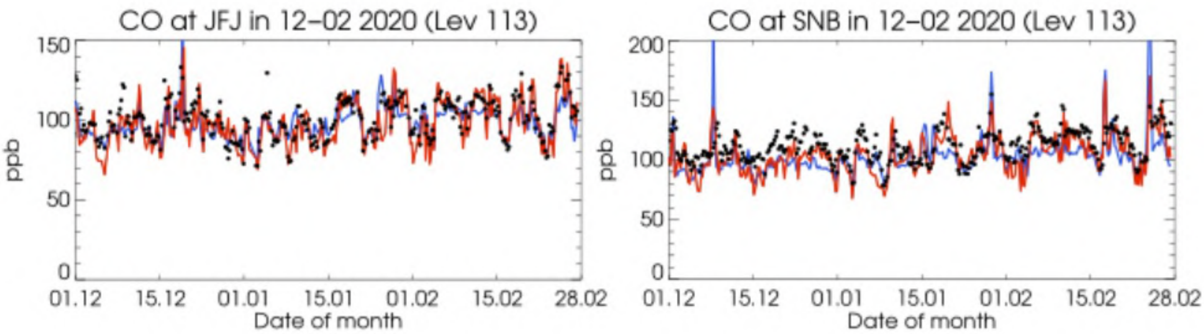

Figure 4.1.3: Time series for the o-suite (red) and control (blue) compared to GAW observations at Jungfraujoch (46.55°N, 7.99°E) and Sonnblick (47.05°N, 12.96°E).

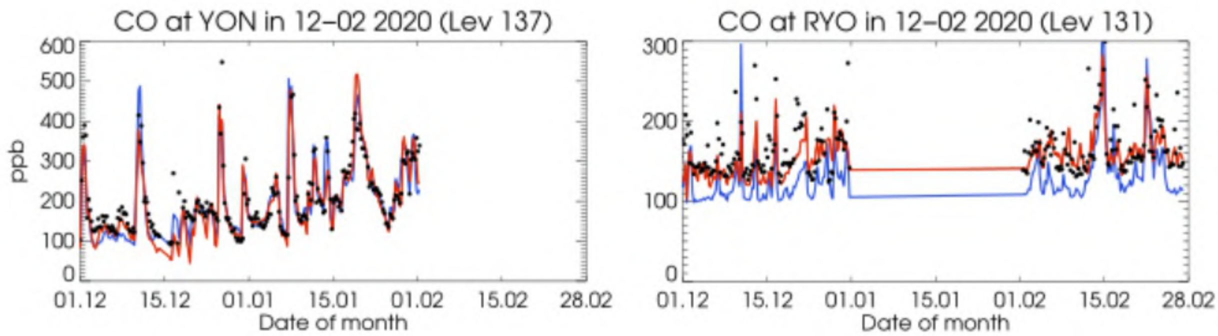

Figure 4.1.4: Time series for the o-suite (red) and control (blue) compared to GAW observations at Yonagunijima (24.47°N, 123.02°E) and Ryori (39.03°N, 141.82°E).

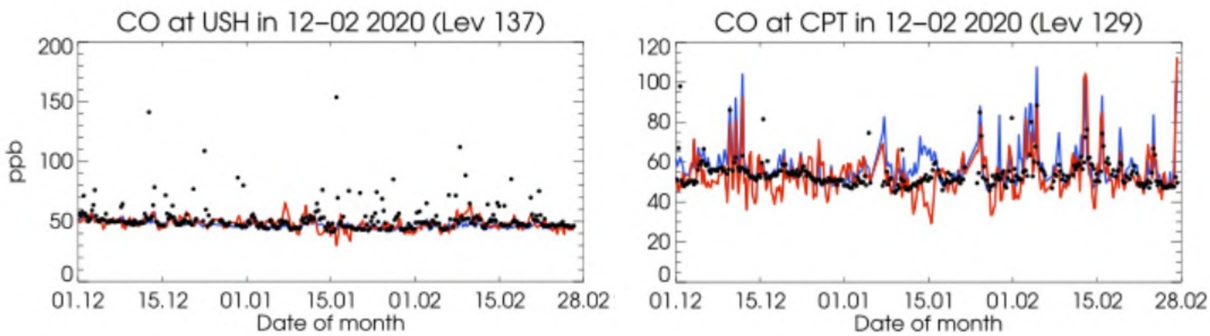

Figure 4.1.5: Time series for the o-suite (red) and control (blue) compared to GAW observations at Ushuaia (54.85°S, -68.32°W) and Cape Point (34.35°S, 18.5°E).

For European stations (Fig. 4.1.3), both runs show an underestimation of observed CO mixing ratios, with MNMBs between -11% and -2%. Correlation coefficients are between 0.3 and 0.73 for the o-suite and between 0.27 and 0.73 for the control run.

For Asian stations, the o-suite corresponds well to the observations with only minimal underestimations <10%. The control run shoes a strong negative offset for Ryori station (Fig. 4.1.4).

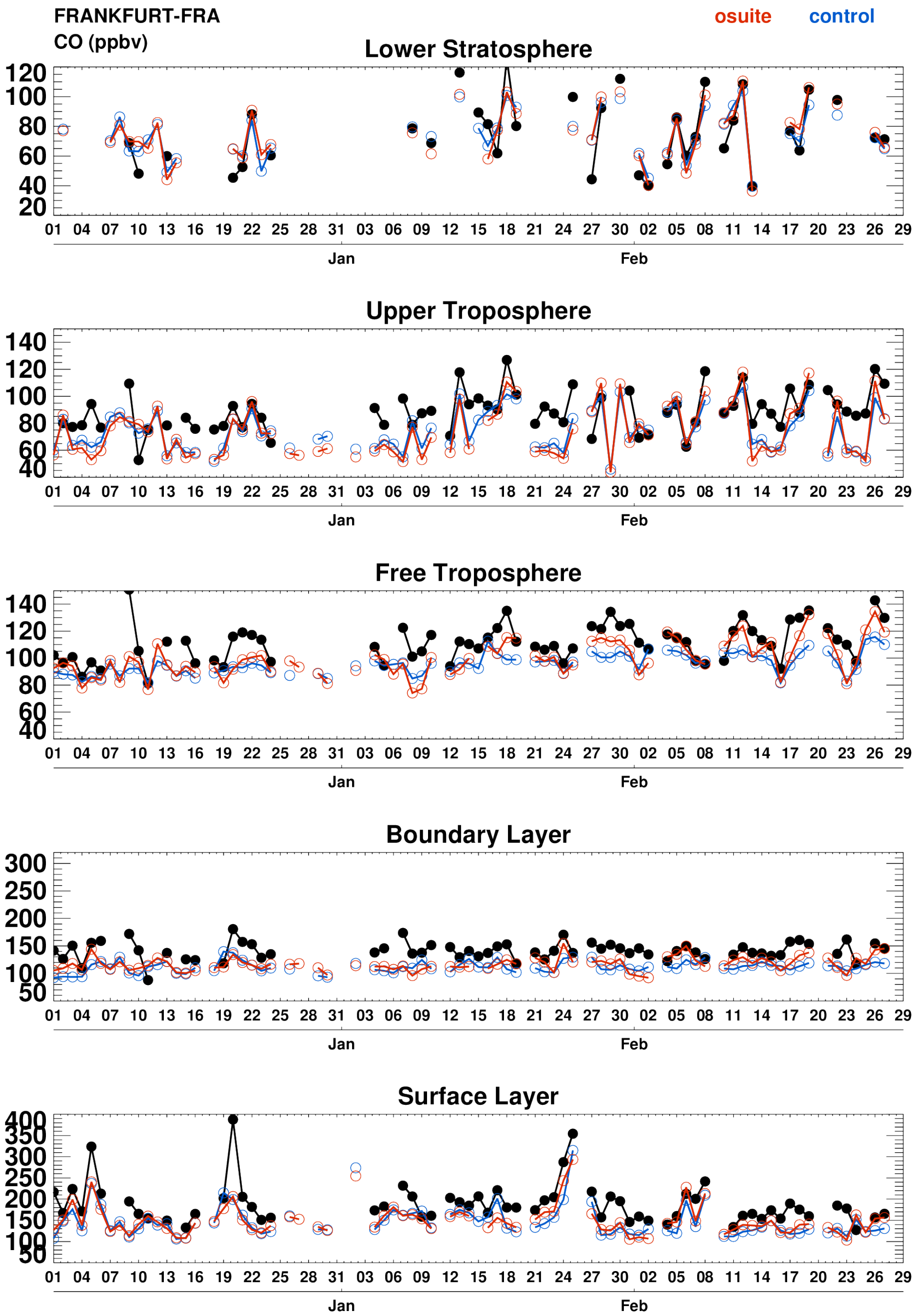

Figure 4.2.1: Time series of daily mean CO over Frankfurt during DJF 2020 for 5 layers: Surface Layer, Boundary Layer, Free Troposphere, Upper Troposphere and Lower Stratosphere. The o-suite is shown in red and associated control run in blue. Units: ppbv.

For CVO, MNMBs are slightly negative for o-suite and control. Correlation is high with 0.85 (control 0.87).

For the two stations in the Southern Mid-latitudes (CPT and USH) MNMBs slightly negative are low (Fig.4.1.5.) for the o-suite and partly positive for the control run. Correlation coefficients for the o-suite are between 0 and 0.36 and range for the control run between 0.36 and 0.51.

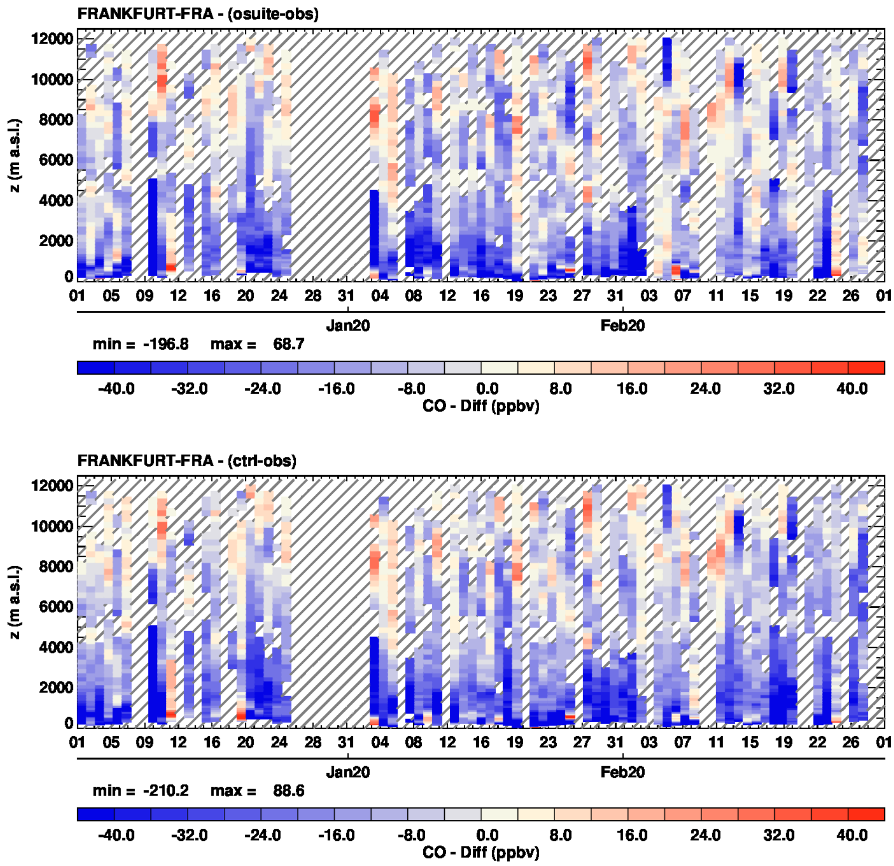

Figure 4.2.2: Time series of the absolute differences (model – IAGOS aircraft observations) in daily profiles for CO over Frankfurt during DJF 2020. The top panel corresponds to o-suite, the bottom panel to control run. Units: ppbv.

4.2 Validation with IAGOS Data

Nearly continuous time series of CO are available at Frankfurt CO during DJF 2020 (Fig. 4.2.1). For CO the behaviour of the two runs is very similar (Fig.2.2) at all levels, CO is mostly underestimated by both o-suite and control run and the largest bias is generally found in the lowest layers (Fig. 4.2.2). A few overestimations are also found in the low troposphere (Fig. 4.2.2). These overestimations are sometimes related to observations of high CO values, but this is not a systematic behaviour (Fig. 4.2.2). While the performances of the two runs are more similar in the lowest layers, the o-suite performs slightly better than the control run in the free troposphere where the runs agree best with the observations, as shown on the time series of Fig. 4.2.1. In the UTLS, the performance of the two runs is very similar and the bias is also small in general.

Three major peaks of CO are observed in the surface layer during DJF-2020 on 5 December, 20 December, and 25 January (Fig. 4.2.1). A secondary peak is also observed on 6 February (Fig. 4.2.1). The corresponding profiles around these dates are presented in Fig. 4.2.3.a-b, showing values reaching close or slightly above 400 ppbv near the surface for some of these profiles. As it can be seen on the time series, the first two peaks of December are largely underestimated by the runs, while the January peak is well reproduced (Fig. 4.2.1), which can also be seen on the individual profiles of Fig. 4.2.3.

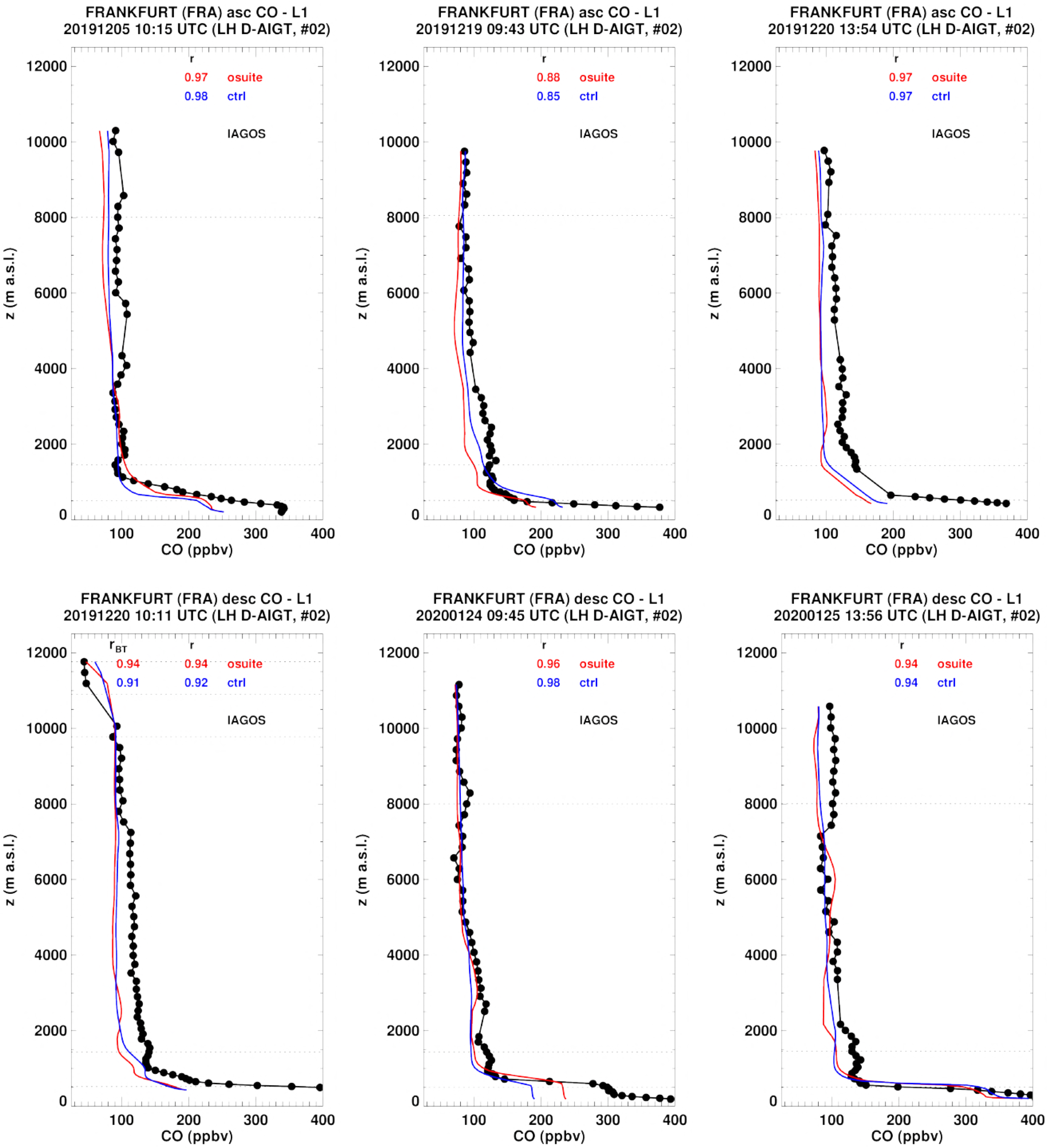

Figure 4.2.3.a: Daily profile for CO from IAGOS (black) and the two NRT runs (o-suite: red, control: blue) over the Europe during DJF 2020.

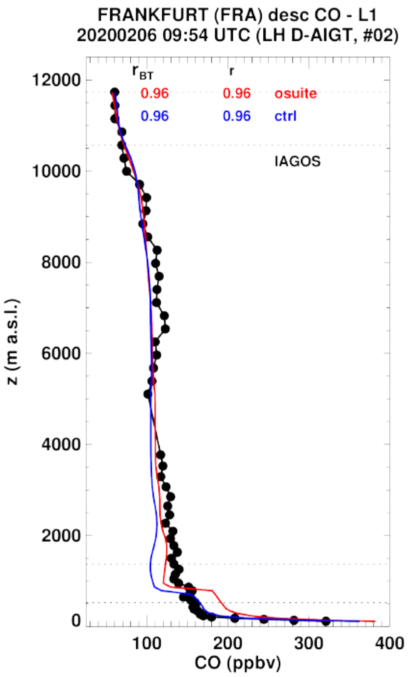

Figure 4.2.3.b Daily profile for CO from IAGOS (black) and the two NRT runs (o-suite: red, control: blue) over the Europe during DJF 2020.

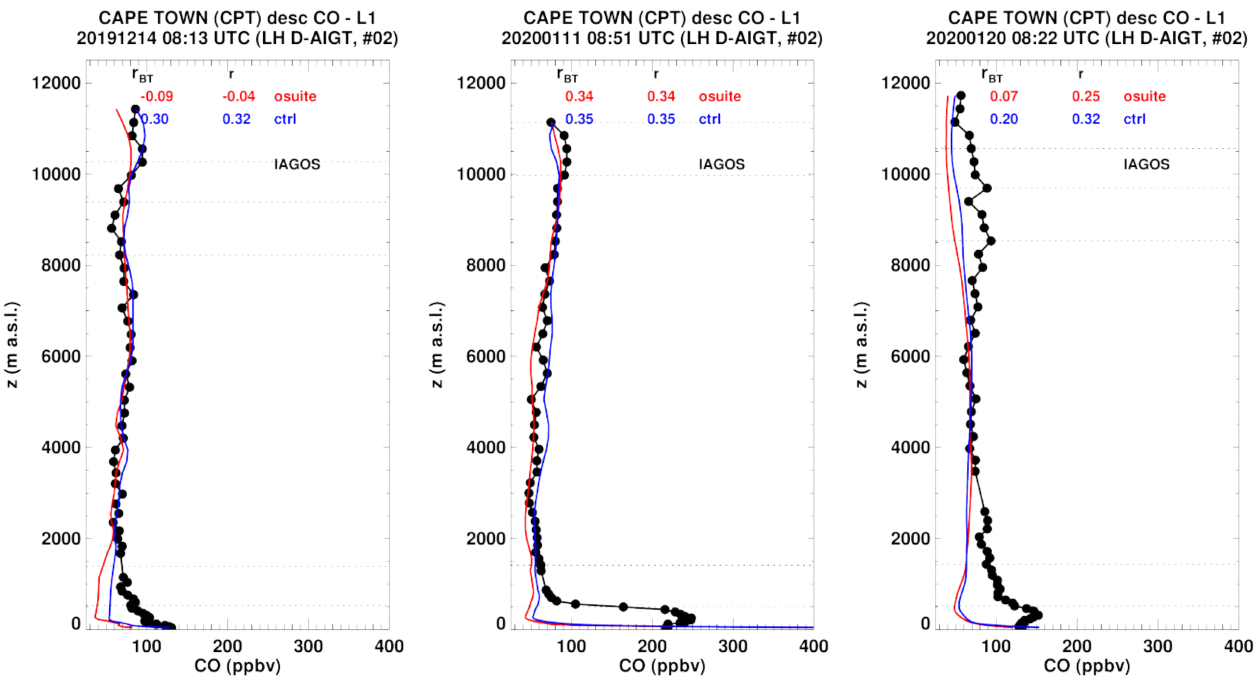

Figure 4.2.4: Daily profile for CO from IAGOS (black) and the two NRT runs (o-suite: red, control: blue) over South Africa during DJF 2020.

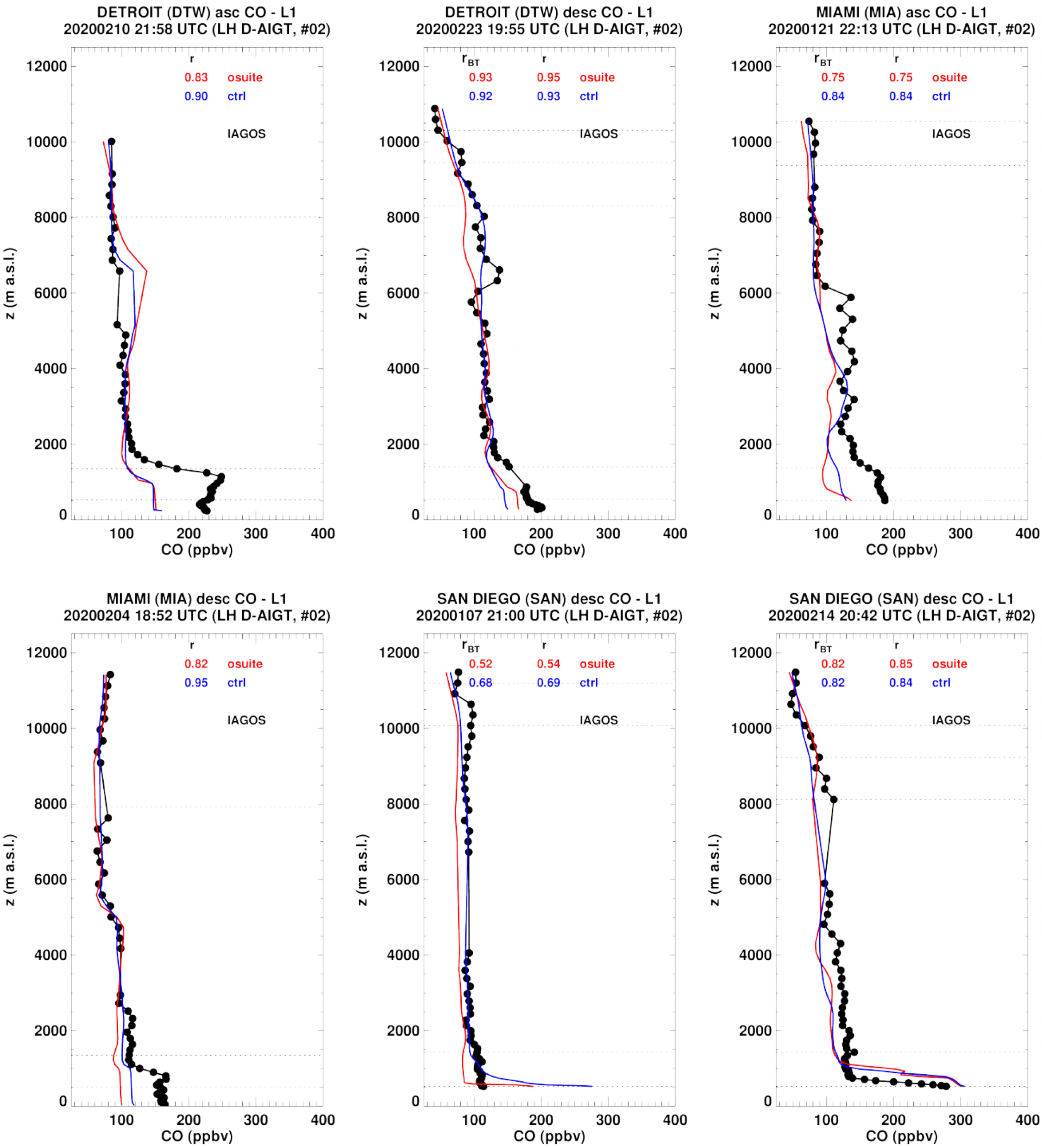

Figure 4.2.5.a: Daily profile for CO from IAGOS (black) and the two NRT runs (o-suite: red, control: blue) over North America during DJF 2020.

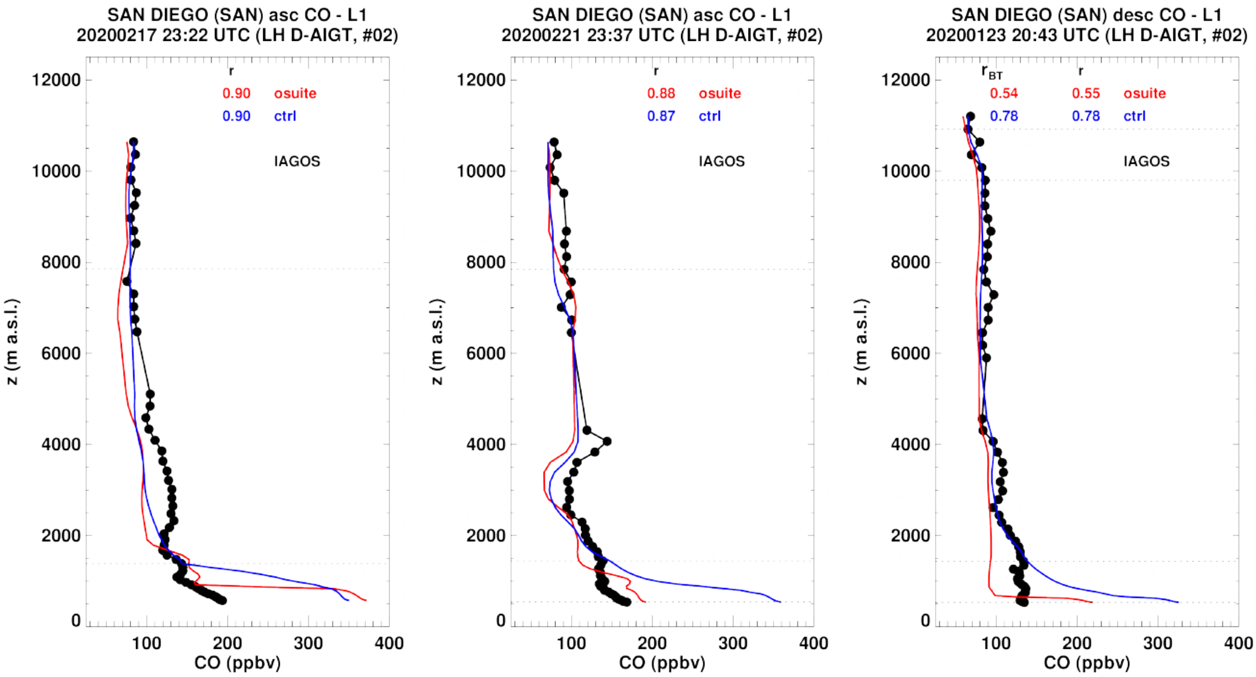

Figure 4.2.5.b: Daily profile for CO from IAGOS (black) and the two NRT runs (o-suite: red, control: blue) over North America during DJF 2020.

South Africa

Over Africa, CO profiles are available only at the South African airport of Cape Town (Fig. 4.2.4). At this airport, the results of the two runs are very similar for this period. In the low troposphere, values are mostly underestimated, although near the surface a case of overestimation is found for the profile of 11 January at 8:51. In the free troposphere and UTLS, o-suite and control run behave similarly and agree well with observations.

North America

CO profiles are available at the airport of Detroit, Miami and San Diego during DJF 2020 (Fig. 4.2.5.a-b). For this period, in the available profiles, CO observed values are mostly in the range 100-200 ppbv in the low troposphere. These values are in general underestimated, similarly by both runs, at the airport of Detroit and Miami. At the airport of San Diego, CO values near the surface are mostly overestimated with sometimes large biases (i.e. 23 January, 20:43), with often a smaller bias from the o-suite than from the control run. In the free troposphere and UTLS the results of both runs behave similarly and agree well with observations at all locations.

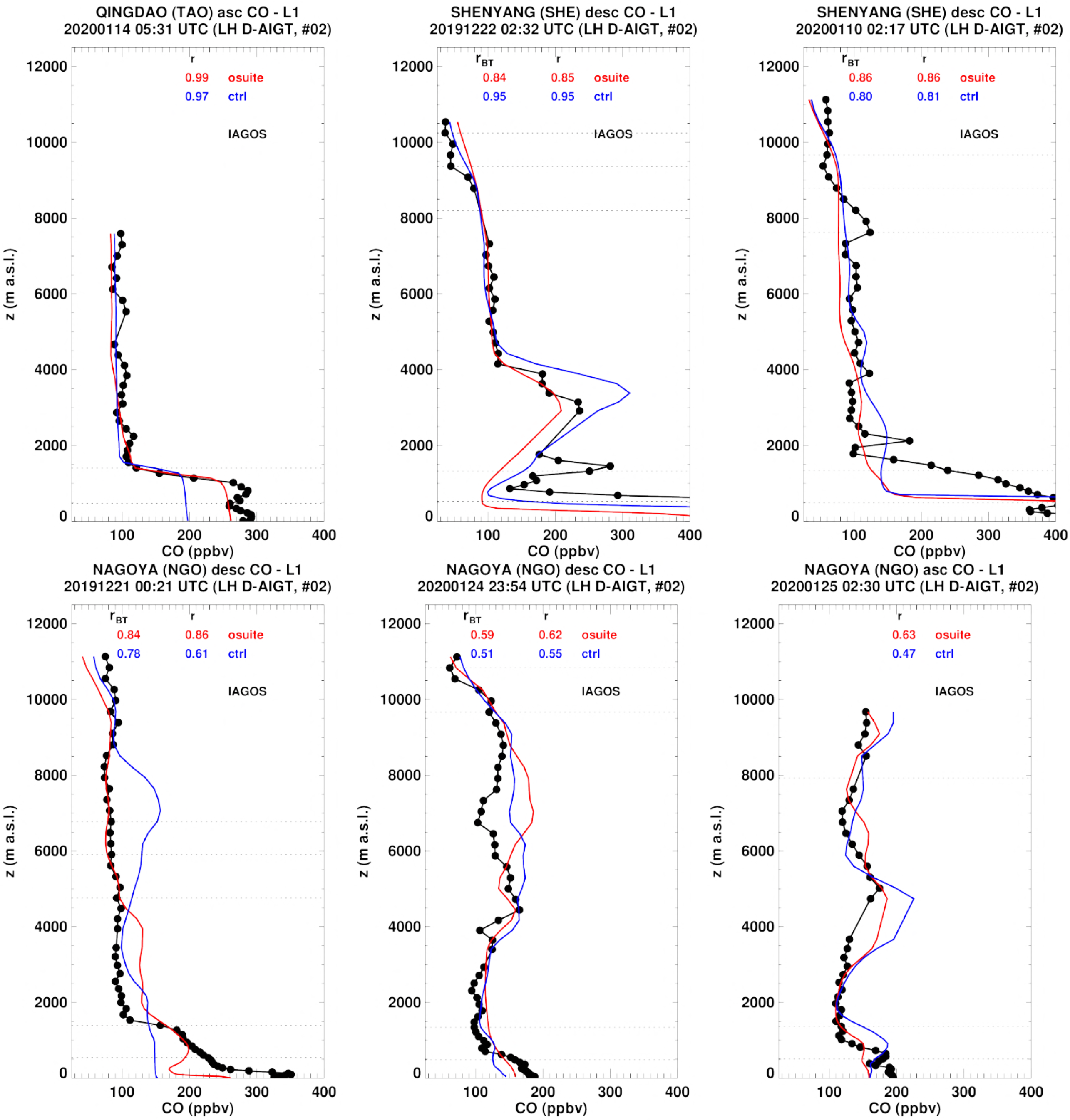

Figure 4.2.6.a: Daily profile for CO from IAGOS (black) and the two NRT runs (o-suite: red, control: blue) over East Asia during DJF 2020.

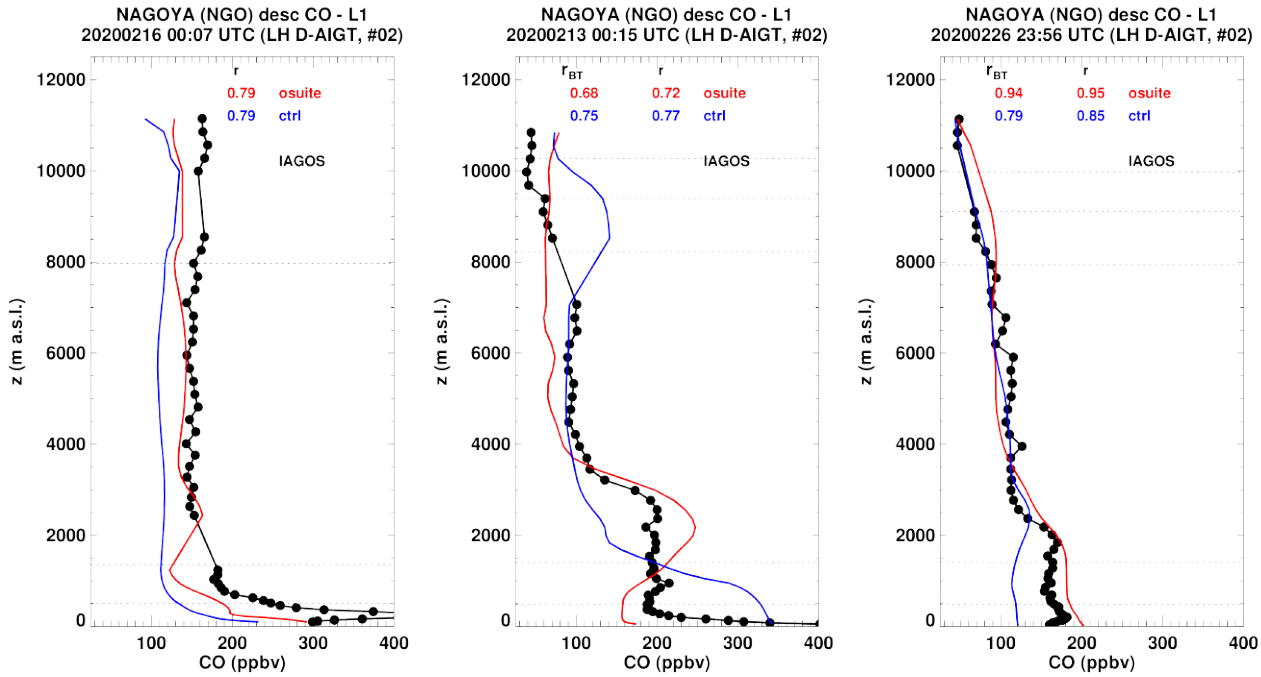

Figure 4.2.6.b: Daily profile for CO from IAGOS (black) and the two NRT runs (o-suite: red, control: blue) over East Asia during DJF 2020.

Eastern Asia

Over East Asia, CO profiles are available at three airports: Qingdao (China) Shenyang (China) and Nagoya (Japan) (see Fig. 4.2.6.a-b). The high CO mixing ratios in the low troposphere and the complex shape of the profiles, with maxima in the free troposphere are in general well reproduced by both runs with often a better performance from the o-suite as compared to the control run. In the UTLS, the agreement is better than in the lowest layers and the performances of the two runs are similar.

Central America

During DJF 2020, a few profiles of CO are available at Panama City (Panama) and Cancun (Mexico), with some examples in Fig. 4.2.7. At both airports, CO values are often largely underestimated in the low to mid-troposphere and especially in the boundary layer by both runs, with often better agreement from the o-suite at Panama City, while the results of the two runs are more similar at Cancun. In the UTLS, CAMS global and control run perform similarly well.

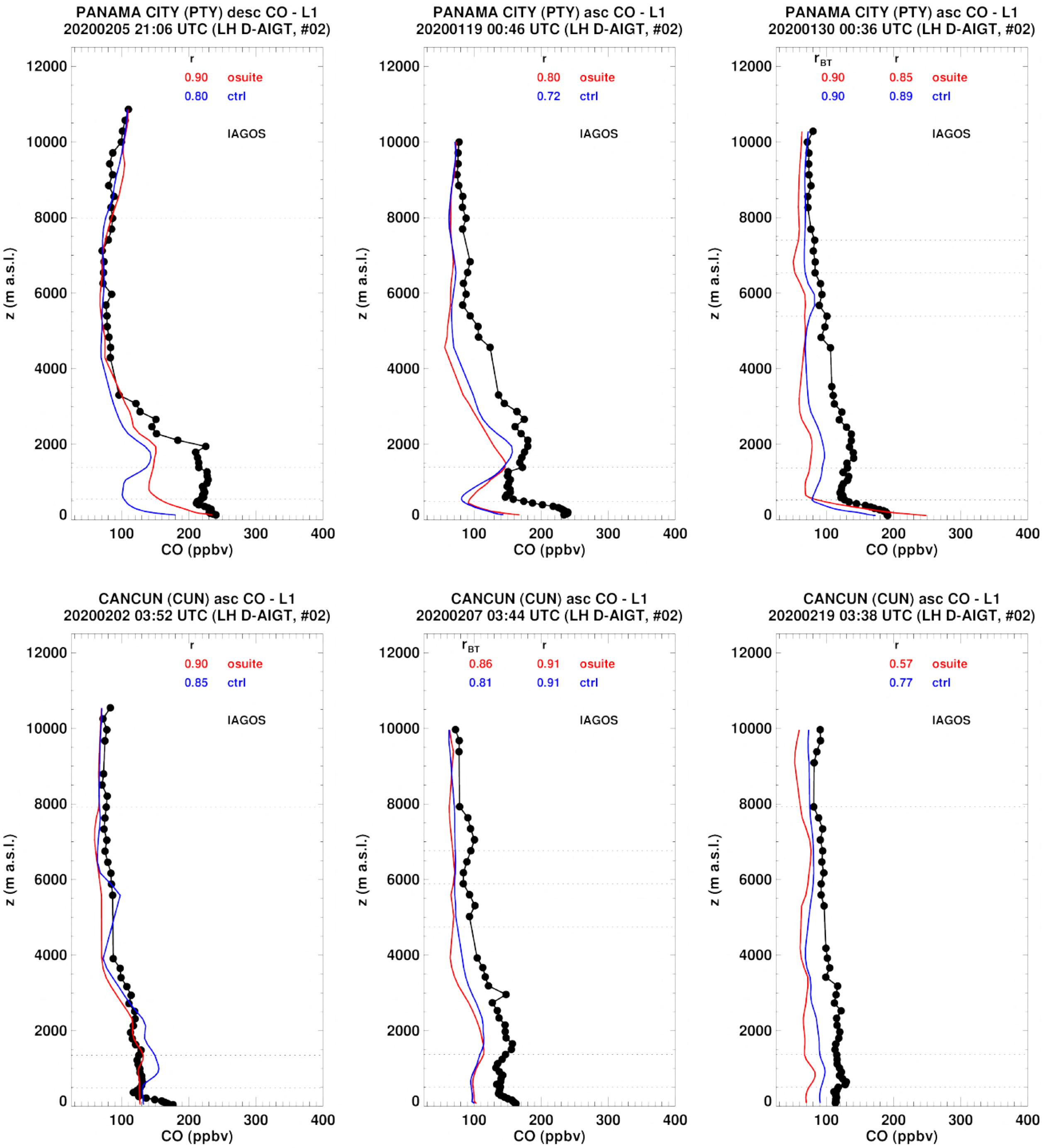

Figure 4.2.7: Daily profile for CO from IAGOS (black) and the two NRT runs (o-suite: red, control: blue) over South America during DJF 2020.

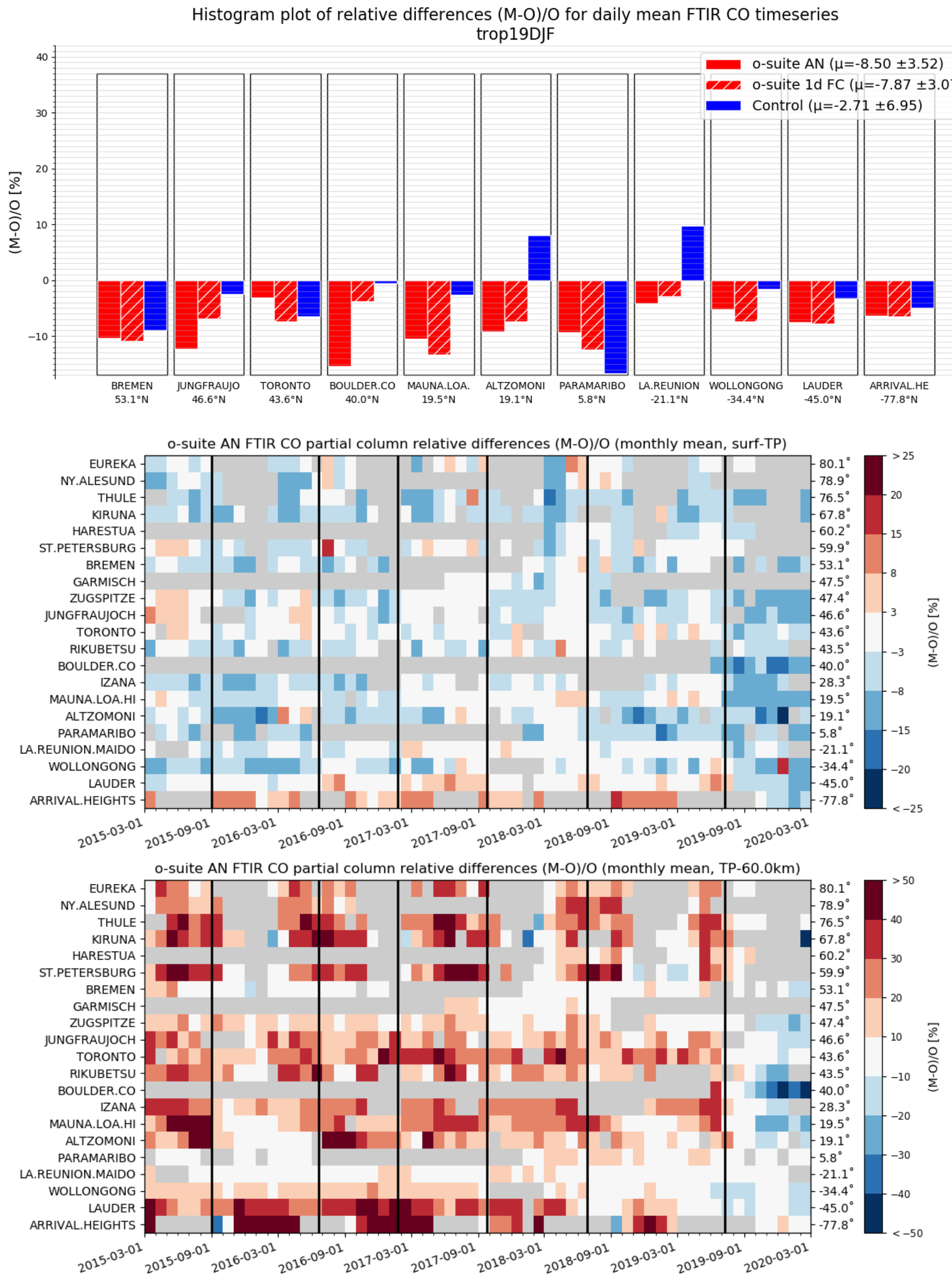

Figure 4.3.1: Seasonal relative mean bias for tropospheric CO columns (MB, %) for the considered period 2019/2020 DJF (top) and monthly mean biases for a longer time period for the tropospheric CO columns (middle) and stratospheric CO columns (bottom) (model upgrades are indicated in black vertical lines).The overall uncertainty for the CO measurements is approximately 3% on the tropospheric columns and 10% for the stratospheric columns. The o-suite analysis averaged bias in tropospheric columns increased to -8.5% for DJF. The bias in the stratosphere reduced to -12% and just exceeds the measurement's uncertainty. Stations are sorted with decreasing latitude (northern to southern hemisphere). In particular at Boulder the o-suite performs significantly worse than the o-suite 1d forecast.

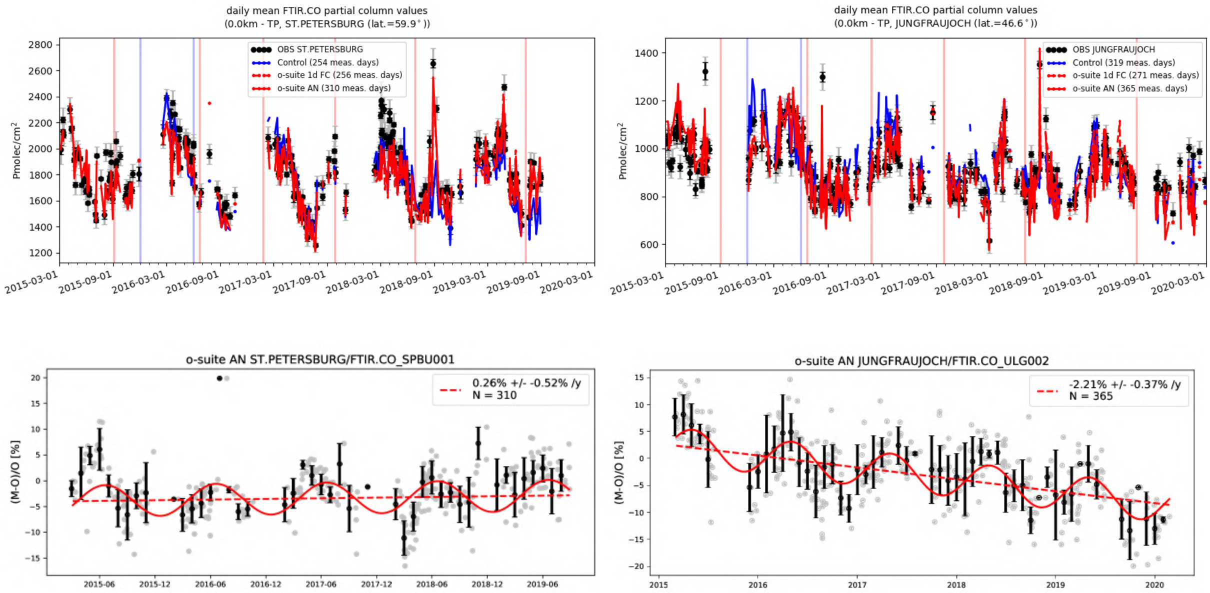

Figure 4.3.2: Top: daily mean values of tropospheric CO columns by the o-suite (AN and 1d FC, red) and the control run (blue) compared to NDACC FTIR data at St Petersburg and Jungfraujoch for the period March 2015-February 2020. During March 2018 the o-suite underestimated the CO columns at St. Petersburg. Bottom row contains a linear fit and seasonal cycle fit through the relative differences for the o-suite AN. An underestimation is observed during the local autumn/winter months. The negative trend at Jungfraujoch is -1%/y in the o-suite 1dFC.

4.3 Validation against FTIR observations from the NDACC network

In this section, we compare the CO profiles of the CAMS products with FTIR measurements at 21 FTIR stations within the NDACC network. These ground-based, remote-sensing instruments are sensitive to the CO abundance in the troposphere and lower stratosphere, i.e. between the surface and up to 20 km altitude. Tropospheric and stratospheric CO partial columns are validated. A description of the instruments and applied methodologies can be found at http://nors.aeronomie.be.

Figure 4.3.1 show that the o-suite tropospheric columns of CO agree well. The model upgrade (60 to 137 levels) implemented in July 2019 changes the overall biases in both the troposphere and stratosphere. The negative bias for the tropospheric columns increased to -8.5% in DJF, -7% in SON (compared to -4% in JJA) and is larger than the reported measurement uncertainty. The stratospheric column bias also increased to -12% in DJF compared to +2% in SON and +6% in JJA.

Figure 4.3.2 shows a trend in the tropospheric CO column at Jungfraujoch (4km – TP) of about 1.5% per year. A similar trend is observed at Zugspitze (3km above sea level), but not at other non-mountain sites like St Petersburg. The trend at the o-suite 1dFC at both mountain stations is much lower (around -0.5%/y), which suggests the trend is located in the upper tropospheric column and is related to the assimilation.

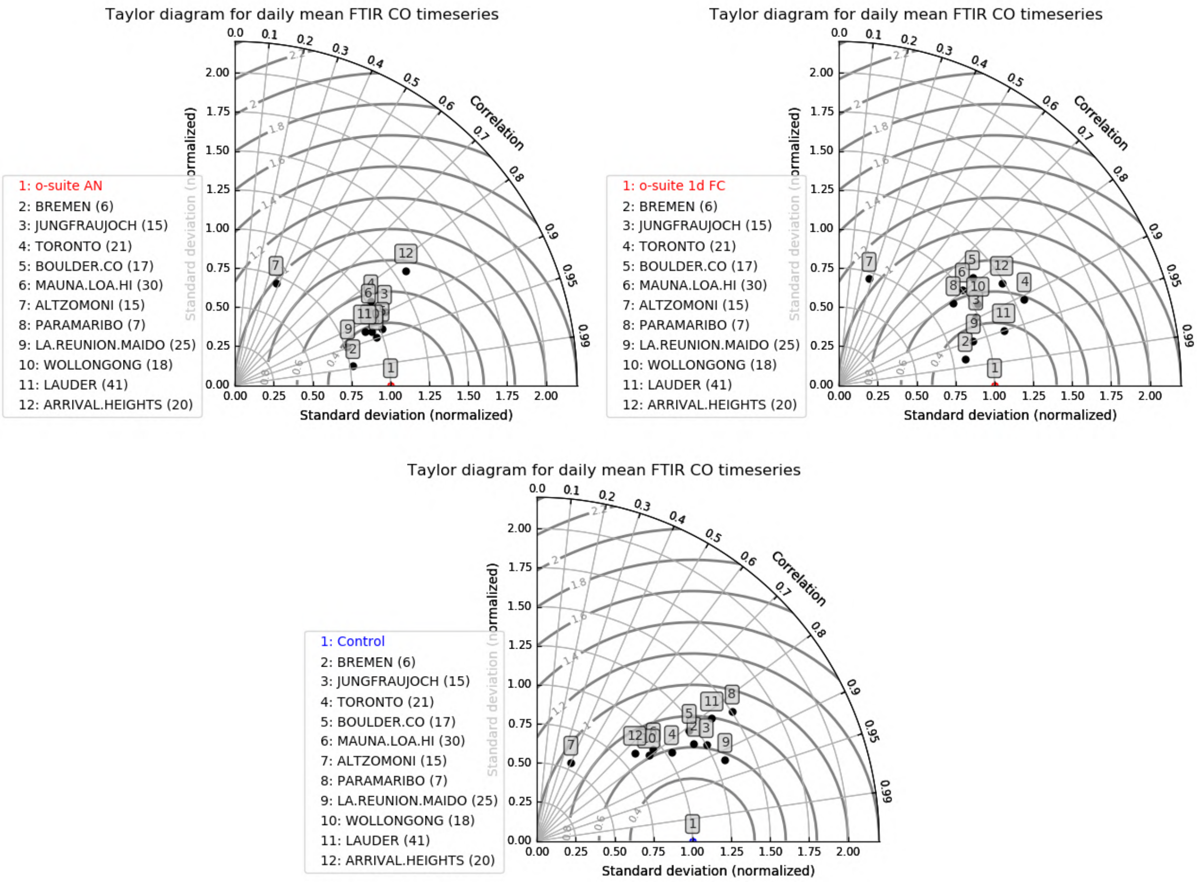

Figure 4.3.3: Taylor diagrams relating the standard deviations for the model /GB time series of tropospheric CO column data and their correlation. All time-series are normalised such that the std of the model is 1. The variability of the CO columns in the o-suite 1dFC deviates more from the variability in the FTIR columns compared to the o-suite AN.

The Taylor diagrams in Figure 4.3.3 provide information on the correlation of all three CAMS products under consideration with the FTIR time series. Leaving out the sites with few measurements, the assimilation has a positive effect on the correlation coefficient. Looking at the correlation values for the period 2019 SON, the o-suite 1d FC (averaged correlation for all sites is 0.78) is comparable to the o-suite AN (averaged correlation for all sites is 0.79).

4.4 Validation against FTIR observations from the TCCON network

CO column averaged mole fractions of the CAMS models are compared with data from the Total Carbon Column Observing Network (TCCON). Column averaged mole fractions provide different information content than the in situ measurements and are therefore complementary to the in situ data. In this section, we compare column averaged mole fractions of CO of the CAMS models with TCCON retrievals. Data from the following TCCON sites have been used:

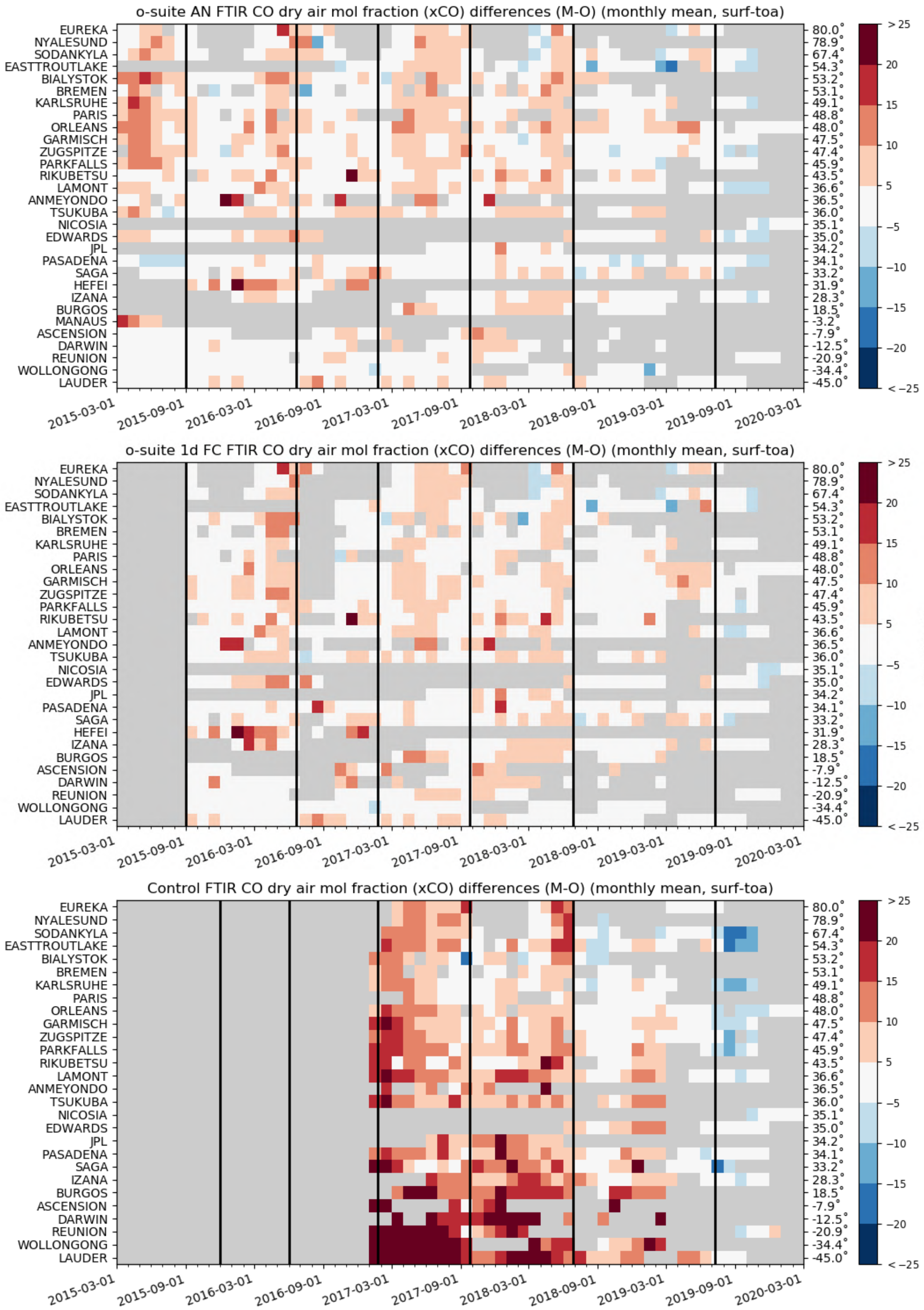

Figure 4.4.1: Monthly differences for the last 4 years. The stations are sorted by latitude (northern to southern hemisphere).

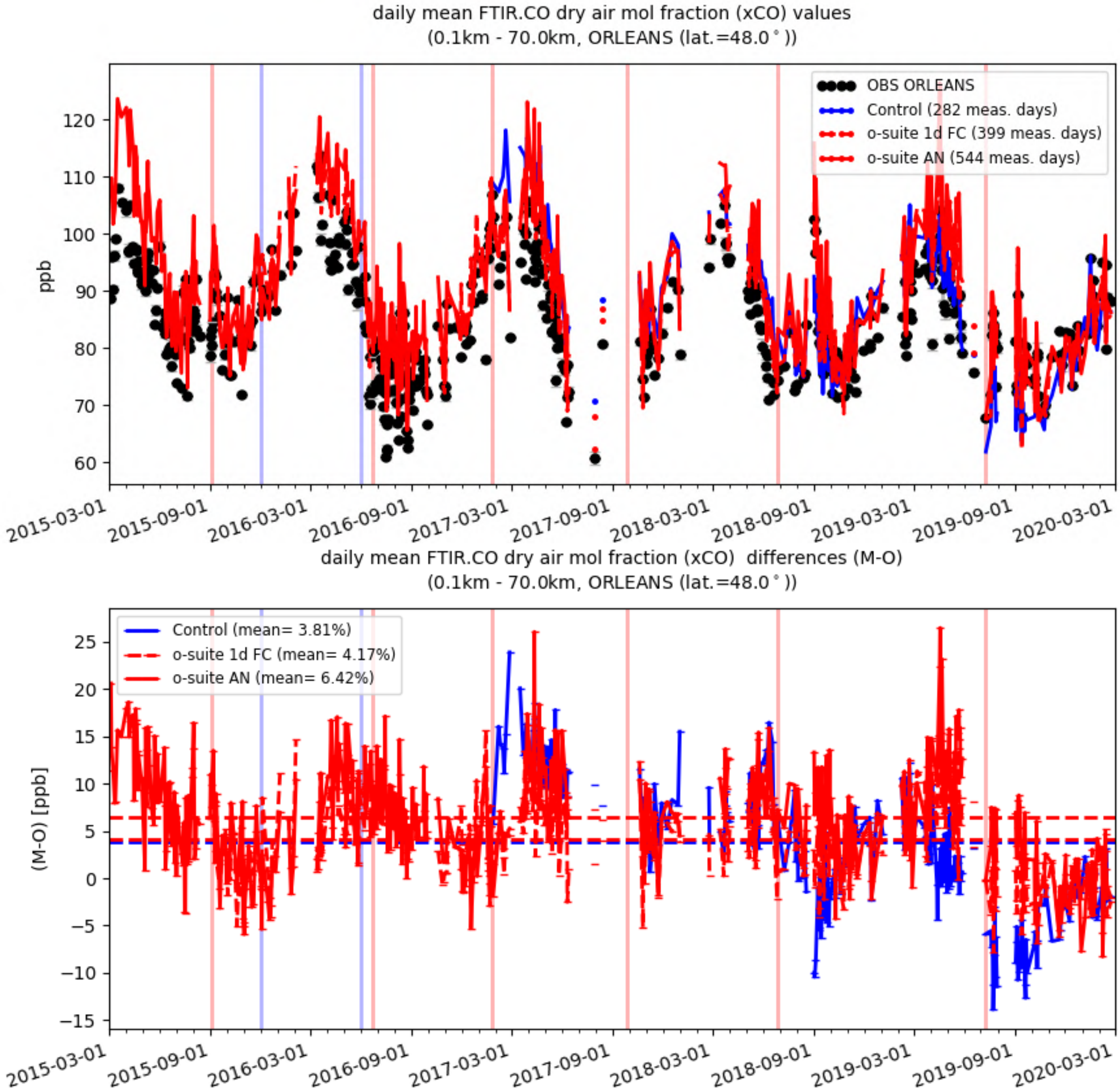

Figure 4.4.2: Comparison of the CO model data with TCCON CO at Orleans.

Izana (Blumenstock et al., 2017), Reunion (De Mazière et al., 2017), Bialystok (Deutscher et al., 2017), Manaus (Dubey et al., 2017), Four Corners (Dubey et al., 2017), Ascension (Feist et al., 2017), Anmeyondo (Goo et al., 2017), Darwin (Griffith et al., 2017), Wollongong (Griffith et al., 2017), Karlsruhe (Hase et al., 2017), Edwards (Iraci et al., 2017), Indianapolis (Iraci et al., 2017), Saga (Kawakami et al., 2017), Sodankyla (Kivi et al., 2017), Hefei (Liu et al., 2018), Tsukuba (Morino et al., 2017), Burgos (Morino et al., 2018), Rikubetsu (Morino et al., 2017), Bremen (Notholt et al., 2017), Spitsbergen (Notholt et al., 2017), Lauder (Sherlock et al., 2017, Pollard et al., 2019), Eureka (Strong et al., 2018), Garmisch (Sussmann et al., 2017), Zugspitze (Sussmann et al., 2018), Paris (Te et al., 2017), Orleans (Warneke et al., 2017), Park Falls (Wennberg et al., 2017), Caltech (Wennberg et al., 2017), Lamont (Wennberg et al., 2017), Jet Propulsion Laboratory (Wennberg et al., 2017), East Trout Lake (Wunch et al., 2017), Nicosia (Petri et al., 2020)

For the validation of the models in December, January and February the sites that made data available were Nicosia, Orleans and Reunion. Nicosia is located on Cyprus and is a new TCCON site, which is operational since mid 2019.

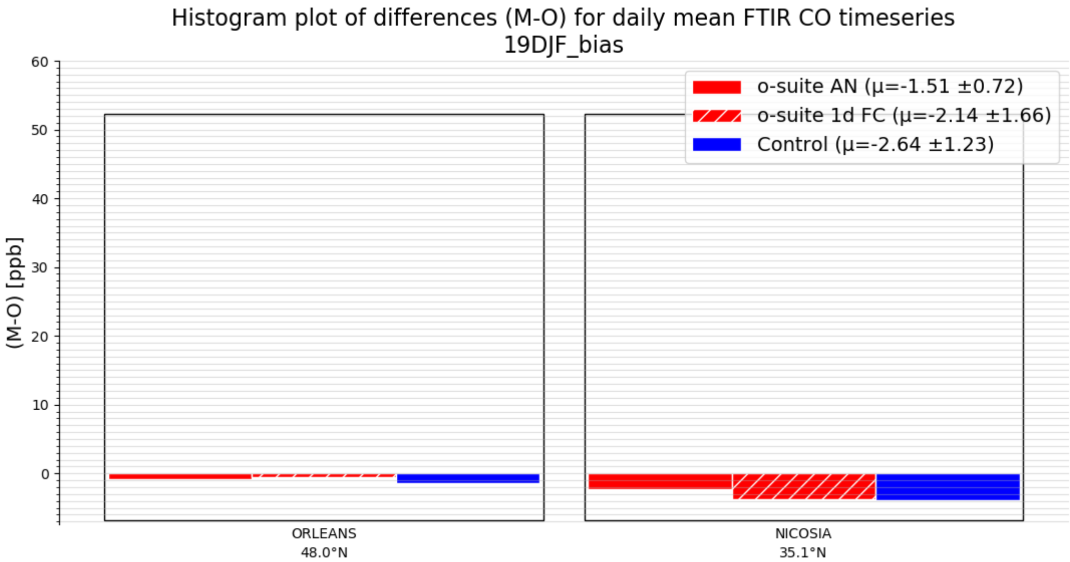

Figure 4.4.3: Differences during the reporting period. The different sites cover different periods of the comparison period.

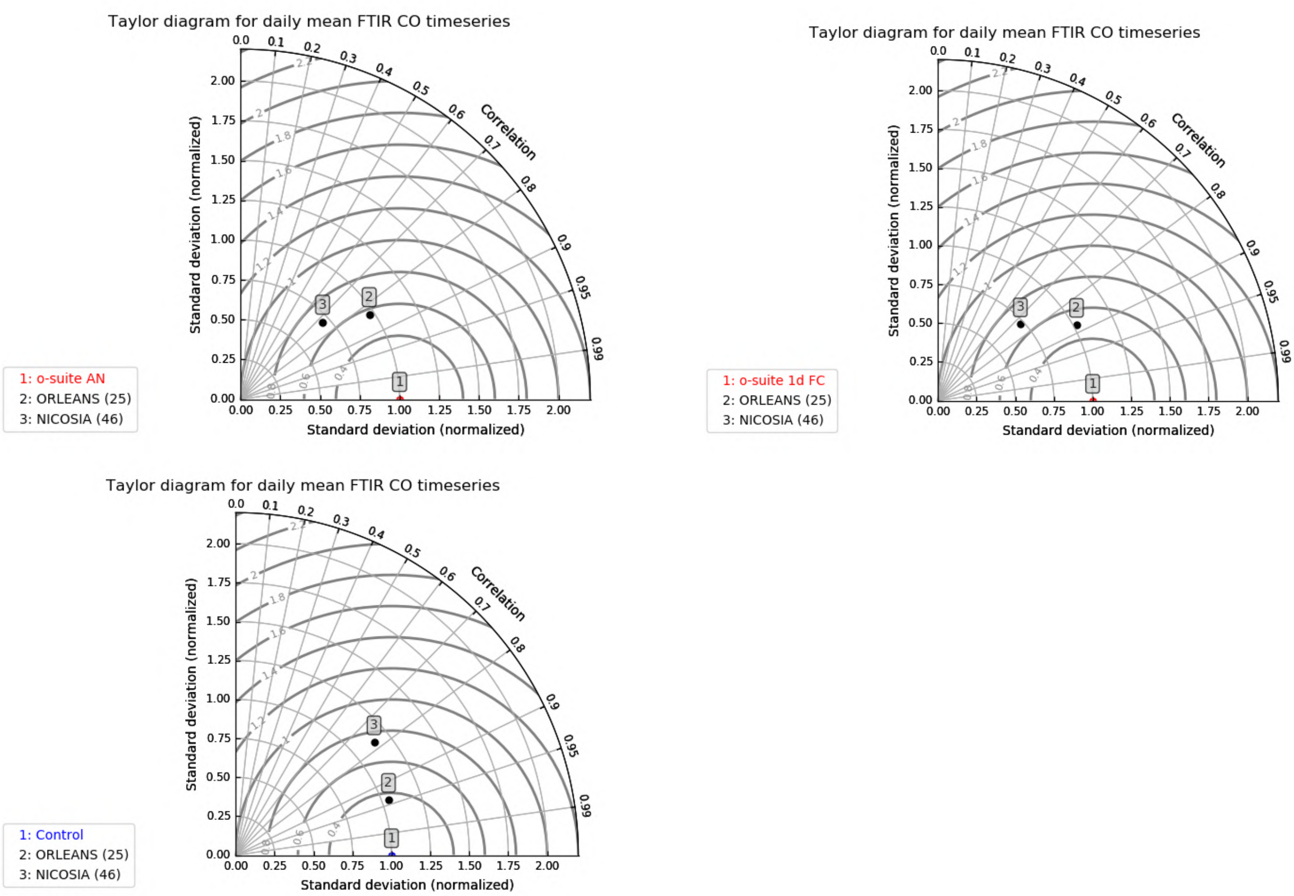

Figure 4.4.4: Taylor diagrams for the comparison period.

The comparisons show that all models capture the seasonality well and the agreement is within 5-10 ppb. For Orleans the comparison is shown in Fig 4.4.2. A significant improvement appears since September 2019 and the differences are small for all 3 sites available for the period of comparison (Fig 4.4.3).

4.5 Evaluation with MOPITT and IASI data

In this section, modelled CO total columns are compared to MOPITT version 8 (thermal infrared radiances) (Emmons et. al., 2009, Deeter et al., 2010) and IASI satellite retrievals (Clerbaux et al., 2009). Figure 4.5.1 shows the global distribution of CO total columns retrieved from MOPITT V8 (top left) and IASI (top right) and the relative biases of the model runs with respect to MOPITT V8 for January 2020.

MOPITT shows high values over the biomass burning area in Central Africa, over the eastern part of China and Indonesia and over the Southeast of Australia and its transportation flux pathway over the Pacific Ocean. IASI shows higher values over the abovementioned regions (except East of China).

The modelled CO geographical distribution and magnitude of values show that the model performs reasonably well. The relative difference between the model runs and MOPITT shows that the o-suite performs better than the control run without data assimilation. The o-suite generally underestimates the satellite data by about 10% with some regional exceptions, where the negative bias reaches 20% (mostly over the land). The model overestimated the Australian CO plume in the transportation pathway over the Pacific Ocean up to 50%. More details about Australian fires are provided in the case study section. The control run shows an overestimation of the satellite data over the low latitudes (except Sahara and biomass burning areas in Africa) and over Eastern China up to 30% and an underestimation over the mid-latitudes up to 20%. The o-suite run shows a growing positive bias on the 4th forecast day over the fire active areas in Central Africa and East of China, as well as a growing negative bias over Sahara and biomass burning area in Africa and some other areas.

Figure 4.5.2 shows time series of CO total column for MOPITT V8, IASI and the model runs over the eight selected regions. For the comparison with MOPITT, the modelled CO concentrations were transformed using MOPITT V8 averaging kernels (Deeter, 2004). Both, MOPITT and IASI CO total columns are assimilated in the o-suite run, while a bias correction scheme is applied to IASI data to bring it in line with MOPITT. MOPITT and IASI CO total columns show a relatively similar variability over different regions. IASI CO values are lower than MOPITT over most regions with some seasonal exceptions till the year 2016. Since then, IASI and MOPITT are more consistent with each other over Europe, the US and East Asia. Significant differences between MOPITT and IASI are observed over the Alaskan and Siberian fire regions in winter seasons, with IASI CO total column values being lower up to 30%. In North and South Africa, deviations become larger since 2016 with IASI values being higher than MOPITT by up to 20%. The modelled seasonality of CO total columns is in relatively good agreement with the retrievals. In general, the comparison between the o-suite and control run shows, that the assimilation of satellite CO has a more positive, pronounced impact on model results over East and South Asia, South Africa, and since the end of 2016, over the US in winter and spring seasons, and smaller impact over the other regions. Since June 2016, the o-suite

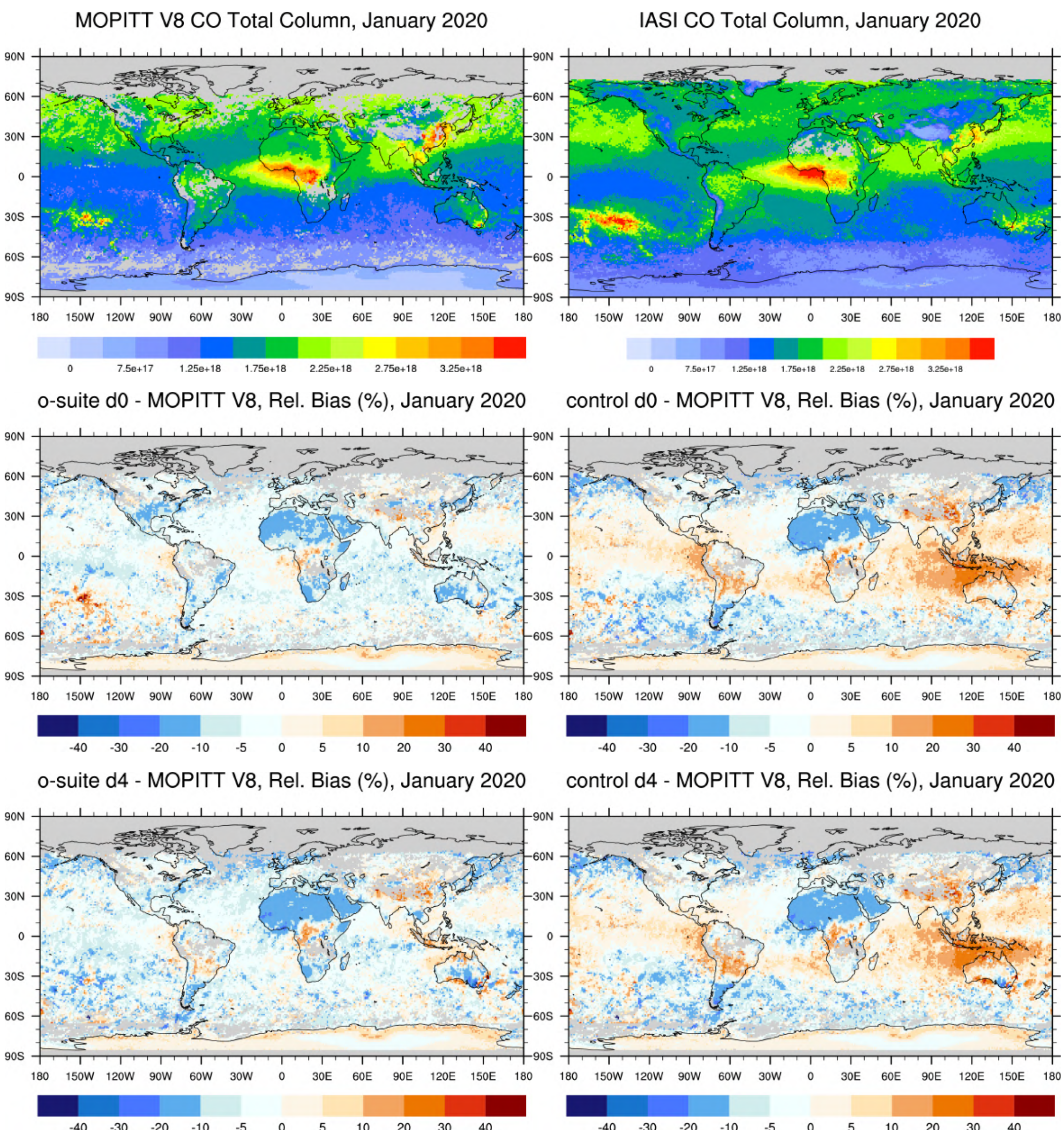

Fig. 4.5.1: CO total columns for MOPITT V8 (top left) and IASI (top right) satellite retrievals and relative difference between the model runs and MOPITT for January 2020: o-suite (middle left), control run (middle right), o-suite 4th forecast day (bottom left), o-suite 4th forecast day (bottom right). Grey colour indicates missing values.

shows very good agreement with the satellite retrievals over Europe and the US with biases less than 5%. In late summer and early autumn of 2018 over Europe, the control run has larger negative biases compared to the satellite data than early in 2018 and the two previous autumn seasons.

A general reduction of CO values from the year 2015 to the year 2018 can be seen over Europe, the US and East Asian regions. The South African region shows a slight increase of the seasonal minimum compared to previous springs.

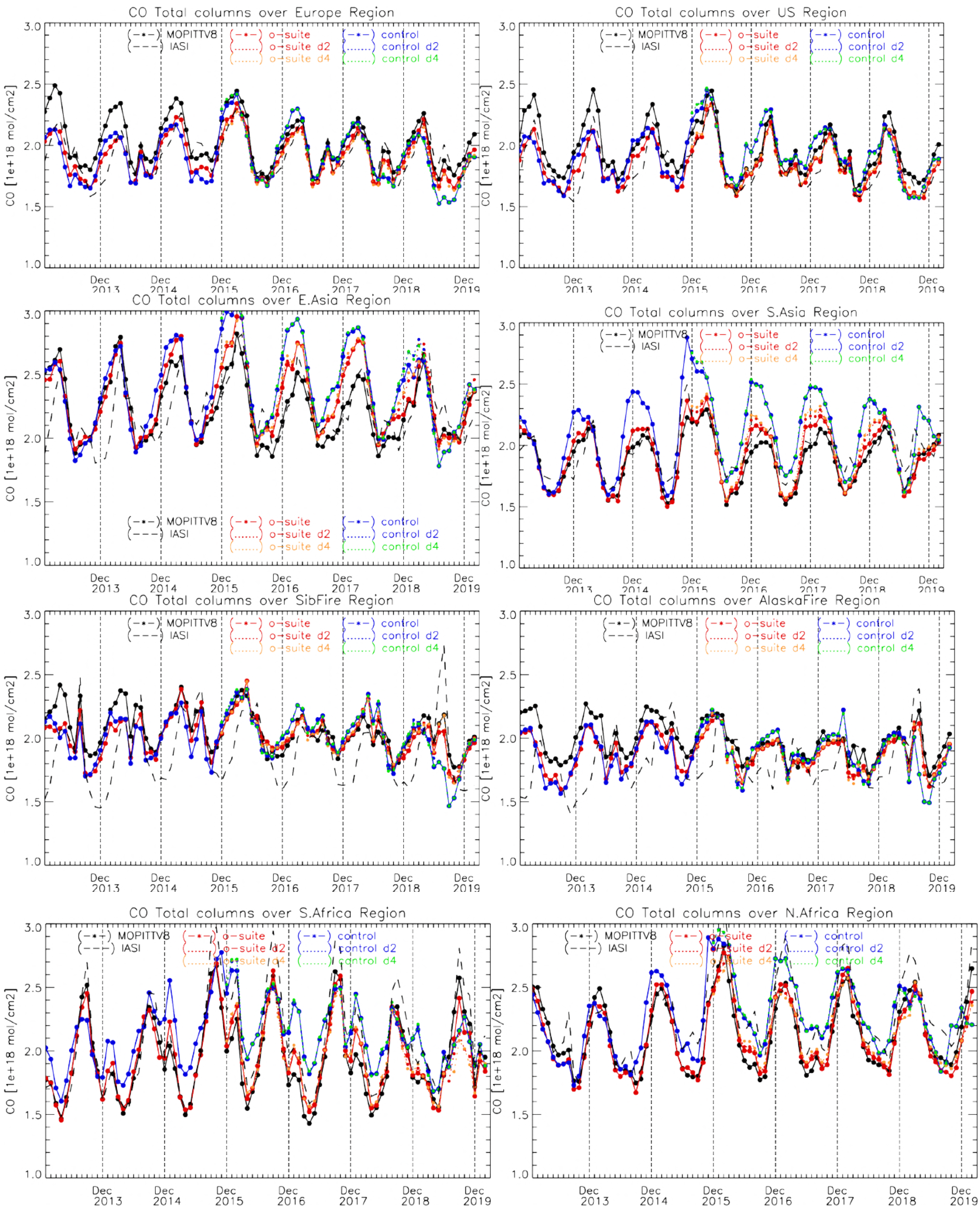

Fig. 4.5.2: Time series of CO total columns for satellite retrievals MOPITT V8, IASI (black) and the model runs over the selected regions: o-suite (red, solid), control (blue, solid), o-suite 2nd forecast day (red, dotted), o-suite 4th forecast day (orange, dotted), control 2nd forecast day (blue, dotted), control 4th forecast day (green, dotted). Period: January 2013 to February 2020.

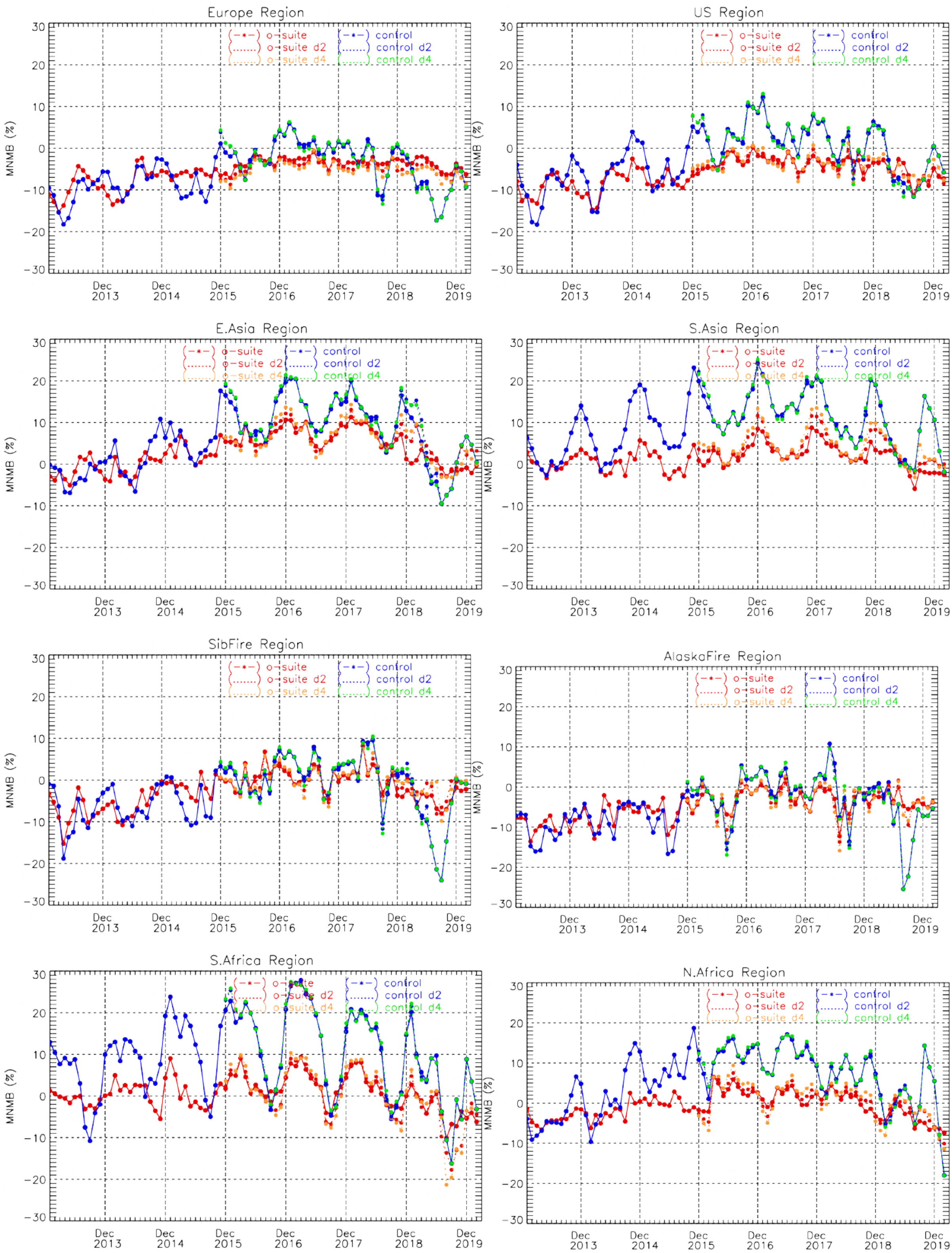

Fig. 4.5.3: Timeseries of modified normalized mean bias (%) for CO total columns from the model simulations vs MOPITT V8 retrievals over selected regions. O-suite (red, solid), control run (blue, solid), o-suite 2nd forecast day (red, dotted), o-suite 4th forecast day (orange, dotted), control 2nd forecast day (blue, dotted), control 4th forecast day (green, dotted). Period: January 2013 to February 2020.

Summer 2019 was characterised by a strong fire events in Siberia. This can be seen in IASI data (peak in August), but it is not reflected in the MOPITT data partly due to only few days of observations available in August.

The modified normalized mean bias (MNMB) of the model runs compared to MOPITT V8 (Fig. 4.5.3) allows quantifying the impact of the assimilation on the model performance. The o-suite model run shows negative biases over Europe, the US and Alaskan fire regions with some seasonal exceptions.

The control run shows a systematic positive bias up to 20% over South Asia in November-December 2014, 2015, 2016, and 2017. Over southern Africa, the control run overestimates satellite retrieved values by up to 25% in winter and spring 2015, 2016, and 2017. In general, the o-suite is within +/- 10% in all regions, while the control run shows larger biases over East and South Asia and North and South Africa, as well as stronger seasonal cycles.

Starting from the second half of the year 2019, the negative biases over Europe and US increase for both runs (from about 5% to about 10% for o-suite). The o-suite results over Asian regions improved and are very close to the observations, especially over East Asia. The control runs also shows strong reductions of biases. A change of bias sign from positive to negative and/or increase of the negative bias can be seen over the Siberian and Alaskan fire regions and African regions for both runs. Non-systematic underestimation of 20% can be seen in the control run in February over North Africa. In general, the increase of underestimation in both runs can be seen over the selected regions, except Asian regions.

5. Tropospheric nitrogen dioxide

5.1 Evaluation against GOME-2 and TROPOMI retrievals

In this section, model columns of tropospheric NO_2 are compared to SCIAMACHY/Envisat NO_2 satellite retrievals (IUP-UB v0.7) [Richter et al., 2005] for model data before April 2012, and to GOME-2/MetOp-A NO_2 satellite retrievals (IUP-UB v1.0) [Richter et al., 2011] for more recent simulations. First comparisons to TROPOMI/Sentinel-5P data (IUP-UB v0.1, preliminary) are provided, using the CAMS o-suite as a-priori in the TROPOMI retrievals. This satellite data provides excellent coverage in space and time and very good statistics. However, only integrated tropospheric columns are available, and the satellite data is always taken at the same local time, roughly 09:30 LT for GOME-2, 10:00 LT for SCIAMACHY and 13:30 LT for TROPOMI and at clear sky only. Therefore, model data are vertically integrated, interpolated in time and then sampled to match the satellite data. The satellite data were gridded to model resolution (currently 0.4° x 0.4° degree). Model data were treated with the same reference sector subtraction approach as the satellite data for all SCIAMACHY/GOME-2 comparisons. For all comparisons to TROPOMI satellite data, tropospheric NO_2 columns over the clean Pacific reference sector simulated by CAMS-global were added to the TROPOMI data, so that the comparison of absolute columns is accomplished. For TROPOMI comparisons before July 2019, the stratospheric contribution has been removed from the measurements according to the method by Hilboll et al. (2013) using simulations from the B3D-CTM (Sinnhuber at al., 2003a; Sinnhuber et al., 2003b; Winkler et al., 2008) scaled to satellite values over the clean Pacific reference sector. Since July 2019, the reference sector method has been applied to the TROPOMI data. Uncertainties in NO_2 satellite retrievals are large and depend on the region and season. Winter values in mid and high latitudes are usually associated with larger error margins. Systematic uncertainties in regions with significant pollution are on the order of 20% – 30%.

Figure 5.1.1 shows global maps of GOME-2 and model monthly mean tropospheric NO_2 columns as well as differences between retrievals and simulations for Jan 2020 as an example for the latest winter. The overall spatial distribution and magnitude of tropospheric NO_2 is well reproduced by both CAMS runs, indicating that emission patterns and NO_x photochemistry are reasonably well represented. Some differences are apparent between observations and simulations, with generally larger shipping signals simulated by the models. For example, shipping signals are much more pronounced in model simulations to the south of India. Emissions over Europe and especially the pollution hotspots around the Benelux countries are regularly underestimated, especially during winter. However, other local maxima of tropospheric NO_2 observed over anthropogenic emission hotspots in East Asia (e.g. over the heavily populated Sichuan Basin; 30°N, 105°E), India and others such as Teheran, Mecca and Moscow and over boreal forest fires (mainly during summer) are regularly overestimated. Likewise, values over the Persian Gulf and the Red Sea are regularly overestimated (mainly summer and autumn). A systematic overestimation of values is visible in the TROPOMI based map comparisons (Figure 5.1.2) in the Northern Hemisphere, resulting in part from the reference sector method applied for stratospheric correction for data since July 2019 (especially for higher northern latitudes) and partly resulting from a more pronounced overestimation over pollution hotspots by the o-suite at the TROPOMI observation time compared to the GOME-2

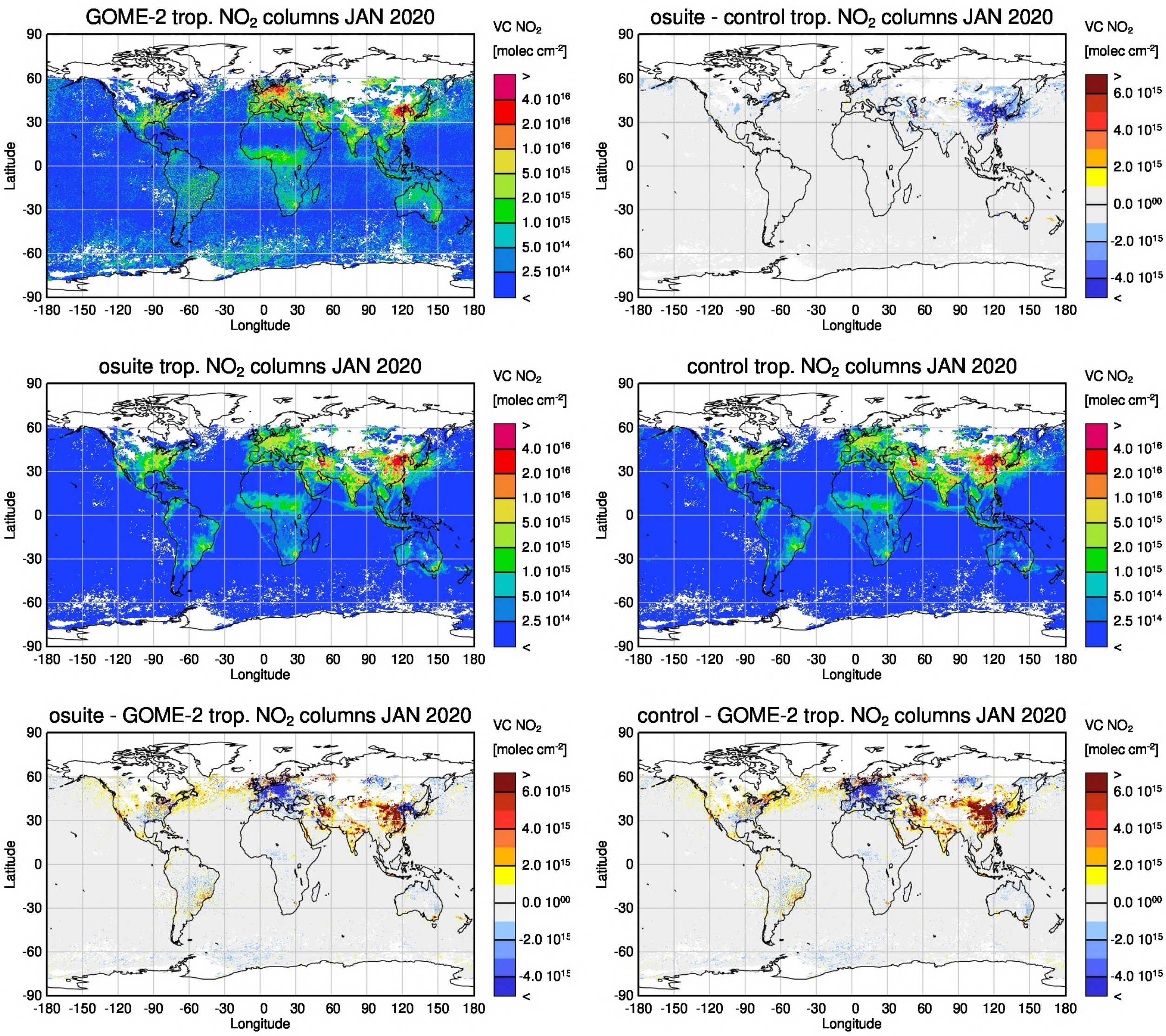

Figure 5.1.1: Global map comparisons of satellite retrieved, and model simulated tropospheric NO_2 columns [molecules cm^{-2}] for Jan 2020. The top row shows monthly mean tropospheric NO_2 columns retrieved from GOME-2 as well as the difference between o-suite and control, the second row shows the corresponding tropospheric NO_2 columns for model simulated averages. The third row shows differences of monthly means between models and GOME-2. GOME-2 data were gridded to model resolution (i.e. 0.4° x 0.4° degree). Model data were treated using the same stratospheric correction method as for the satellite data.

observation time. A first comparison to the operational TROPOMI retrieval product shows similar values on the order of magnitude as the Bremen retrieval product and will be included within one of the next reports.

Closer inspection of the seasonal variation of tropospheric NO_2 in some selected regions (Fig. 5.1.3) reveals significant differences between measurements and model results and points to some simulation problems. Over regions where anthropogenic emissions are major contributors to NO_x emissions, models correctly simulate the occurrence of maxima and minima in seasonality in time, but fail to reproduce the inter-annual variability observed by GOME-2. Over East-Asia, absolute

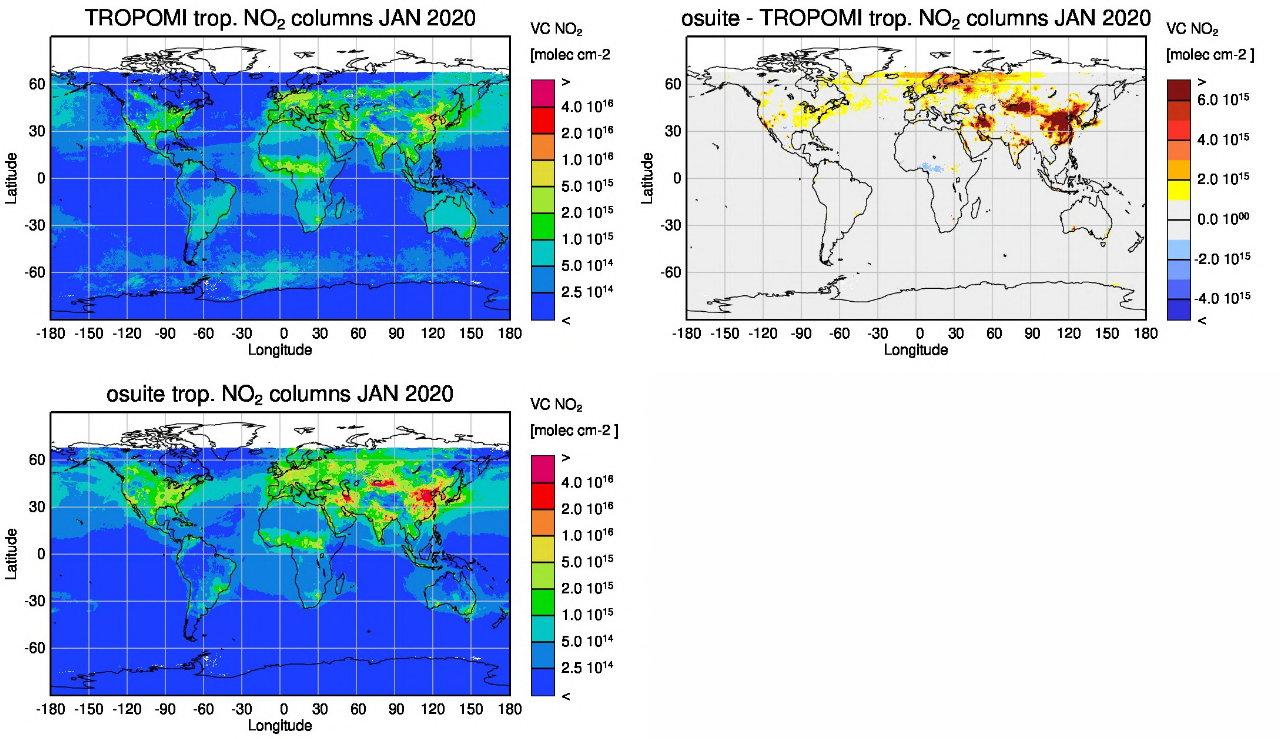

Figure 5.1.2: Global map comparisons of satellite retrieved, and model simulated tropospheric NO_2 columns [molecules cm-2] for Jan 2020: (top left) TROPOMI, (top right) o-suite minus TROPOMI, (bottom left) o-suite. TROPOMI data were gridded to model resolution (i.e. 0.4° x 0.4° degree) and the CAMS o-suite was used as a-priori in the retrievals. Comparisons to the control are not available for this report.

values and seasonality were strongly underestimated before 2014 by all model runs (most likely due to an underestimation of anthropogenic emissions) for all seasons apart from summertime minima, with the o-suite showing the best results since an upgrade in July 2012. As wintertime NO_2 column retrievals decreased significantly in 2014, model simulated wintertime maxima previously have been in better agreement with the satellite retrieved ones for recent years. However, the observed NO_2 decrease was not reproduced by the simulations and therefore the better agreement for more recent years could not be attributed to model improvements. Moreover, summertime model minima increased in 2015 compared to previous years, which is in contrast to the satellite retrievals, so that the simulated values for the summers since 2015 are about 50% larger than satellite retrieved ones. For the first time in the time series, model results for the latest winter season (DJF 2019/2020) overestimate the peak in seasonality, with the control showing a significantly larger overestimation compared to the o-suite. Note that the overestimation occurs already for Dec 2019, in advance of the COVID-19 pandemic in China. The long-term development of model simulated tropospheric NO_2 columns over East-Asia points to inadequate scenarios of emission development.

As for East-Asia, a decrease in satellite retrieved values also occurred in 2015 over Europe where a peak is usually found around January, which was, as a result, only slightly underestimated by the models for January 2015. The underestimation of tropospheric NO_2 columns over Europe may be caused to some extent by a change of emission inventories in 2012. However, the situation changed for the three winter periods between 2015 and 2017, for which GOME-2 shows (compared to previous years) a strong increase in January peak values, combined with a decrease in values for

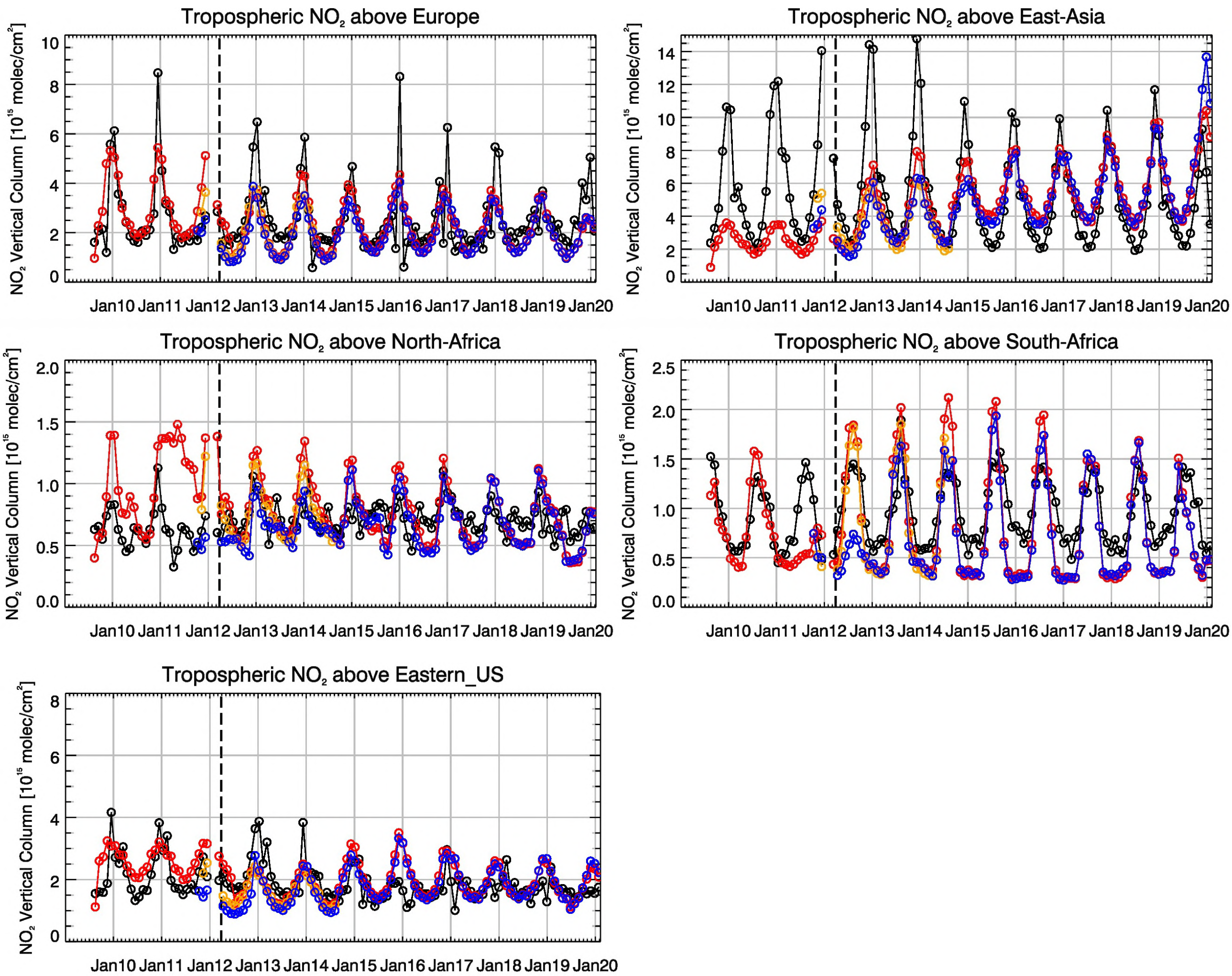

Figure 5.1.3: Time series of average tropospheric NO_2 columns [10^{15} molec cm^{-2}] from SCIAMACHY (up to March 2012, black) and GOME-2 (from April 2012 onwards, black) compared to model results (red: o-suite; blue: MACC-TM5 forecast, MACC-CIFS forecast or control; orange: MACC-MOZART forecasts) for different regions (see Annex 2). The upper panels and lower panel represent regions dominated by anthropogenic emissions, and the panels for Africa represent those dominated by biomass burning. Vertical dashed black lines mark the change from SCIAMACHY to GOME-2 based comparisons in April 2012.

December and February that is not reproduced by the models. It is not clear if the GOME-2 observations are realistic here, although an inspection of daily GOME-2 satellite images did not point to problems regarding the retrieval. The simulations show the same pattern as the retrievals however for winter 2018/2019 but strongly underestimate the retrievals again for the last winter (DJF 2019/2020).

Over regions where biomass burning is the major contributor to NO_x emissions, seasonality and amplitude of model columns are determined by fire emissions. The seasonality for the two regions in Africa was simulated reasonably well for 2010 and after October 2011. In the time period in between, a bug in reading fire emissions lead to simulation errors for all MOZART runs. Over North-Africa, the o-suite shows improved results since an update in July 2012 and the change to IFS-CB05 in September 2014. However, tropospheric NO_2 columns around December are still overestimated

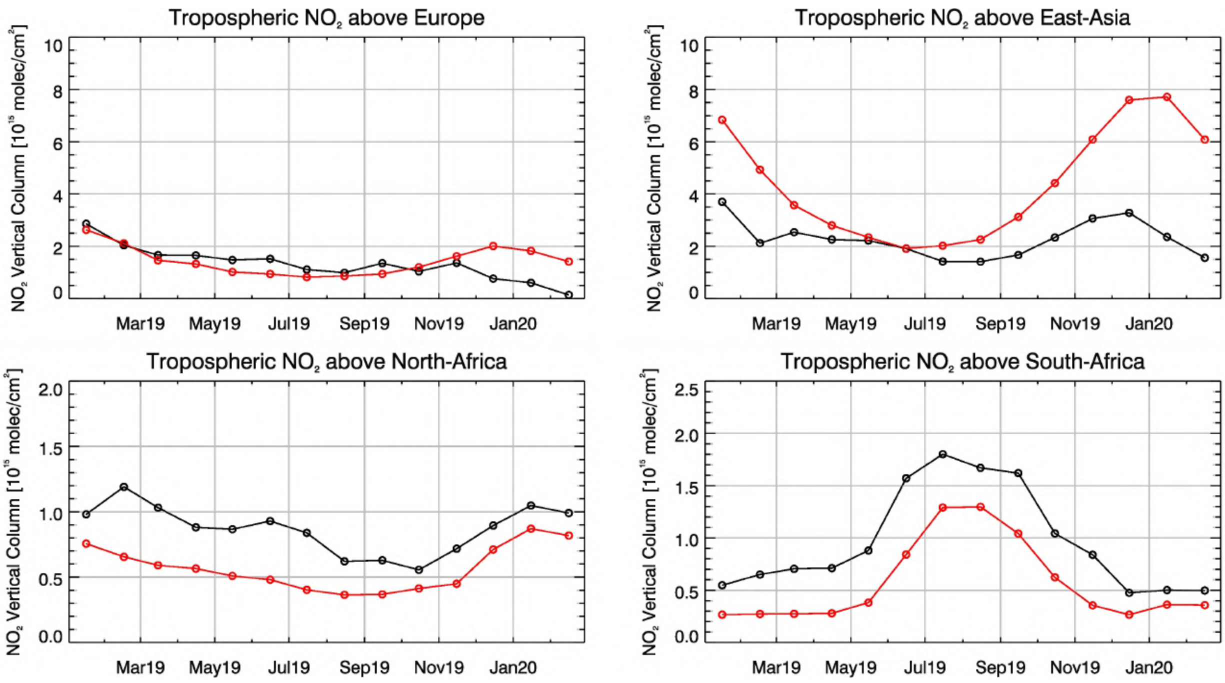

Figure 5.1.4: Time series of average tropospheric NO_2 columns [10^{15} molec cm^{-2}] from (black) TROPOMI compared to (red) o-suite model results since Jan 2019 (see Annex 2 for definition of regions). The upper panels represent regions dominated by anthropogenic emissions, and the lower panels represent those dominated by biomass burning.

by the models. Summer to autumn NO_2 columns over North-Africa are underestimated compared to the satellite data from 2015 onwards and especially for 2019. The models (especially the o-suite) generally overestimate the seasonal cycle for South-Africa, particularly for 2014-2016 with an overestimation of the seasonal maximum, which usually occurs around August (e.g. by a factor of 1.4 larger compared to GOME-2 retrievals in 2016). However, August maxima are in better agreement since the upgrade of the o-suite in 2017, but minima during SH summer remain underestimated.

Time series comparisons between the o-suite and TROPOMI are shown in Figure 5.1.4 since January 2019. They show some differences with respect to the GOME-2 based ones: the o-suite generally overestimates values over East-Asia and underestimates values over the African regions and simulations are close to the satellite observations over Europe according to the TROPOMI based comparisons. In contrast to the GOME-2 comparisons, the seasonal cycle over South-Africa is not overestimated Differences in comparison results are in principal due to differences in observation time or differences in the retrieval products.

More NO_2 evaluation plots can be found on the CAMS website, see table 1.2.

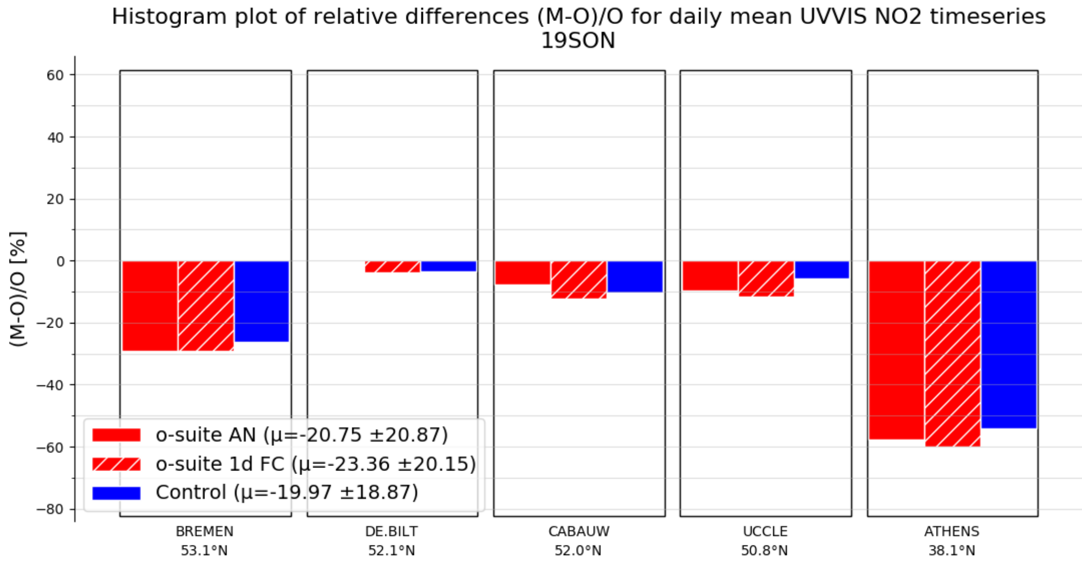

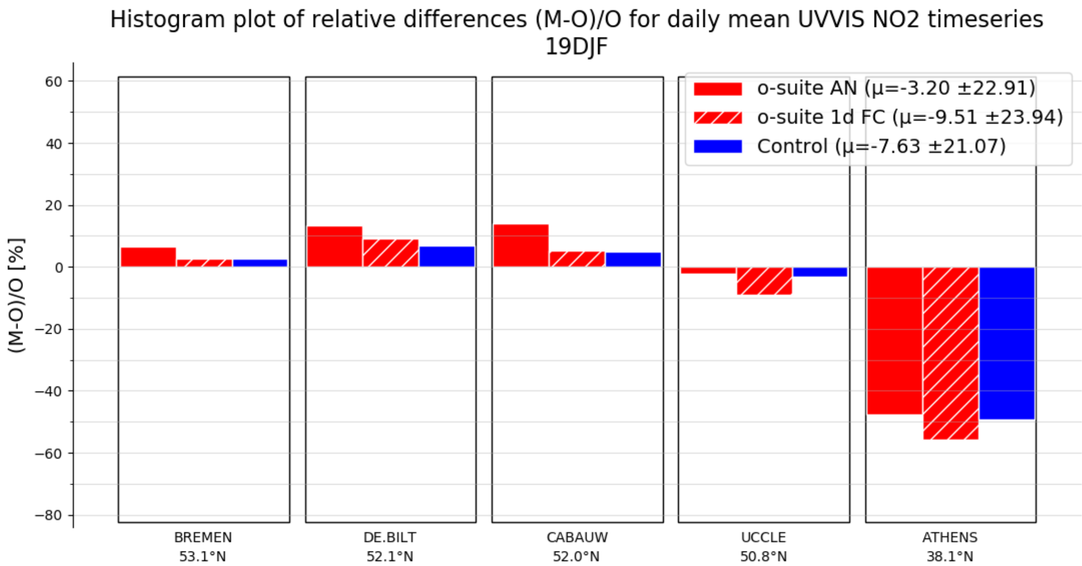

Figure 5.2.1: Table diagram showing the seasonal bias Sep-Nov 2019 (top) and Dec-Feb 2020 (bottom) for five stations, sorted by latitude. Compared to the previous validation period SON, the relative biases in DJF did not change significantly. Figure 5.2.1 shows the biases for the latest validation periods Sept-Nov 2019 and Dec-Feb 2020 at the different sites. At the urban sites at Uccle and Athens a strong underestimation is observed. For the other sites (Bremen, De Bilt and Cabauw) the o-suite AN is able to capture only few of the high pollution events.

5.2 Evaluation against ground-based DOAS observations

In this section, we compare the NO_2 columns of the CAMS products with UVVIS DOAS profile measurements at Uccle and column data from the other stations.[1] This ground-based, remote-sensing instrument is sensitive to the NO_2 abundance in the lower troposphere, up to 1km altitude

[1] No contribution from Xianghe, Reunion and OHP due to instrument failure.

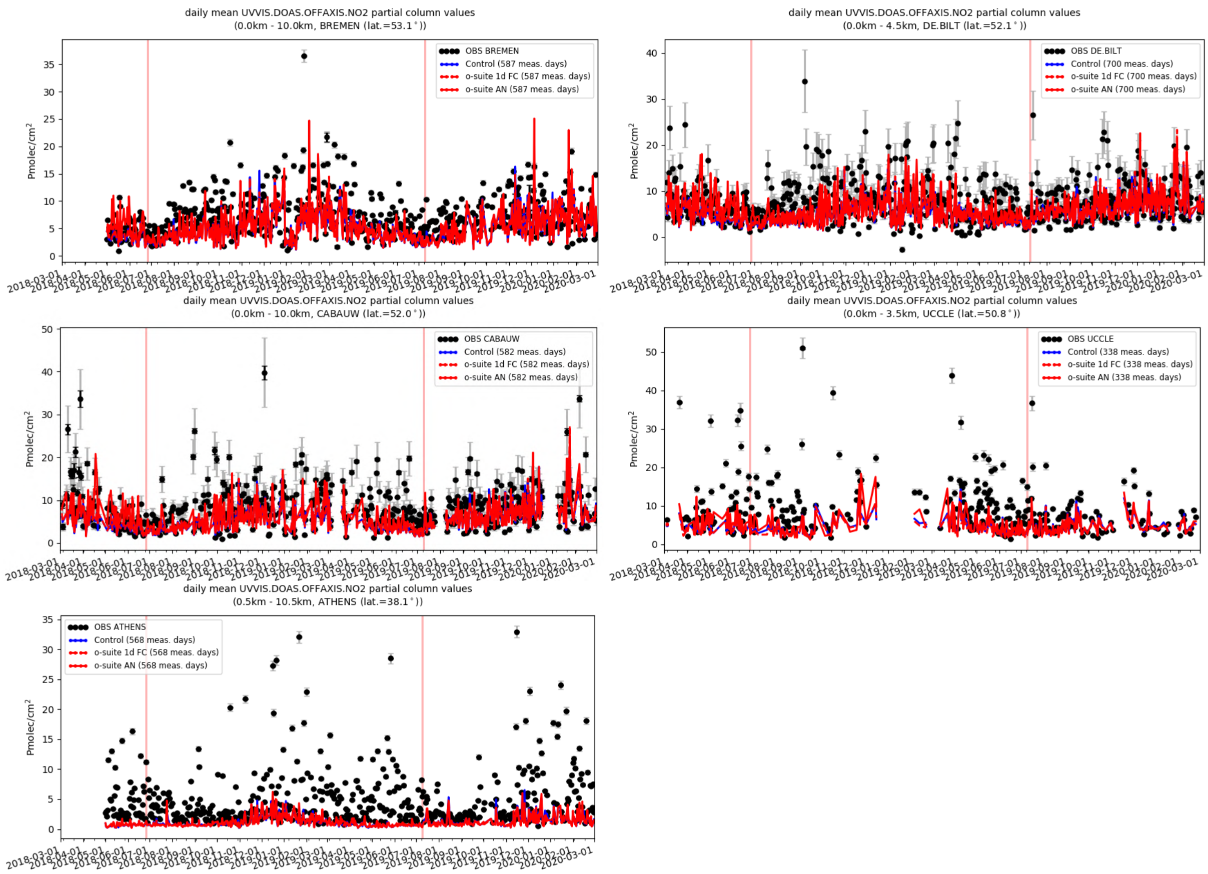

Figure 5.2.2: Time series of NO_2 partial columns at the five different sites. For all sites except Athens, background concentrations are well captured by the CAMS products. The o-suite and control product show little difference.

with an estimated uncertainty of 8%. Tropospheric NO_2 profiles and columns are validated (up to 3.5km or 10km). A description of the instruments and applied methodologies is the same for all DOAS OFFAXIS measurements, see http://nors.aeronomie.be. It is important to mention here that the model partial column values are calculated from the smoothed model profiles. This guarantees that the model levels where the measurement is not sensitive do not contribute to the observed bias. We should mention that the measurement data is still catalogued as rapid delivery and not in the consolidated NDACC database.

Figure 5.2.1 shows the biases for the latest validation periods Sept-Nov 2019 and Dec-Feb 2020 at the different sites. The corresponding time series are shown in Fig. 5.2.2. At the urban sites at Uccle and Athens a strong underestimation is observed. For the other sites (Bremen, De Bilt and Cabauw) the o-suite is able to capture only few of the high pollution events.

6. Formaldehyde

6.1 Validation against satellite data

In this section, simulations of tropospheric formaldehyde are compared to SCIAMACHY/Envisat HCHO satellite retrievals (IUP-UB v1.0) [Wittrock et al., 2006] for model data before April 2012 and to GOME-2/MetOp-A HCHO data (IUP-UB v1.0) [Vrekoussis et al., 2010] afterwards. First comparisons to TROPOMI/Sentinel-5P data (IUP-UB v1.0) are provided, using the CAMS o-suite as a-priori in the TROPOMI retrievals. The HCHO retrievals are described in Alvarado et al. (2019). As the retrieval is performed in the UV part of the spectrum where less light is available and the HCHO absorption signal is smaller than that of NO_2, the uncertainty of monthly mean HCHO columns is relatively large (20% – 40%) and both noise and systematic offsets have an influence on the results. However, absolute values and seasonality are retrieved more accurately over HCHO hotspots.

In Figure 6.1.1, monthly mean satellite HCHO columns from GOME-2 are compared to model results for Jan 2020 as an example for the latest winter. The magnitude of oceanic and continental background values and the overall spatial distribution are well represented by the o-suite and control. The models regularly overestimate values over regions in Central Africa, which could be due to fire or biogenic emissions. This appears less pronounced for autumn 2019 compared to recent years. Moreover, HCHO columns over regions with fire and biogenic emissions in Northern Australia were regularly overestimated mainly during SON and DJF, but this appears much less pronounced since 2019. So far similar conclusions arise from TROPOMI based map comparisons (see Figure 6.1.2 for Jan 2019) though the magnitude of the differences between observations and simulations differs and though an overestimation over Northern Australia still occurs. Differences in comparison results are in principal due to differences in observation time or differences in the retrieval products.

Time series in Fig. 6.1.3 highlight three cases:

- East-Asia and the Eastern US, where HCHO is dominated by biogenic emissions. Model results and measurements generally agree rather well. However, all model runs underestimate the yearly cycle over East-Asia since 2012. In contrast to MOZART runs, MACC_CIFS_TM5 overestimated satellite values for the Eastern US since the middle of 2013. However, the newer IFS-CB05 runs perform well for Eastern US since 2015. For recent years and both regions, there is virtually no difference between the most recent o-suite run with IFS-CB05 chemistry and the corresponding control run without data assimilation. The variability or “ups and downs” in HCHO columns observed by GOME-2 since December 2014 is due to the lack of data (caused by instrument degradation) for these regions during winter in the Northern Hemisphere, leading to e.g. the negative values in the GOME-2 time series for Eastern US since December 2015. Summertime maxima are still underestimated over East-Asia despite of the higher resolution of the model runs since 2016.

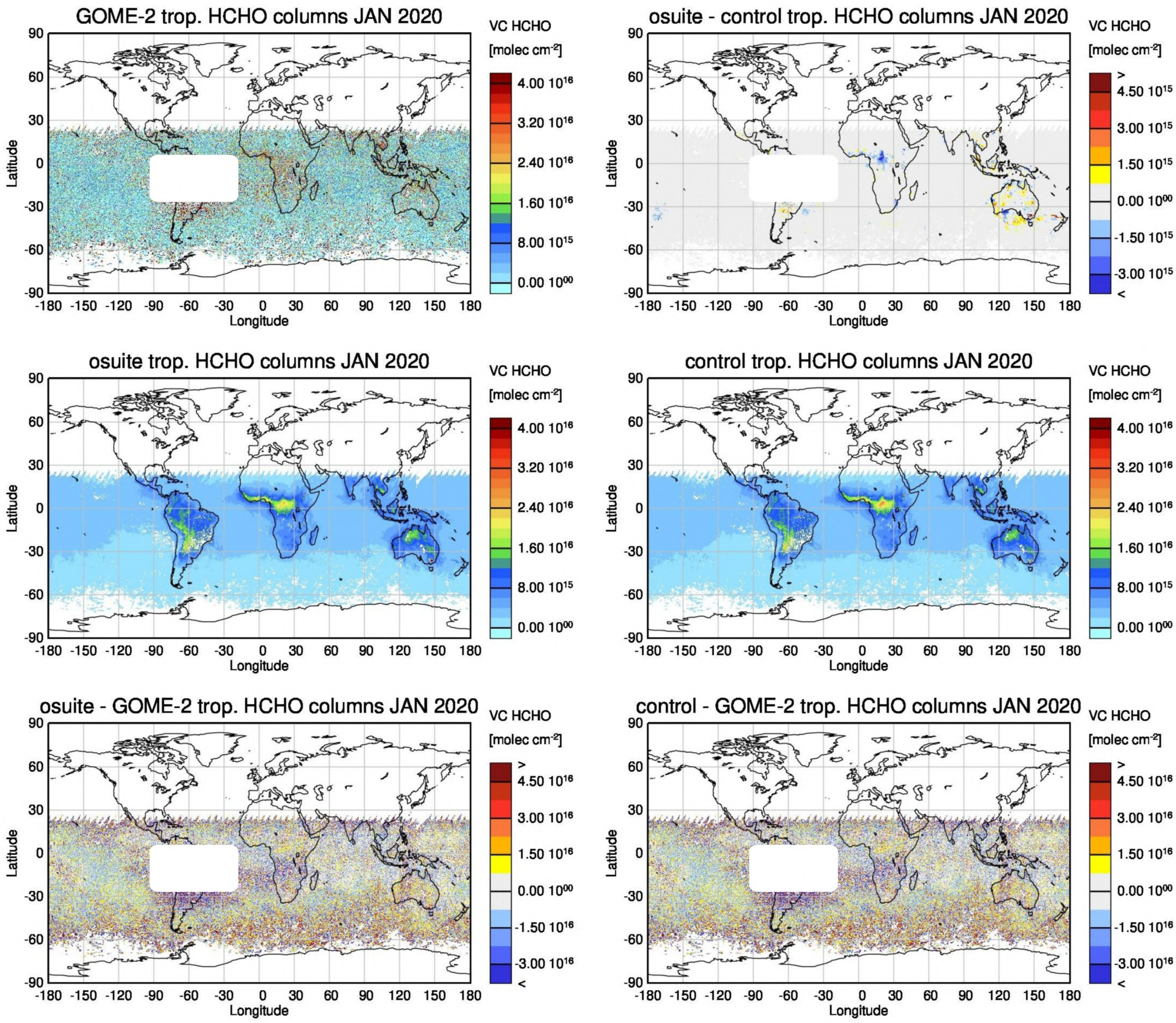

Figure 6.1.1: Global map comparisons of satellite-retrieved and model-simulated tropospheric HCHO columns [molec cm-2] for Jan 2020. The top row shows monthly mean tropospheric HCHO columns retrieved by GOME-2, the second row shows the same but for model simulated averages. The third row shows differences of monthly means between models and GOME-2. GOME-2 data were gridded to model resolution (i.e. 0.4° deg x 0.4° deg). Model data were treated with the same reference sector subtraction approach as the satellite data. Satellite retrieved values in the region of the South Atlantic anomaly are not valid and therefore masked out (white boxes in all images except those which show model results only).

- North-Africa, where biomass burning as well as biogenic sources largely contribute to HCHO and its precursors. Satellite observations over North-Africa tend to be slightly overestimated by IFS-CB05 chemistry model runs since 2014 and also the latest higher resolution model versions since July 2016. However, GOME-2 values are higher, and model values a bit lower for summer 2019 compared to previous years, resulting in a pronounced underestimation with respect to the satellite observations. Moreover, the model simulated HCHO columns increase from summer throughout autumn 2019, though the satellite observed columns show opposite development.

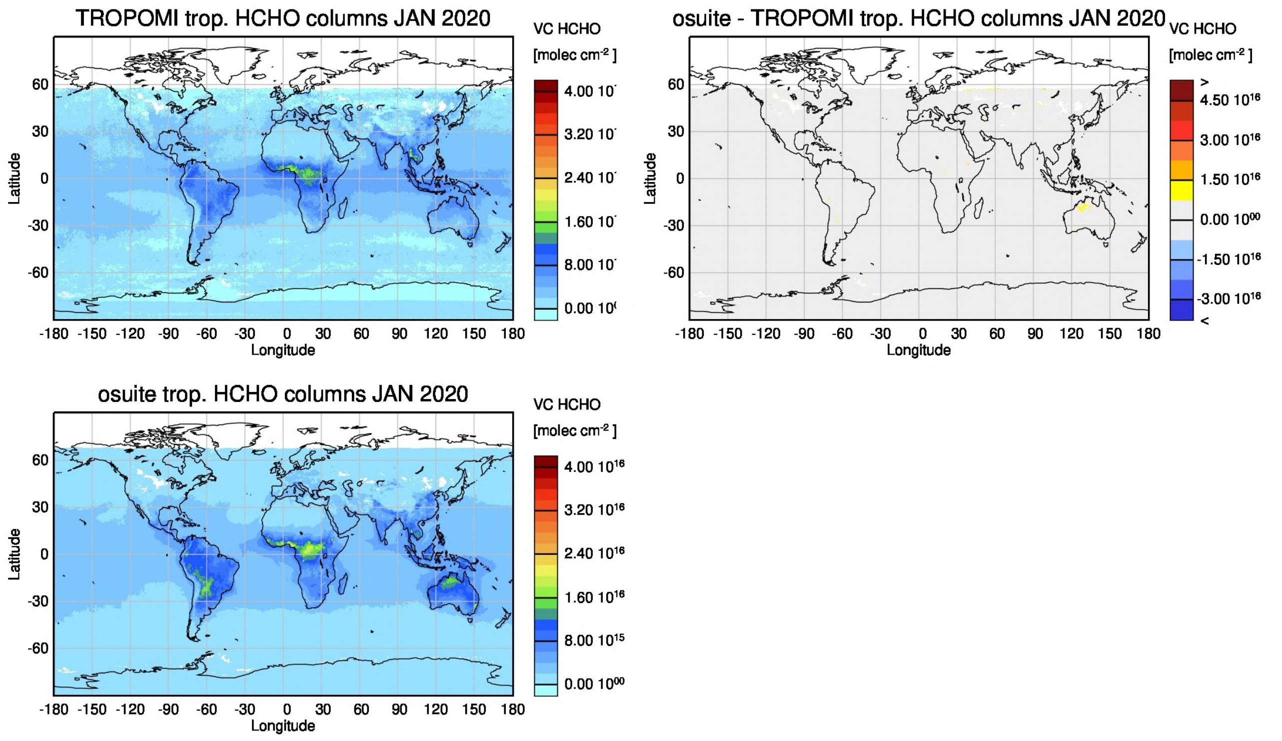

Figure 6.1.2: Global map comparisons of satellite retrieved, and model simulated tropospheric HCHO columns [molec cm^{-2}] for Jan 2020: (top left) TROPOMI, (top right) o-suite minus TROPOMI, (bottom left) o-suite. TROPOMI data were gridded to model resolution (i.e. 0.4° x 0.4° degree) and the CAMS o-suite was used as a-priori in the retrievals. Comparisons to the control are not available for this report.

- Indonesia, where HCHO is also dominated by biogenic sources and biomass burning. Old MOZART based model versions generally overestimated satellite values here (by a factor of 3 – 4 in the second half of 2010) and failed to reproduce the observed seasonality. This may be due to the use of fire emissions including El Nino years, which experience much larger fire activities. MOZART simulations and observations agreed much better since late 2012. IFS-CB05 runs agree very well with satellite retrieved ones for December 2014 to August 2015. For September and October 2015, satellite retrieved HCHO columns show a pronounced maximum. 2015 was a strong El Nino year, which caused droughts and higher fire activity in Indonesia. Another pronounced, but by the models overestimated, increase in satellite observed values associated with comparatively weaker El Nino conditions occurs for Sep 2019. As for previous El Nino years, fire emissions used by IFS-CB05 seem to be largely overestimated, resulting in model-simulated HCHO columns, which are up to twice as large as those retrieved by GOME-2. Further investigations (see previous reports) show that this is not caused by cloud flagging applied to the satellite and model data. Between the middle of 2016 and Sep 2019 there was mainly little variation from one month to another in both, satellite observations and model simulations and the magnitude of model and satellite values agreed overall well.

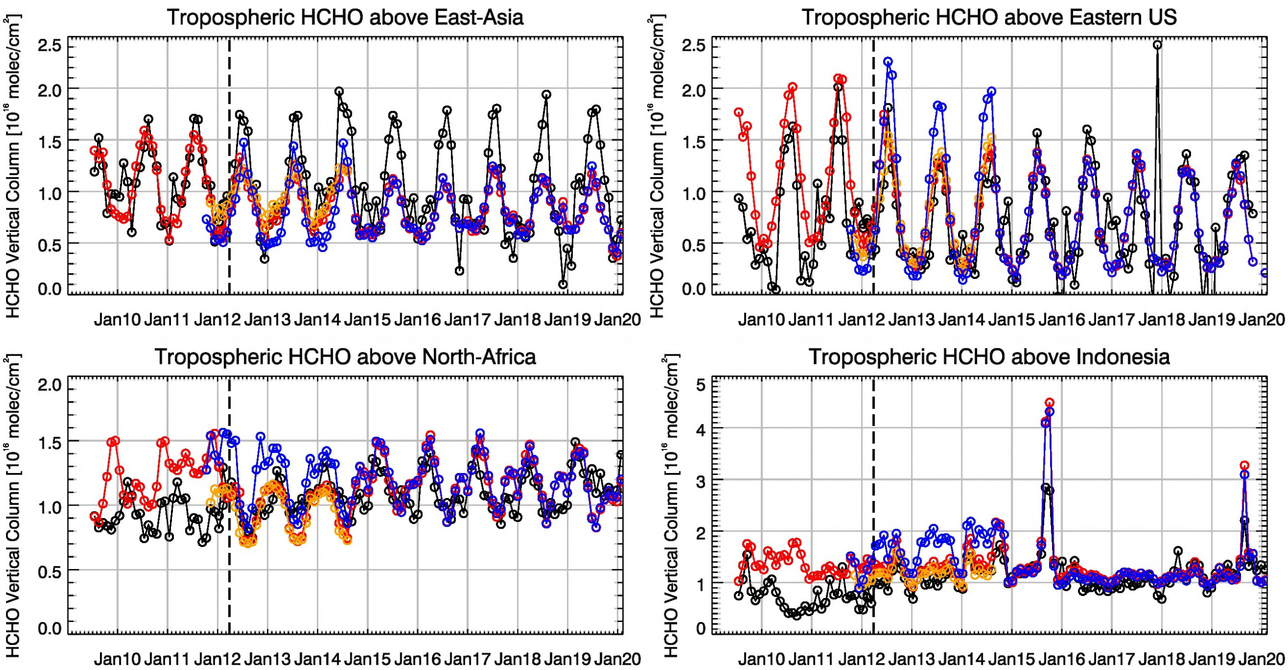

Figure 6.1.3: Time series of average tropospheric HCHO columns [1016 molec cm-2] from SCIAMACHY (up to March 2012, black) and GOME-2 (from April 2012 onwards, black) compared to model results (red - osuite, blue - MACC_fncrt_TM5/MACC_CIFS_TM5/control, orange - MACC_fcnrt_MOZ) for different regions. The blue line shows MACC_fcnrt_TM5 from November 2011 to November 2012, MACC_CIFS_TM5 results from December 2012 to August 2014 and control results from September 2014 onwards (the model run without data assimilation is termed control since Sep 2014). The regions differ from those used for NO2 to better focus on HCHO hotspots: East-Asia (25-40°N, 110-125°E), Eastern US (30-40°N, 75-90°W), Northern Africa (0-15°N, 15°W-25°E) and Indonesia (5°S-5°N, 100-120°E). Negative satellite retrieved values over Eastern US are due to a lack of data (caused by instrument degradation) during Northern Hemisphere winter months for this region. Vertical dashed black lines mark the change from SCIAMACHY to GOME-2 based comparisons in April 2012.

Time series comparisons between the o-suite and TROPOMI are shown in Figure 6.1.4 since September 2019. They show differences with respect to the GOME-2 based ones: the peak over Indonesia for Sep 2019 is much less pronounced for both the o-suite and satellite observations, the development of values in time is in agreement over North-Africa. Apart from Indonesia, the osuite agrees well with the retrievals over Eastern-US for the latest winter, differences between observations and the o-suite are generally less pronounced. Differences in comparison results are in principal due to differences in observation time or differences in the retrieval products.

For details on the HCHO evaluation: http://www.doas-bremen.de/macc/macc_veri_iup_home.html

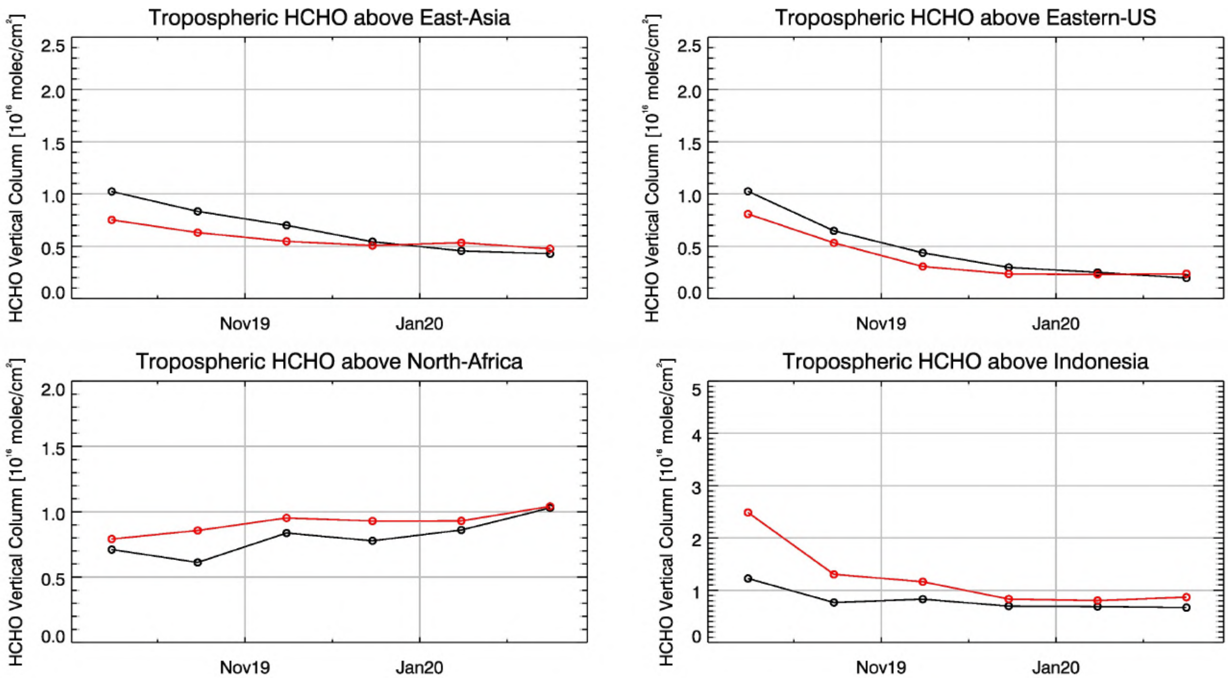

Figure 6.1.4: Time series of average tropospheric HCHO columns [1016 molec cm-2] from (black) TROPOMI compared to (red) o-suite model results since September 2019 (see Annex 2 for definition of regions). The regions differ from those used for NO2 to better focus on HCHO hotspots: East-Asia (25-40°N, 110-125°E), Eastern US (30-40°N, 75-90°W), Northern Africa (0-15°N, 15°W-25°E) and Indonesia (5°S-5°N, 100-120°E).

6.2 Evaluation against ground-based DOAS observations

In this section, we compare the HCHO columns of the CAMS products with UVVIS DOAS measurements at Uccle, Cabauw and De Bilt.[2] These ground-based, remote-sensing instruments are sensitive to the HCHO abundance in the lower troposphere. Tropospheric HCHO profiles and columns are validated (up to 3.5km (Uccle) or 10km (Cabauw and De Bilt)). The validation methodology is the same as for the MWR O_3 and FTIR O_3 and CO validations see http://nors.aeronomie.be. It is important to mention here that the model partial column values are calculated for the smoothed model profiles. This guarantees that the model levels where the measurement is not sensitive do not contribute to the observed bias. We should mention that the measurement data is catalogued as rapid delivery and not in the consolidated NDACC database.

Figure 6.2.1 shows the absolute biases December 2019 – February 2020 at the different sites and indicates strongly reduced biases for the different sites. At all three sites high pollution events are not captured by the model and leads to a higher overall underestimation (Fig 6.2.2). From Fig. 6.2.1 and 6.2.2 we see little difference between the o-suite and the control run. Although the background column values are well captured by the products, the high emission events are not.

[2] No contribution from Reunion, Xianghe and OHP due to instrument failure.

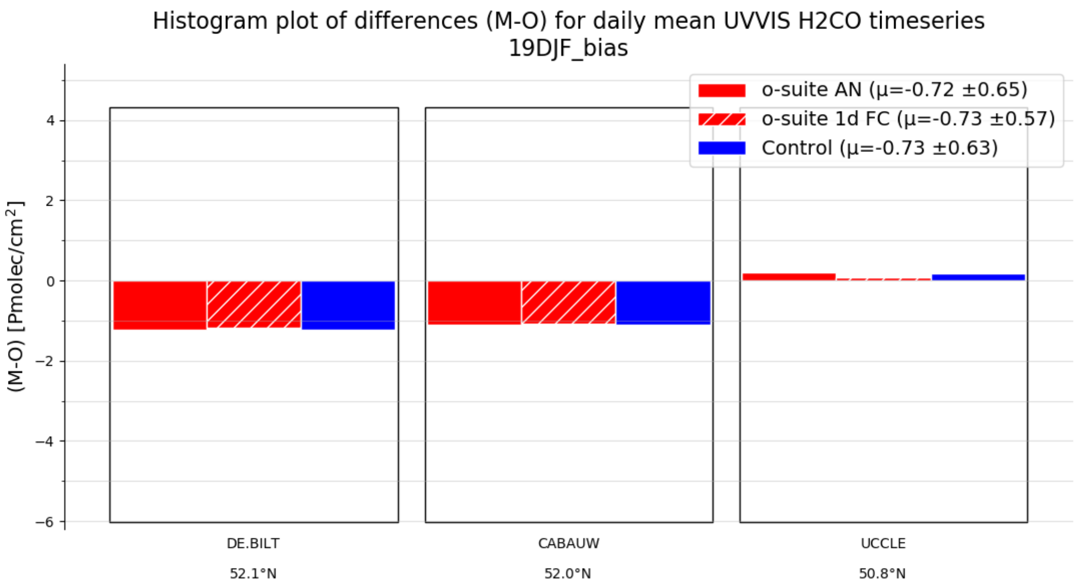

Figure 6.2.1: Table diagram showing the seasonal absolute bias in DJF 2019/2020 for three stations, sorted by latitude.

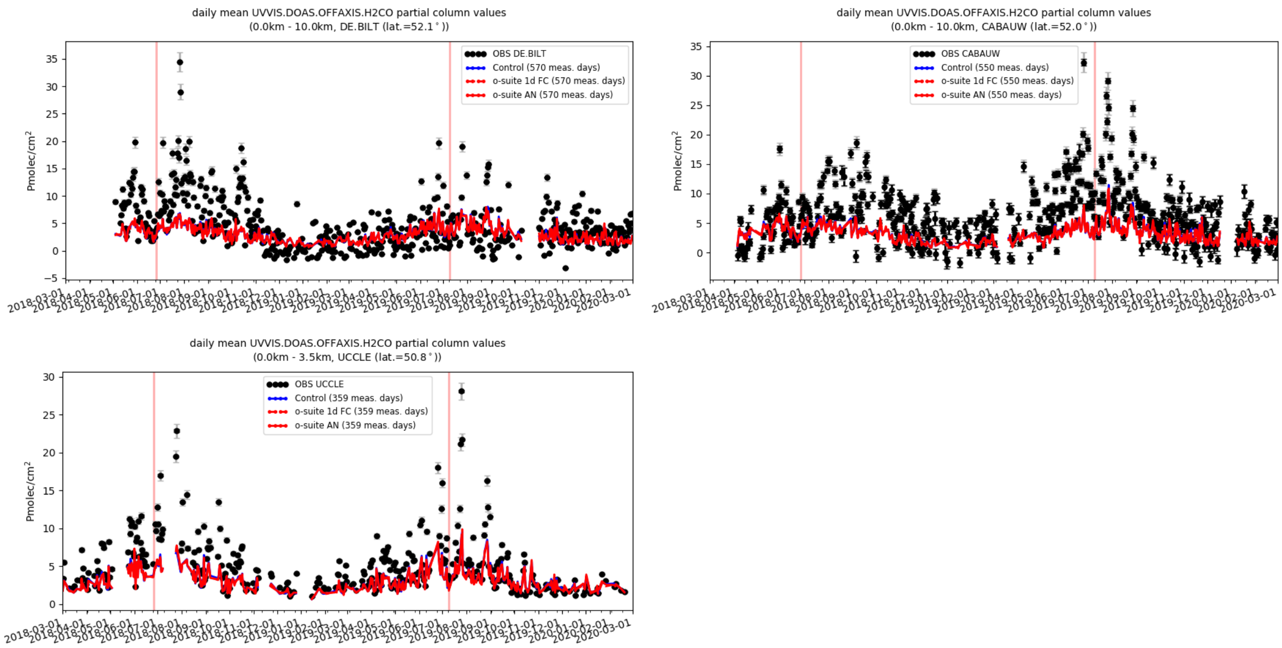

Figure 6.2.2: Time series of HCHO partial columns at the five different sites. All CAMS products underestimate the HCHO concentrations, except at De Bilt, where the model overestimates during the winter months.

7. Water vapour

Water vapour observations are available almost continuously from IAGOS take-offs and landings at Frankfurt during DJF 2020 until mid-February (Fig. 7.1). The results from the o-suite and control run are very similar at all levels for water vapour, as expected (Fig.7.1, Fig. 7.2 and Fig. 7.3). The variability of water vapour during DJF is well represented by the models in all layers (Fig. 7.1). In the lowest layers, the two runs agree well with the observations with a small bias (mostly positive) with values generally below 20% (Fig. 7.2) and a correlation coefficient higher than 90% (Fig. 7.3).

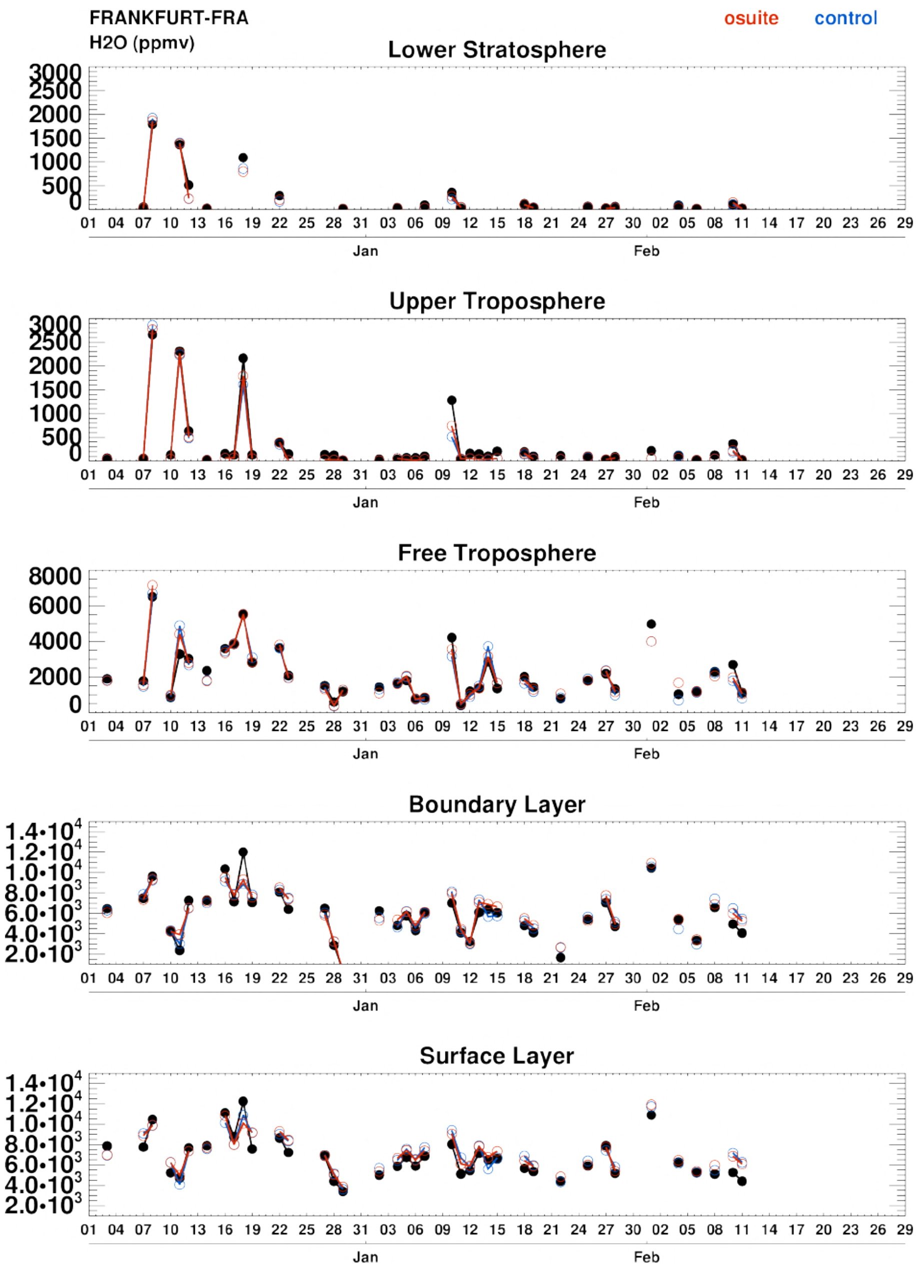

Figure 7.1: Time series of daily mean H_2O vapour over Frankfurt during DJF 2020 for 5 layers: Surface Layer, Boundary Layer, Free Troposphere, Upper Troposphere and Lower Stratosphere. The o-suite is shown in red and associated control run in blue. Units: ppmv.

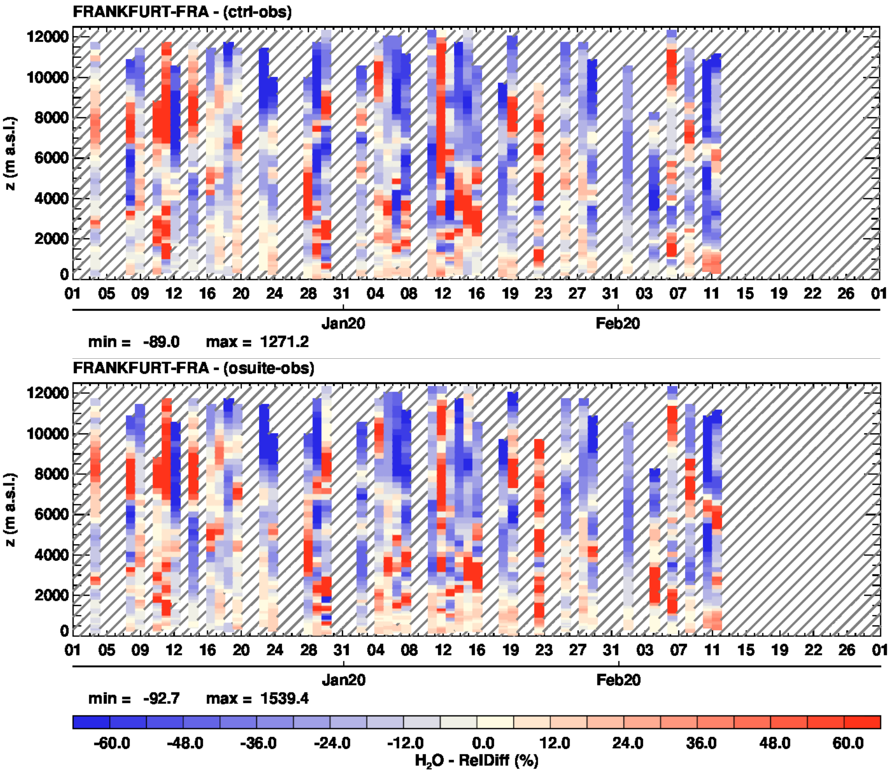

Figure 7.2: Time series of the relative differences ([model – observations]/observations) in daily profiles for CO over Frankfurt during DJF 2020. The top panel corresponds to o-suite the bottom panel to control run. Units: %.

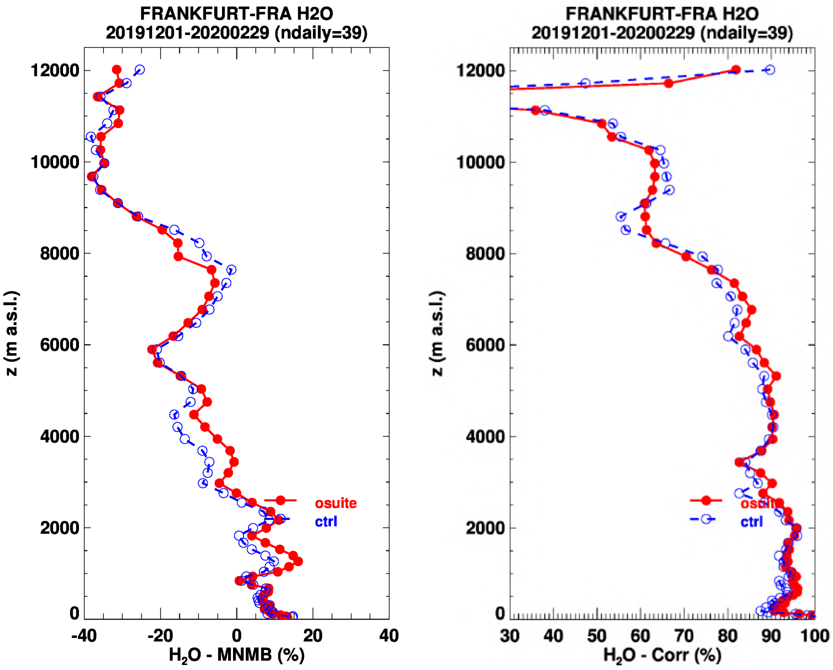

Figure 7.3: Model scores (MNMB and Correlation coefficient) for water vapour at Frankfurt calculated over the period DJF 2020. The left panel corresponds to MNMB and the rightpanel to Correlation coefficient. The o-suite is shown in red and associated control run in blue. Units: %.

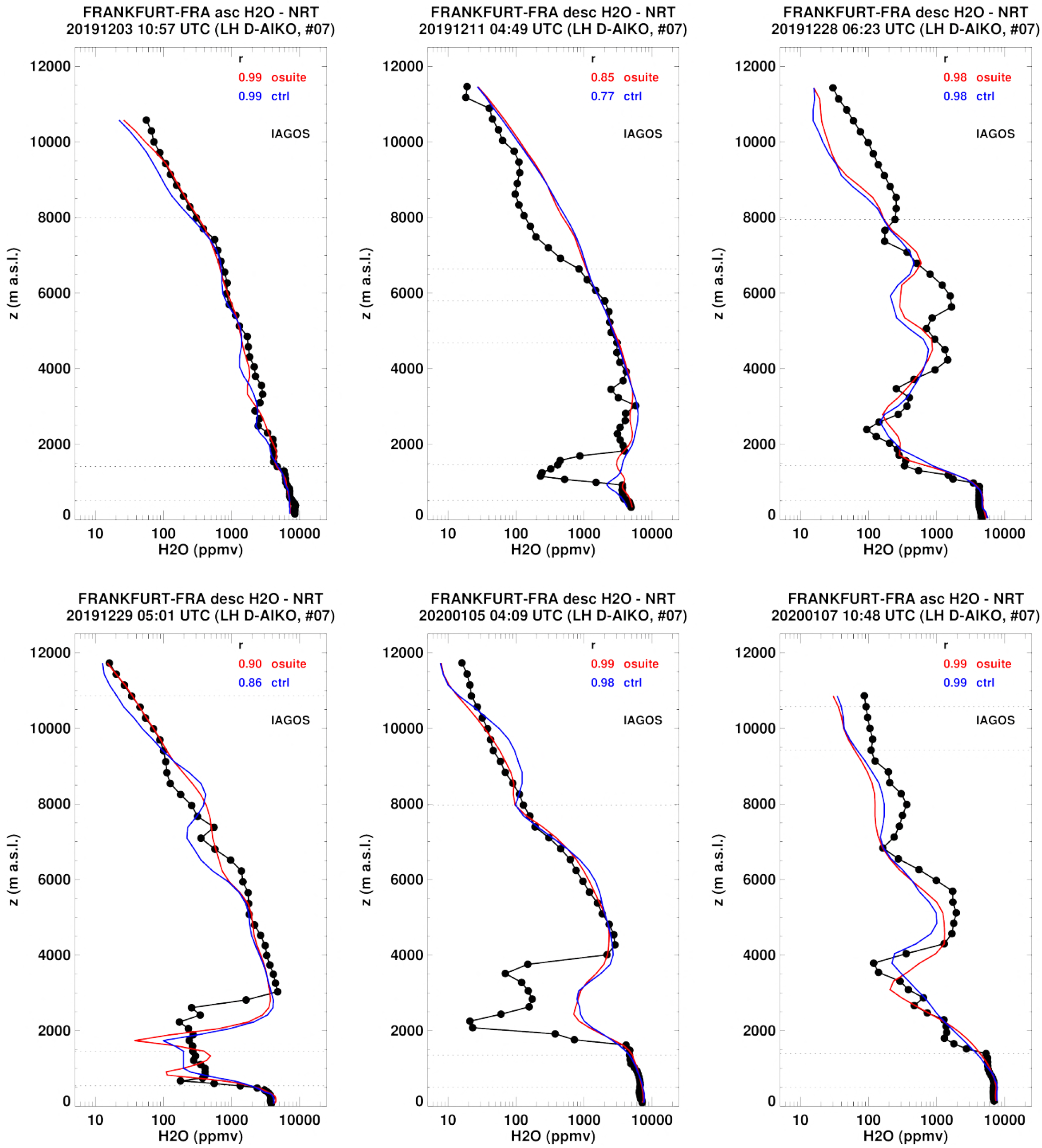

Figure 7.4.a: Daily profile for H_2O from IAGOS (black) and the two NRT runs (o-suite: red, control: blue) over Frankfurt during DJF 2020. Units: ppmv.

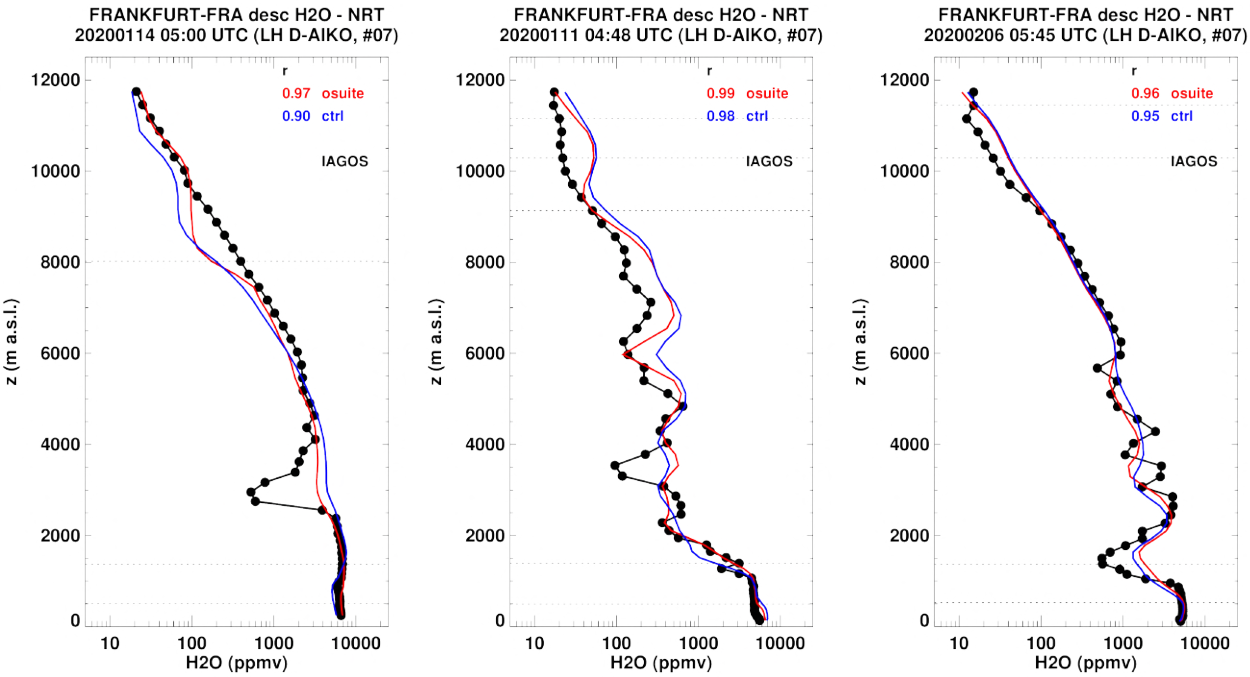

Figure 7.4.b: Daily profile for H_2O from IAGOS (black) and the two NRT runs (o-suite: red, control: blue) over Frankfurt during DJF 2020. Units: ppmv.

The agreement is worse in the upper layers, with larger biases and smaller correlation (Fig. 7.2 and Fig. 7.3). In the free troposphere, both underestimations and overestimations are found, and the correlation is on average between 80% and 90%. These overestimations often reach more than 60%, while underestimations spread generally in the range of 30 to 60 %. In the UTLS, the bias of the models is mostly negative as shown on the time series (Fig. 7.2), with an MNMB of -40% (Fig. 7.3). However, sometimes large overestimations also occur in the UTLS, as it was the case in the free troposphere but less frequently. Above 8000 m, the values of the correlation coefficient drop below 60%.

Several examples of individual profiles at Frankfurt are shown on Fig. 7.4.a-, which illustrate the aforementioned results. As shown in some of these profiles, the models often fail at reproducing sharp water vapour minima, that are observed in the low to mid-troposphere, which leads to large overestimations (i.e. 1211 09:49, 0105 04:09, 0114 05:00), while maxima are in general better represented. Individual profiles from other regions of the world are also presented in Fig. 7.5-10 for respectively: the Middle East, West and East Africa, South Africa, East Asia, North America and Central America. For all these regions the models present results similar to those observed over Europe at Frankfurt.

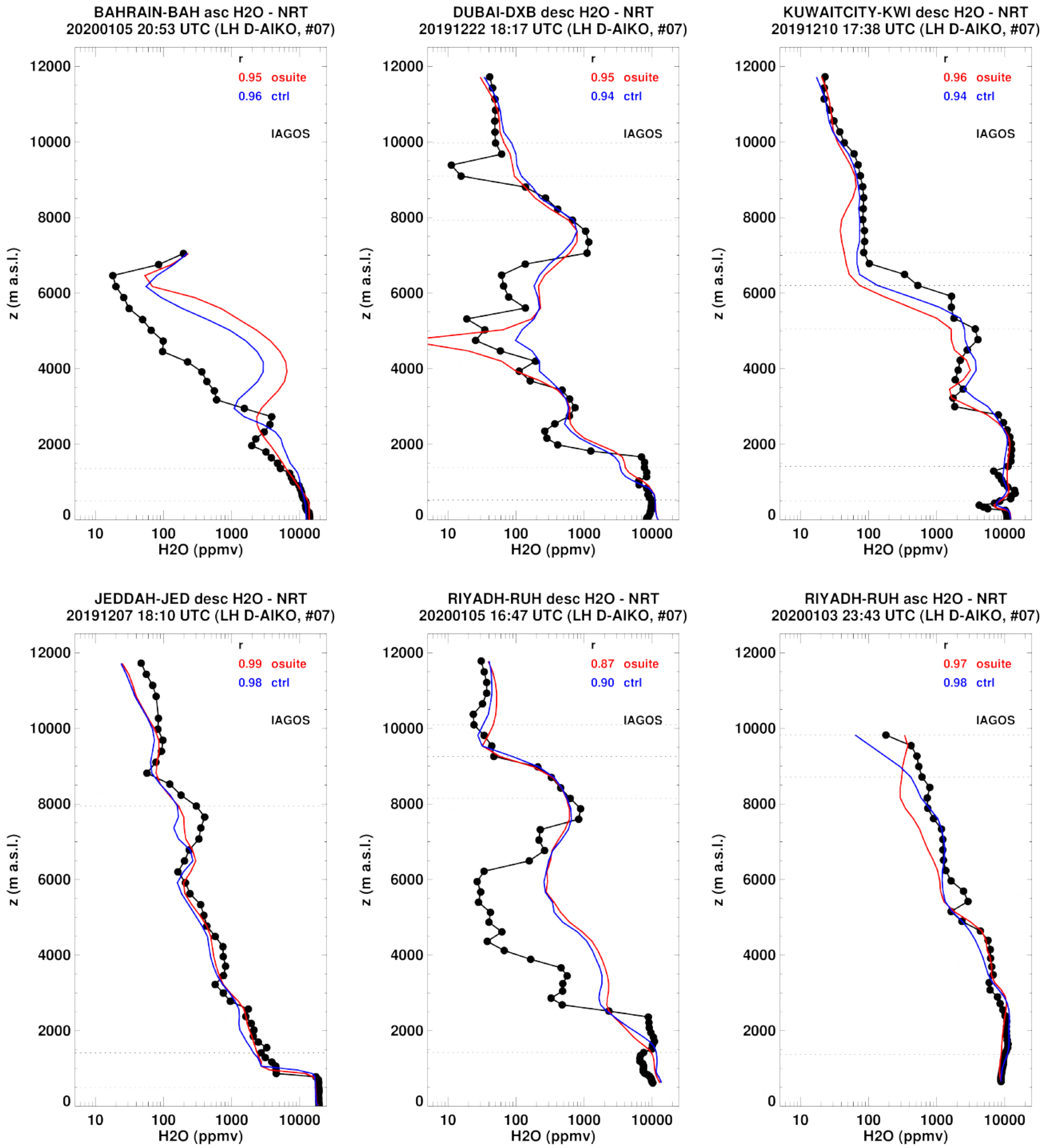

Figure 7.5: Daily profile for H_2O from IAGOS (black) and the two NRT runs (o-suite: red, control: blue) over the Middle East during DJF 2020. Units: ppmv.

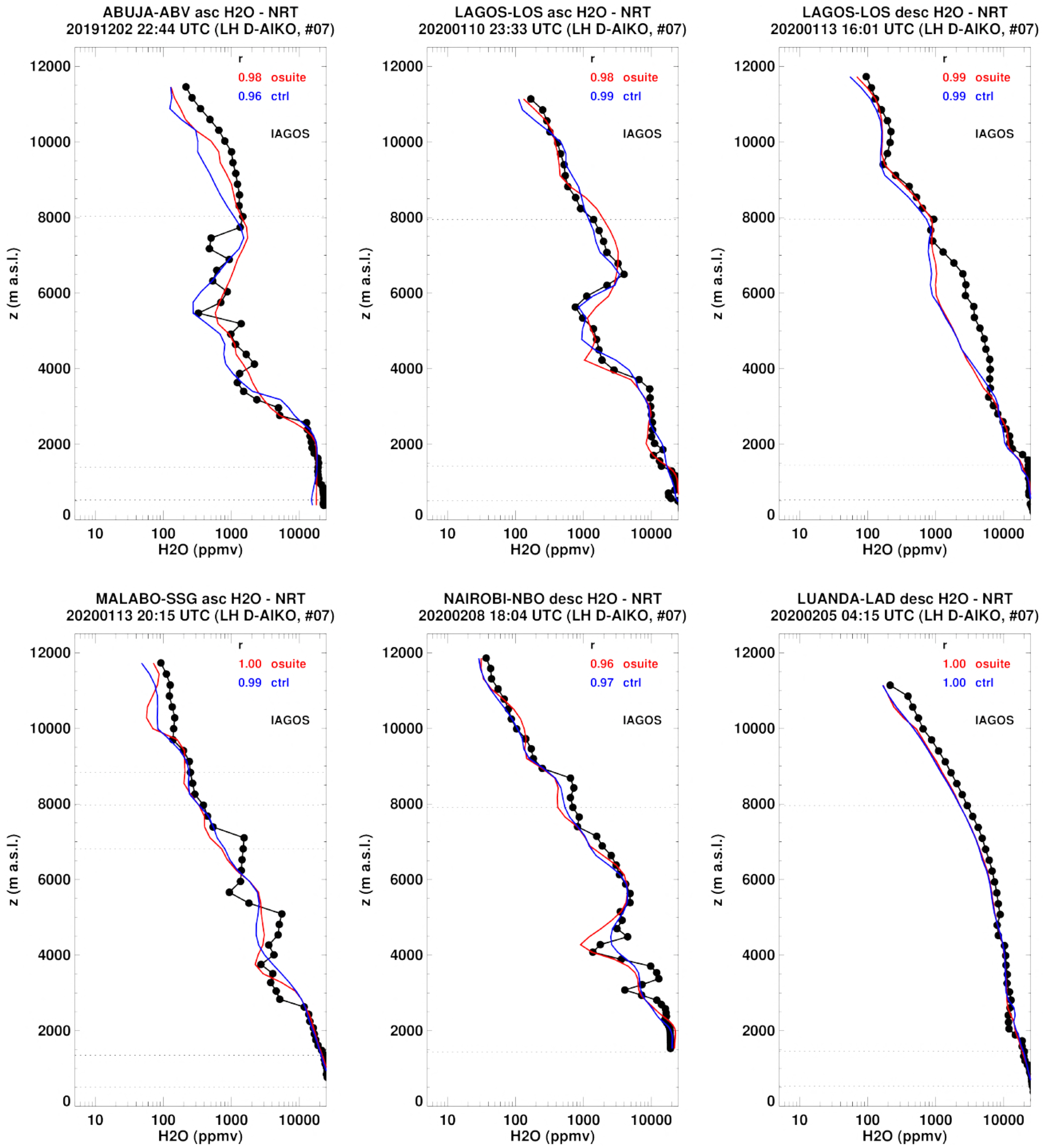

Figure 7.6: Daily profile for H_2O from IAGOS (black) and the two NRT runs (o-suite: red, control: blue) over the West and East Africa during DJF 2020. Units: ppmv.

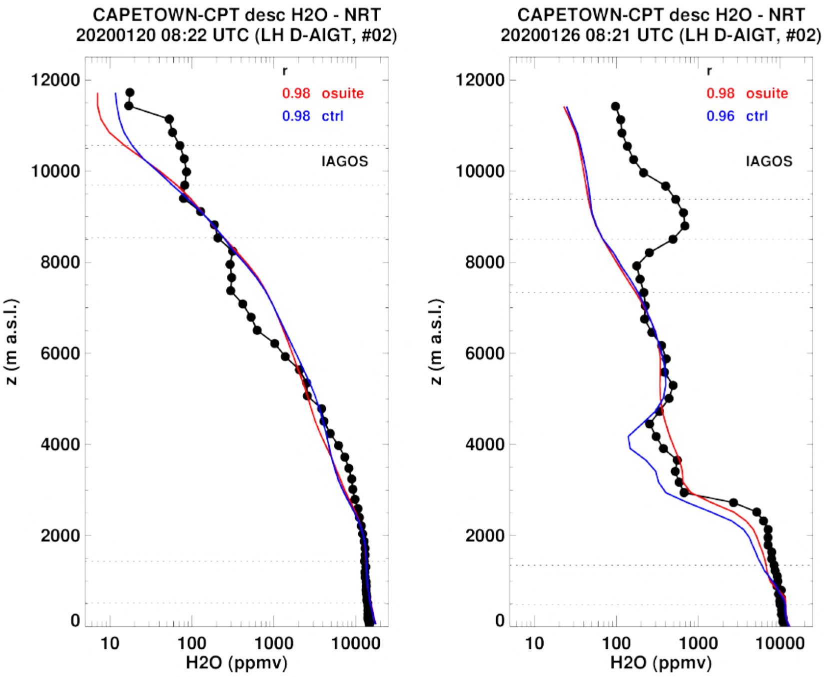

Figure 7.7: Daily profile for H_2O from IAGOS (black) and the two NRT runs (o-suite: red, control: blue) over the South Africa during DJF 2020. Units: ppmv.

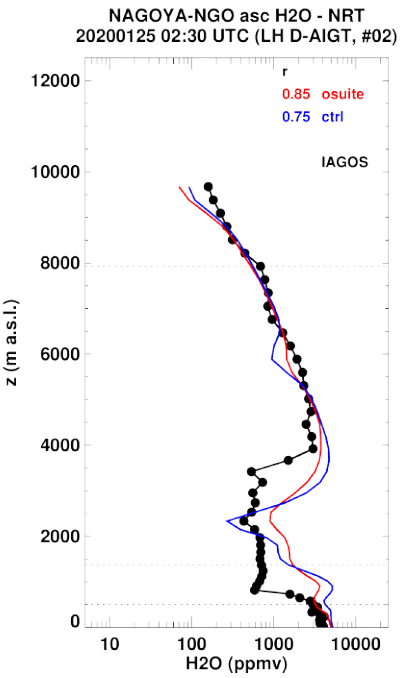

Figure 7.8: Daily profile for H_2O from IAGOS (black) and the two NRT runs (o-suite: red, control: blue) over East Asia during DJF 2020. Units: ppmv.

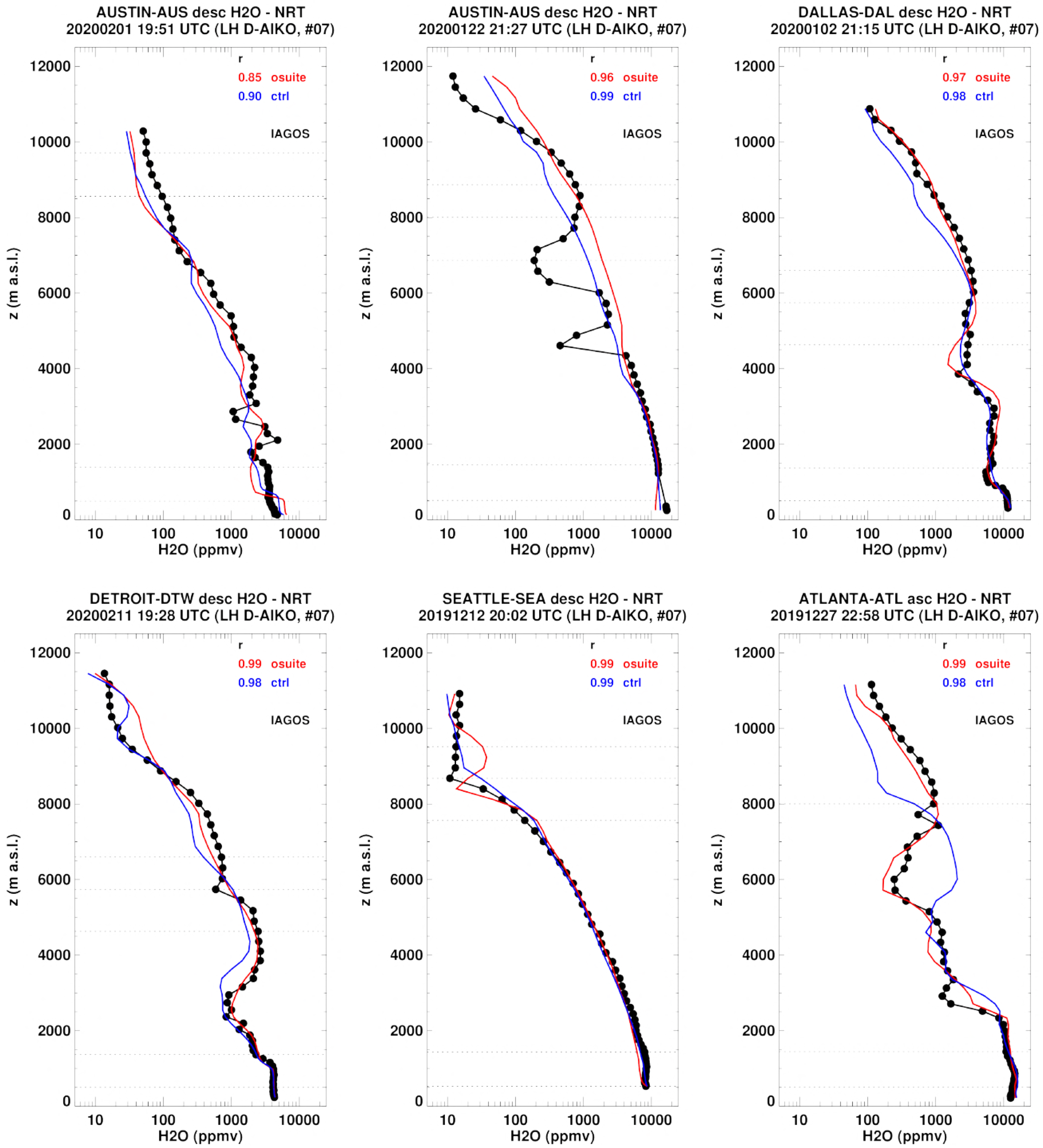

Figure 7.9: Daily profile for H_2O from IAGOS (black) and the two NRT runs (o-suite: red, control: blue) over North America during DJF 2020. Units: ppmv.

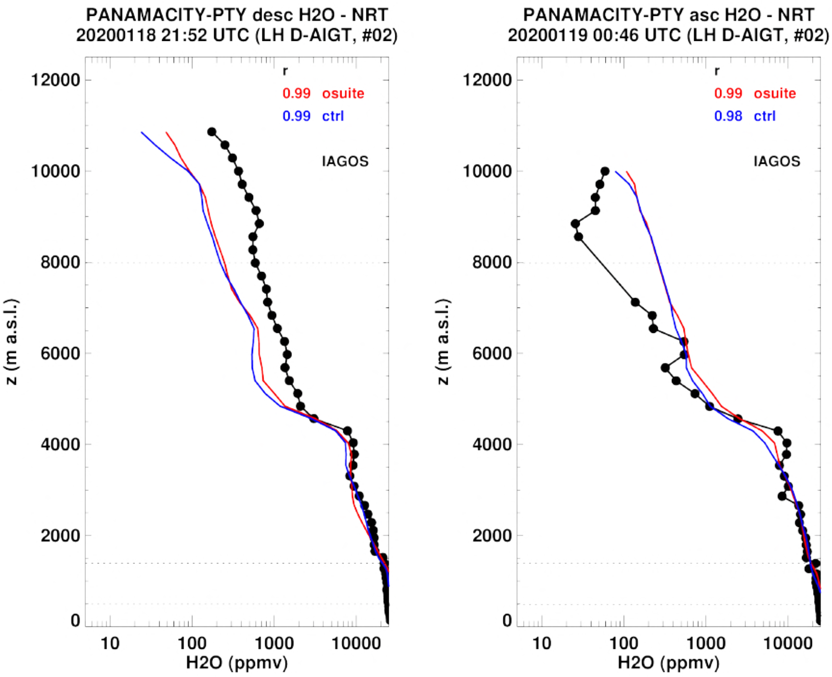

Figure 7.10: Daily profile for H_2O from IAGOS (black) and the two NRT runs (o-suite: red, control: blue) over Central America during DJF 2020. Units: ppmv.

8. Aerosol

8.1 Global comparisons with Aeronet and EMEP

The comparison of the CAMS simulation of time series of aerosol optical depth can be found for all Aeronet stations at: http://aerocom.met.no/cams-aerocom-evaluation/

More detailed evaluation including scores, maps, scatterplots, bias maps and histograms illustrating the performance of the aerosol simulation in the IFS system are made available through the AeroCom web interface. The model run can be compared here to e.g. the CAMS interim reanalysis and other models, such as the AeroCom Median model.

Correlation, based on daily aerosol optical depth and NRT Aeronet observations, has been rather stable recently. The o-suite forecast at +3 days shows only slightly lower correlation. See figure S3.

Part of the month-to-month variation in correlation is due to the varying quality and coverage of the Aeronet network. This has been improved by the version 3 from Aeronet. We use therefore version 3 level 1.5 for all global comparison to Aeronet.

The performance of the o-suite model exhibits some seasonal variation in AOD depending on region (Fig. 8.1.1). Noteworthy is the persistent AOD overestimation over North America (Fig. 8.1.1-bottom), but also a long-term trend to overestimation in East Asia. The latitudinal display of model and Aeronet AOD in the period investigated here (Fig. 8.1.2) shows a small positive bias against Aeronet in the Southern Hemisphere.

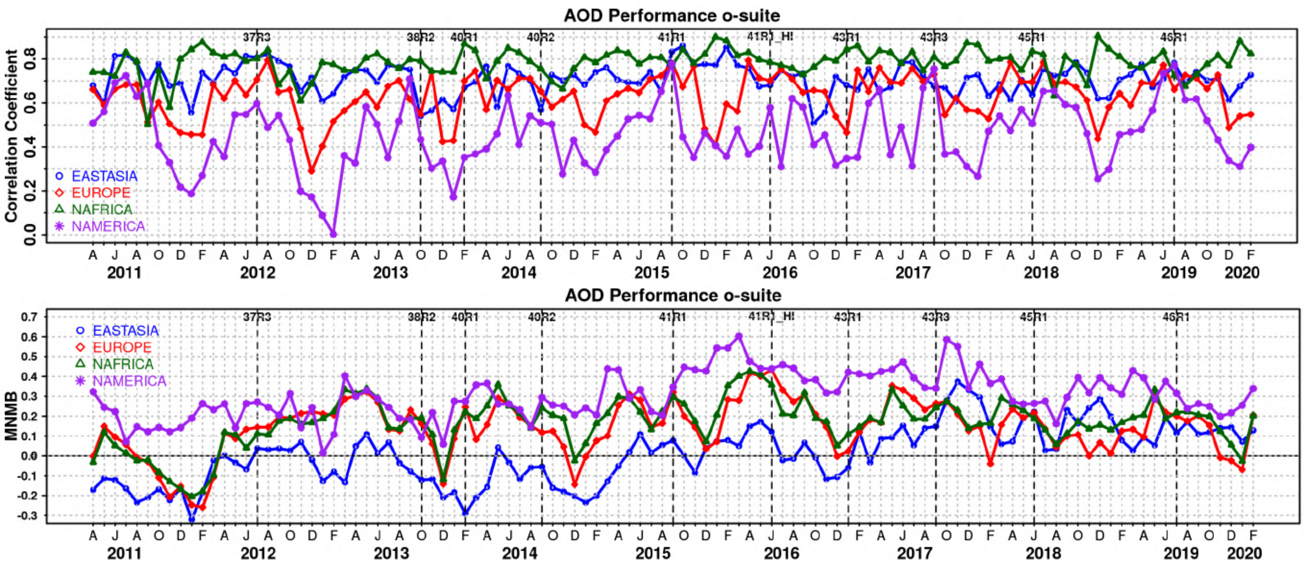

Figure 8.1.1. (top) Correlation coefficient and (bottom) modified normalized mean bias (MNMB) in AOD, since 2011, based on daily AOD comparison (Aeronet V3 level 1.5 data) in four world regions [East-Asia (blue); Europe (red); North Africa (green); North America (purple)] for the o-suite.

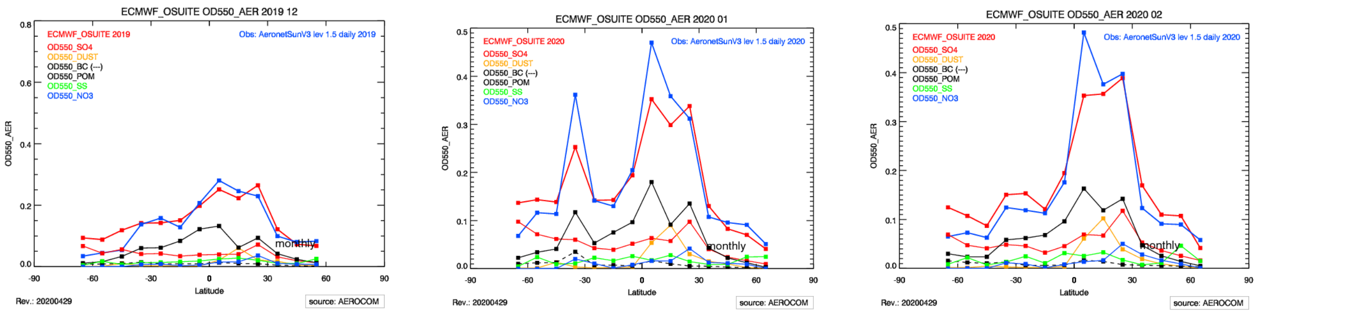

Figure 8.1.2. Aerosol optical depth of o-suite (red) compared to latitudinally aggregated Aeronet V3 level 1.5 data (blue) for the three months covered by this report.

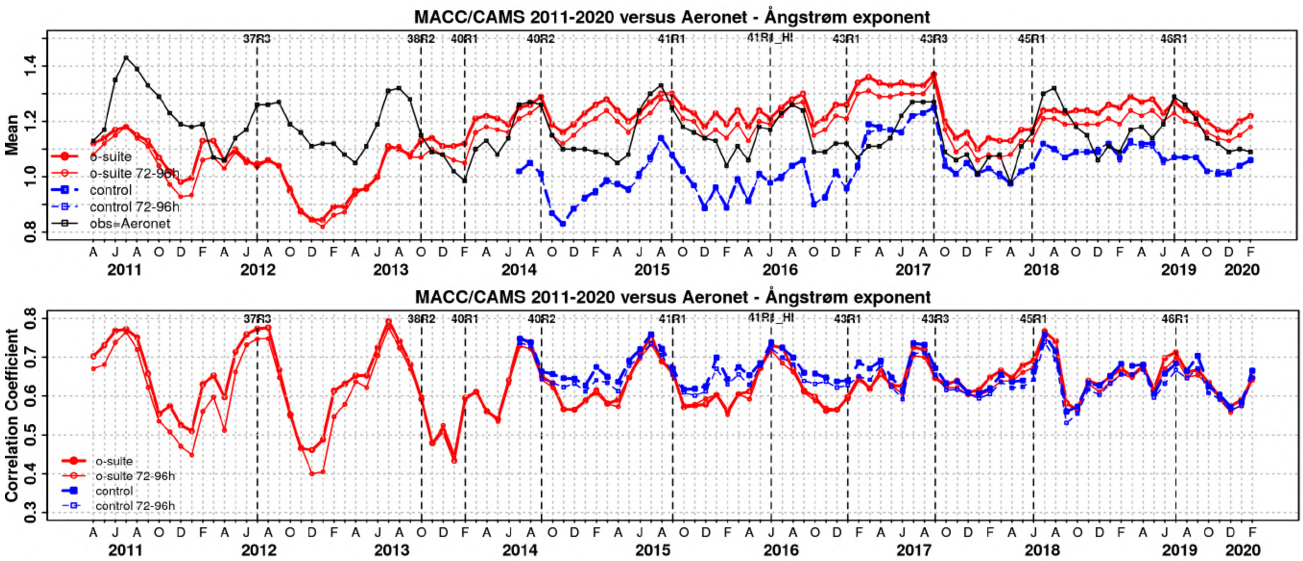

Figure 8.1.3. a) (top) Evolution of mean Ångström exponent in o-suite and control at Aeronet sites (Aeronet V3 level 1.5 data), based on matching monthly mean values. o-suite (thick red curve); o-suite at last forecast day (light red curve); control (blue dashed curve); control at last forecast day (light blue dashed curve). b) (bottom) Correlation using daily matching Ångström exponent.

o-suite				
	Mean SON 2019 0-24h	Change wrt to first day on day 4	Mean DJF 2019/20 0-24h	Change wrt to first day on day 4
AOD@550	0.158	-14%	0.153	-15%
BC-OD@550	0.005	-19%	0.005	-23%
Dust-OD@550	0.015	13%	0.011	13%
OA-OD@550	0.048	-24%	0.043	-27%
SO4-OD@550	0.036	-22%	0.036	-23%
SS-OD@550	0.053	-6%	0.056	-6%

Table 8.1.1. Mean global total and speciated AOD in the o-suite for the last two periods covered by the VAL report and change after 3 forecast days.

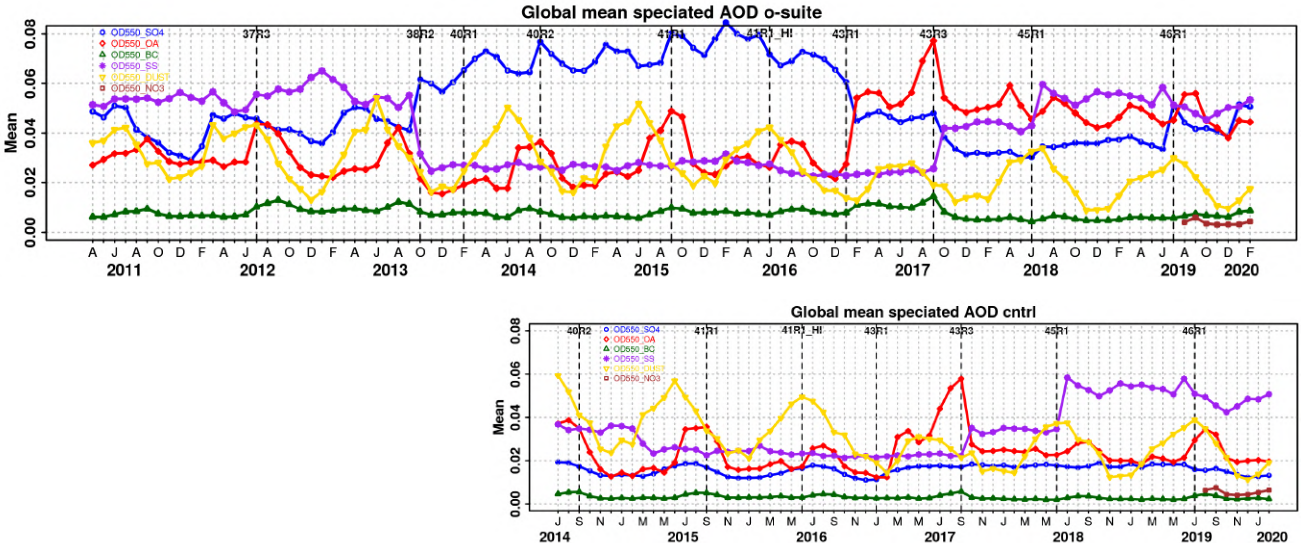

Figure 8.1.4. Evolution of the aerosol components of total AOD@550nm [OD550_SO4 = sulphate(blue); OD550_OA = organics(red); OD550_BC = black carbon(green); OD550_SS = sea salt(purple); OD550_DUST = dust(yellow); OD550_NO3 = nitrate(brown)] in o-suite and control simulation.

The simulated aerosol size distribution may be validated to first order using the wavelength-dependent variation in AOD, computed as Ångström exponent, with higher Ångström exponents indicative of smaller particles. We find in DJF 2019-20 a small bias (Figure 8.1.3-a). Temporal and spatial variability is difficult to capture, but correlation from all daily data is lower than for AOD (Figure 8.1.3-b and S3). Figure 8.1.4 shows that the Sep 2017 and Jun 2018 model changes are responsible for a shift in Ångström exponent. More organic matter seems to shift the size distribution to smaller sizes. The model upgrade in Feb 2017 with a bugfix for sea salt and improved parameterisations for SO4 lead to that sea salt increased with 45% while sulphate further decreased a bit. Sea salt has increased further due to a new sea salt emission scheme implemented in the Jun 2018 model upgrade and is back to earlier 2011-2013 levels. Since the latest model upgrade with the improvement to the sulphur cycle, the SO4 seem to have increased to same levels as before the Sep 2017 upgrade.

The o-suite uses data assimilation to obtain an analysis of the aerosol field. In the forecast period, however, a-priori model parameterisations and emissions (except fire emissions, which are kept in the forecast equal to the latest GFAS emission values) determine increasingly the aerosol fields. The performance of the day three forecasted AOD fields as compared to the first guess is shown in Figure S3 in the summary of this report. Table 8.1.1 shows an average global decrease in total aerosol optical depth during the first four forecast days, dominated by sulphate and organics. The control run with no assimilation shows somewhat less AOD (-39% compared to o-suite, see figure S3). All this supports the conclusion that either a-priori IFS aerosol and aerosol precursor sources are too small, or sinks are too effective in the IFS model.

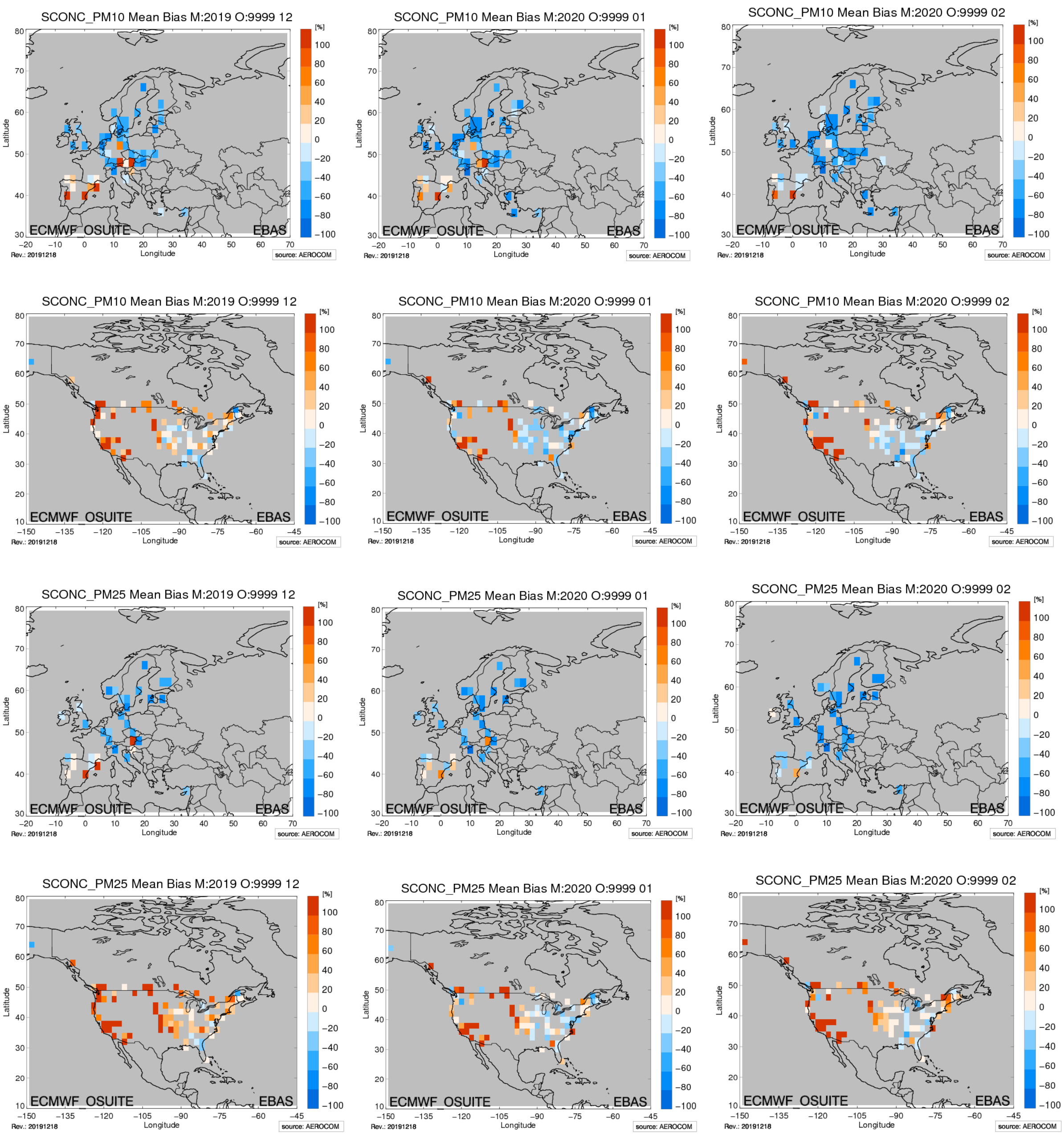

Figure 8.1.5. Bias [%] map of monthly mean PM10 and PM2.5 concentrations at EMEP (Europe, first and third row) and IMPROVE sites (North America, second and fourth row) for December 2019 (left column), January (middle) and February 2020 (right); simulated o-suite versus EMEP/IMPROVE derived climatological average (2000-2009).

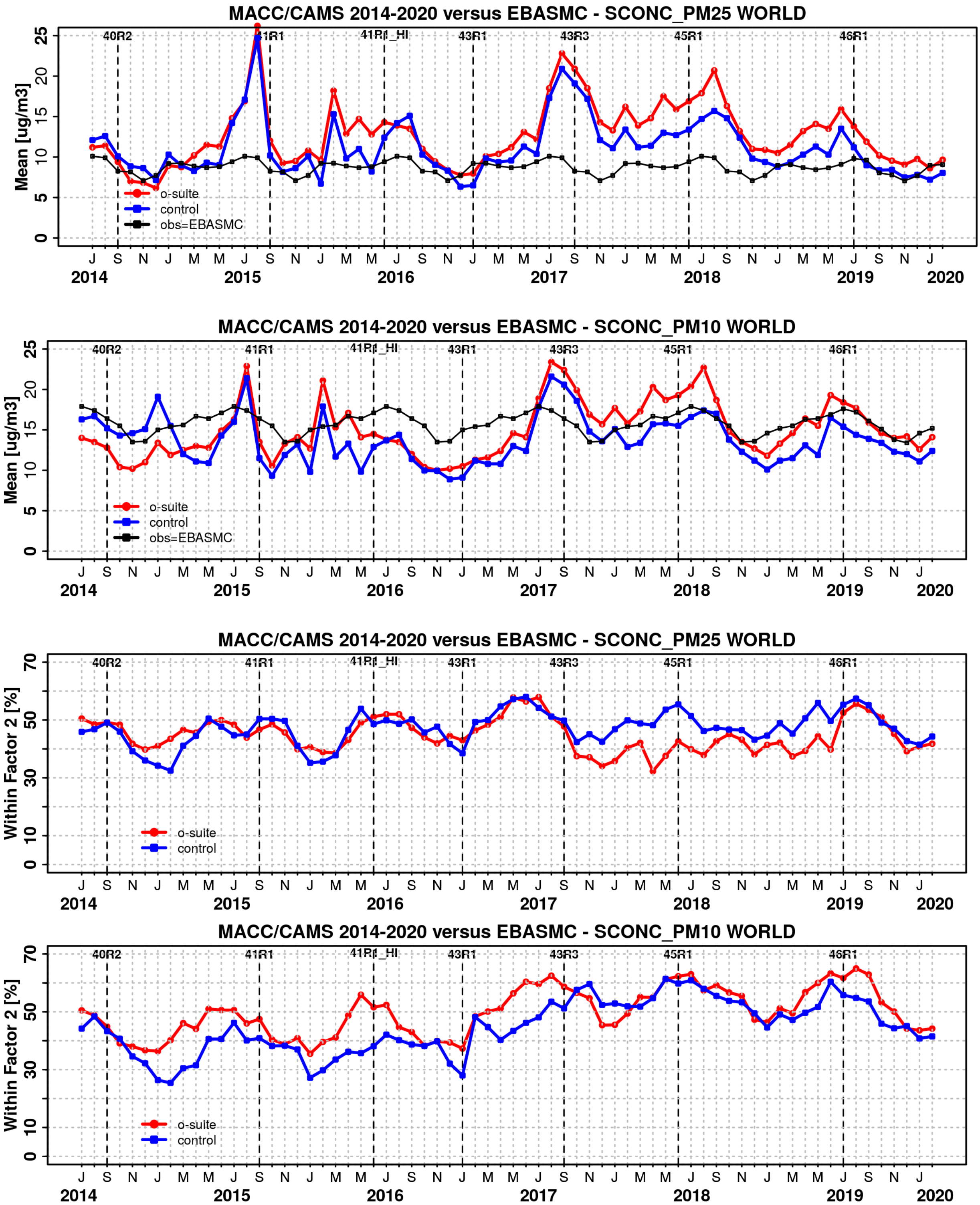

Figure 8.1.6. Temporal evolution of monthly mean average PM25 and PM 10 concentrations at EMEP (Europe) and IMPROVE sites (North America) and data fraction within a factor 2 of observed; ca 160 sites, observed data averaged from data available in EBAS from 2000-2009.

Surface concentration of particulate matter below 10 µm (PM10) and below 2.5 µm (PM25) from the o-suite experiment have been validated against data from 160 background IMPROVE and EMEP stations. A climatological average has been constructed from data in the period 2000-2009 as available in the EBAS database hold at NILU. The data availability is not the same at all stations, and sometimes covers only a few years.

A negative MNMB bias of PM10 in Europe and an overestimate in North America PM2.5 appears (Fig. 8.1.5), consistent with the AOD bias in the two regions. Figure 8.1.6 shows the evolution of mean observed and simulated PM10 and PM2.5. The biggest change appeared in July 2017 with the bias of o-suite now becoming positive almost overall. Shown is also the statistics of being within factor 2, a more robust metrics for a comparison to climatological data. This statistical indicator has clearly improved over time, indicating best PM10 and PM25 performance in summer months for the o-suite. O-suite is also better most of the times than the control simulation for PM10. For PM25 the difference is less clear, but since September 2017 (upgrade to 43R3) the control is performing better than the o-suite, except since latest upgrade with a performance of o-suite as good as the control.

8.2 Validation of dust optical depth against AERONET, and comparisons with the Multi-model Median from SDS-WAS

The 72-hour forecasts (on a 3-hourly basis) of dust aerosol optical depth (DOD) from CAMS o-suite and control have been validated for the period 1 December 2019 – 29 February 2020 against the AERONET Spectral Deconvolution Algorithm (SDA) cloud-screened observations, MODIS/Terra and Aqua Collection 6.1 Level 3 (1º x 1º) and SDS-WAS Multi-model Median DOD. The SDS-WAS Multi-model Median DOD is obtained from (currently) twelve dust prediction models participating in the Sand and Dust Storm Warning Advisory and Assessment System (SDS-WAS) Regional Center for Northern Africa, Middle East and Europe (http://sds-was.aemet.es/). At those sites where the SDA products are available, the dust AOD evaluation will be complemented with AOD-coarse, which is fundamentally associated to maritime/oceanic aerosols and desert dust. Since sea-salt is related to low AOD (< 0.03; Dubovik et al., 2002) and mainly affects coastal stations, high AOD-coarse values are mostly related to mineral dust.

During this season, satellites (see MODIS in Figure 8.2.1) detect the presence of biomass burning from Savanah fires and show that major dust activity in Northern Africa (seasonal AOD up to 0.3) is concentrated in latitudes between 15 and 20ºN with maximum seasonal AOD values over 0.9. Meanwhile, in the Middle East, high AOD values up to 0.2 are observed in Iraq and Saudi Arabia. In general, the CAMS o-suite shows lower season values than the control run, which are in general higher than the SDS-WAS multi-median product.

The CAMS o-suite can reproduce the dust transport over the North Atlantic region. However, the maximum dust activity is shifted to Chad, Mali, Niger and Algeria border and Sudan as shown in MODIS (see Figure 8.2.1). Also, DOD over Iraq and in the Mediterranean Basin appears overestimated in comparison with the SDS-WAS multi-model ensemble. These changes in dust activity in the main source regions are linked to the new dust module implemented in the operational CAMS model since early-July 2019.

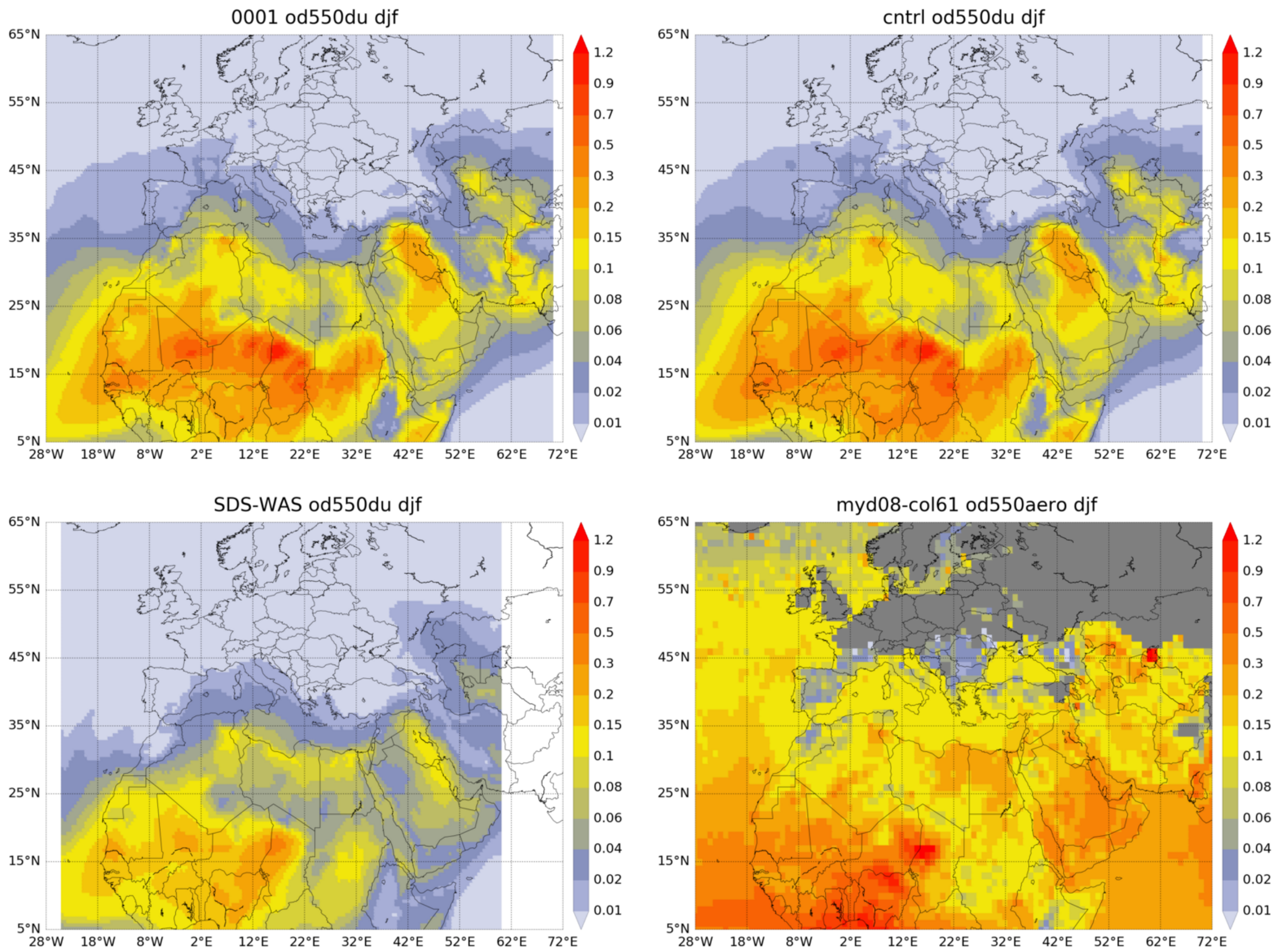

Figure 8.2.1: Averaged DOD 24h forecast from o-suite (top left) and control (top right), DOD of the multi-model SDS-WAS Median product (bottom left) as well as AOD from MODIS/Aqua Collection 6.1 Level 3 combined Dark target and Deep Blue product (bottom right) for the study period.

From December to February, the o-suite (control) experiments reproduce the daily variability of AERONET SDA observations (see Figure 8.2.2 and Table 8.2.1), with a correlation coefficient of 0.59 (0.52) averaged over all AERONET sites, which is lower than the SDS-WAS multi-model product which has a correlation coefficient of 0.82. Regarding mean bias (MB), the CAMS o-suite tends to underestimate the AERONET observations with a MB of -0.04 for o-suite and -0.03 for the control experiment. The SDS-WAS multi-model underestimates (MB of -0.04) the AERONET dust-filtered observations.

Over desert dust sources in the Sahara (see Table 8.2.1 as well as Zinder Airport AERONET site in Figure 8.2.3a), CAMS does reproduce the daily variability with correlation coefficients of 0.60 and 0.53 for o-suite and control. Overestimations are observed in both CAMS products over the Sahara (MB of 0.08 for control and 0.06 for o-suite). The SDS-WAS Multi-model results for Sahara shows better skills for this season (with a seasonal correlation of 0.83 and MB of 0.01). In the Middle East, the comparison with AERONET SDA AOD coarse product observations shows correlations of 0.55 for o-suite and 0.49 for control (see Table 8.2.1). These results in the Middle East are closer to the SDS-

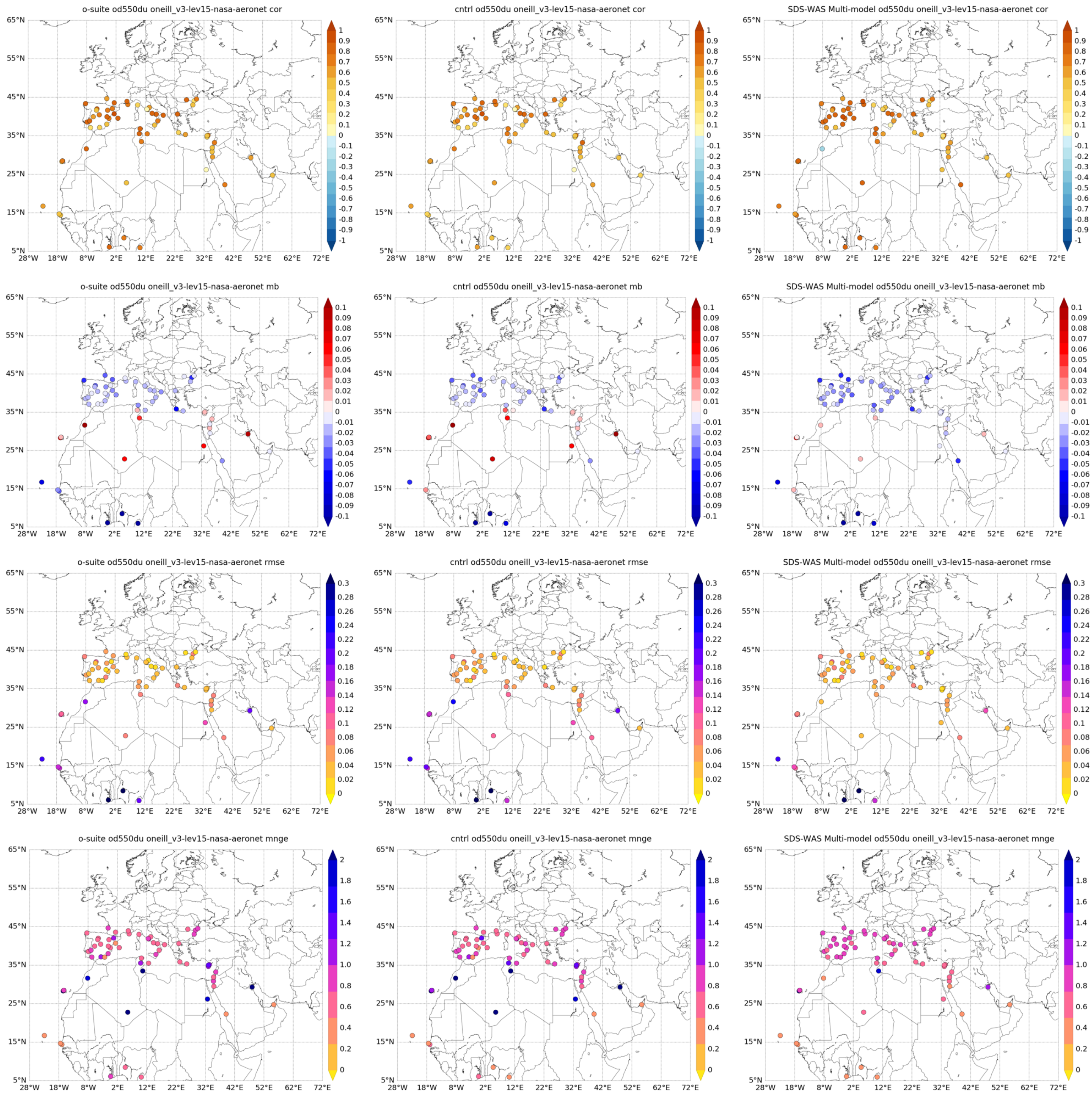

Figure 8.2.2: Skill scores (correlation coefficient, MB, RMSE and FGE) for 24-hour forecasts of CAMS o-suite (left column), control (central column) and DOD Multi-model SDS-WAS Median (right column) for the study period. AOD-coarse from AERONET SDA is the reference.

WAS Multi-model (with a seasonal correlation of 0.58 and MB of -0.04). As shown in Figure 8.2.3a, the CAMS overestimations in the Middle East of the control run are reduced in the o-suite experiment. As indicated before, these changes in the dust activity in the main source regions are linked to the new dust module implemented in the operational CAMS model since 9th July 2019.

Table 8.2.1: Skill scores (MB, FGE, RMSE and r) of 24h forecasts for CAMS o-suite, CAMS control and SDS-WAS Multi-model Median for the study period, and the number of data (NDATA) used. DOD (SDA AOD coarse product) from AERONET is the reference.

		Control				o-suite DOD				SDS-WAS Median DOD			
	NDATA	MB	FGE	RMSE	r	MB	FGE	RMSE	r	MB	FGE	RMSE	r
Sahara	195	0.08	0.94	0.10	0.61	0.06	0.80	0.08	0.53	0.01	0.04	0.04	0.83
Sahel	783	-0.16	-0.31	0.32	0.44	-0.21	-0.66	0.33	0.63	-0.13	-0.26	0.26	0.78
Tropical North Atlantic	202	-0.05	-0.09	0.22	0.61	-0.07	-0.23	0.22	0.66	-0.07	-0.19	0.21	0.72
Subtropical North Atlantic	508	0.05	0.03	0.14	0.56	0.03	-0.08	0.11	0.61	0.02	-0.01	0.10	0.65
North Western Maghreb	21	0.04	-0.10	0.13	0.26	0.02	-0.15	0.10	0.40	-0.01	-0.36	0.04	0.78
Western Iberian Peninsula	390	-0.02	-0.59	0.07	0.66	-0.02	-0.68	0.06	0.83	-0.03	-1.17	0.07	0.78
Iberian Peninsula	766	-0.02	-0.80	0.06	0.51	-0.02	-0.86	0.05	0.62	-0.02	-1.29	0.06	0.70
Western Mediterranean	921	-0.01	-0.52	0.03	0.73	-0.01	-0.55	0.03	0.76	-0.02	-1.44	0.04	0.81
Central Mediterranean	1399	0.01	-0.36	0.07	0.63	0.00	-0.43	0.06	0.63	-0.02	-0.98	0.04	0.68
Eastern Mediterranean	1627	0.00	-0.38	0.05	0.58	0.00	-0.39	0.05	0.58	-0.01	-0.88	0.04	0.65
Eastern Sahara	-	-	-	-	-	-	-	-	-	-	-	-	-
Middle East	560	0.04	0.09	0.14	0.49	0.03	0.03	0.13	0.55	-0.01	-0.07	0.10	0.58
All sites	**8755**	**-0.03**	**-0.37**	**0.17**	**0.52**	**-0.04**	**-0.45**	**0.17**	**0.59**	**-0.04**	**-0.82**	**0.14**	**0.79**

In the Sahel (see Figure 8.2.2 and Table 8.2.1), the o-suite shows strong underestimations (MB of -0.21) in comparison with control (with MB of -0.16). However, the o-suite better reproduces the observed daily variability (with a correlation of 0.63 for o-suite in comparison to 0.44 for control). The underestimations observed in o-suite in the Sahel are also spread to the Tropical North Atlantic (MB of -0.07 for o-suite, see Table 8.2.1).

Over long-range transport regions (see Figure 8.2.2), the CAMS o-suite model results perform better than control over the sub-Tropical North Atlantic region with correlations of 0.56 for control and 0.61 for the o-suite (see Santa Cruz de Tenerife in Figure 8.2.3b and Table 8.2.1).

Over the Iberian Peninsula and the Mediterranean, both CAMS products show correlations between 0.51 and 0.83 and slight underestimations (MB between -0.01 and -0.02) except in Central and Eastern Mediterranean region (see Table 8.2.1 and Tunis Carthage and Agia Marina Xyliatou in Figure 8.2.3b). Western Iberian Peninsula has the best results in the AERONET comparison in terms of correlation (of 0.83 for o-suite and 0.66 for control). The Eastern Mediterranean (see Table 8.2.1 and Agia Marina Xyliatou in Figure 8.2.3b) presents slightly lower correlation values (0.58 for control and o-suite). This is related to the minimum in dust activity during this period in this region and the associated low AOD. In the case of the North-Western Maghreb, both CAMS products present low correlation coefficients (of 0.26 for control and 0.40 for o-suite), and o-suite reduced the overestimation observed in control (MB of 0.04 for control and 0.02 for o-suite. This poorer performance in this region in comparison to the previous season is associated with the low AOD values observed and the number of observations during this season when there is more presence of clouds.

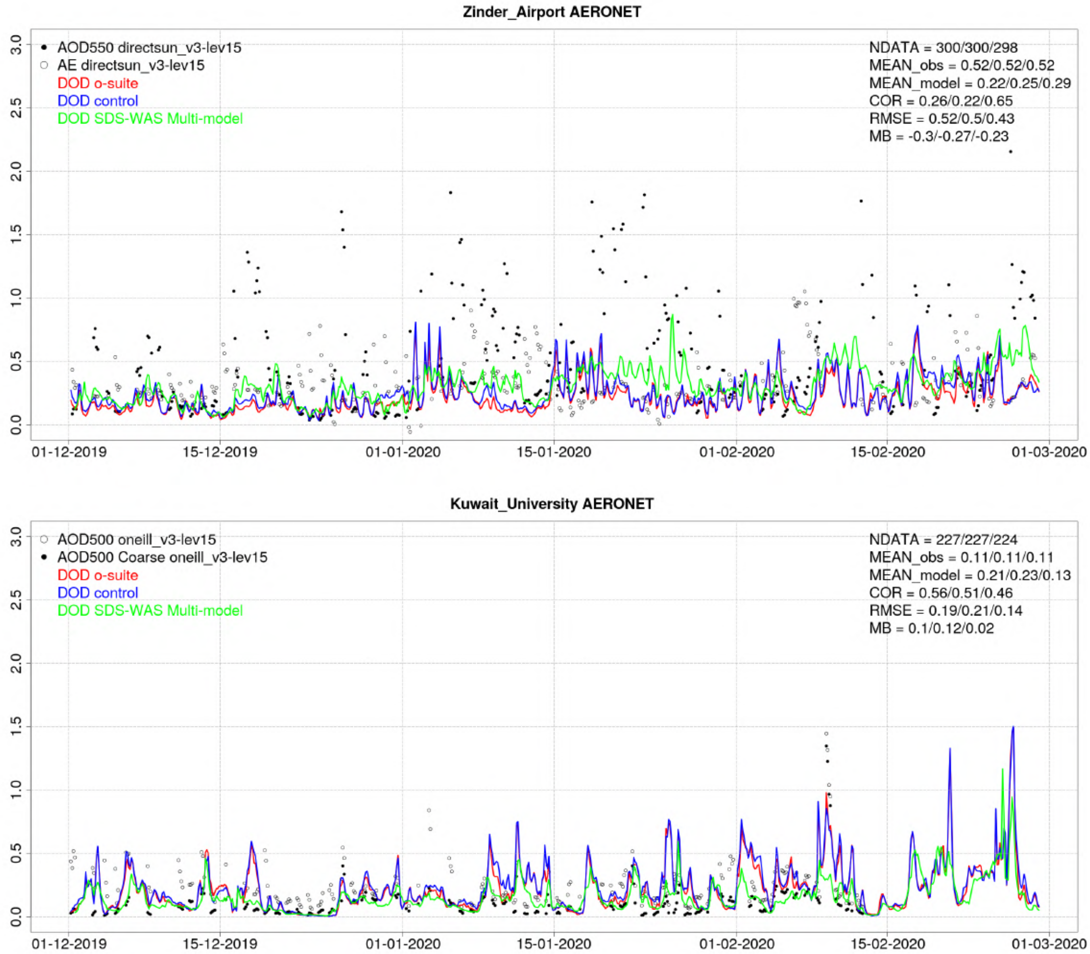

Figure 8.2.3a: AOD and Angstrom Exponent from AERONET Direct-sun (black dots), DOD o-suite (red line), DOD control (blue line) and DOD Multi-model SDS-WAS Median (green line) for the study period over Zinder Airport (Sahara) and Kuwait University (Middle East). Skill scores per each individual site and model (o—suite/control/ SDS-WAS Multi-model) are shown in the upper right corner (NDATA: available 3-hourly values used for the calculations, MEAN observations, MEAN model, COR, RMSE, MB).

The comparison of the 1- to 3-day forecasts shows that the prediction is stable during the forecasts in comparison with AERONET direct-sun observations with correlation coefficients of 0.59 (0.52), 0.60 (0.60), and 0.57 (0.58) respectively for 24, 48 and 72h forecasts for all the sites, for o-suite (control).

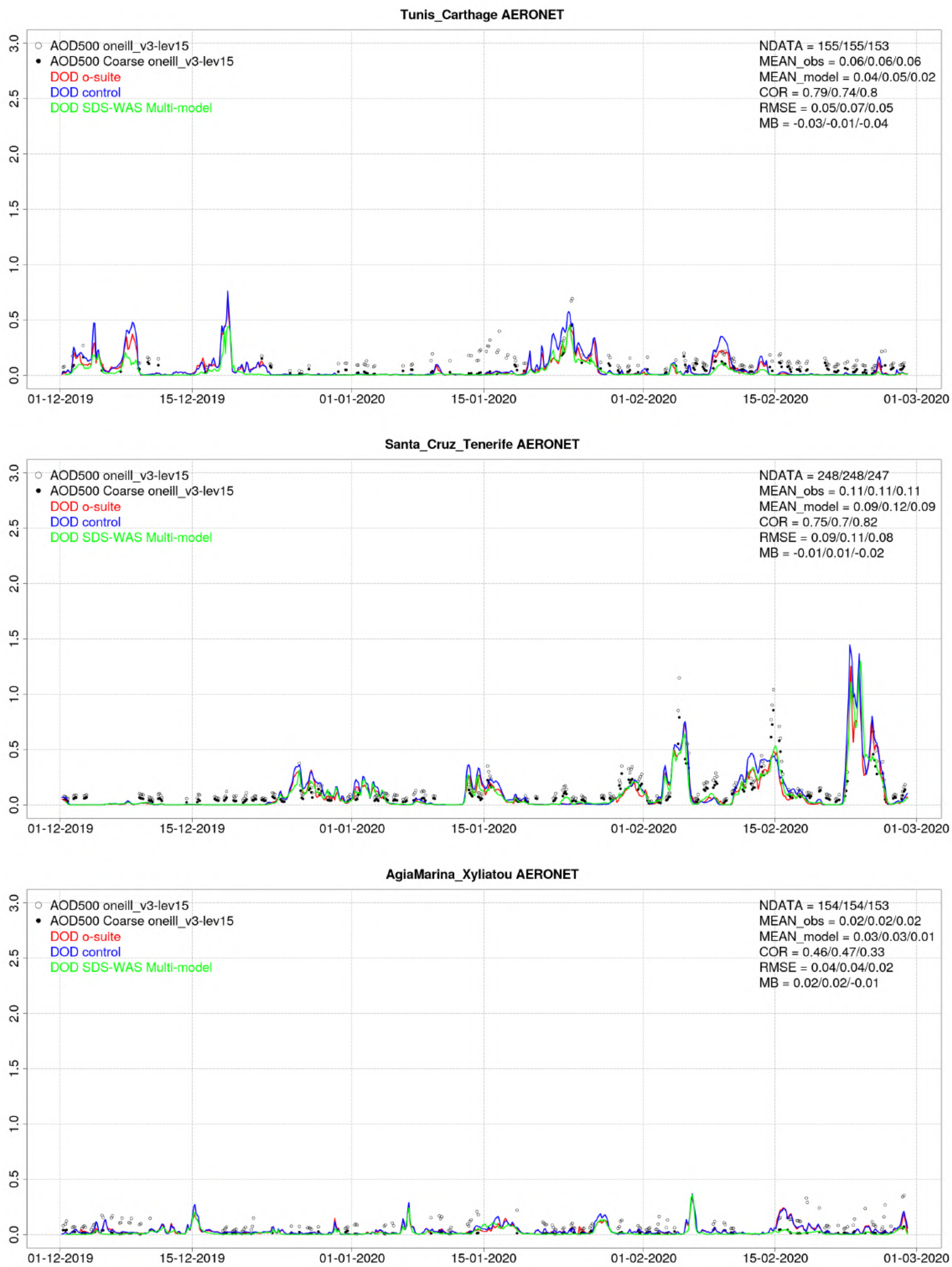

Figure 8.2.3b: AOD and AOD-coarse from AERONET SDA (black dots), DOD o-suite (red line), DOD control (blue line) and DOD Multi-model SDS-WAS Median (green line) for the study period over Tunis Carthage (Central Mediterranean), Santa Cruz de Tenerife (SubTropical North Atlantic) and Agia Marina Xyliatou (Eastern Mediterranean) Skill scores per each individual site and model (o—suite/control/SDS-WAS Multi-model) are shown in the upper right corner (NDATA: available 3-hourly values used for the calculations, MEAN observations, MEAN model, COR, RMSE, MB).

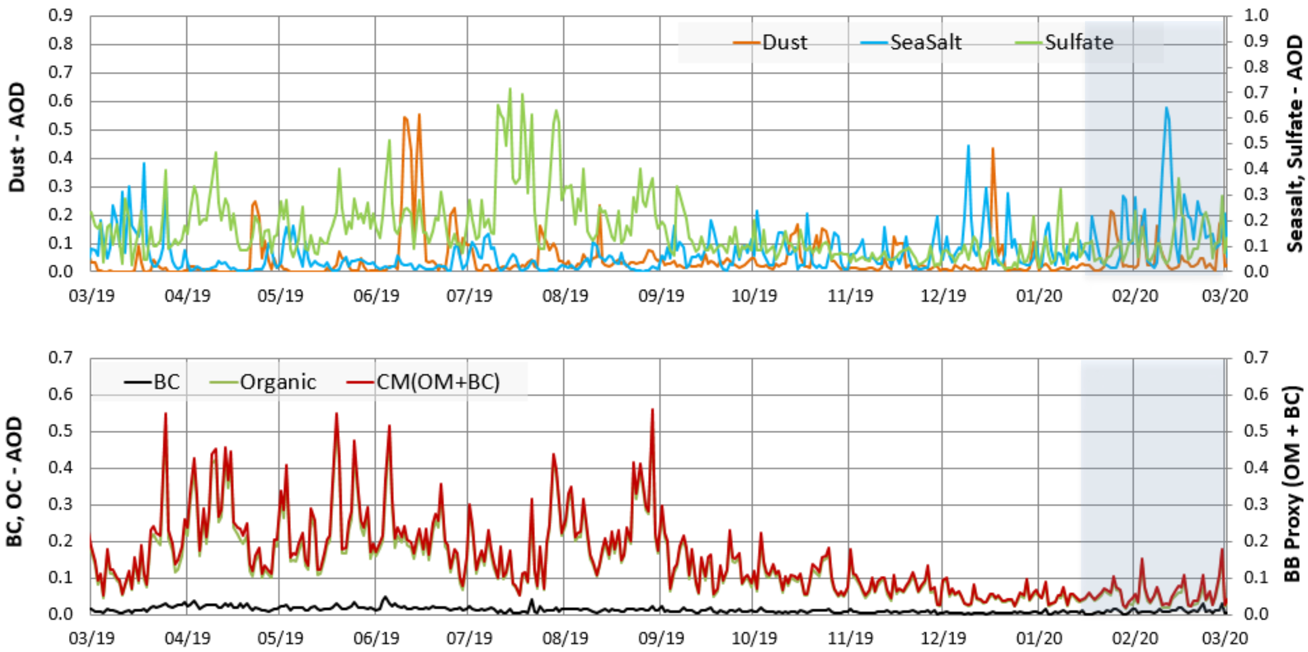

Figure 8.3.1: Maximum daily AOD over Germany for aerosols included in the IFS model from 12/2017 - 02/2020: sea salt (blue), dust (orange), sulphate (light green), black carbon (BC, black), organic matter (green), proxy for 'biomass burning' (as OC+BC - red). Note the different y-axes for the aerosol species.

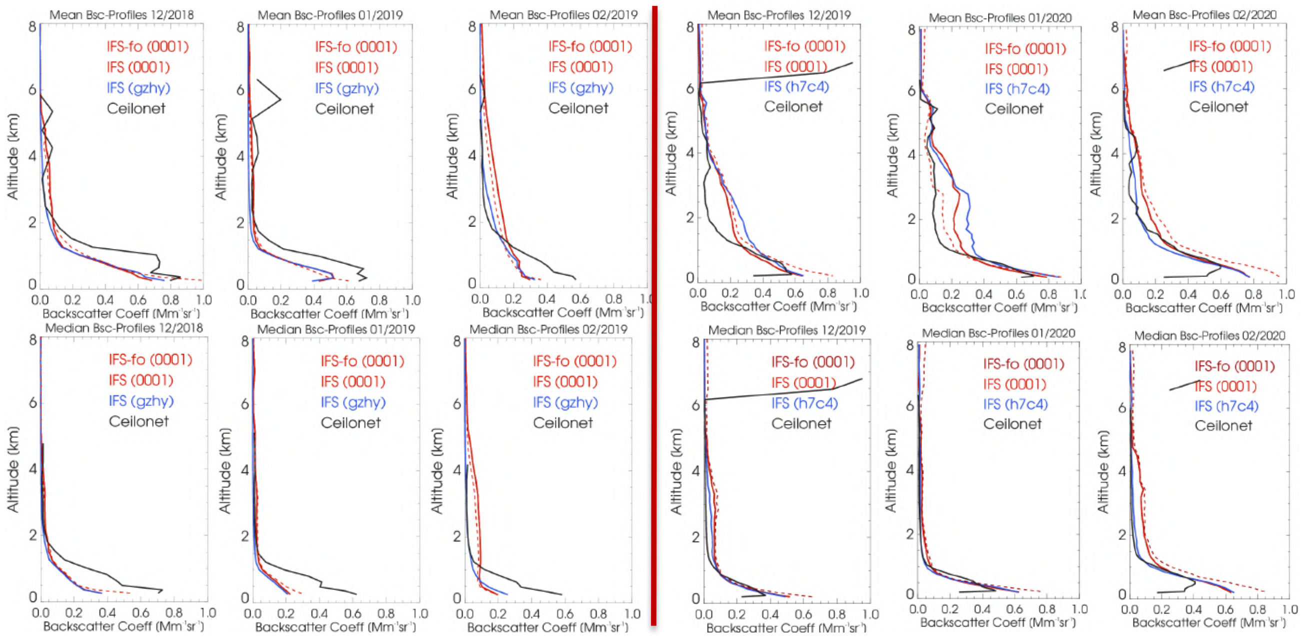

Figure 8.3.2: Left 2018/19 (0001/gzhy), right 2019/20 (0001/h7c4: Monthly mean profiles (upper panel) and median profiles (lower panel) of backscatter coefficients from o-suite (red), control run (blue), and ceilometers (black) combined from 21 German stations in Dec 2019 to Feb 2020.

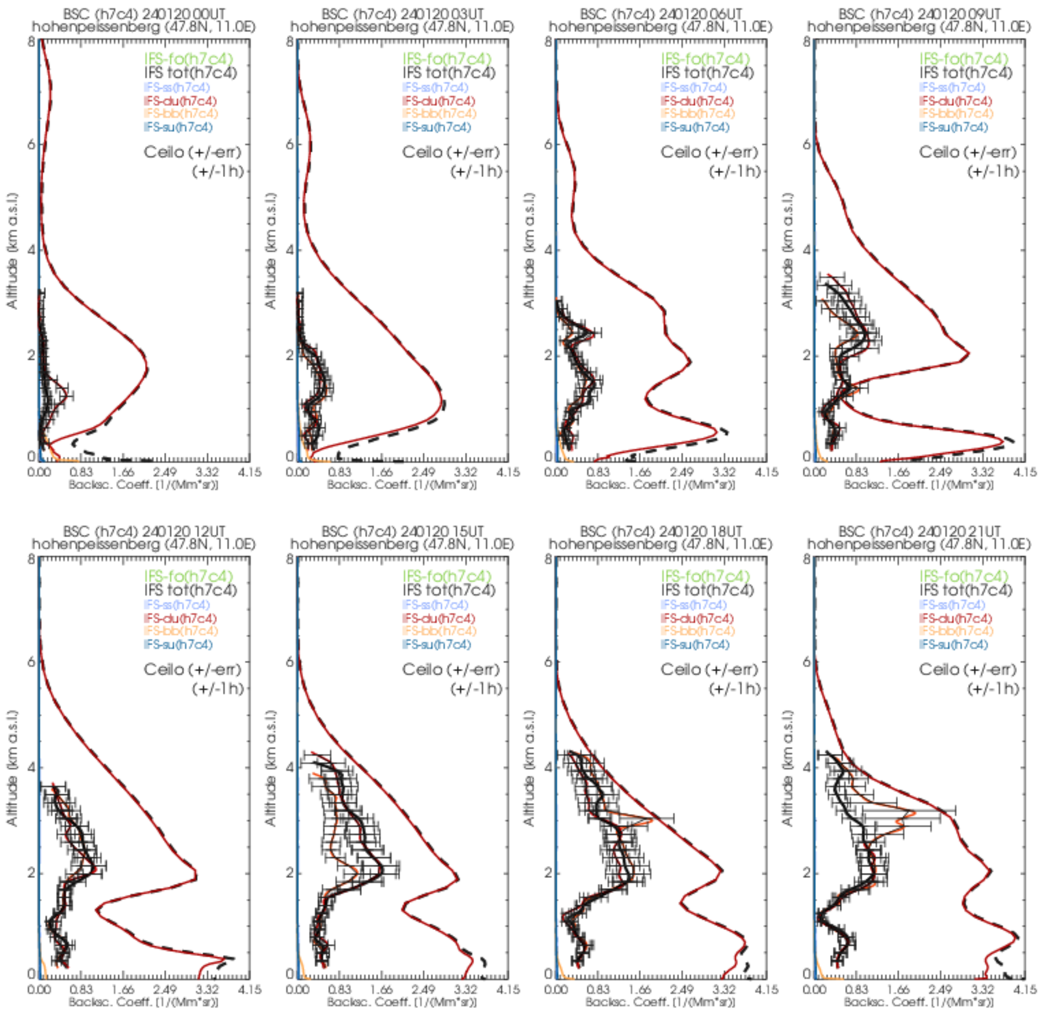

Figure 8.3.3: Exemplary foehn Situation with high number of predicted model dust (24.01.20) from o-suite dust load (red) and total load (dashed black line), control run gzhy/g7h4 (blue), forward operator (green), and ceilometers (solid black).

8.3 Ceilometer backscatter profiles

The technical specification of data sources, evaluated parameters and methods are given in the observations specification report (Eskes et al., 2019). In this section, the temporal and vertical variation of the backscatter coefficient (bsc) profiles are evaluated, statistically as bias, correlation, and standard deviation of o-suite '0001' and control run ‘g7h4’ vs ceilometers, and summarized in Taylor plots.

Period Overview

In Figure 8.3.1 showing the maximum AOD over Germany, the model aerosol optical depth (AOD) indicates initially higher (starting with the update on 10 July) but then decreasing SO4 concentrations, while all other components show no marked changes. Saharan dust events occurred in Oct 2019. With respect to AOD, all aerosol components follow their usual seasonality.

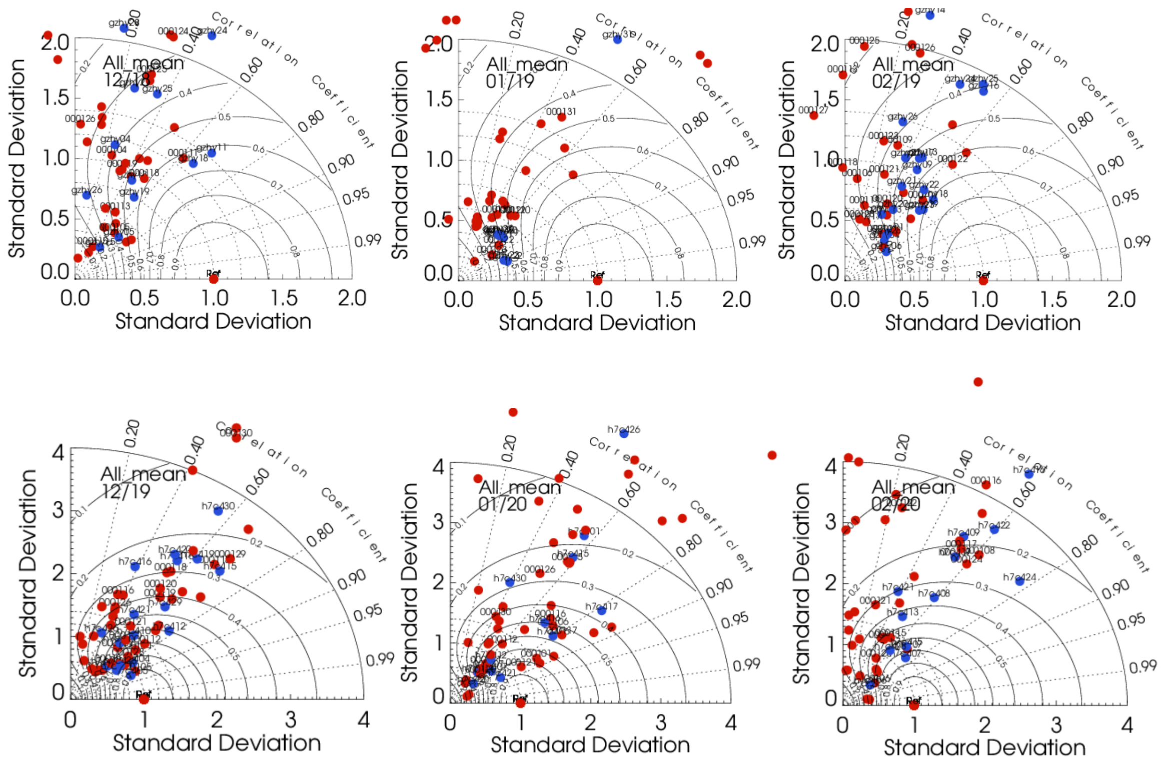

Fig. 8.3.4: Taylor polar plots with daily average standard deviation of vertical profiles vs correlation coefficient, averaged over 21 German ceilometer sites for Dec 2018 to Feb 2019 (top) and Dec2019- Feb 2020 (bottom). The O-suite in red, control run in blue.

Mean profiles:

In the new IFS cycle 46r1, implemented on 9 July 2019, nitrate NO_3 and ammonia NH_4 have been added and, likewise sulphate SO_4, have been coupled w.r.t homogeneous (gas-phase) and heterogeneous (particle phase) chemical processes. They contribute roughly 10-30% of aerosol mass in the rural central European PBL, as neutralized forms NO_3NH_4 or $(NH_4)_2SO_4$. Simultaneously, emissions of most aerosol components were significantly upgraded.

The negative Bias of the model has significantly decreased from 60L to 137L model version. The median for December to February 2020 shows only minimal bias. Mean values for Dec19 and Jan20 shown a positive Bias in the middle troposphere (see Figure 8.3.2).

The mean value offset in December and Janauary could be explained by two factors. First during Winter 2019/20 athmospheric conditions often poduce westerly winds. This leads to relativly warm and dryer weather condictions increasing the dust load. Also foehn situations over the alps including some transport of Sharian dust into germany. One example is the situation on January the 24th (see Figure 8.3.3).

For this day the model predicts a long range transport over the alps, including a high load of dust. The measured amount was factor two to three lower then predicted.

Taylor Plots:

The average coefficient of correlation between modelled and observed vertical backscatter profiles has improved from the 60L to the 137L model version and now ranges between r = 0.4 – 0.8 rather than r = 0.2-0.6 before. (Fig. 8.3.4). This is mainly due to better representation of the PBL top height. The absolute standard deviation (SD) are normalized to the SD of observations per day, as reference value at SD ≡ 1.0. In winter 2019/20, o-suite (red dots) and control run (blue dots) show that the both suites show better correlation (0.2-0.8) with the observation then the previous winter (0-0.6). The o-suits even showed a stronger correlation in some cases then the control run. There is a large day-to-day and a seasonal variation of the performance. It must be noted, that small vertical displacements decrease the correlation coefficient, although the SD plumes are mostly reproduced at geographically truthful positions.

Summary

Conclusion concerning the changes due to the model upgrades in July 2019 and the development in Winter 2019/2020:

- Very low bias of the model bsc during winter
- The high bias of model bsc in the FT has not changed notably
- The step at the top of the PBL is captured notably better with 137 levels than with 60 levels (51L instead of 27L <8 km altitude), same for o-suite and control.
- The amplitude of the model vertical profile is now very close the the observation (reference)

Daily averages of Pearsons correlation coefficients in June/July (run gzhy) cluster around r= 0.2-0.8 for the 137L model in contrast to r=0.0-0.6 for the 60L version before.

8.4 Aerosol validation over Europe and the Mediterranean

Three-hourly aerosol optical depth (AOD) and surface concentration (PM10 and PM2.5) from the o-suite and control run have been validated for the period 1 December 2019 – 29 February 2020 against AERONET direct-sun cloud-screened observations.

Aerosol optical depth over the Mediterranean

The CAMS o-suite does reproduce the daily variability of AERONET direct-sun observations. In Western, Central and Eastern Mediterranean, the correlation coefficient increases from (0.49, 0.67 and 0.56), to (0.51, 0.66 and 0.46), respectively for control and o-suite during winter (see Figure 8.4.1). This poorer performance in this region in comparison to the previous season is associated with the low AOD values observed and the number of observations during this season when there is more presence of clouds. In general, both CAMS experiments overestimated the AERONET observations in the Mediterranean basin in control (MB of 0.02, 0.05 and 0.07 for Western, Central and Eastern Mediterranean regions respectively) and o-suite (MB of 0.06, 0.06 and 0.11 for Western, Central and Eastern Mediterranean regions respectively) as shown in Figure 8.4.1. The

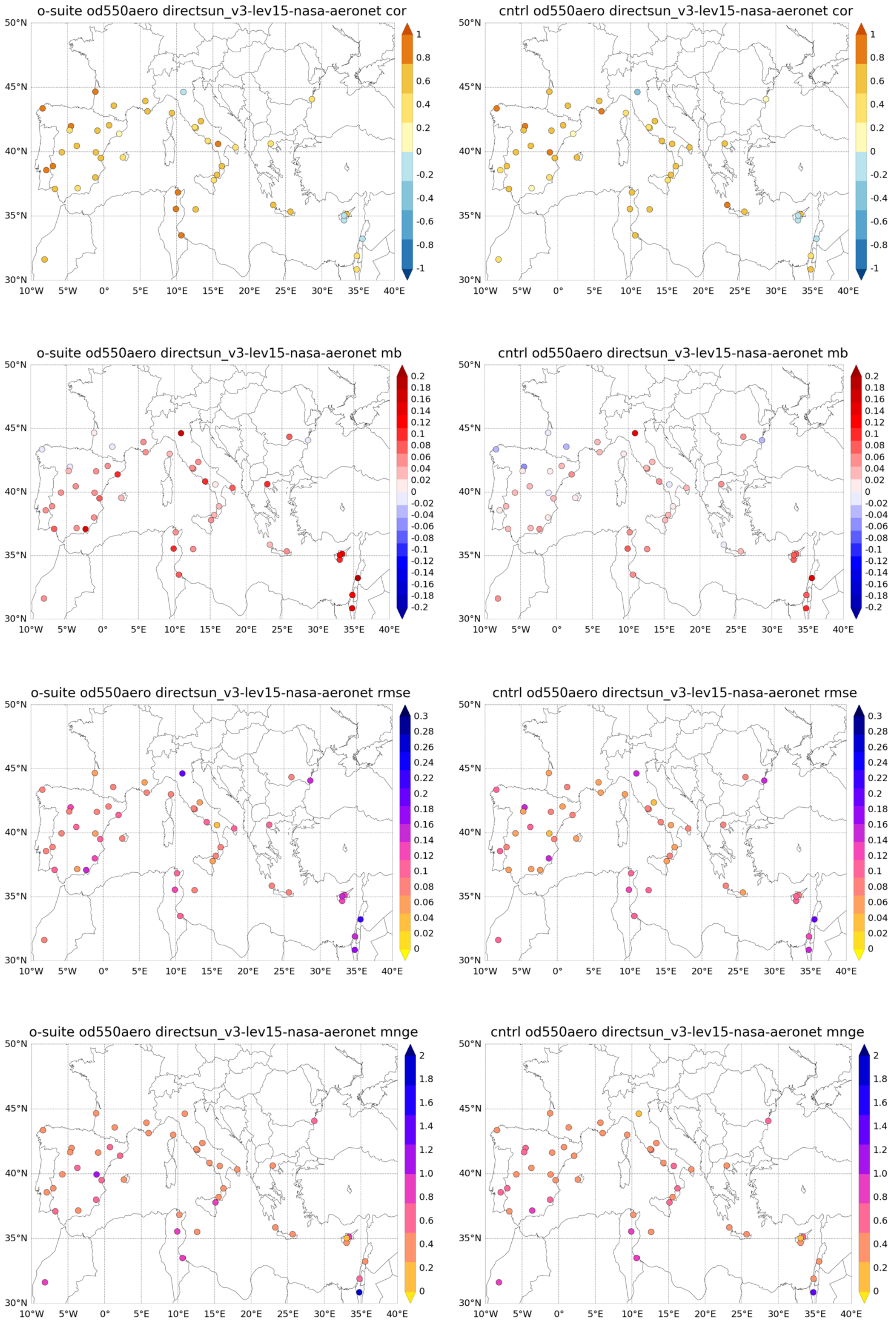

Figure 8.4.1: Skill scores (correlation coefficient, MB, RMSE and FGE) for 24-hour forecasts of CAMS o-suite and control for the study period. AOD from AERONET direct-sun is the reference.

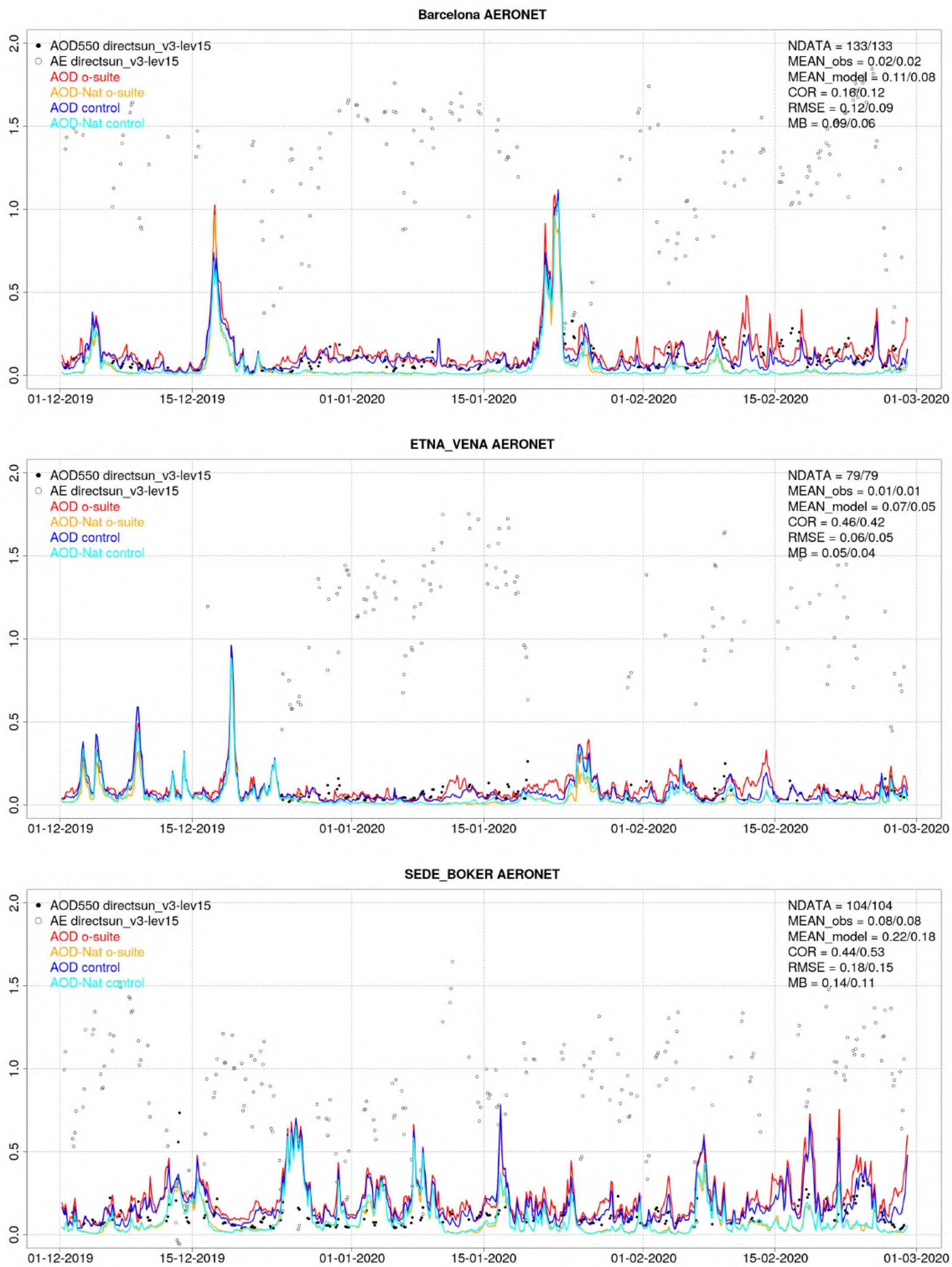

Figure 8.4.2: AOD from AERONET (black dot), AOD o-suite (red line), AOD control (blue line), AOD-Nat o-suite (orange line), AOD-Nat control (cyan line), for the study period over Barcelona (Spain), ETNA Vena (Italy) and SEDE BOKER (Crete). AOD-Nat corresponds to the natural aerosol optical depth that includes dust and sea-salt. Skill scores per each individual site and model (o—suite/control) are shown in the upper right corner (NDATA: available 3-hourly values used for the calculations, MEAN observations, MEAN model, COR, RMSE, MB).

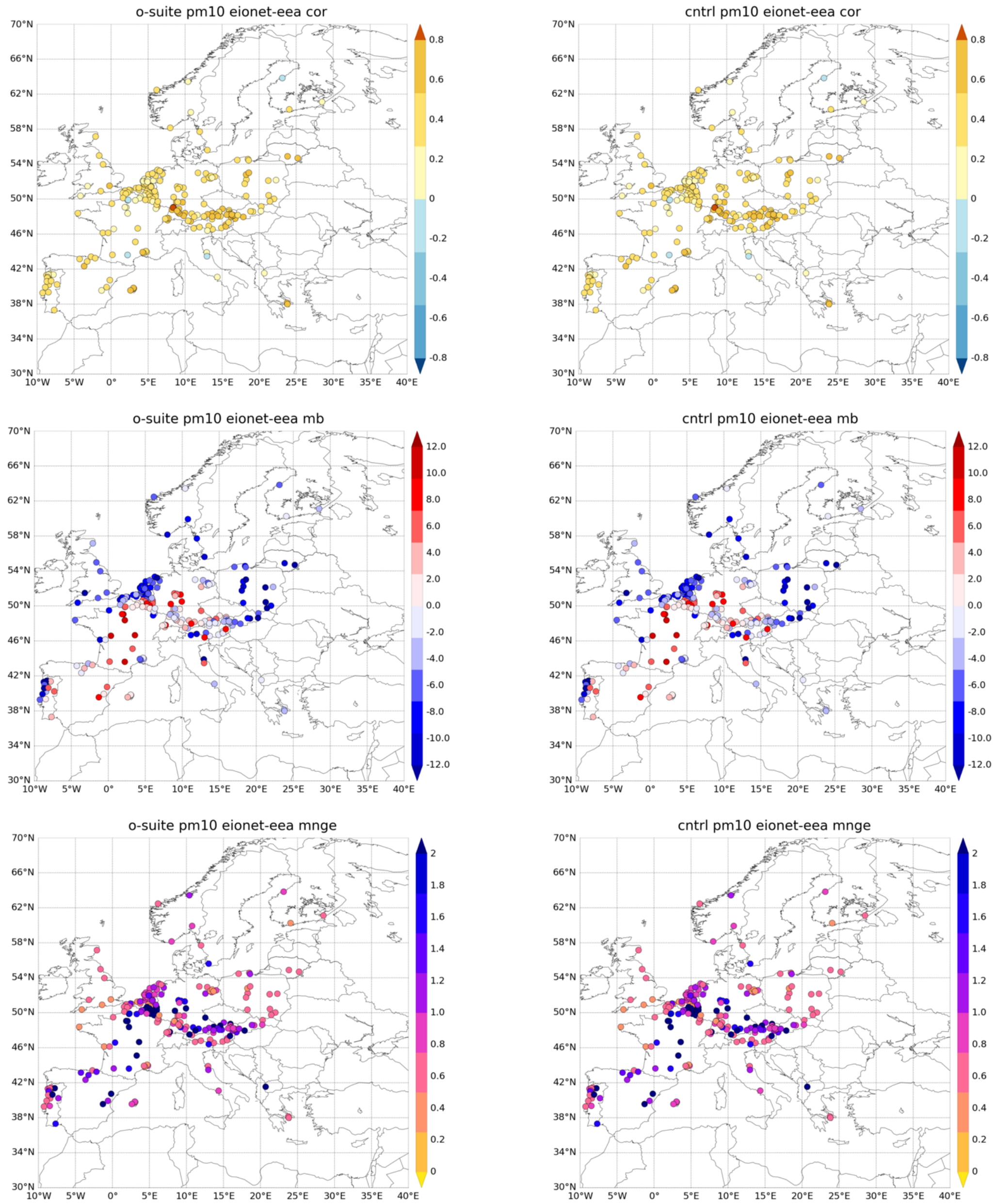

Figure 8.4.3: Skill scores (correlation coefficient, MB, RMSE and FGE) for 24-hour forecasts of CAMS o-suite and control for the study period. PM10 from EIONET are the reference. Only background suburban and rural available stations are displayed.

highest peaks on CAMS AOD simulations are linked to desert dust intrusions occurring during the whole season in the whole Mediterranean basin. This is shown in the Barcelona (Spain), Rome (Italy) and Sede Boker (Crete) AERONET sites (see Figure 8.4.2). In Barcelona, AOD values up to 1.0 are observed. In February 2020, elevated AOD values are observed in Sede Boker (up to 0.5) that are not associated with natural aerosols (i.e. dust or sea-salt). This can be associated with the latest model upgrade with the improvements implemented for the sulphur cycle.

Surface aerosol concentrations in Europe

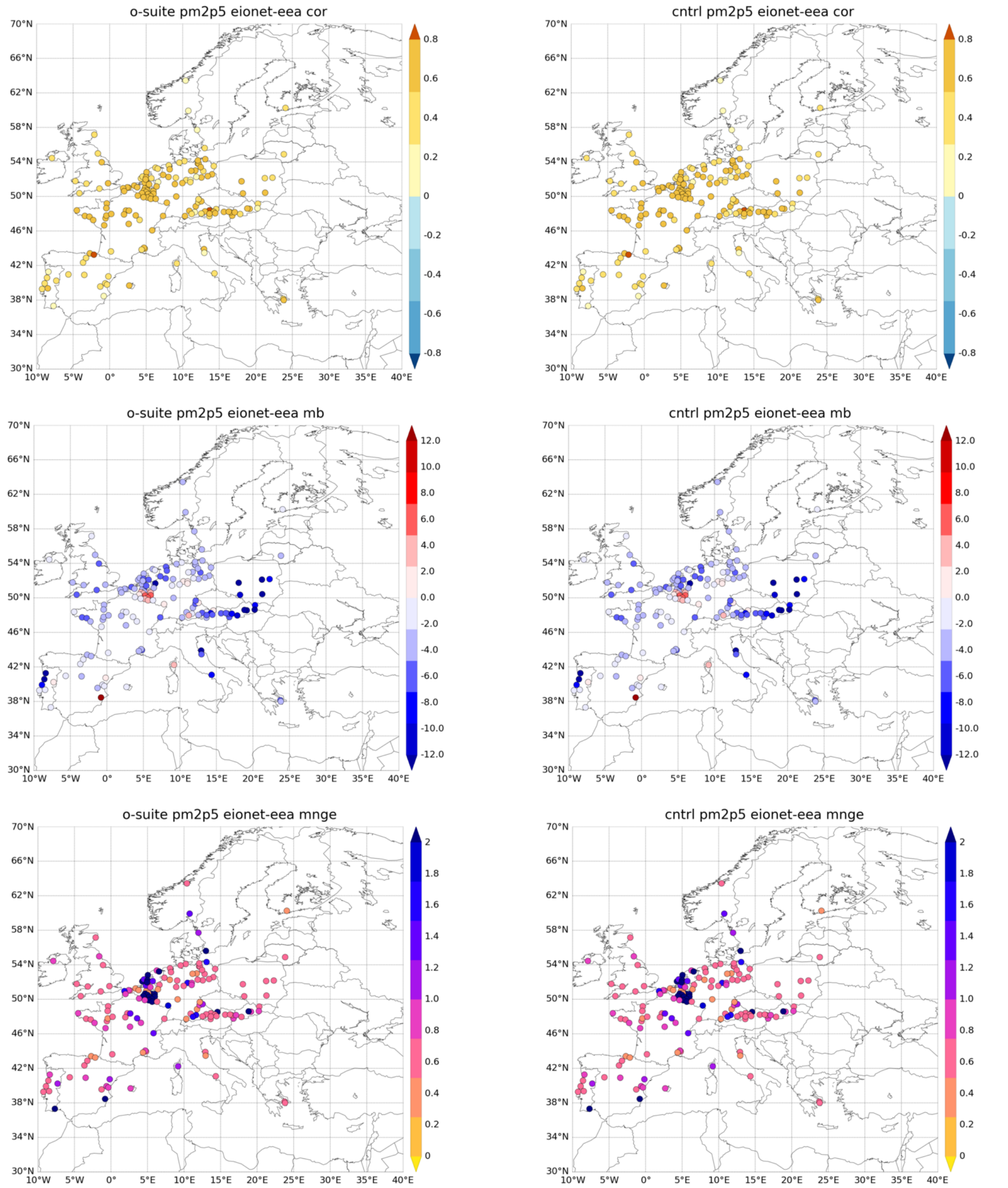

Figure 8.4.4: Skill scores (correlation coefficient, MB, RMSE and FGE) for 24-hour forecasts of CAMS o-suite and control for the study period. PM2.5 from EIONET are the reference. Only background suburban and rural available stations are displayed.

For winter, CAMS o-suite and control show very similar skill scores for PM10 and PM2.5 in comparison with EIONET-Airbase observations (see Figure 8.4.3). The CAMS experiments tend to underestimate the surface concentration EIONET-Airbase observations with MB of -3.46 and -3.92 µg/m3, respectively for PM10 and PM2.5 (see Figure 8.4.3 and Figure 8.4.4). However, overestimations are observed in Central and Southern European sites (see Figure 8.2.5).

The upgrade of the CAMS o-suite during July 2019 led to an increase of the coarse particles at the surface, as shown in Figure 8.2.5. During the whole study period peaks above 50 µg/m^3 for PM10 are observed.

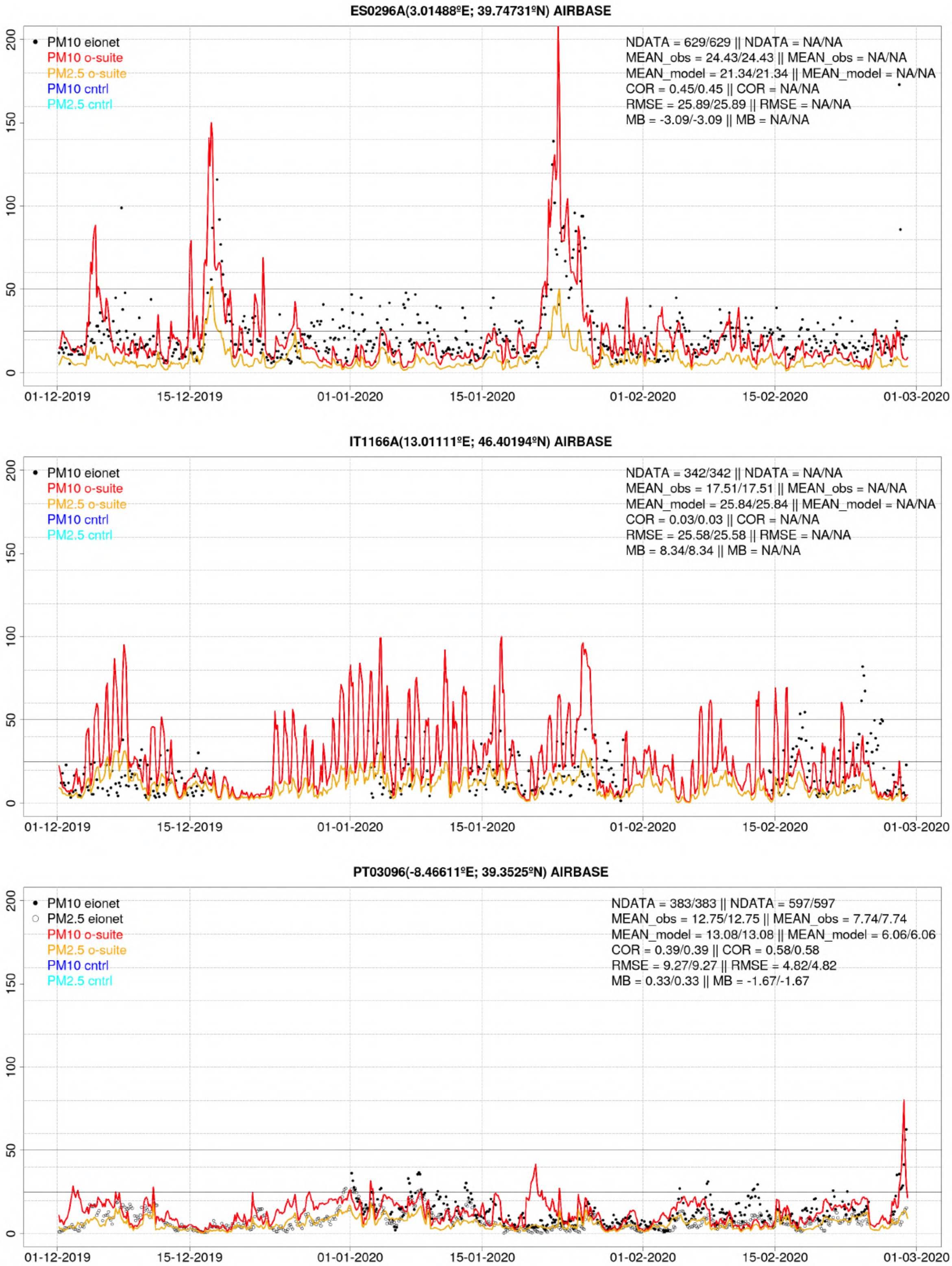

Figure 8.4.5: PM10 and PM2.5 Airbase observations (black and grey dots, respectively), PM10 and PM2.5 o-suite (red and orange lines, respectively) and PM10 and PM2.5 control (blue and cyan lines, respectively) for the study period over ES1691A (Spain), IT1166A (Italy) and PT03096 (Portugal).

9. Stratosphere

9.1 Validation against ozone sondes

In this section, we present the results of the stratospheric ozone evaluation against ozone soundings from the NDACC, WOUDC, NILU and SHADOZ databases. The sondes have a precision of 3-5% (~10% in the troposphere for Brewer Mast) and an uncertainty of 5-10%. For further details see Cammas et al. (2009), Deshler et al. (2008) and Smit et al (2007). Model profiles of the o-suite are compared to balloon sondes measurement data of 44 stations for the period January 2013 to February 2020 (please note that towards the end of the validation period fewer soundings are available). As C-IFS-CB05 stratospheric composition products beyond O_3 in the o-suite is not useful we provide only a very limited evaluation of the control experiment. A description of the applied methodologies and a map with the sounding stations can be found in Eskes et al. (2019). Please note that recent scientific findings (https://tropo.gsfc.nasa.gov/shadoz/Archive.html, Thompson et al., 2017; Witte et al., 2017; 2018, Stauffer, et al. in preparation 2020) show a drop-off in Total Ozone at various global ozone stations in comparison with satellite instruments. This drop-off amounts between 5-10% for stratospheric ozone. Changes in the ECC ozone instrument are associated with the drop-off, but no single factor has been identified as cause yet.

The o-suite shows MNMBs within the range ±14%, for all regions and months (some exceptions with MNMBs of up to ±18% for single months in the high latitude regions). Figure 9.1.1 shows the results for the past year.

Fig. 9.1.2 compares the averaged profiles in each region during January 2020. The vertical distribution of stratospheric ozone is quite well represented for all regions by the o-suite (MNMBs between -2.7 to 2.1% for DJF 2019/2020). The control run shows a strong overestimation of stratospheric ozone in the Arctic stratosphere and underestimations for Antarctica.

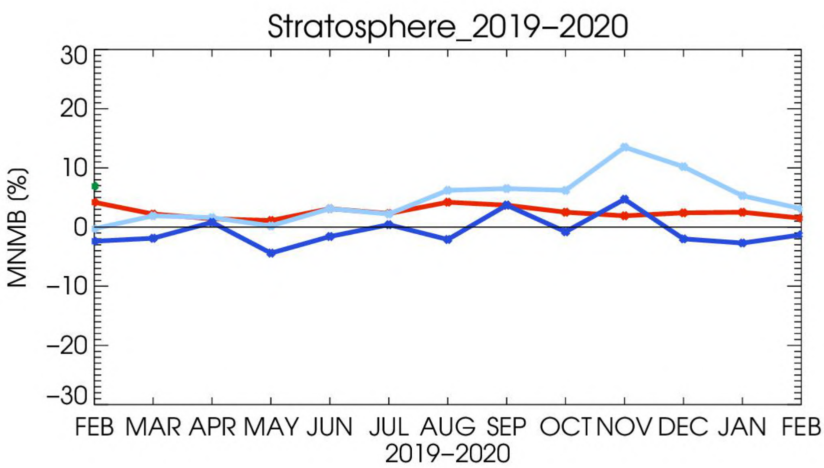

Figure 9.1.1: MNMBs (%) of ozone in the stratosphere from the o-suite against aggregated sonde data in the Arctic (light blue), Antarctic (dark blue) and northern midlatitudes (red). Period February 2019 to February 2020. The stratosphere is defined as the altitude region between 90 and 10 hPa.

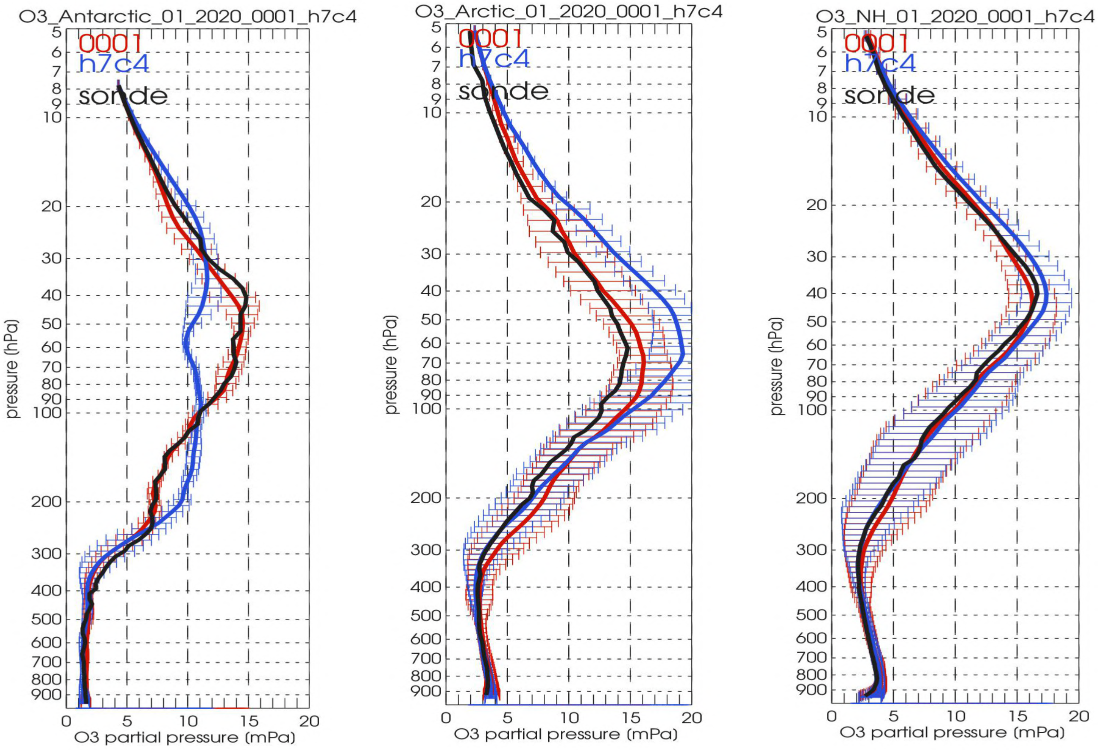

Figure 9.1.2: Comparison between mean O_3 profiles (units: mPa) of o-suite (red), and control (blue) in comparison with observed O_3 sonde profiles (black) for January 2020 for the various latitude bands: Arctic, NH-mid latitudes and Antarctic.

9.2 Validation against observations from the NDACC network

UVVIS column and FTIR stratospheric columns

Since the start of the CAMS27 project, the number of UVVIS Zenith ozone measurements have increased on NDACC. Currently sixteen sites provided data in the recent quarter allowing for a representative picture on the latitude dependence of the model data.

The systematic uncertainty of the UVVIS measurements is typically 5%, hence the relative biases for most sites for both the AN and 1d FC of the o-suite are very close to each other and within the uncertainty ranges, see Figure 9.2.1. The averaged bias for the 14 UVVIS sites is comparable to the measurement uncertainty of 5%, the averaged correlation is above 0.9 for the entire time period (2016-2020).

The correlations between the sites and the model are presented in the Taylor diagrams in Figure 9.2.2. Again, the o-suite AN and 1d FC perform very similarly in correlation coefficients.

Figure 9.2.3 depicts the FTIR stratospheric columns showing a discontinuity in the o-suite 1d FC model for the tropical sites (Mauna Loa, Altzomoni and Reunion) in the June 2016 model update. The worse performance of the tropical sites is also seen in lower correlations in Figure 9.2.2.

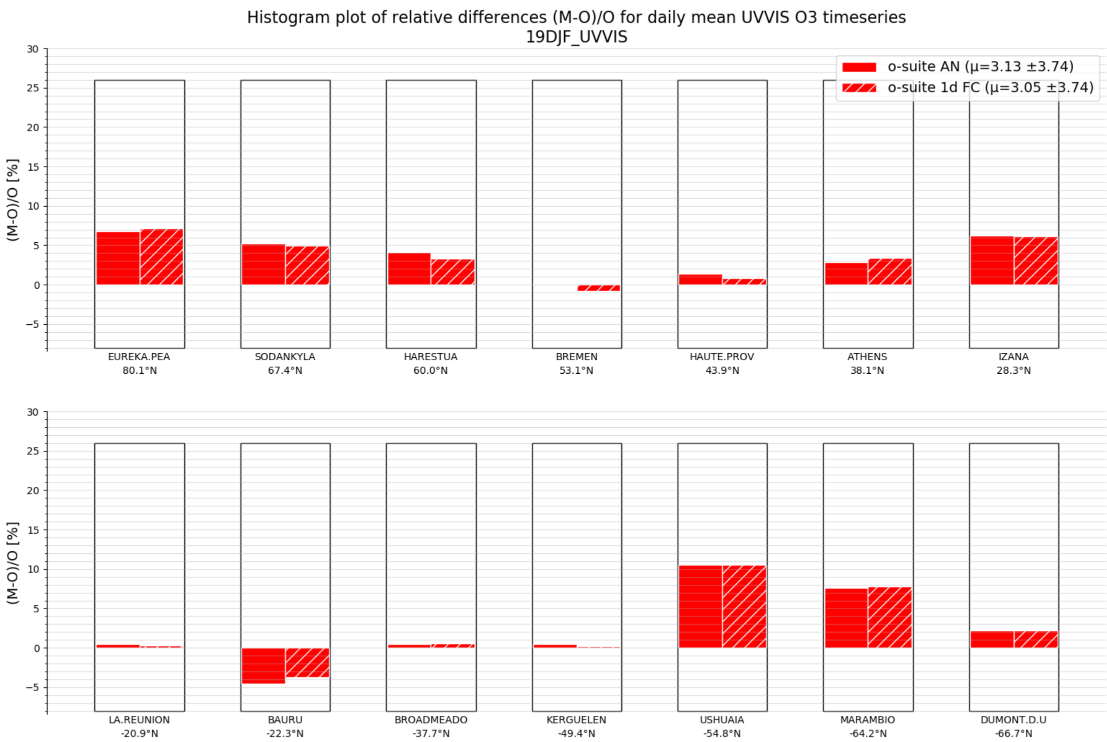

Figure 9.2.1. Relative biases during quarter DJF 2020 for 14 UVVIS stations measuring stratospheric ozone columns with ZENITH measurement geometry (stations sorted with decreasing latitude). The overall relative bias is positive for all latitudes and comparable to the typical measurement uncertainty of 5% for most of the sites.

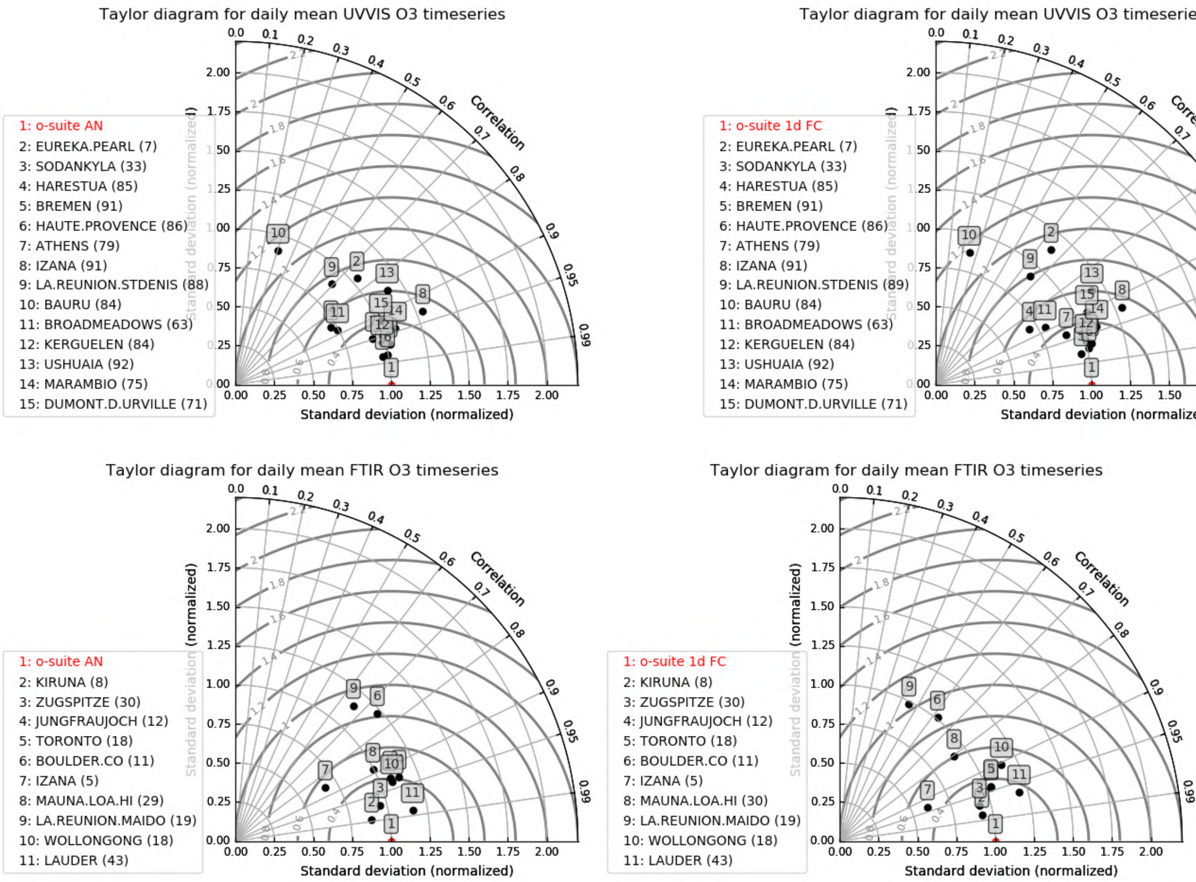

Figure 9.2.2. Taylor diagrams relating the standard deviations for the model and GB stratospheric column time series and their correlation for the time period DJF-2020. All time-series are normalized such that the standard deviation of the model is 1. The performance for the o-suite is slightly better (averaged correlation is 0.89 for FTIR and 0.85 for UVVIS) compared to the 1-day forecast (averaged correlation is 0.85 for FTIR and 0.84 for UVVIS). Again, the correlation for the tropical sites are worse in the 1-day forecast compared to the analysis.

Profile comparison using LIDAR and MWR

In this section we present a comparison between the CAMS o-suite and control products against MWR and LIDAR observations from the NDACC network. A detailed description of the instruments and applied methodologies for all NDACC instruments can be found at http://nors.aeronomie.be. MWR (microwave) at Ny Alesund (79°N, 12°E, Arctic station) and Bern (47°N, 7°E, northern midlatitude station). LIDAR at Observatoire Haute Provence (OHP), France (43°N, 5.7°E, altitude 650m), Hohenpeissenberg, Germany (47°N, 11°E, altitude 1km) and Mauna Loa, Hawaii (19.5°N, 204°E, altitude 3.4km)

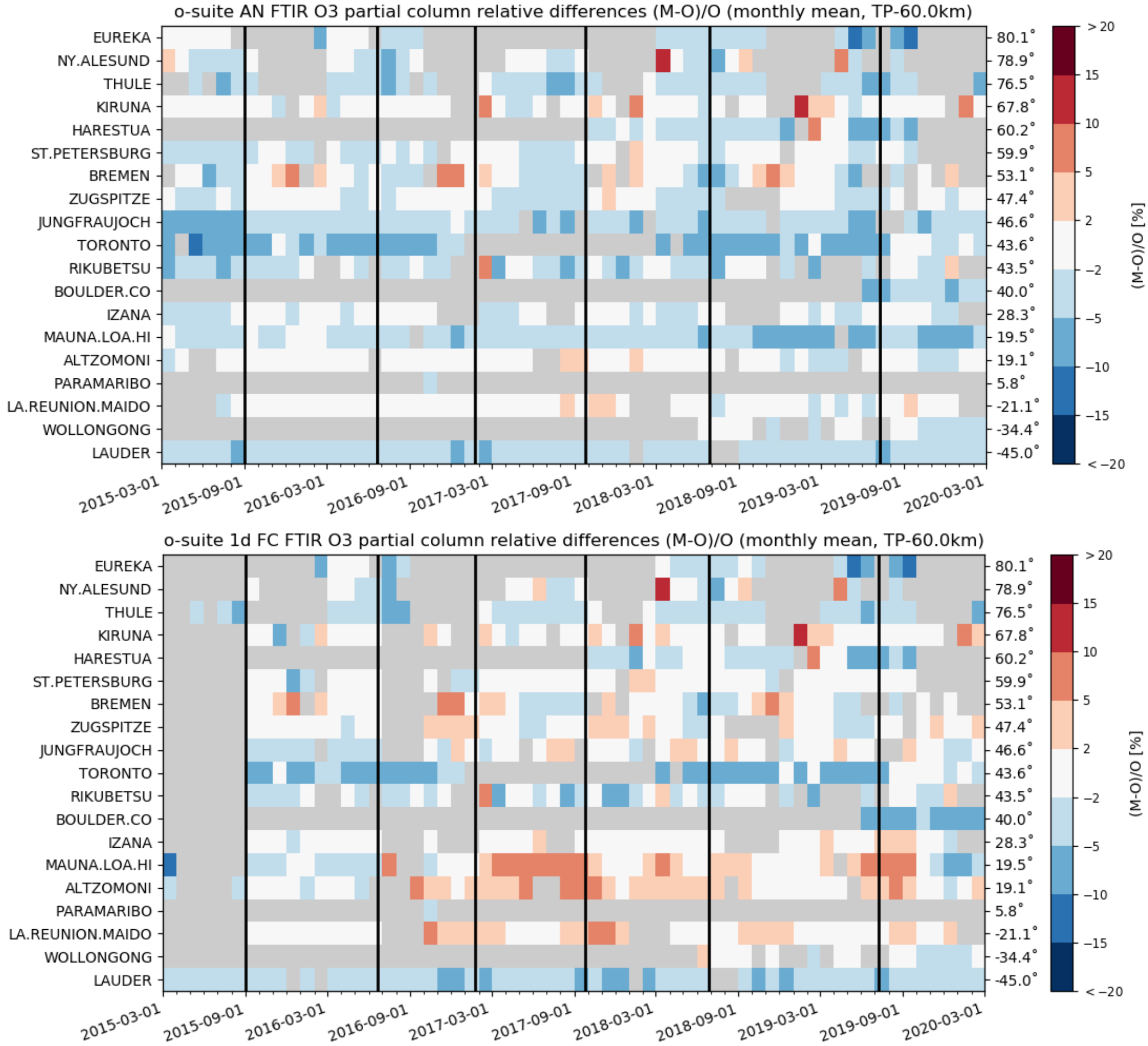

Figure 9.2.3 Time series of monthly mean relative differences for stratospheric FTIR columns along with model cycle updates (black vertical lines) (o-suite AN top, o-suite 1d FC bottom). The stratospheric FTIR columns for the tropical sites at Izana, Mauna Loa, Altzomoni and Reunion show a higher overestimation for the 1dFC compared to the AN.

At OHP, Hohenpeissenberg and Mauna Loa (LIDAR, see Figure 9.2.4), the o-suite slightly overestimates the observed ozone (<10%) between 25km and 35km. The uncertainty on the LIDAR concentration increases with altitude and above 35km the observed differences are comparable to the measurement uncertainty (>10%, see http://nors.aeronomie.be/projectdir/PDF/NORS_D4.2_DUG.pdf).

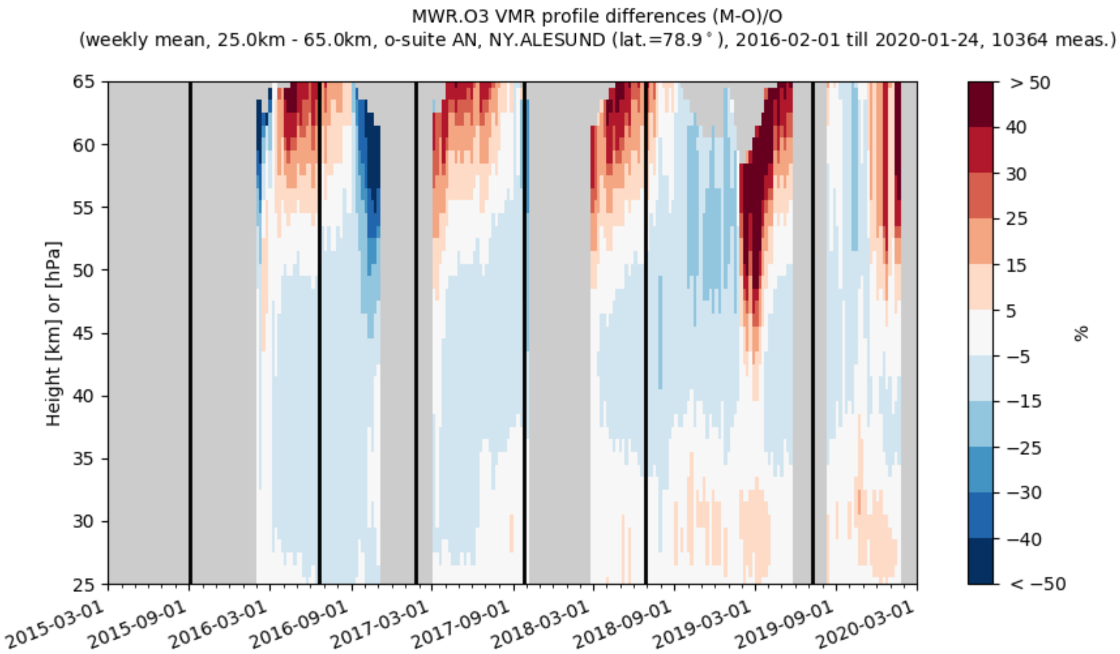
MWR.O3 VMR profile differences (M-O)/O
(weekly mean, 25.0km - 65.0km, o-suite AN, NY.ALESUND (lat.=78.9 °), 2016-02-01 till 2020-01-24, 10364 meas.)
Height [km] or [hPa]
%
> 50
40
30
25
15
5
−5
−15
−25
−30
−40
< −50
2015-03-01
2015-09-01
2016-03-01
2016-09-01
2017-03-01
2017-09-01
2018-03-01
2018-09-01
2019-03-01
2019-09-01
2020-03-01

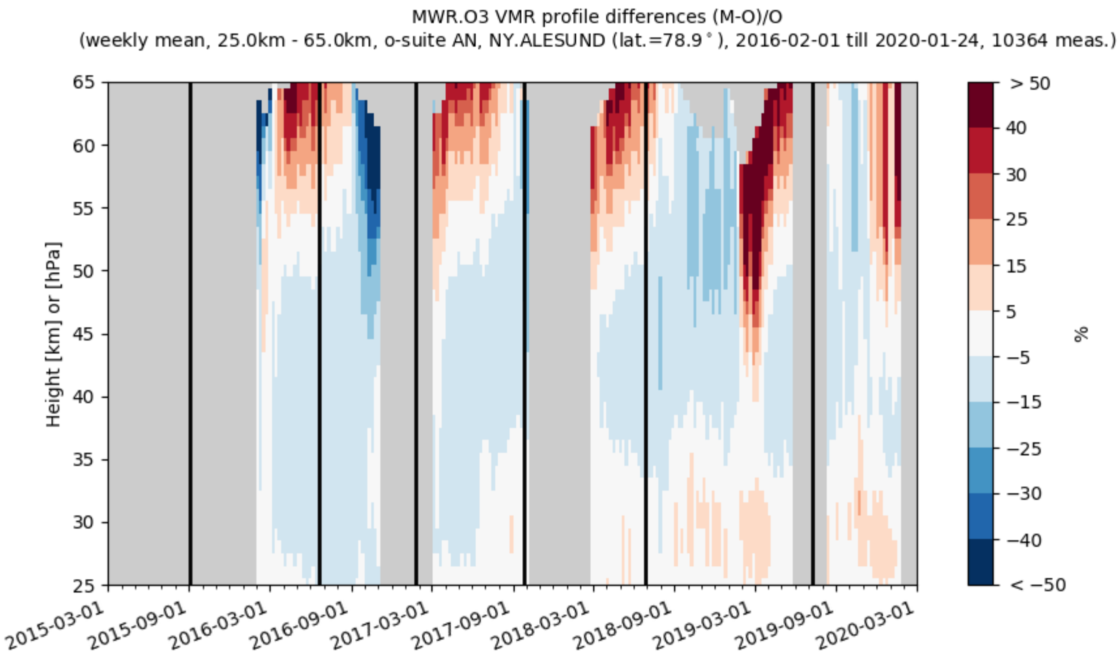
MWR.O3 VMR profile differences (M-O)/O
(weekly mean, 25.0km - 65.0km, o-suite AN, NY.ALESUND (lat.=78.9 °), 2016-02-01 till 2020-01-24, 10364 meas.)
Height [km] or [hPa]
%
> 50
40
30
25
15
5
−5
−15
−25
−30
−40
< −50
2015-03-01
2015-09-01
2016-03-01
2016-09-01
2017-03-01
2017-09-01
2018-03-01
2018-09-01
2019-03-01
2019-09-01
2020-03-01

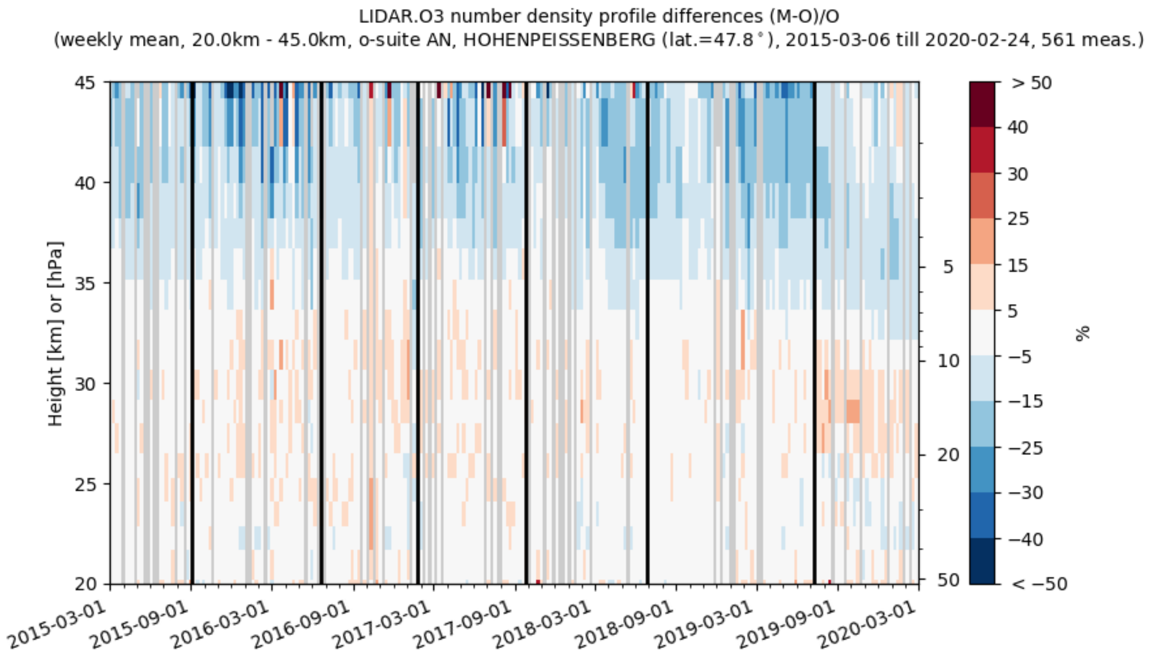
LIDAR.O3 number density profile differences (M-O)/O
(weekly mean, 20.0km - 45.0km, o-suite AN, HOHENPEISSENBERG (lat.=47.8°), 2015-03-06 till 2020-02-24, 561 meas.)
Height [km] or [hPa]
%
2015-03-01
2015-09-01
2016-03-01
2016-09-01
2017-03-01
2017-09-01
2018-03-01
2018-09-01
2019-03-01
2019-09-01
2020-03-01

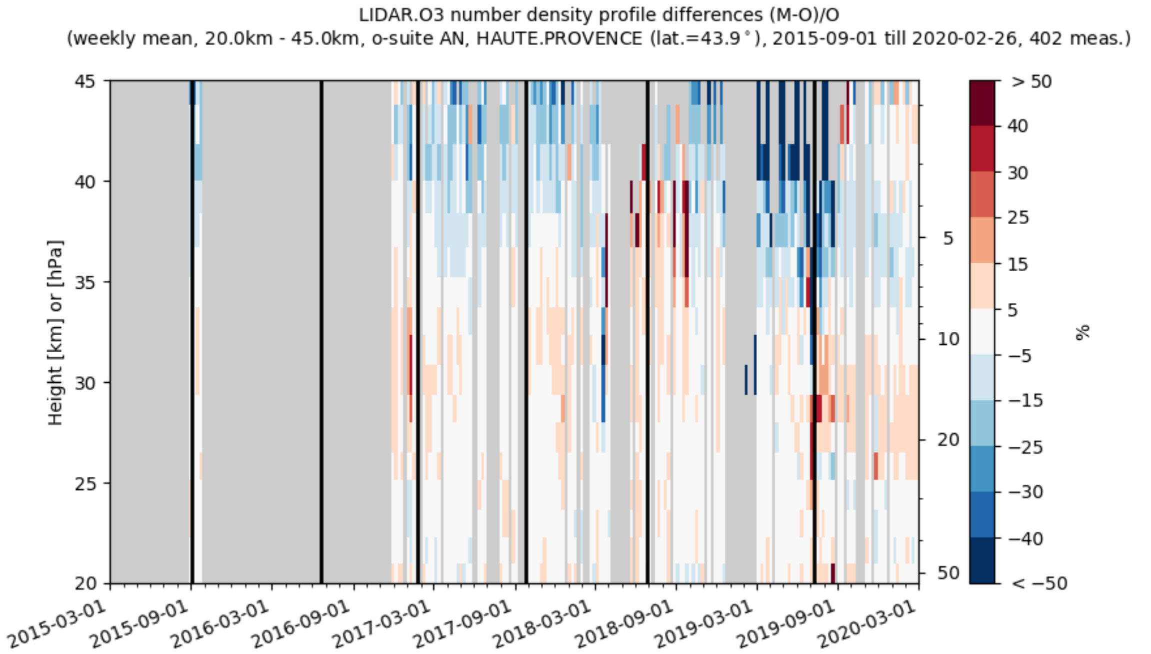
LIDAR.O3 number density profile differences (M-O)/O
(weekly mean, 20.0km - 45.0km, o-suite AN, HAUTE.PROVENCE (lat.=43.9°), 2015-09-01 till 2020-02-26, 402 meas.)
Height [km] or [hPa]
%
2015-03-01
2015-09-01
2016-03-01
2016-09-01
2017-03-01
2017-09-01
2018-03-01
2018-09-01
2019-03-01
2019-09-01
2020-03-01

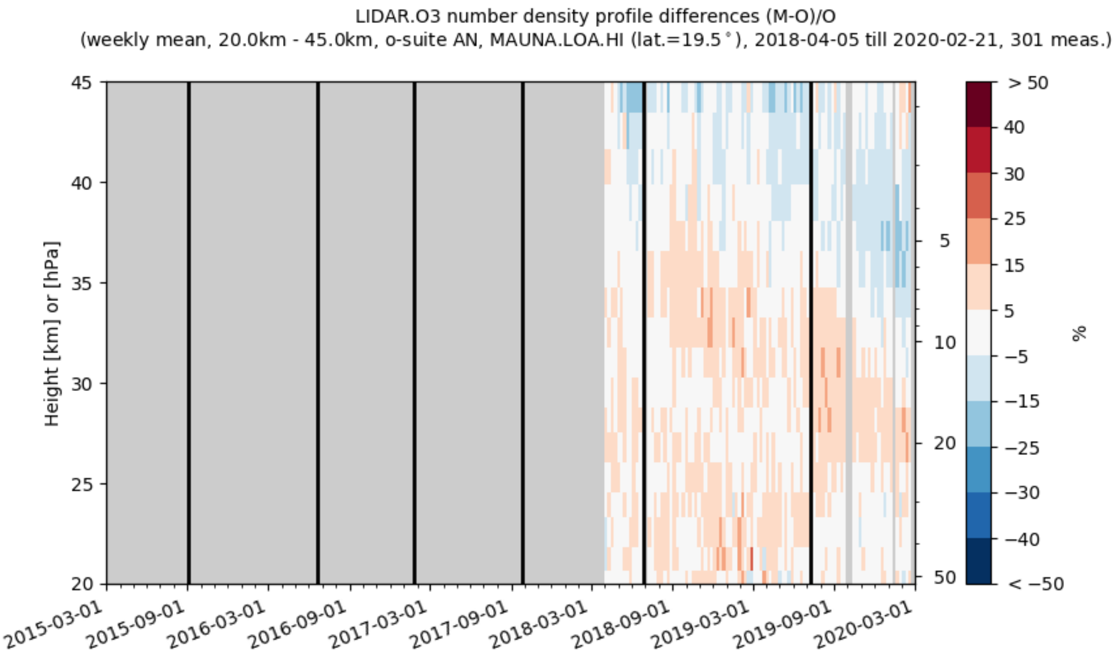

Figure 9.2.4: Comparison of the weekly mean profile bias between the O3 mixing ratios of o-suite AN and the NDACC station at Ny Alesund, Bern, Hohenpeissenberg, OHP and Mauna Loa. For the LIDAR stations, the measurement uncertainty above 35km is comparable to the observed profile bias.

9.3 Comparison with dedicated systems and with observations by limb-scanning satellites

This section compares the output of the o-suite for the last period with observations by limb-scanning satellite instruments, using the methodology described by Lefever et al. (2015). We also include the comparisons for the o-suite 4th day forecasts (96h to 120h) of stratospheric ozone. These forecasts are represented by dotted lines in the figures.

All datasets are averaged over all longitudes and over the three most interesting latitude bands for stratospheric ozone: Antarctic (90°S-60°S), Tropics (30°S-30°N) and Arctic (60°N-90°N). In order to provide global coverage, the two mid-latitude bands (60°S-90°S and 60°N-90°N) are also included in some comparisons with satellite observations.

The level-2 data from limb scanning instrument used in this section are:

- ACE-FTS version 3.6, on board SCISAT-1
- SAGE-III version 5.1, on board the International Space Station (ISS); among the 3 different ozone profiles delivered by the solar occultation (denoted Mesospheric, MLR and AO3), we use the AO3 retrieval which is recommended by the mission science team.
- OMPS-LP version 2.5, on board NPP

For reference, we include also the BASCOE analyses which are very constrained by the AURA MLS offline profiles.

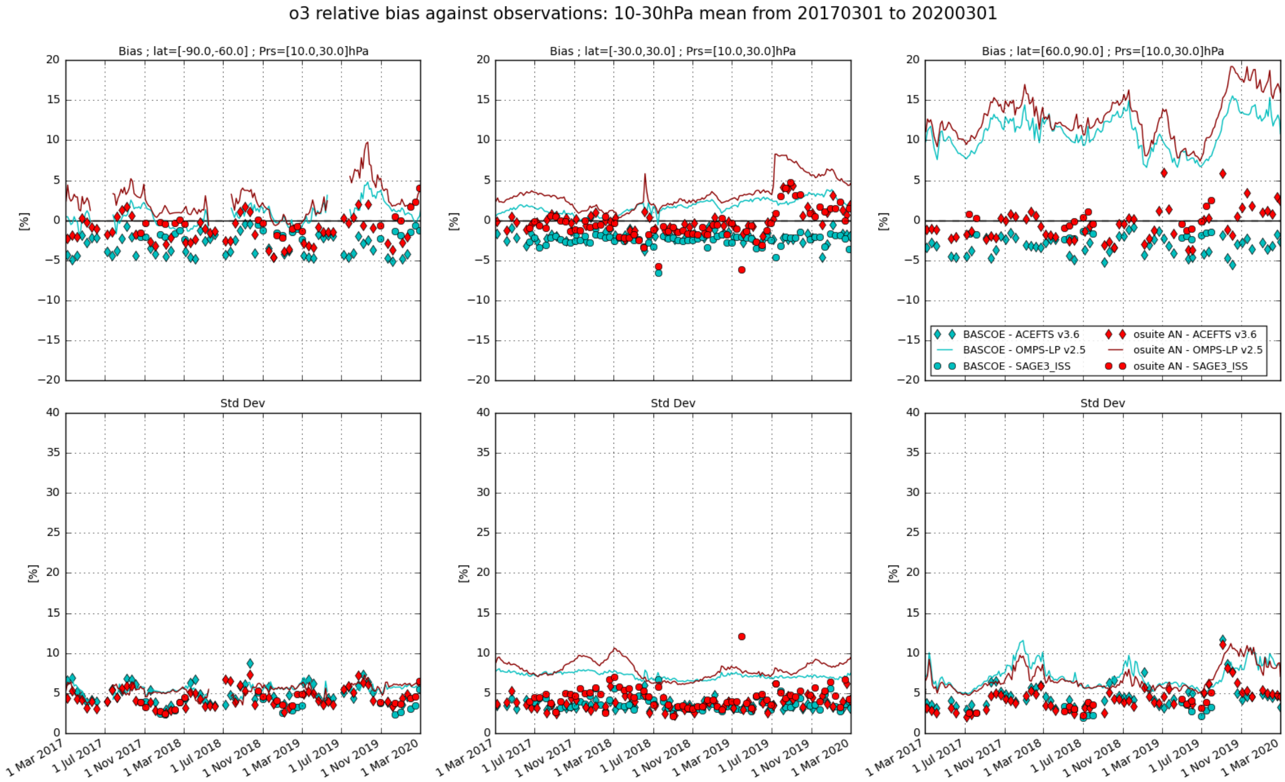

Figure 9.3.1: Time series comparing models to observations for the period 2017-03-01 to 2020-03-01 in the upper stratosphere (10-30hPa averages): o-suite analyses (red) and BASCOE (cyan) vs OMPS-LP (solid), ACE-FTS (diamonds) and SAGE-III (bullets). Top row: normalized mean bias (model-obs)/obs (%); bottom row: standard deviation of relative differences (%).

Figure 9.3.1 to 9.3.3 present, in the upper row, the time series over the last 36 months of the bias of the o-suite against the three satellite measurements for respectively three layers of the stratosphere (10-30hPa upper, 30-70hPa middle, and 70-100hPa lower and UTLS); the bottom row of the figures shows the standard deviation of the differences and can be used to evaluate the random error in the analyses.

In the tropics for the 70-100hPa region, the comparison with all instruments is unreliable (highly scattered bias and large standard deviations)

The agreement with ACE-FTS is good: the bias is generally within ±5% for all regions.

The SAGE-III onboard ISS provide observations since June 2017. The latitudinal coverage is more limited than ACE-FTS; the polar regions are not covered for long periods of time (data available only in the summer). Where available, the agreement of the osuite with SAGE-III is good, with biases similar to those observed against ACE-FTS, except in the tropics in the 30-70hPa region where they are more positive (3-13%).

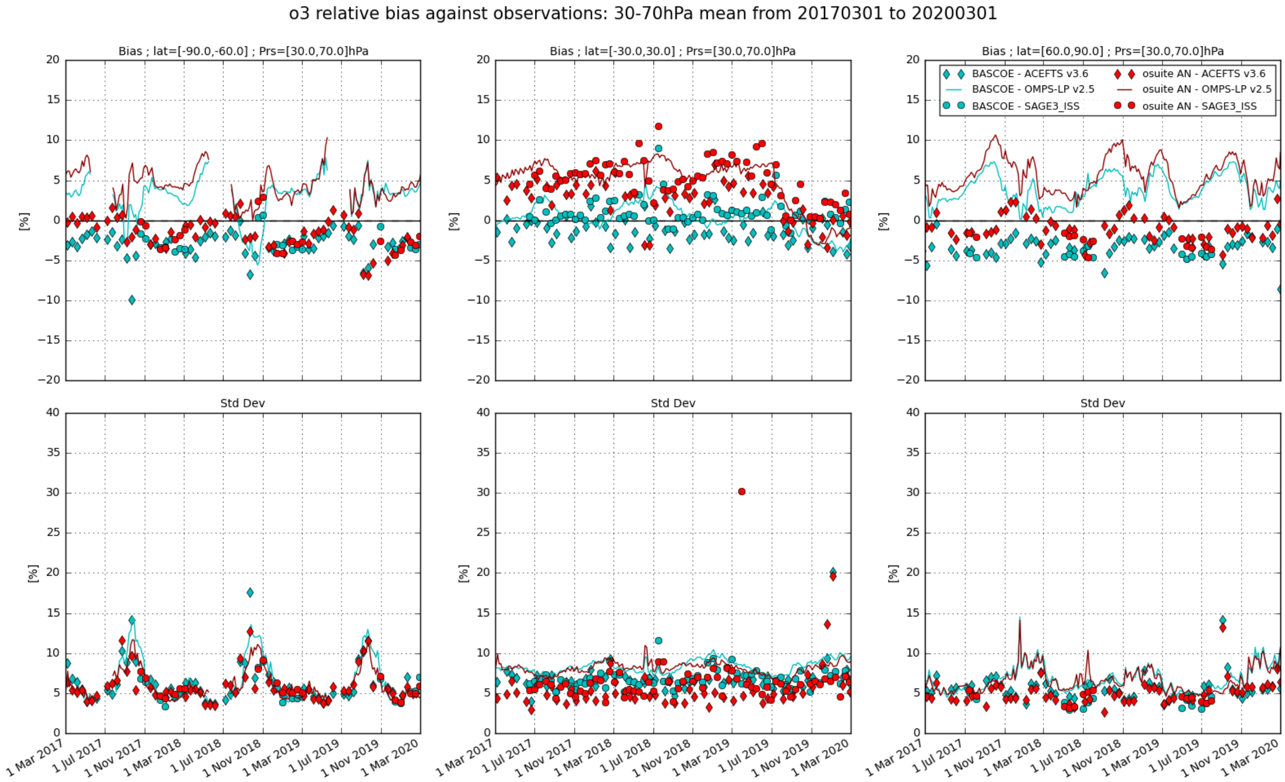

Figure 9.3.2: Time series comparing models to observations for the period 2017-03-01 to 2020-03-01 in the middle stratosphere (30-70hPa averages): o-suite analyses (red) and BASCOE (cyan) vs OMPS-LP (solid), ACE-FTS (diamonds) and SAGE-III (bullets). Top row, normalized mean bias (model-obs)/obs (%); bottom row, standard deviation of relative differences (%).

Compared to OMPS-LP, there is an almost systematic overestimation by the o-suite; the biases are more variable and more marked than for the other instruments (10% to 15% in the north polar at 10-30hPa region, up to 10% at 30-70hPa and up to 20% at 70-100hPa).

The bias of BASCOE against the satellite observations for the considered regions is systematically lower, but follows a similar evolution as the o-suite. Using the BASCOE bias as a reference for the evolution of the osuite bias, the change of model settings in the osuite in July 2019 causes an increase of ~3% in the 10-30hPa pressure range, and a decrease of ~3% in the Tropics in the 30-70hPa.

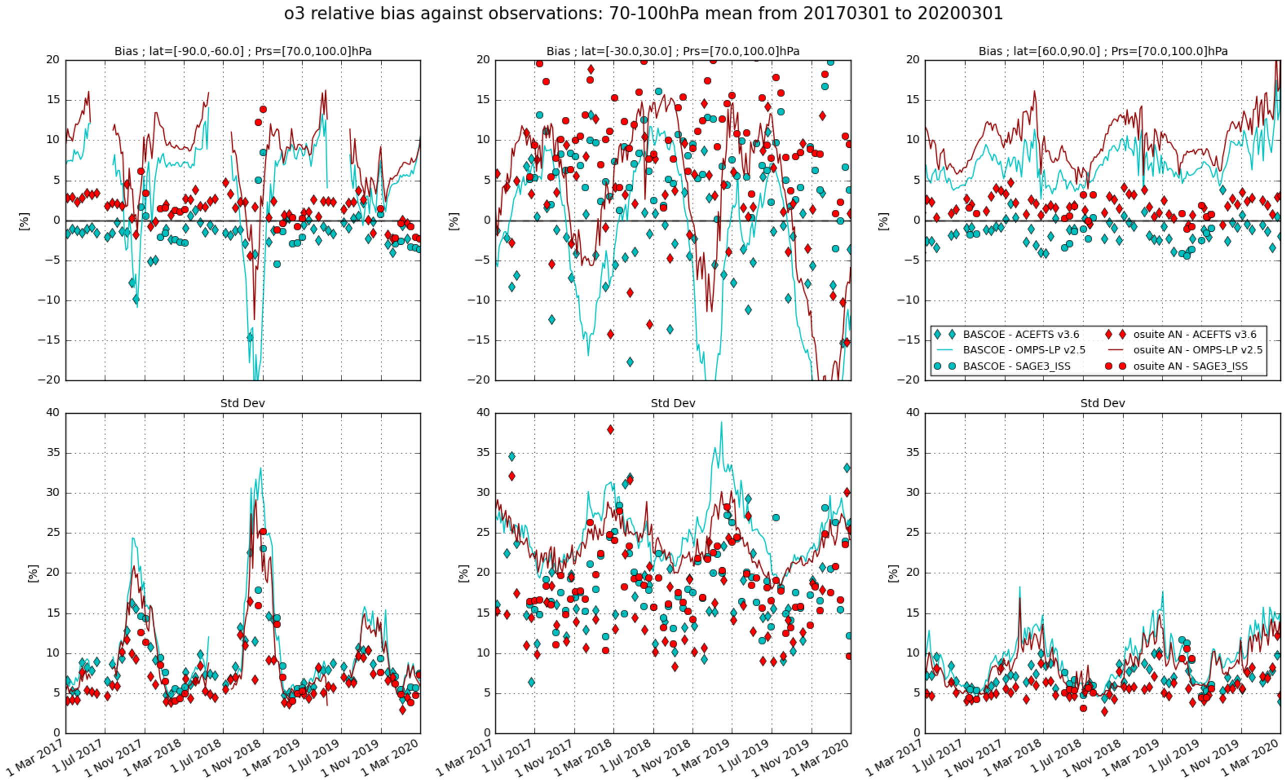

Figure 9.3.3: Time series comparing models to observations for the period 2017-03-01 to 2020-03-01 in the lower stratosphere (70-100hPa averages): o-suite analyses (red) and BASCOE (cyan) vs OMPS-LP (solid), ACE-FTS (diamonds) and SAGE-III (bullets). Top row, normalized mean bias (model-obs)/obs (%);bottom row, standard deviation of relative differences (%).

Figure 9.3.4 to 9.3.7 display vertical profiles of the relative biases between the o-suite or BASCOE and the satellite measurements. The difference is averaged over the most recent 3-month period considered in this validation report, i.e. DJF 2020.

All o-suite profiles present a common feature of a slight overestimation at around 30km, followed by a stronger underestimation at around 40km, which is evidenced in the 4th day forecast.

The profiles of OMPS-LP in the northern hemisphere present irregularities (mainly in the part contributed by the sensor in the visible), which are not found in the other instruments nor in the o-suite or the BASCOE models; hence they should be disregarded for this validation.

At the higher part of the north polar profiles, an overestimation of ~1.5 ppm is seen above 55km compared to ACE-FTS and 0.5 hPa compared to MLS. This is a typical phenomenon in the osuite which appears systematically above the south polar region in the months of August-September and above the north polar region in February-March.

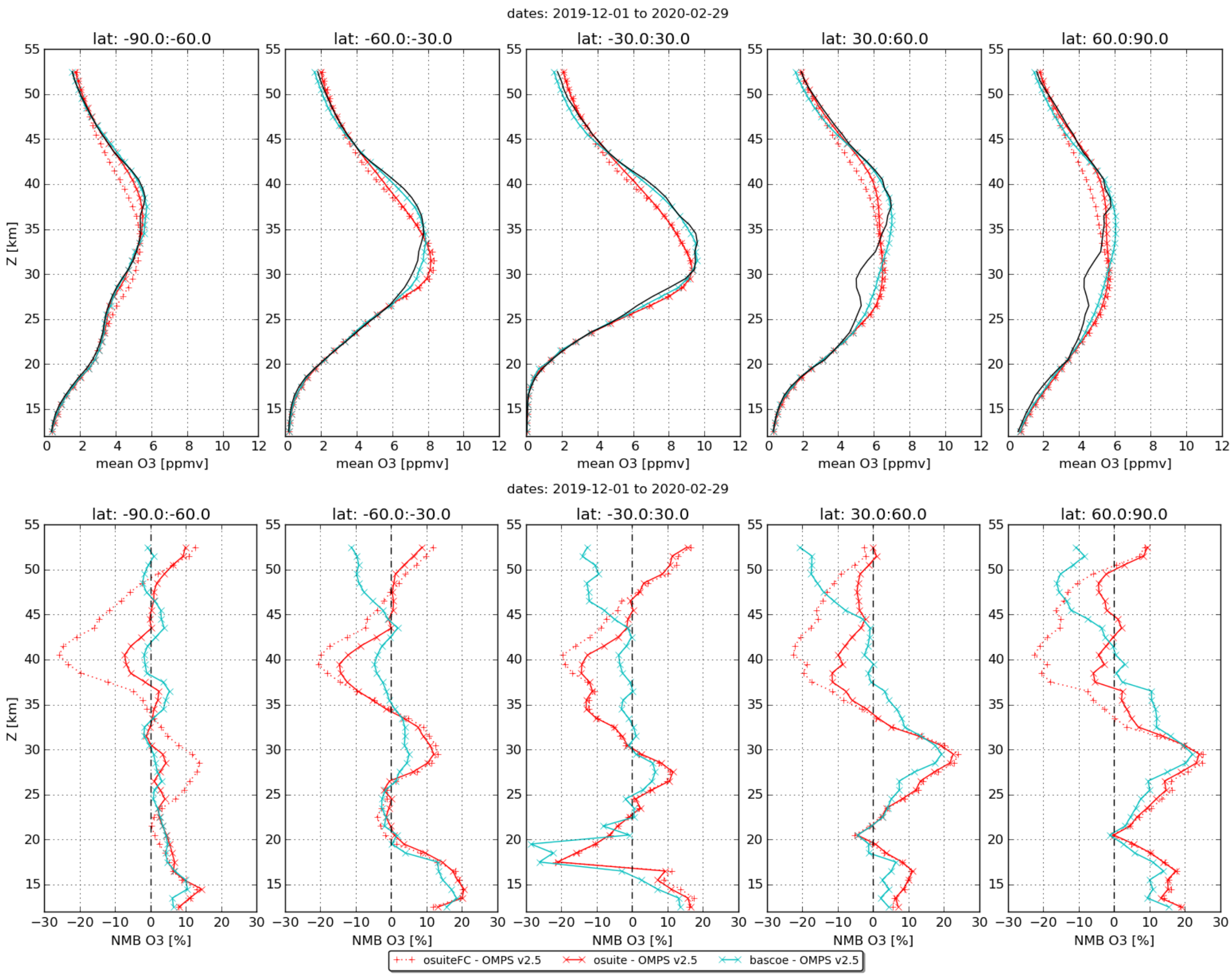

Figure 9.3.4: Mean value (top) and normalized mean bias (bottom) of the ozone profile between o-suite analyses (red, solid), o-suite forecasts 4th day (red, dotted) and BASCOE (cyan line) with OMPS-LP v2.5 observations for the period DJF2020.

It must be noted that the different instruments have a variety of spatial and temporal coverage: for a 3 month period and over the latitude bands considered, OMPS and Aura MLS provide daily data with more than 40000 valid profiles, while ACE-FTS provides around 700 profiles in the polar region and 200 profiles in the tropics, and SAGE-III around 800 profiles in each latitude band except the north polar region (none).

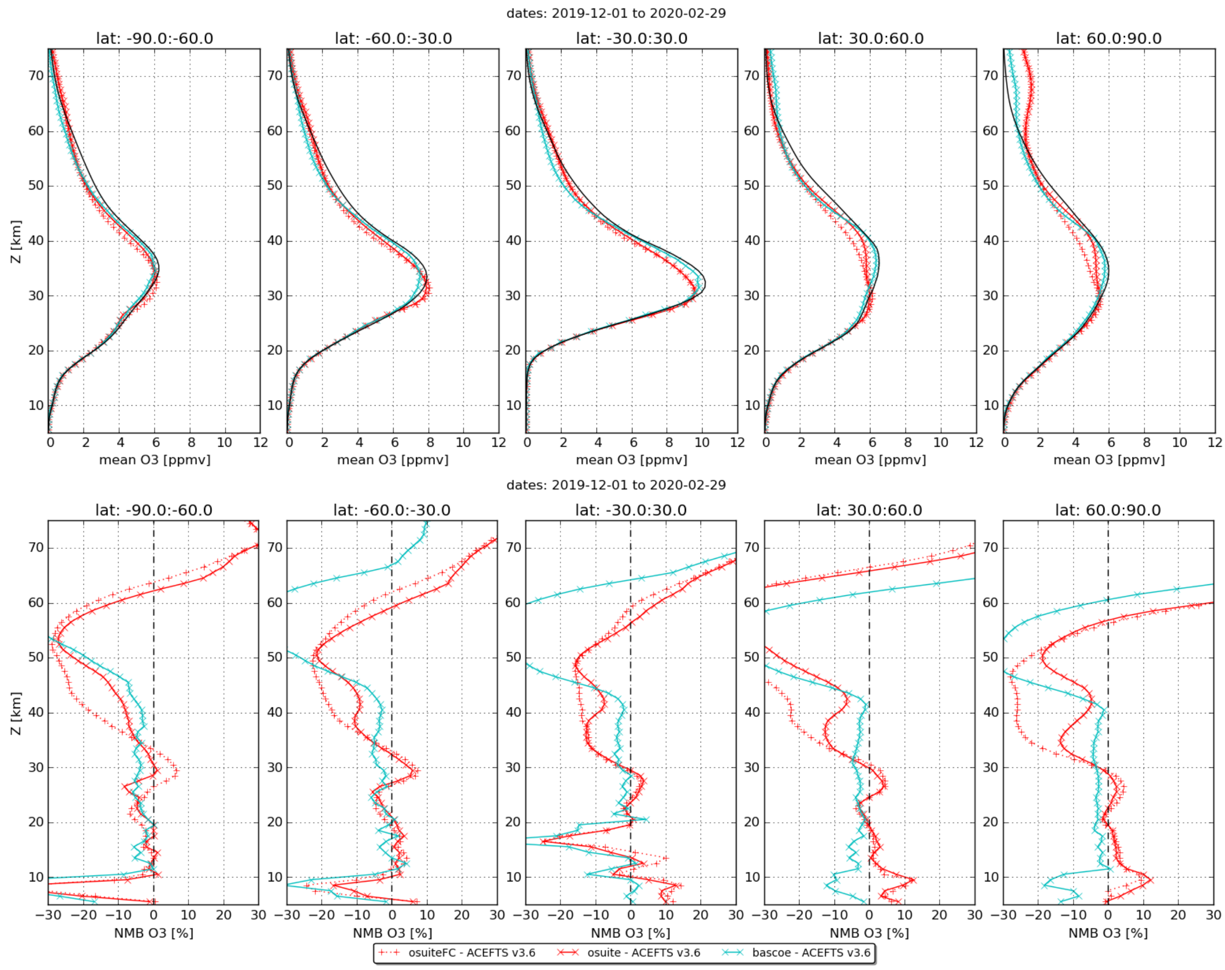

Figure 9.3.5: Mean value (top) and normalized mean bias (bottom) of the ozone profile between o-suite analyses (red, solid), o-suite forecasts 4th day (red, dotted) and BASCOE (cyan line) with ACE-FTS observations for the period DJF 2020.

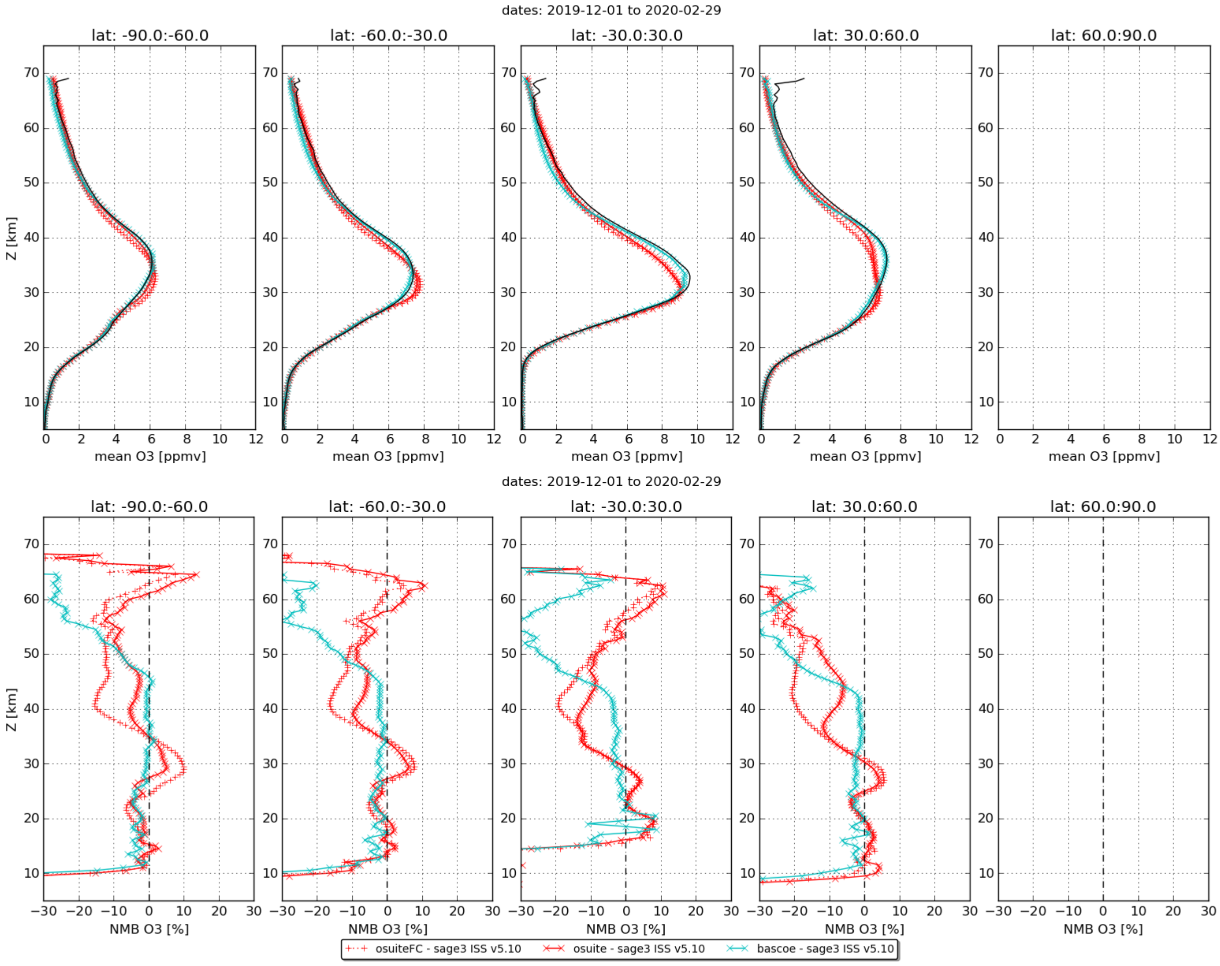

Figure 9.3.6: Mean value (top) and normalized mean bias (bottom) of the ozone profile between o-suite analyses (red, solid), o-suite forecasts 4th day (red, dotted) and BASCOE (cyan line) with SAGE-III observations for the period DJF 2020.

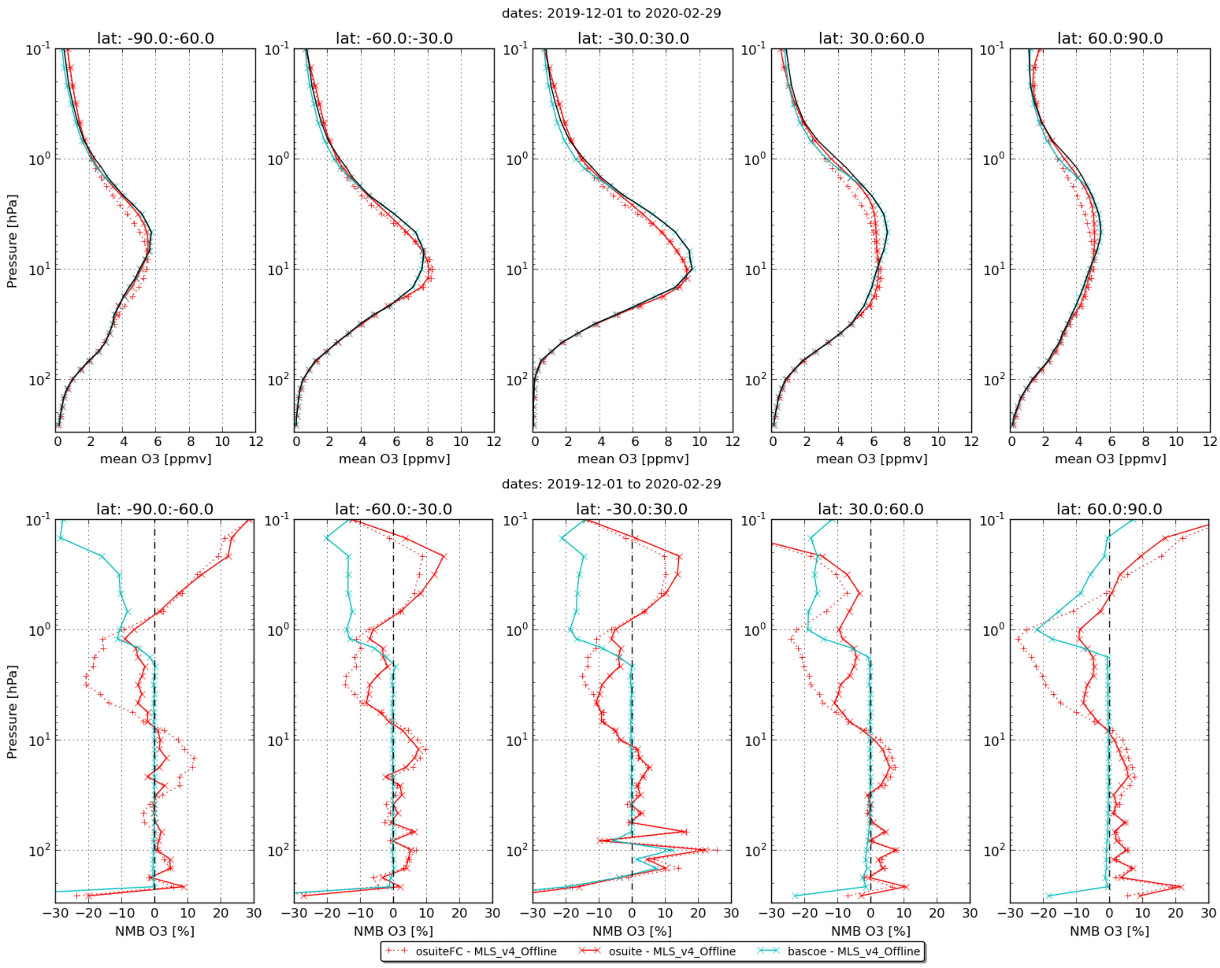

Figure 9.3.7: Mean value (top) and normalized mean bias (bottom) of the ozone profile between o-suite analyses (red, solid), o-suite forecasts 4th day (red, dotted) and BASCOE (cyan line) with MLS observations for the period DJF 2020.

9.4 Stratospheric NO_2

The CAMS model uses a tropospheric chemistry scheme in combination with a parameterization for stratospheric ozone. Stratospheric ozone is well constrained by satellite observations. Therefore, the only useful product in the stratosphere is ozone, and all other compounds, including NO_2, should not be used, as demonstrated by the validation results presented here.

In this section, nitrogen dioxide from SCIAMACHY/Envisat satellite retrievals (IUP-UB v0.7) and GOME-2/MetOp-A satellite retrievals (IUP-UB v1.0) are compared to modelled stratospheric NO_2 columns. Monthly mean stratospheric NO_2 columns from SCIAMACHY and GOME-2 have relatively small errors on the order of 20% in the tropics and in mid-latitudes in summer and even lower errors at mid-latitudes in winter. As the time resolution of the saved model files is rather coarse and NO_x photochemistry in the stratosphere has a large impact on the NO_2 columns at low sun, some uncertainty is introduced by the time interpolation at high latitudes in winter.

As shown in Figure 9.4.1, amplitude and seasonality of satellite stratospheric NO_2 columns are poorly modelled with CB05-based chemistry runs including the more recent versions of the o-suite.

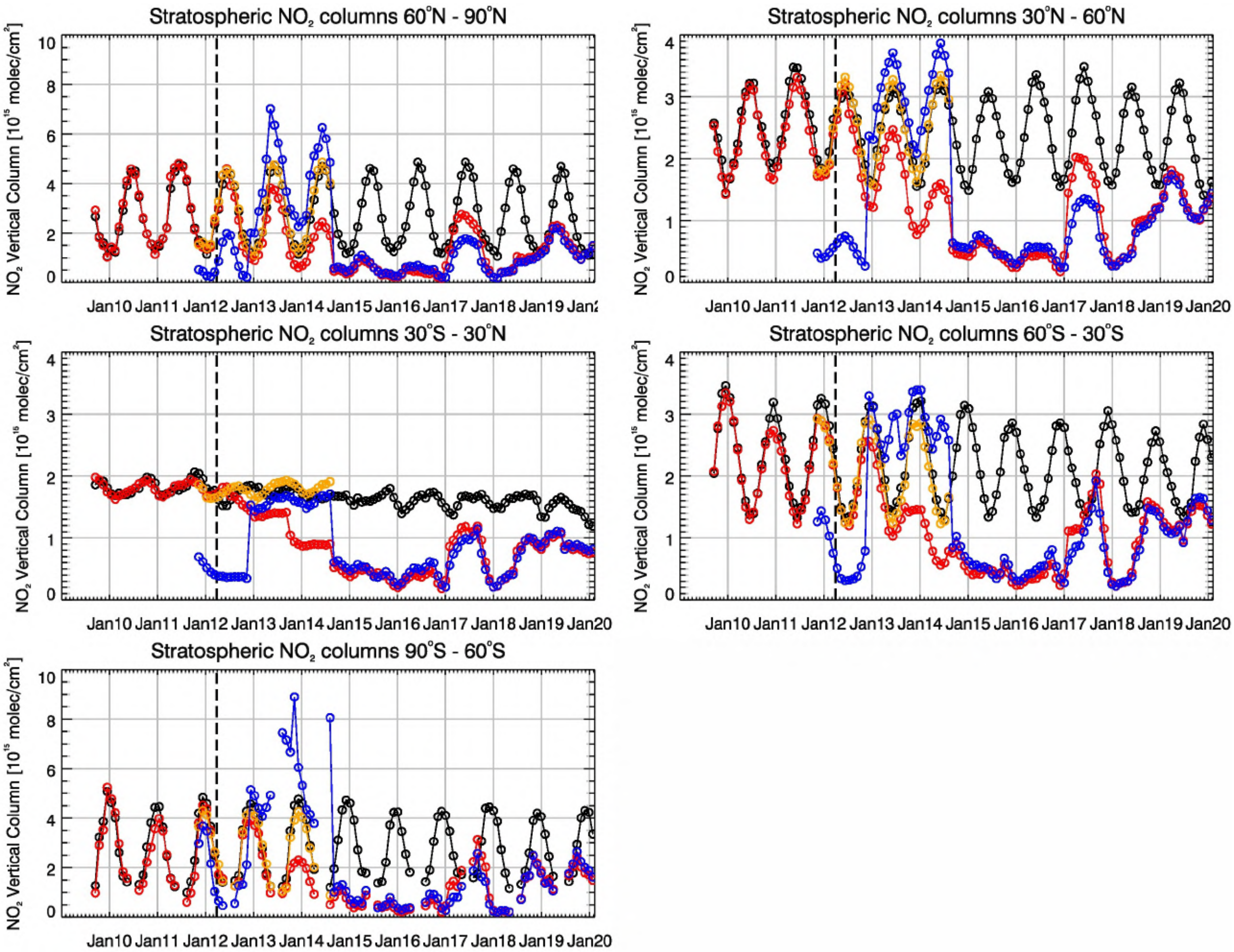

Figure 9.4.1: Time series of stratospheric NO2 columns [10^{15} molec cm-2] from SCIAMACHY (up to March 2012) and GOME-2 (from April 2012, black) compared to model results (red: o-suite, blue: MACC fcnrt TM5/MACC CIFS TM5/control, orange: MACC forecast based on MOZART stratospheric chemistry) for different latitude bands. The blue line shows TM5-based forecasts from November 2011 until August 2014 and CAMS control results from September 2014 onwards. The vertical dashed black lines mark the change from SCIAMACHY to GOME-2 based comparisons in April 2012.

The significant differences between observations and CB05 chemistry runs, i.e. a strong underestimation of satellite retrievals by models, can be explained by the missing stratospheric chemistry for these model versions. The only constraint on stratospheric NO_x is implicitly made by fixing the HNO_3/O_3 ratio at the 10 hPa level. This assumption, in combination with the changing model settings for stratospheric O_3 for control compared to MACC_CIFS_TM5, may explain some of the jumps we see in stratospheric NO_2. In any of these runs the stratospheric NO_2 is poorly constrained. It clearly indicates that stratospheric NO_2 in the latest versions of the o-suite is not a useful product and should be disregarded.

Comparison of the o-suite from July 2012 until August 2014 with stratospheric NO_2 column satellite observations shows that the previous MACC o-suite had a systematically lower bias for all latitude bands. The best performance was achieved with the MOZART chemistry experiments without data assimilation (orange, running until September 2014), especially northwards of 30°S. Details on the NO_2 evaluation can be found at: http://www.doas-bremen.de/macc/macc_veri_iup_home.html.

10. Validation results for greenhouse gases

This section describes the NRT validation of the pre-operational, high resolution forecast of CO_2 and CH_4 from 1st March 2019 to 1st March 2020 based on observations from 17 surface stations, located in Western Europe; 10 TCCON stations measuring XCO_2 and XCH_4 total columns, and 13 NDACC stations measuring partial and total CH_4 columns. We compare the observations to the high-resolution forecast experiments (*gznv/h9sp, Tco1279L137; 9x9 km*), coupled to the analysis experiment (*gwx3/h72g, Tco399L137, 25x25 km*). The *gznv/gwx3* experiments, based on IFS CY45R1, are used from 1st December 2018 to 30 November 2019. The *h9sp/h72g* experiments, based on IFS CY46R1, are used from 1st December 2019 onwards.

10.1 CH4 and CO2 validation against ICOS observations

The CO_2 and CH_4 simulations from the analysis and high-resolution forecast have been compared to the 17 ICOS stations. The near–real time data processing of the in-situ measurements is ensured by the Atmospheric Thematic Center (Hazan et al., 2016). Among the 17 stations we can distinguish three sites located on top of mountains (PUY, JFJ, CMN), two background sites (PAL, ZEP) and 12 tall towers. For the later we consider only in this report the highest sampling levels which are at least at 100m above the ground.

The figure 10.1.1 shows the time varying biases (observations minus model), averaged on a weekly basis, for all ICOS stations. The CO_2 biases from the previous experiments (prior to Dec.2019) were characterized by a clear seasonal cycle at most sites with maximum values in Summer/Autumn, and minimum in Winter/Spring. The new experiments, started on 1st Dec. 2019, correspond to a step change for all sites, and both in the forecast and analysis. The bias changes from positive to negative biases at all sites. Ispra (IPR), a tall tower located in the Po valley, appears as an outlier probably due to the complex orography. Two examples are detailed on Figure 10.1.2 for Jungfrauhoch (Switzerland) and Trainou tall tower (France). The first one is typical of the mountain sites, with an overestimation of the CO_2 concentration up to 2% in September 2019, decreasing down to 1% in December 2019, and close to zero with the new experiment. Trainou is representative of most ICOS stations. The CO2 bias is quite similar to JFJ with a less marked change between the two experiments in December 2019.

The seasonal cycle of the CO_2 bias calculated from the average of all European sites is shown on figure 10.1.4. It was ranging between 4 and 8 ppm from March 2019 to December 2019. With the new experiment started in December 2019 the bias is now negative ranging from -2 to 0 ppm. It should also be noted that the RMS are significantly higher in summer.

For CH_4 the figure 10.1.1 shows also a significant step change with the new experiments starting on December 2019, with similar feature on the high-resolution forecast and the analysis. Before this date we observe two distinct patterns in the model-observations differences: a seasonal and a latitudinal one. At the Scandinavian sites the model overestimates (up to 50 ppb) the observations almost all along the year. The example of Norunda (Figure 10.1.3) clearly shows that both the baseline and the CH_4 spikes are overestimated by the model, which could indicate that the wetland

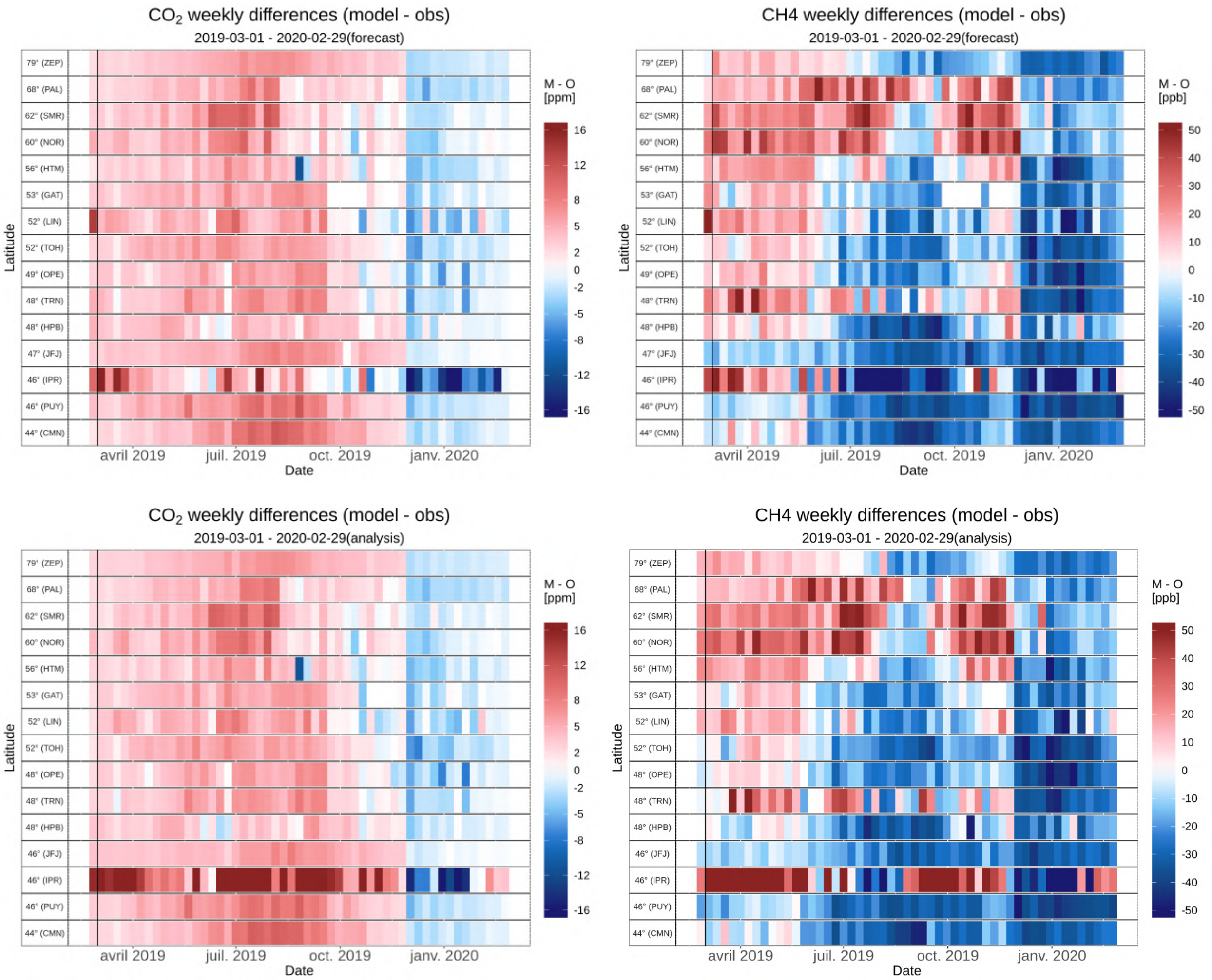

Figure 10.1.1: Mosaic plot of CO_2 (left, in ppm) and CH_4 (right, in ppb) biases of the CAMS high resolution forecast (top panel) and analysis (bottom panel), compared to surface station observations. Each vertical colored line represents a weekly mean.

emissions are overestimated. There is only a period in August/September 2019 when the observations are greater than the simulated values (Figure 10.1.3). The more we go at lower latitudes, the more we observe negative biases. In Germany and North France the bias is negative in Summer/Autumn. Negative biases are observed all year long for the mountain sits of Puy de dome. Then from December to March 2019 we observe negative biases at all sites, ranging from 0 to –50 ppb. When considering the average signal from 15 European sites (Figure 10.1.4), we observe a mean positive bias up 20 ppb until May 2019, and negative bias (0 to -20 ppb) from June to November 2019. The new experiment does not improve the mean bias (-30 ppb on average from December to March 2019), but the dispersion among the stations and the latitudes is clearly reduced (Figure 10.1.4, 10.1.1).

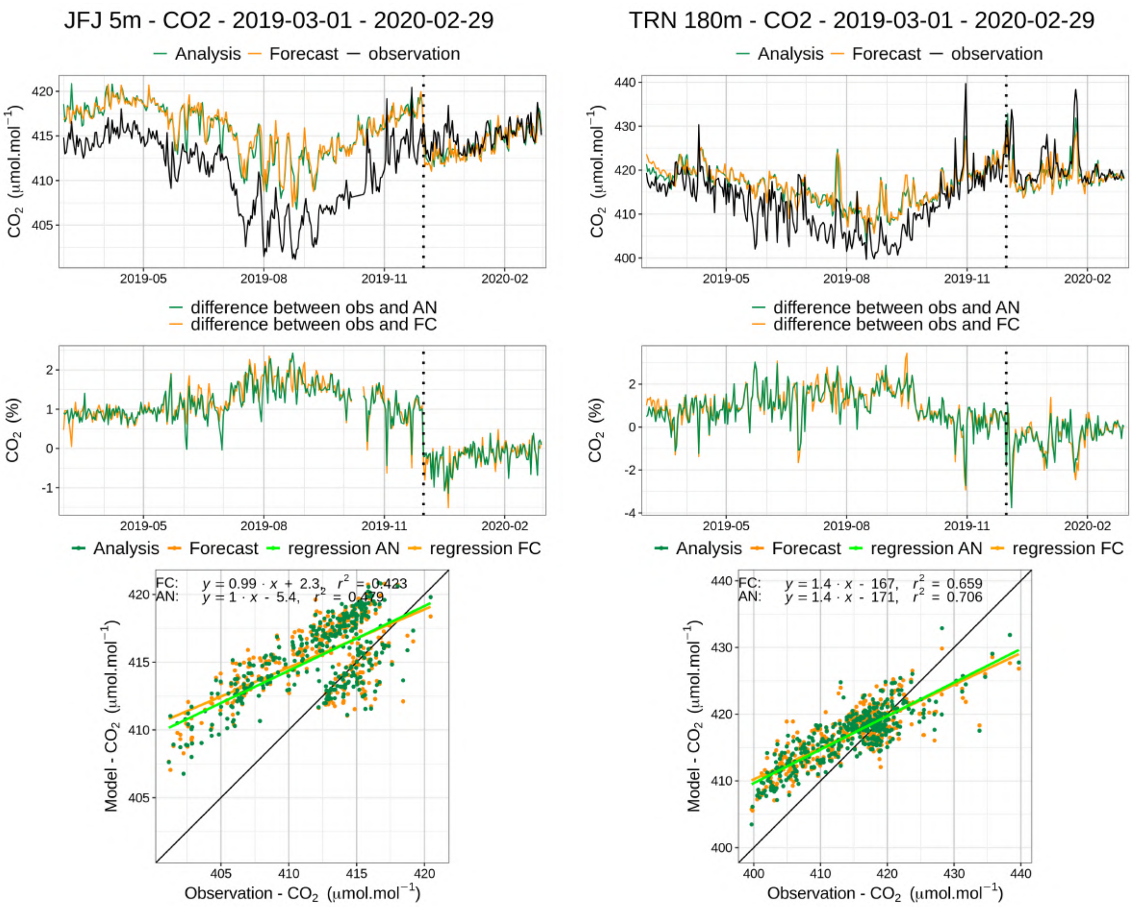

Figure 10.1.2: Comparison of CO_2 daily means observed (black) with the analysis run (green) and the high-resolution forecast (orange) at Jungfrauhoch (left) and Trainou (right). Middle: differences of the observations minus the simulations. Below: Linear fit between observations and simulations. The dashed vertical line represents the change of experiments in December 2018.

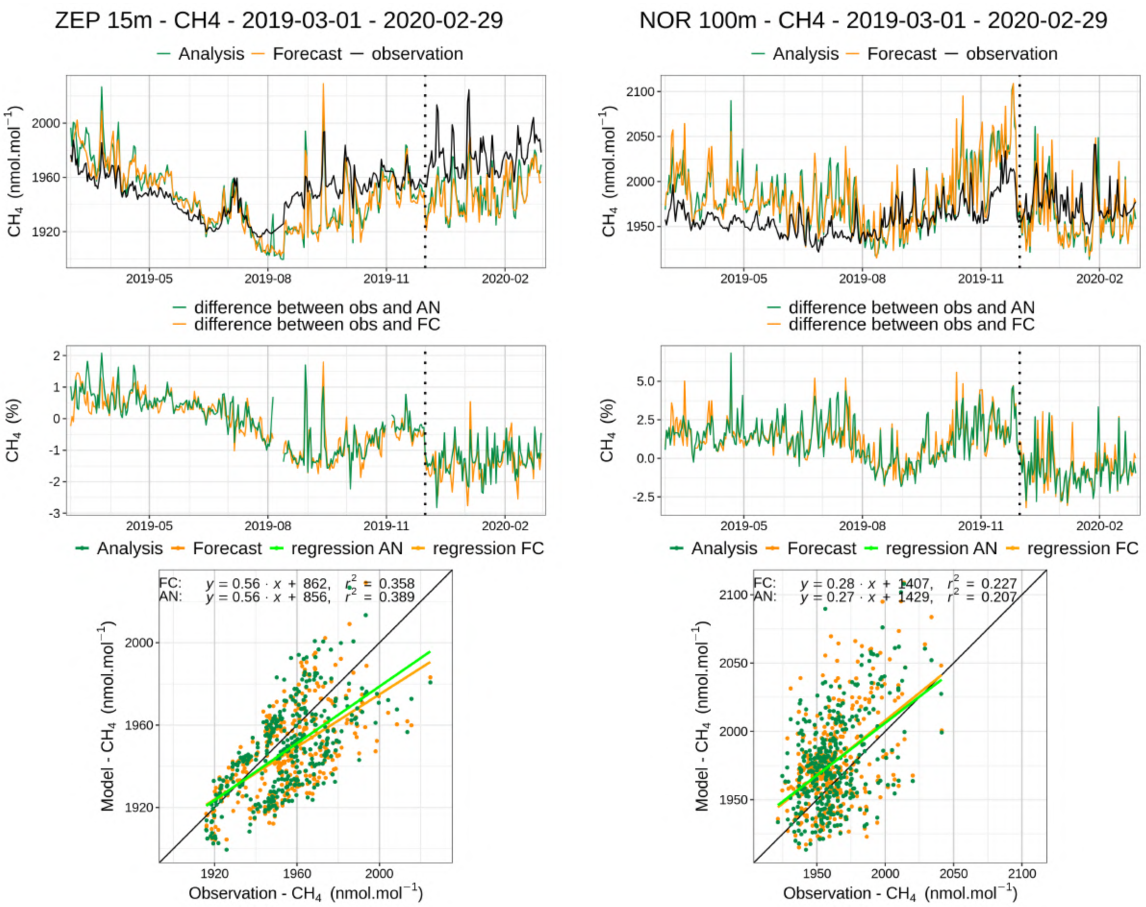

Figure 10.1.3: Comparison of CH_4 daily means observed (black) with the analysis run (green) and the high-resolution forecast (orange) at Zeppelin (left) and Norunda (right). Middle: differences of the observations minus the simulations. Below: Linear fit between observations and simulations. The dashed vertical line represents the change of experiments in December 2018.

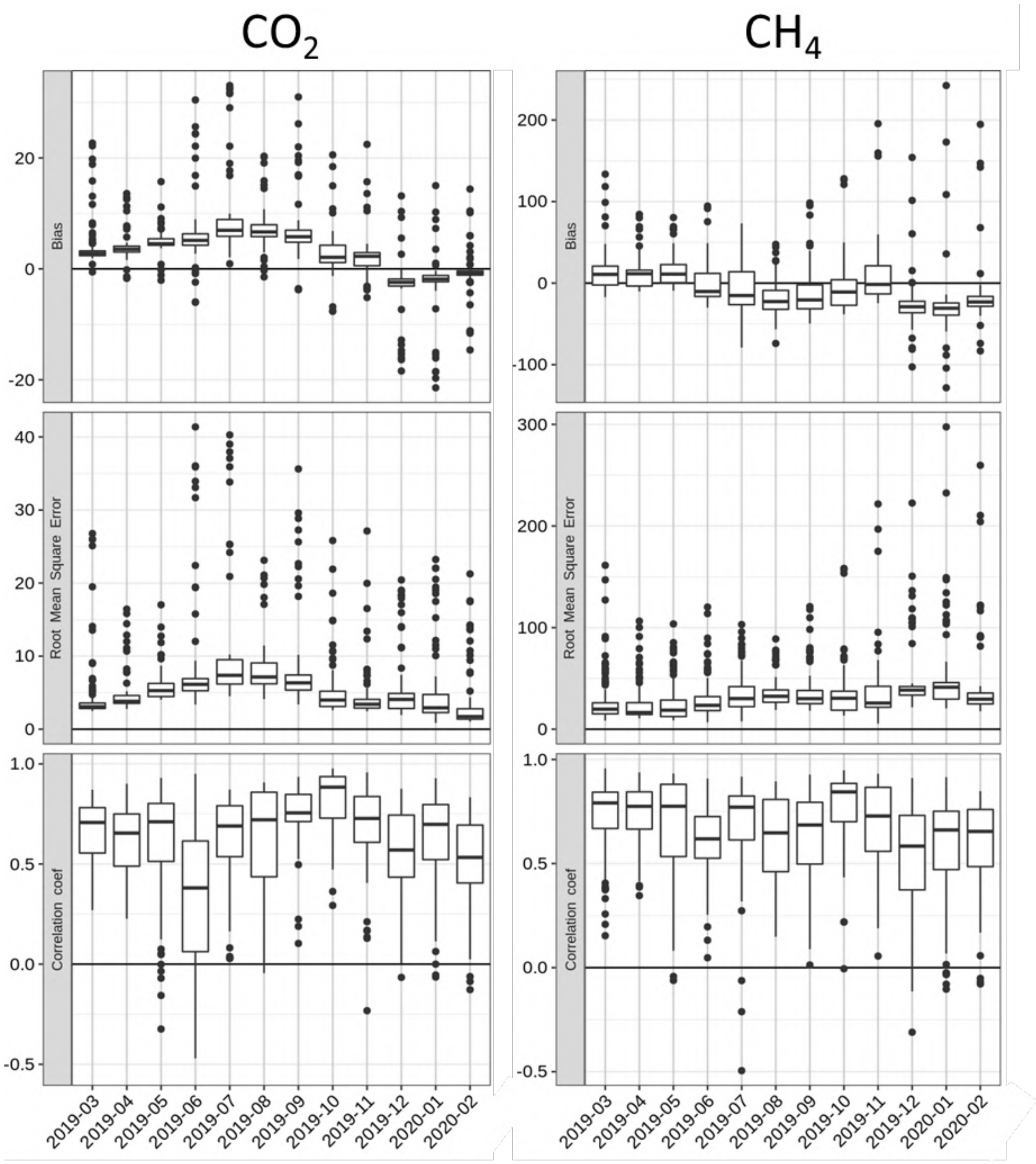

Figure 10.1.4: Monthly statistics (bias, RMSE, correlation coefficients) of the analysis experiment compared to CO_2 (left) and CH_4 (right) surface measurements at ICOS sites. The results obtained for all European sites (CMN, GAT, HPB, HTM, IPR, JFJ, LIN, NOR, OPE, PAL, PUY, SMR, TOH, TRN, ZEP) are averaged. September 2019 is not representative, since using only one day.

10.2 CH_4 and CO_2 validation against TCCON observations

For the validation column averaged mole fractions of CO_2 and CH_4 (denoted as XCO_2 and XCH_4) from the Total Carbon Column Observing Network (TCCON) are used. Column averaged mole fractions provide different information than the in situ measurements and are therefore complementary to the in situ data. The validation routines used for TCCON data are the same as used for the NDACC network and are documented in Langerock et al. (2015). In this section, we compare column averaged mole fractions of CH_4 and CO_2 of the CAMS models with TCCON retrievals. Data from the following TCCON sites has been used:

Izana (Blumenstock et al., 2017), Reunion (De Mazière et al., 2017), Bialystok (Deutscher et al., 2017), Manaus (Dubey et al., 2017), Four Corners (Dubey et al., 2017), Ascension (Feist et al., 2017), Anmeyondo (Goo et al., 2017), Darwin (Griffith et al., 2017), Wollongong (Griffith et al., 2017), Karlsruhe (Hase et al., 2017), Edwards (Iraci et al., 2017), Indianapolis (Iraci et al., 2017), Saga (Kawakami et al., 2017), Sodankyla (Kivi et al., 2017), Hefei (Liu et al., 2018), Tsukuba (Morino et al., 2017), Burgos (Morino et al., 2018), Rikubetsu (Morino et al., 2017), Bremen (Notholt et al., 2017), Spitsbergen (Notholt et al., 2017), Lauder (Sherlock et al., 2017, Pollard et al., 2019), Eureka (Strong et al., 2018), Garmisch (Sussmann et al., 2017), Zugspitze (Sussmann et al., 2018), Paris (Te et al., 2017), Orleans (Warneke et al., 2017), Park Falls (Wennberg et al., 2017), Caltech (Wennberg et al., 2017), Lamont (Wennberg et al., 2017), Jet Propulsion Laboratory (Wennberg et al., 2017), East Trout Lake (Wunch et al., 2017), Nicosia (Petri et al., 2020)

For the validation of the models in December, January and February TCCON data was available from the sites Orleans, Nicosia and Reunion. The site Nicosia (Cyprus) was installed mid-2019 and is used for the first time for a comparison with the CAMS models.

Methane (CH_4)

Figure 10.2.1 shows the data for the last 3 years. The only data for the reporting period is from Orléans, Nicosia and Réunion Island. The data from these two stations show that the model data continues to underestimate the CH_4 for these stations by 20-35 ppb.

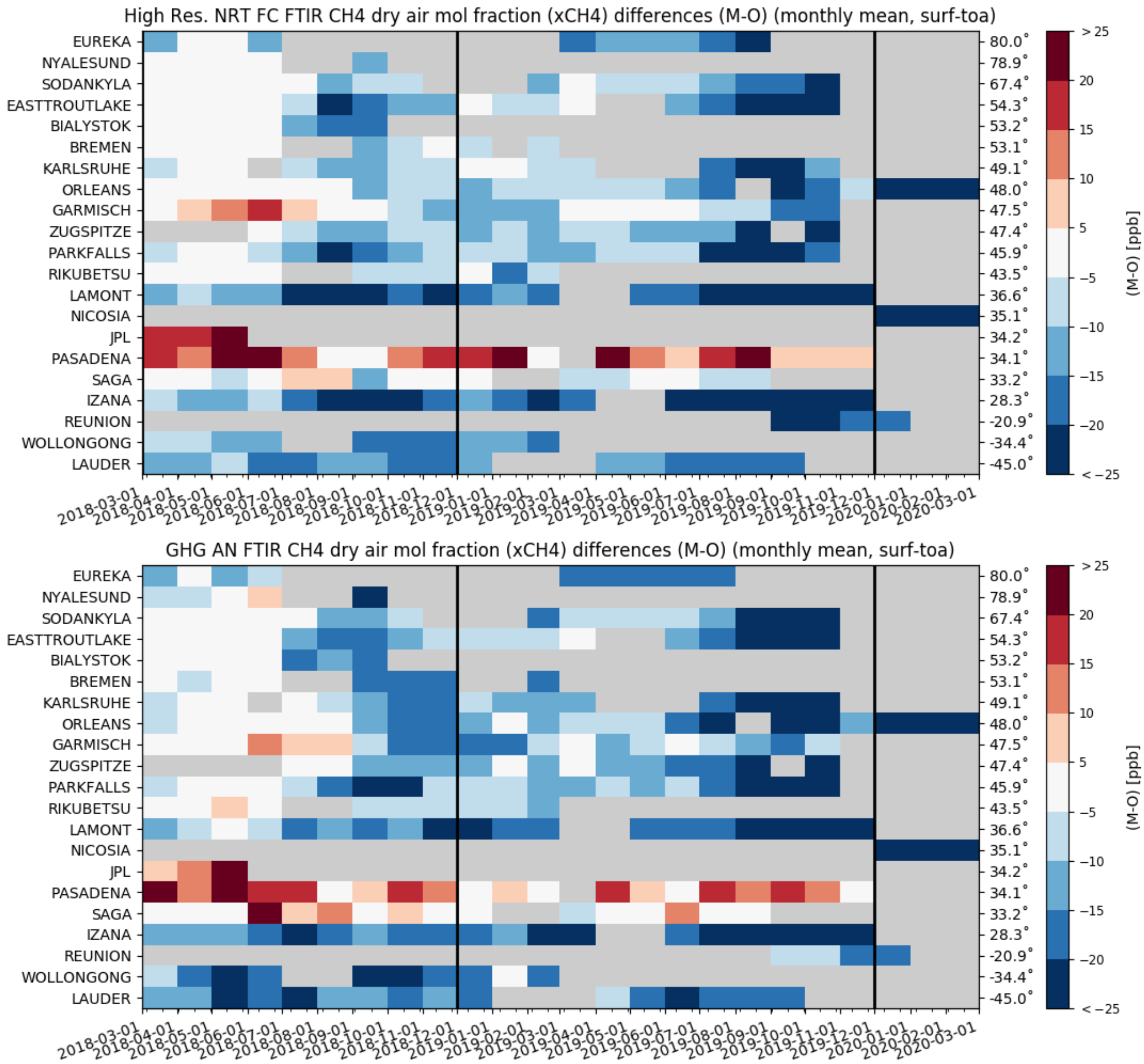

Figure 10.2.1: Monthly differences for the last 3 years (upper plot: high-resolution NRT forecast, lower plot: methane analysis). The stations are sorted by latitude (northern to southern hemisphere).

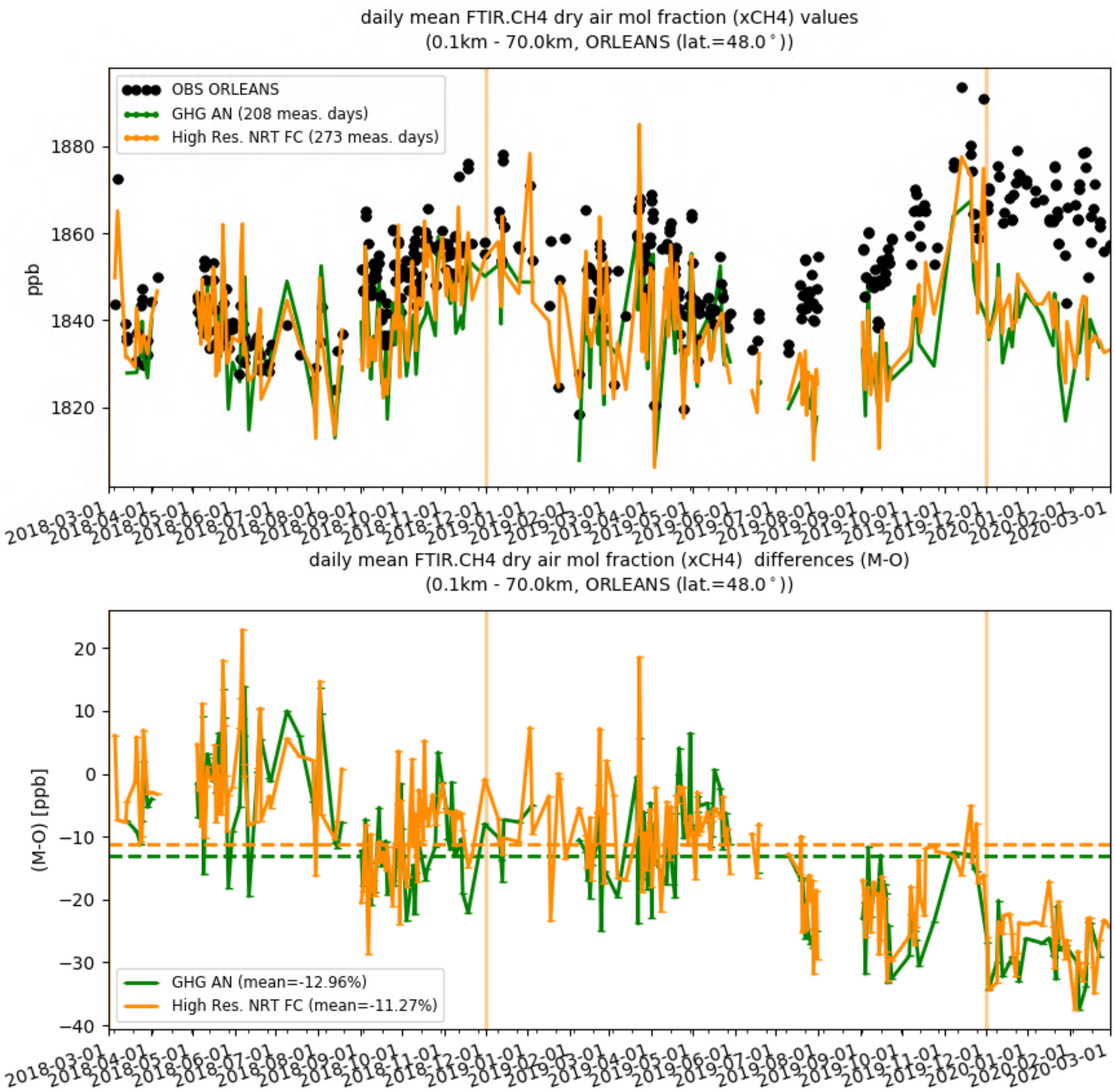

Figure 10.2.2: Comparison of the CH_4 model data with TCCON CH_4 at Orleans.

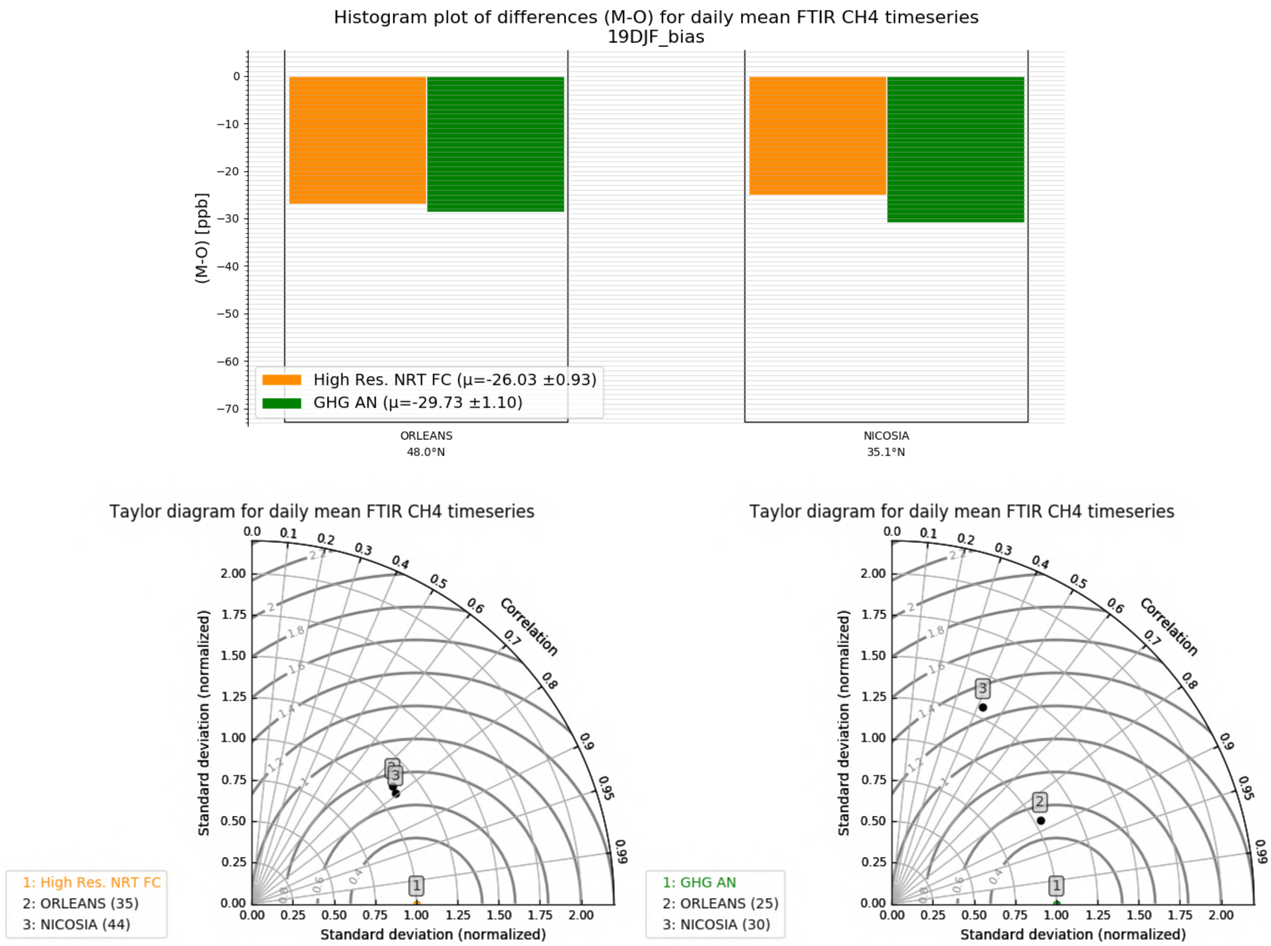

Figure 10.2.3: Model-minus-observation differences during the reporting period (top) and Taylor diagrams (bottom) for the two sites Orleans and Nicosia that cover the whole reporting period.

Carbon dioxide (CO_2)

Figure 10.2.4 shows the comparisons for the last 3 years. The only data for the reporting period is from Orléans, Nicosia and Réunion Island. The data from these stations show that for the reporting period (December-March 2019) the model data agrees very well with the observations. This is a strong improvement: prior the reporting period the models strongly overestimated the CO_2 (up to 6 ppm).

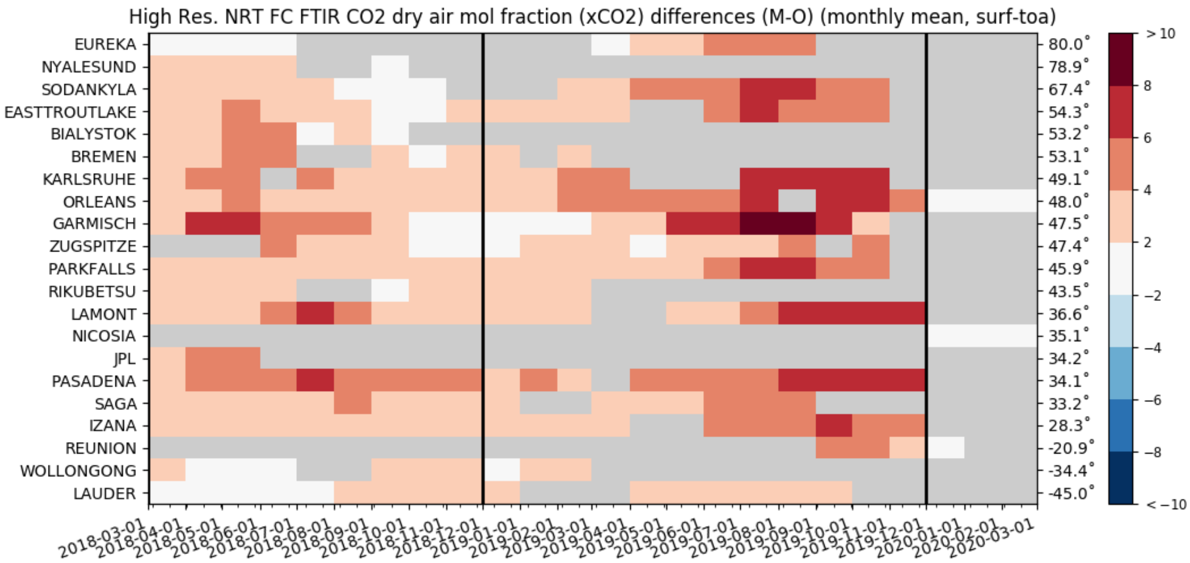

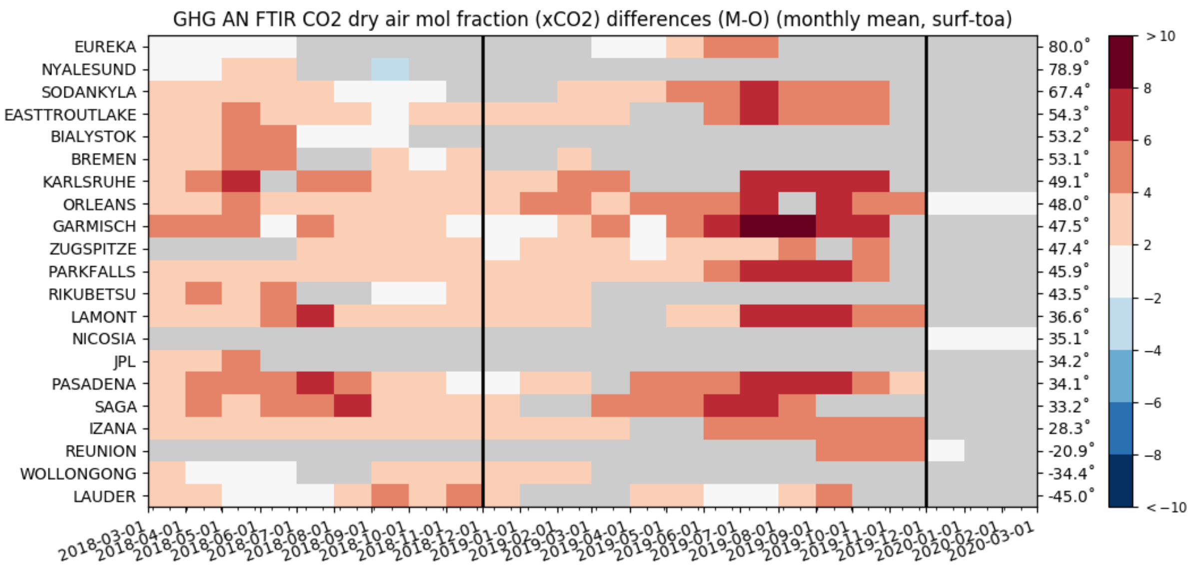

Figure 10.2.4: Monthly differences for the last 3 years (upper plot: high res NRT, lower plot: GHG AN). The stations are sorted by latitude (northern to southern hemisphere).

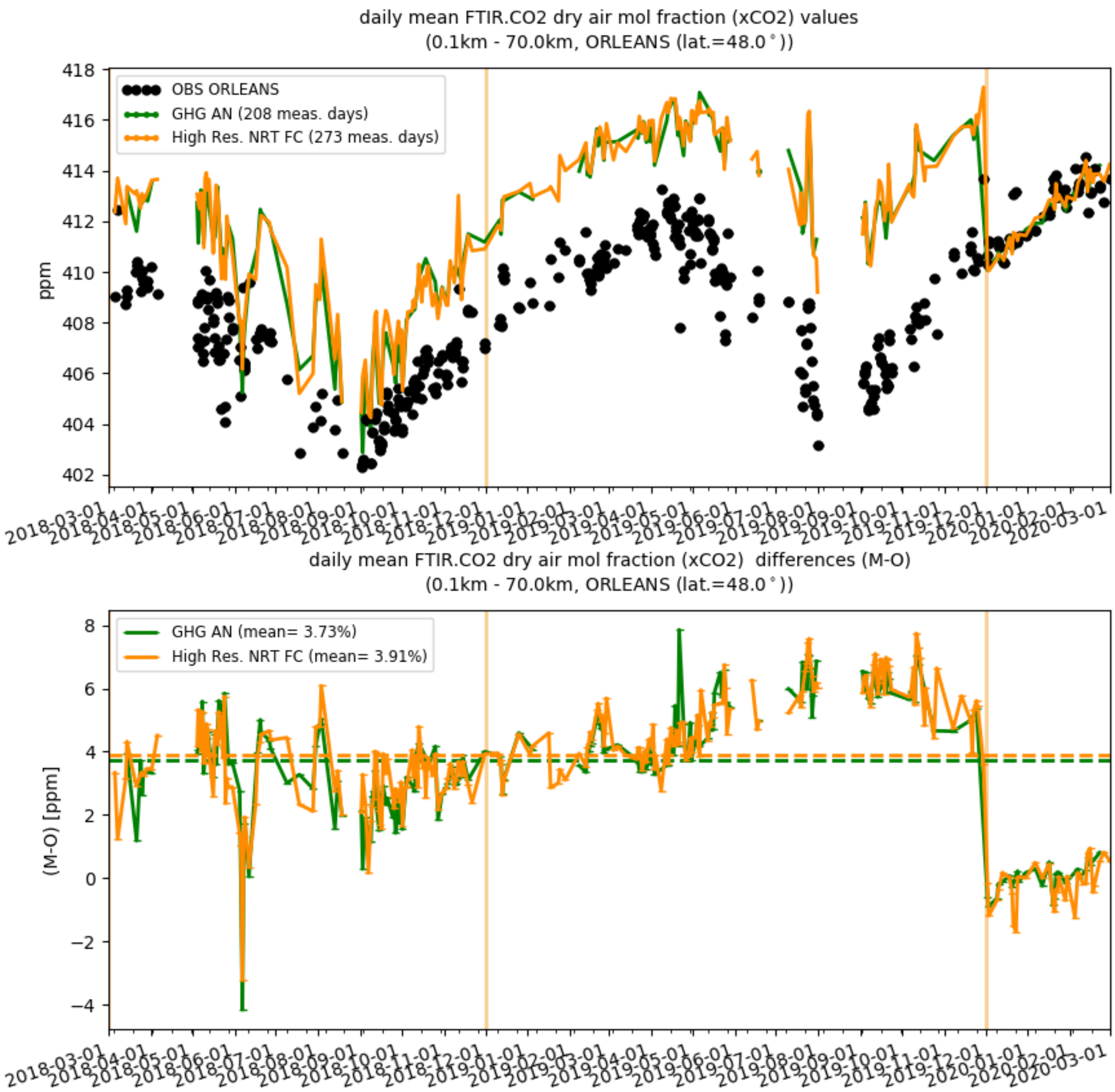

Figure 10.2.5: Comparison of the CO_2 model data with TCCON CO_2 at Orleans.

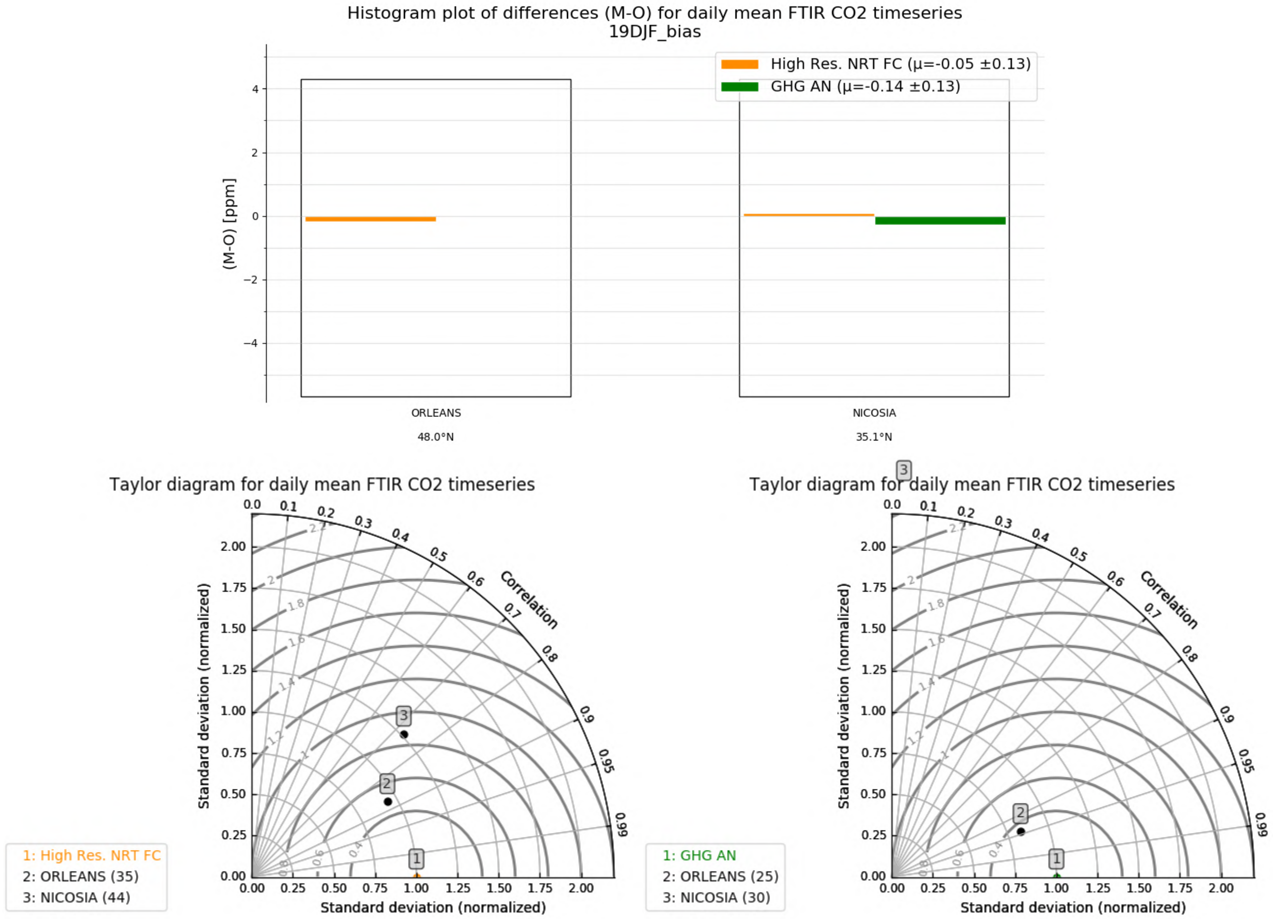

Figure 10.2.6: Differences during the reporting period and Taylor diagrams for the two sites that cover the whole reporting period

10.3 Validation against FTIR observations from the NDACC network

In this section, we compare the CH_4 profiles of the CAMS GHG products with FTIR measurements at different FTIR stations within the NDACC network. These ground-based, remote-sensing instruments are sensitive to the CH4 abundance in the troposphere and lower stratosphere, i.e. between the surface and up to 25 km altitude. Tropospheric and stratospheric CH4 columns are calculated from the FTIR profile data and used to validate corresponding columns obtained from the model data. A description of the instruments and applied methodologies can be found at http://nors.aeronomie.be. The typical uncertainty on the FTIR tropospheric column is 2%, while the uncertainty on the stratospheric column is 7.5%, adding together to a 3% uncertainty on the total column. The systematic uncertainty is large for the NDACC methane product mostly due to higher spectroscopic uncertainties.

Figure 10.3.1 (middle row) shows that the tropospheric columns of CH4 agree well and only small differences appear between the analysis and the high resolution model. In comparison with the measurement uncertainty, a slight underestimation is observed in the tropospheric columns which is in agreement with the TCCON results. The Paramaribo measurements have reduced sensitivity and the tropospheric/stratospheric split is not valid in this case.

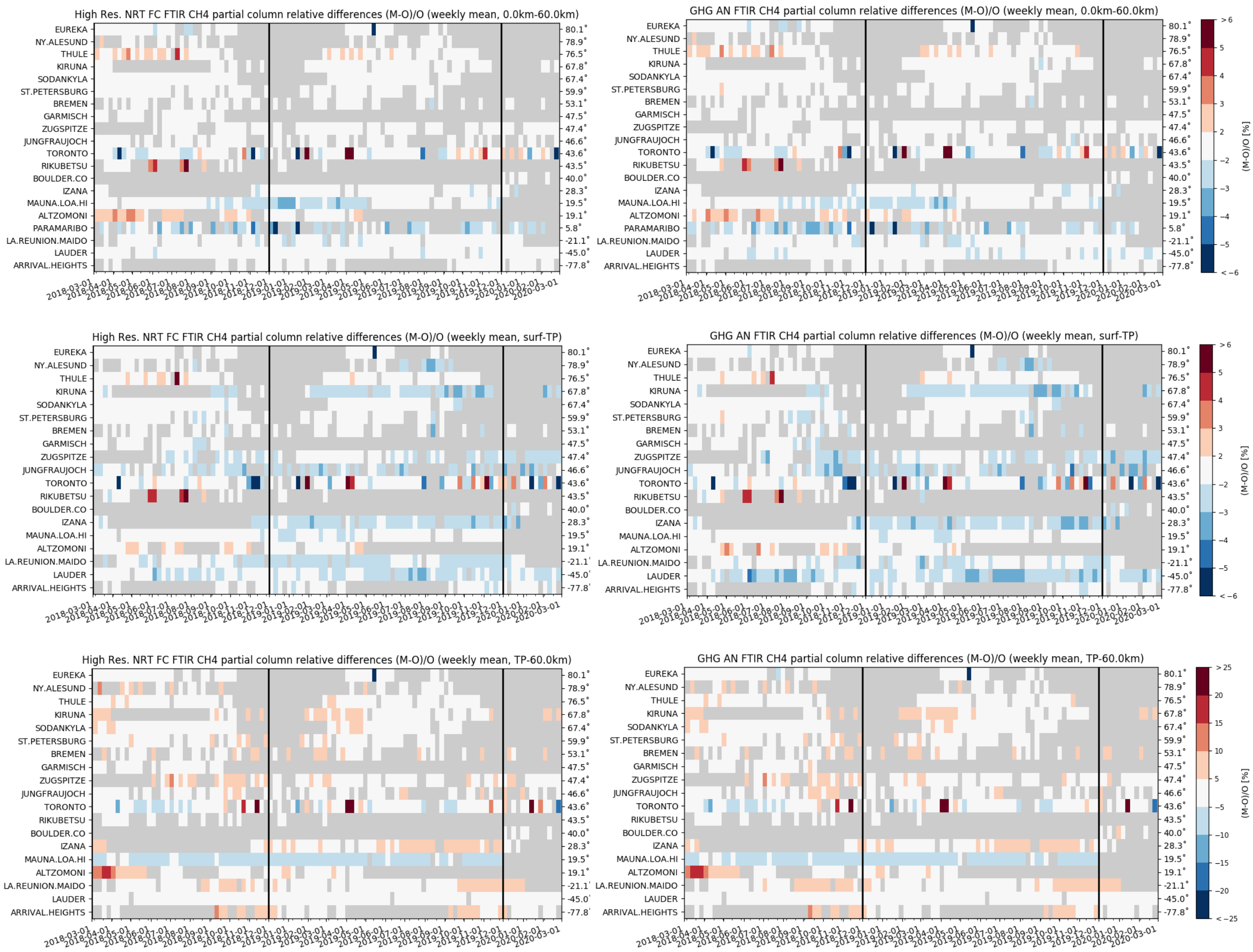

Figure 10.3.1: Weekly mean relative bias for total (top row), tropospheric (middle row) and stratospheric CH_4 columns (bottom row) for the period March 2018 – February 2020 for high resolution forecast (left) and the analysis (right). The overall uncertainty for the CH_4 total column measurements is approximately 4%. The overall uncertainty for the CH_4 total/tropospheric column measurements is approximately 2%, while the stratospheric uncertainty is 7.5% (the colour scale for the mosaic plots follows uncertainty scale)

The stratospheric columns (Figure 10.3.1, bottom row) show a slight overestimation compared to the measurement uncertainty.

At some sites a seasonal change is observed in either the tropospheric or stratospheric concentrations. Due to the short time period, it is unclear if this is a recurring seasonal dependent model performance. In Figure 10.3.2 the tropospheric and stratospheric relative difference time series are plotted at Thule and St. Petersburg.

Figure 10.3.3 shows Taylor diagrams for the DJF time period and for a selected number of sites (many high latitude stations are not measuring during SON/DJF): some stations have limited observations and should be treated with care. Assimilation has a small effect on the correlation coefficients for most sites: the average correlation for 11 stations is 0.76 for the analysis and 0.84 for the high-resolution forecast.

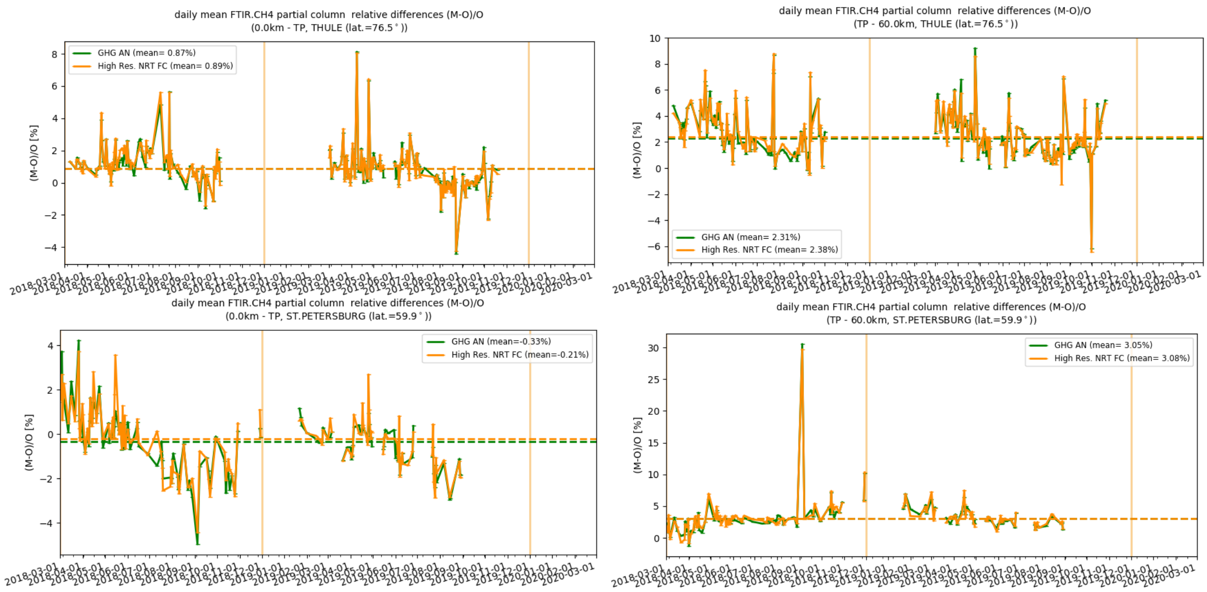

Figure 10.3.2: Daily mean of relative differences for tropospheric CH_4 columns (left) and stratospheric CH_4 columns (right) at Thule (top) and St Petersburg (bottom). At Thule the stratospheric column shows a reduced bias during the summer months, while at St Petersburg the tropospheric column performs worse during June-October.

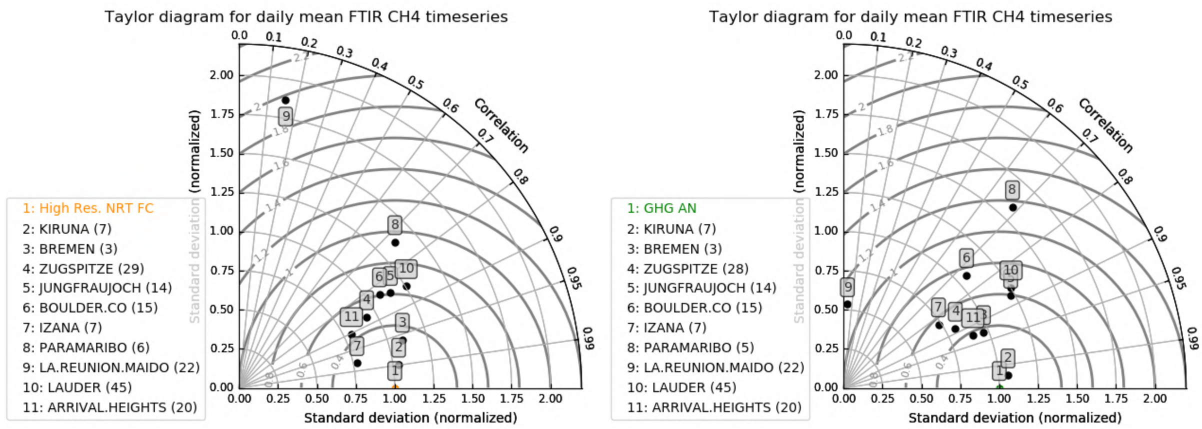

Figure 10.3.3: Taylor diagrams relating the standard deviations for the model /GB time series of total CH_4 column data and their correlation for the period 2019 DJF (the stations with a limited number of measurements should be ignored). All time-series are normalized such that the standard deviation of the model column time series is 1. For the tropical site Reunion (9) the instrument broke down end of 2019 and only a limited coverage is obtained in this reporting period.

11. Event studies

11.1 Australian fires in early 2020

Heatwaves in Australia with temperature exceeding 40°C in the time period from December to February 2020 led to many fire events. Fig. 11.1.1 shows the evolution of CO during December - February. IASI satellite data indicate a plume of CO in the south-east of Australia on 16 December and significant increase on 21 December. The easterly transportation patterns are clearly seen on 2 January with very high CO values over the south of the Pacific Ocean and extended further on 7 January. The model run does not show the plume on 16 December, but it captured well the location of the plume during other days, but with smaller CO values. The transportation pathways are captured as well, but not as extended and with reduced CO values.

Enhancements in CO were observed locally south of Sydney at Wollongong (Fig. 11.1.2). The peak early January was well captured by the CAMS o-suite and control run.

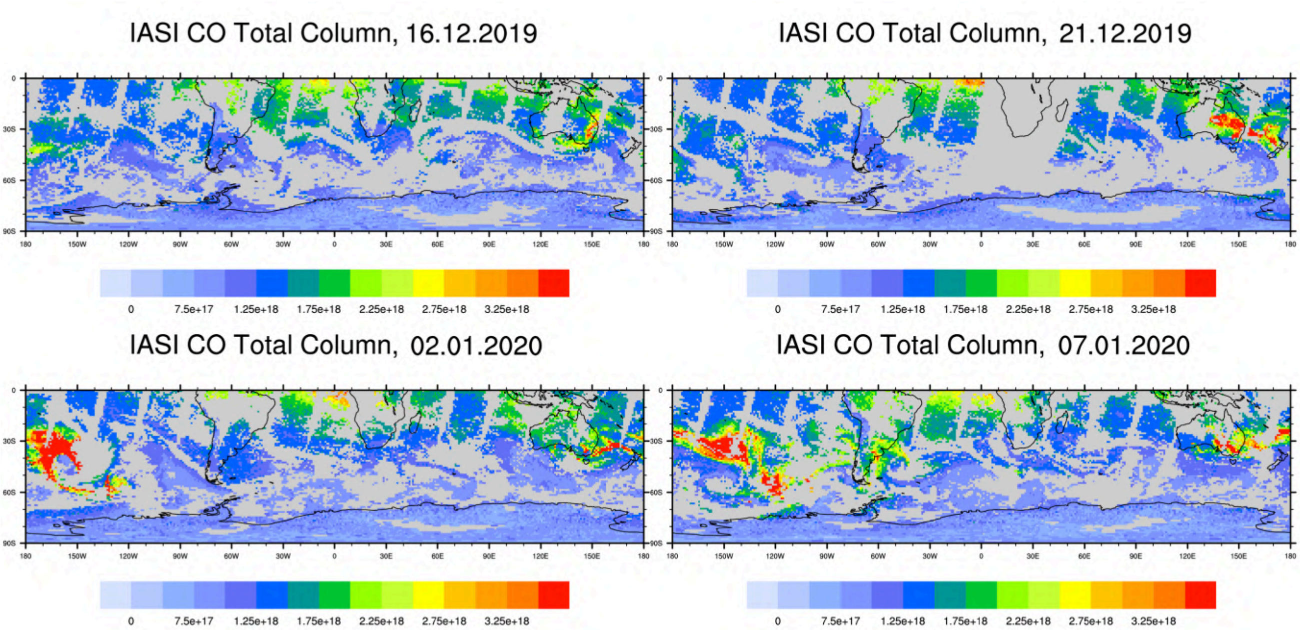

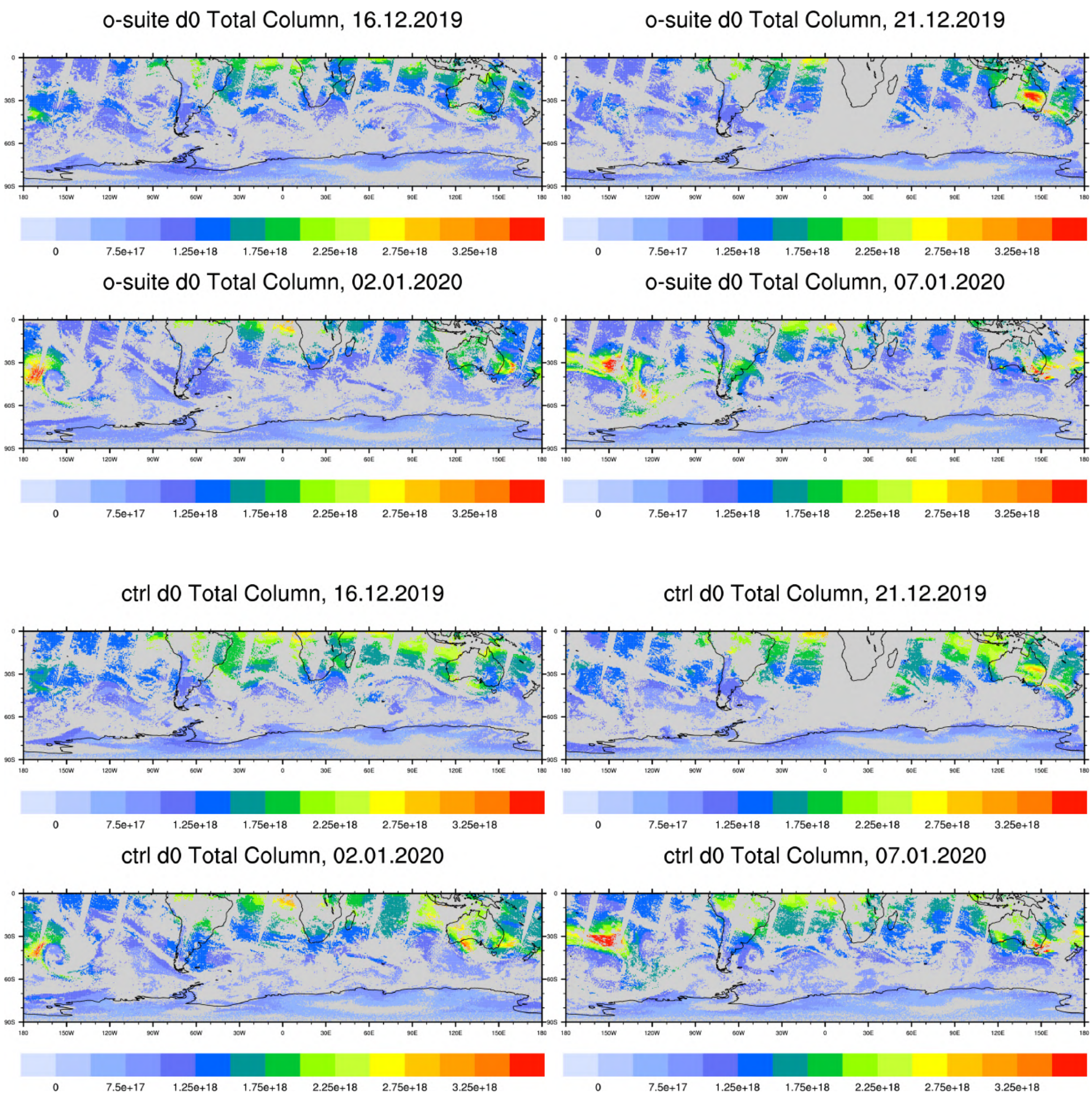

Fig. 11.1.1: CO total column for IASI (top two rows), o-suite (middle two rows) and control runs (bottom rows) for 16 December 2019, 21 December 2019, 2 January 2020 and 7 January 2020.

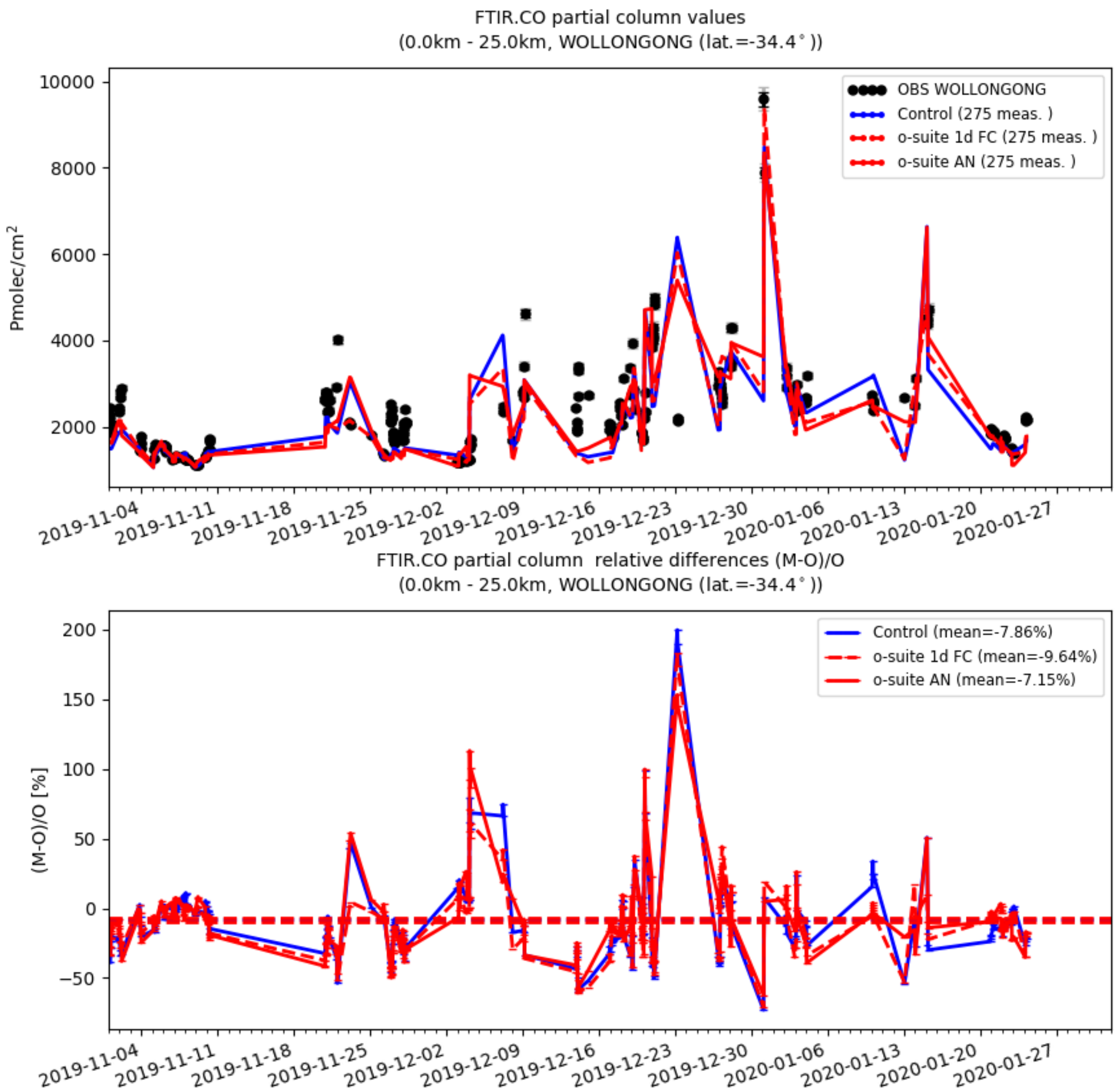

Fig. 11.1.2: FTIR observed partial column time series of CO (0-25 km) at Wollongong, south of Sydney. Top: column amount in 10^{15} molecules/cm^2. Bottom: relative difference in %.

11.2 Exceptional dust event over Canary Islands in late-February 2020

In late-February 2020, strong Saharan winds picked up dust from Africa and carried it over the Canary Islands, achieving surface concentrations over 3000µg/m^3 and reducing visibility to less than 10m. Due to strong winds and poor visibility, all airports across the Canary Islands were closed on February 22, and most stayed closed until February 24. Close to 800 flights were cancelled or re-routed. Some roads were also shut down due to limited visibility. Schools and universities were closed on February 24, and people were advised to keep their windows shut and to stay indoors due to poor air quality. Some Carnival events were postponed or curtailed due to the dusty conditions. The strong winds spread several wildfires in Tenerife and Gran Canaria (the largest island in the archipelago).

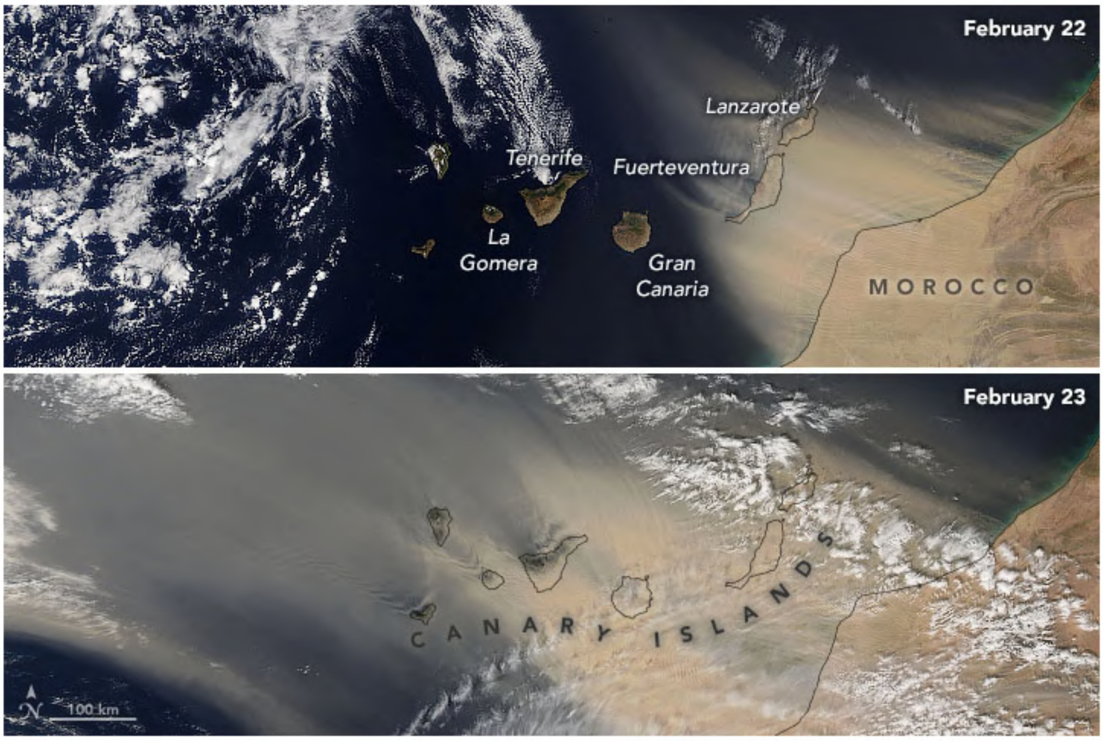

Figure 11.2.1: MODIS images on 22-23 February 2020. Source NASA Earth Observatory.

MODIS satellite detected an intense outbreak of dust over Canary Islands (see Figure 11.2.1 and Figure 11.2.2) achieving maximum AOD values up to 5. The event is originating in Mauritania on 22nd February in the early morning. Dust was transported towards the West achieving Canary Islands few hours later (see Santa Cruz de Tenerife in Figure 8.2.3).

The event was associated with the presence of some clouds as shown in Figure 11.2.1. The comparison with the MODIS AOD product show that The CAMS o-suite AOD reproduces the spatial distribution and timing of the dust plume as shown by the comparison with MODIS/Aqua (see Figure 11.2.2). However, the comparison shows that CAMS o-suite underestimates the aerosol concentrations during this event, reaching AOD values up to 1.5 and PM10 up to 300 μg/m^3 in over Canary Islands.

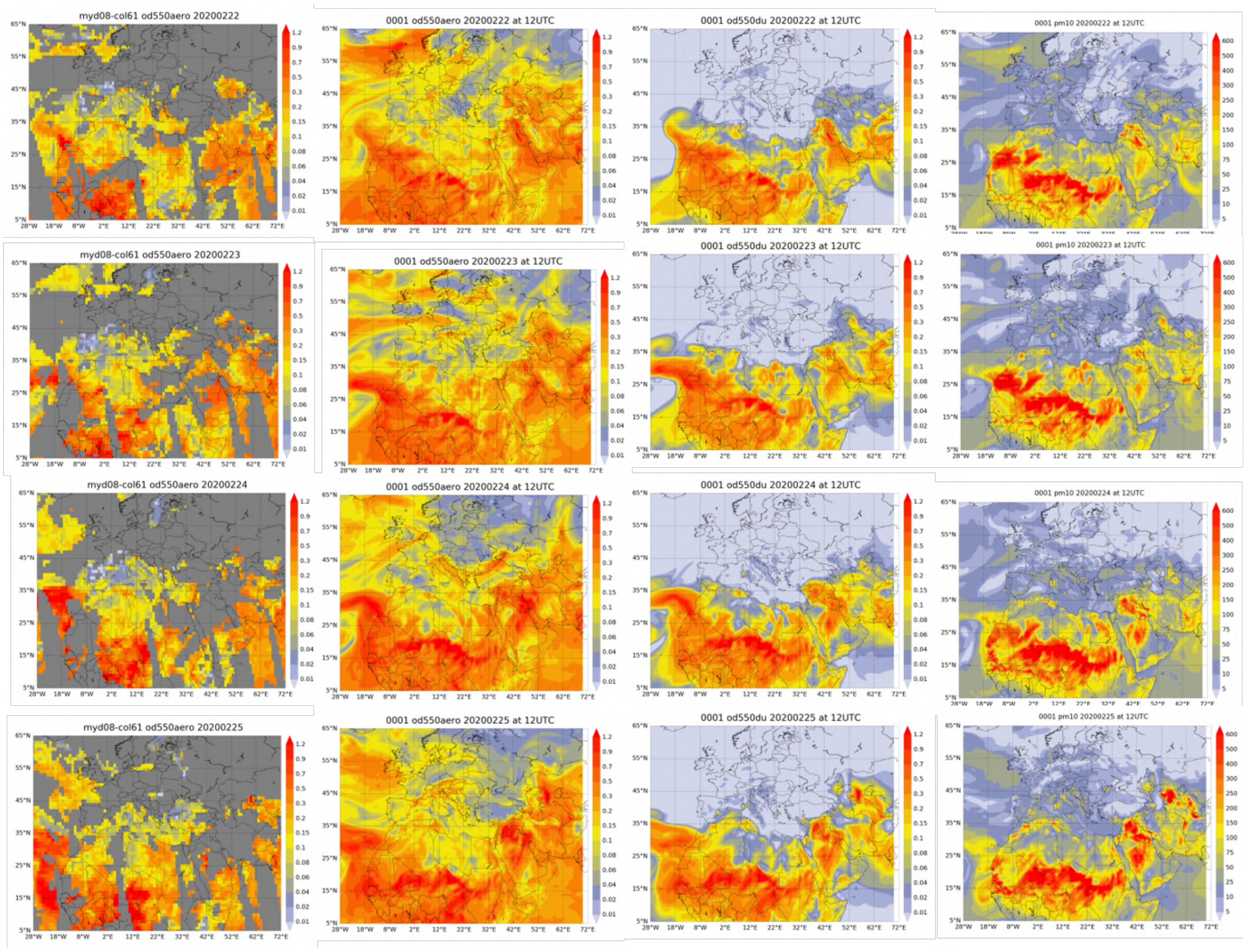

Figure 11.1.2: Daily composite of NASA MODIS/Aqua well as AOD, DOD and PM10 at 12UTC from o-suite) for 22-25 February 2020.

12. References

Agusti-Panareda, A., Monitoring upgrades of analysis/forecast system, MACC-III Deliverable D44.04, June 2015.

Basart, S, A. Benedictow, Y. Bennouna, A.-M. Blechschmidt, S. Chabrillat, Y. Christophe, E. Cuevas, H. J. Eskes, K. M. Hansen, O. Jorba, J. Kapsomenakis, B. Langerock, T. Pay, A. Richter, N. Sudarchikova, M. Schulz, A. Wagner, C. Zerefos, Upgrade verification note for the CAMS near-real time global atmospheric composition service: Evaluation of the e-suite for the CAMS upgrade of July 2019, Copernicus Atmosphere Monitoring Service (CAMS) report, CAMS84_2018SC1_D3.2.1-201907_esuite_v1.pdf, July 2019.

Bergamaschi, P., Frankenberg, C., Meirink, J. F., Krol, M., Villani, M. G., Houweling, S., Dentener, F., Dlugokencky, E. J., Miller, J. B., Gatti, L. V., Engel, A., and Levin, I.: Inverse modeling of global and regional CH4 emissions using SCIAMACHY satellite retrievals, J. Geophys. Res., 114, D22301, doi:10.1029/2009JD012287, 2009.

Benedetti, A., J.-J. Morcrette, O. Boucher, A. Dethof, R. J. Engelen, M. Fisher, H. Flentjes, N. Huneeus, L. Jones, J. W. Kaiser, S. Kinne, A. Mangold, M. Razinger, A. J. Simmons, M. Suttie, and the GEMS-AER team: Aerosol analysis and forecast in the ECMWF Integrated Forecast System. Part II : Data assimilation, J. Geophys. Res., 114, D13205, doi:10.1029/2008JD011115, 2009.

Birmili, W., Schepanski, K., Ansmann, A., Spindler, G., Tegen, I., Wehner, B., Nowak, A., Reimer, E., Mattis, I., Müller, K., Brüggemann, E., Gnauk, T., Herrmann, H., Wiedensohler, A., Althausen, D., Schladitz, A., Tuch, T., and Löschau, G.: A case of extreme particulate matter concentrations over Central Europe caused by dust emitted over the southern Ukraine, Atmos. Chem. Phys., 8, 997–1016, https://doi.org/10.5194/acp-8-997-2008, 2008.

Boussetta, S., Balsamo, G., Beljaars, A., Agusti-Panareda, A., Calvet, J.-C., Jacobs, C., van den Hurk, B., Viterbo, P., Lafont, S., Dutra, E., Jarlan, L., Balzarolo, M., Papale, D., and van der Werf, G.: Natural carbon dioxide exchanges in the ECMWF Integrated Forecasting System: implementation and offline validation, J. Geophys. Res.-Atmos., 118, 1–24, doi: 10.1002/jgrd.50488, 2013.

Braathen, WMO Arctic Ozone Bulletin No 1/2016, DOI:10.13140/RG.2.1.4929.6403, 2016.

Cammas, J.P., Brioude J., Chaboureau J.-P., Duron J., Mari C., Mascart P., Nédélec P., Smit H., Pätz H.-W., Volz-Thomas A., Stohl A., and Fromm M., Injection in the lower stratosphere of biomass fire emissions followed by long-range transport: a MOZAIC case study. Atmos. Chem. Phys., 9, 5829-5846, 2009

Cariolle, D. and Teyssèdre, H.: A revised linear ozone photochemistry parameterization for use in transport and general circulation models: multi-annual simulations, Atmos. Chem. Phys., 7, 2183-2196, doi:10.5194/acp-7-2183-2007, 2007.

Dee, D. P. and S. Uppala, Variational bias correction of satellite radiance data in the ERA-Interim reanalysis. Quart. J. Roy. Meteor. Soc.,135, 1830-1841, 2009.

Deeter, M. N., Emmons, L. K., Edwards, D. P., Gille, J. C., and Drummond, J. R.: Vertical resolution and information content of CO profiles retrieved by MOPITT, Geophys. Res. Lett., 31, L15112, doi:10.1029/2004GL020235, 2004.

Deeter, M. N., et al. (2010), The MOPITT version 4 CO product: Algorithm enhancements, validation, and long-term stability, J. Geophys. Res., 115, D07306, doi:10.1029/2009JD013005.

Dentener, F., et al., 2006: Emissions of primary aerosol and precursor gases in the years 2000 and 1750 prescribed data-sets for AeroCom, Atmos. Chem. Phys., 6, 4321 – 4344.

Deshler, T., J.L. Mercer, H.G.J. Smit, R. Stubi, G. Levrat, B.J. Johnson, S.J. Oltmans, R. Kivi, A.M. Thompson, J. Witte, J. Davies, F.J. Schmidlin, G. Brothers, T. Sasaki (2008) Atmospheric comparison of electrochemical cell ozonesondes from different maufacturers, and with different cathode solution strengths: The Balloon Experiment on Standards for Ozonsondes. J. Geophys. Res.113, D04307, doi:10.1029/2007JD008975

Dupuy, E., et al.: Validation of ozone measurements from the Atmospheric Chemistry Experiment (ACE), Atmos. Chem. Phys., 9, 287-343, doi:10.5194/acp-9-287-2009, 2009.

Elbern, H., Schwinger, J., Botchorishvili, R.: Chemical state estimation for the middle atmosphere by four-dimensional variational data assimilation: System configuration. Journal of Geophysical Research (Atmospheres) 115, 6302, 2010.

Emmons, L. K., D. P. Edwards, M. N. Deeter, J. C. Gille, T. Campos, P. Nédélec, P. Novelli, and G. Sachse, Measurements of Pollution In The Troposphere (MOPITT) validation through 2006 Atmos. Chem. Phys., 9, 1795-1803, 2009

Errera, Q., Daerden, F., Chabrillat, S., Lambert, J. C., Lahoz, W. A., Viscardy, S., Bonjean, S., and Fonteyn, D., 4D-Var Assimilation of MIPAS chemical observations: ozone and nitrogen dioxide analyses, Atmos. Chem. Phys., 8, 6169-6187, 2008.

Errera, Q. and Ménard, R.: Technical Note: Spectral representation of spatial correlations in variational assimilation with grid point models and application to the belgian assimilation system for chemical observations (BASCOE), Atmos. Chem. Phys. Discuss., 12, 16763-16809, doi:10.5194/acpd-12-16763-2012, 2012.

Eskes, H.J., S. Basart, A. Benedictow, Y. Bennouna, A.-M. Blechschmidt, S. Chabrillat, Y. Christophe, E. Cuevas, H. Flentje, K. M. Hansen, J. Kapsomenakis, B. Langerock, M. Ramonet, A. Richter, M. Schulz, N. Sudarchikova, A. Wagner, T. Warneke, C. Zerefos, Observation characterisation and validation methods document, Copernicus Atmosphere Monitoring Service (CAMS) report, December 2019, doi: 10.24380/0nsd- wb26. Available from: http://atmosphere.copernicus.eu/user-support/validation/verification-global-services

Eskes, H. J., S. Basart, A. Benedictow, Y. Bennouna, A.-M. Blechschmidt, S. Chabrillat, Y. Christophe, H. Clark, E. Cuevas, K. M. Hansen, U. Im, J. Kapsomenakis, B. Langerock, K. Petersen, M. Schulz, A. Wagner, C. Zerefos, Upgrade verification note for the CAMS near-real time global atmospheric composition service, Copernicus Atmosphere Monitoring Service (CAMS) report, CAMS84_2015SC3_D84.3.1.5_201802_esuite_v1.pdf, February 2018 (2018b)

Eskes et al., Upgrade verification note for the CAMS near-real time global atmospheric composition service, Addendum July 2018, CAMS84_2015SC3_D84.3.1.5_201802_esuite_v1.pdf (2018c).

Flemming, J., Huijnen, V., Arteta, J., Bechtold, P., Beljaars, A., Blechschmidt, A.-M., Diamantakis, M., Engelen, R. J., Gaudel, A., Inness, A., Jones, L., Josse, B., Katragkou, E., Marecal, V., Peuch, V.-H., Richter, A., Schultz, M. G., Stein, O., and Tsikerdekis, A.: Tropospheric chemistry in the Integrated Forecasting System of ECMWF, Geosci. Model Dev., 8, 975-1003, doi:10.5194/gmd-8-975-2015, 2015.

Flemming, J., Benedetti, A., Inness, A., Engelen, R. J., Jones, L., Huijnen, V., Remy, S., Parrington, M., Suttie, M., Bozzo, A., Peuch, V.-H., Akritidis, D., and Katragkou, E.: The CAMS interim Reanalysis of Carbon Monoxide, Ozone and Aerosol for 2003–2015, Atmos. Chem. Phys., 17, 1945-1983, doi:10.5194/acp-17-1945-2017, 2017.

Franco, B., et al., Retrievals of formaldehyde from ground-based FTIR and MAX-DOAS observations at the Jungfraujoch station and comparisons with GEOS-Chem and IMAGES model simulations, Atmos. Meas. Tech., 8, 1733-1756, 2015

Gielen, C., Van Roozendael, M., Hendrick, F., Pinardi, G., Vlemmix, T., De Bock, V., De Backer, H., Fayt, C., Hermans, C., Gillotay, D., and Wang, P.: A simple and versatile cloud-screening method for MAX-DOAS retrievals, Atmos. Meas. Tech., 7, 3509-3527, doi:10.5194/amt-7-3509-2014, 2014.

Granier, C. et al.: Evolution of anthropogenic and biomass burning emissions of air pollutants at global and regional scales during the 1980–2010 period. Climatic Change (109), 2011

Holben, B. N., Eck, T. F., Slutsker, I., Tanré, D., Buis, J. P., Setzer, A., Vermote, E., Reagan, J. A., Kaufman, Y. J., Nakajima, T., Lavenu, F., Jankowiak, I., and Smirnov A.: AERONET – a federated instrument network and data archive for aerosol characterization, Remote Sens. Environ., 66, 1–16, 5529, 5533, 5537, 5544, 1998.

Hommel, R., Eichmann, K.-U., Aschmann, J., Bramstedt, K., Weber, M., von Savigny, C., Richter, A., Rozanov, A., Wittrock, F., Khosrawi, F., Bauer, R., and Burrows, J. P.: Chemical ozone loss and ozone mini-hole event during the Arctic winter 2010/2011 as observed by SCIAMACHY and GOME-2, Atmos. Chem. Phys., 14, 3247-3276, doi:10.5194/acp-14-3247-2014, 2014.

Huijnen, V., et al.: The global chemistry transport model TM5: description and evaluation of the tropospheric chemistry version 3.0, Geosci. Model Dev., 3, 445-473, doi:10.5194/gmd-3-445-2010, 2010.

Inness, A., Blechschmidt, A.-M., Bouarar, I., Chabrillat, S., Crepulja, M., Engelen, R. J., Eskes, H., Flemming, J., Gaudel, A., Hendrick, F., Huijnen, V., Jones, L., Kapsomenakis, J., Katragkou, E., Keppens, A., Langerock, B., de Mazière, M., Melas, D., Parrington, M., Peuch, V. H., Razinger, M., Richter, A., Schultz, M. G., Suttie, M., Thouret, V., Vrekoussis, M., Wagner, A., and Zerefos, C.: Data assimilation of satellite-retrieved ozone, carbon monoxide and nitrogen dioxide with ECMWF's Composition-IFS, Atmos. Chem. Phys., 15, 5275-5303, doi:10.5194/acp-15-5275-2015, 2015.

Janssens-Maenhout, G., Dentener, F., Aardenne, J. V., Monni, S., Pagliari, V., Orlandini, L., Klimont, Z., Kurokawa, J., Akimoto, H., Ohara, T., Wankmueller, R., Battye, B., Grano, D., Zuber, A., and Keating, T.: EDGAR-HTAP: a Harmonized Gridded Air Pollution Emission Dataset Based on National Inventories, JRC68434, EUR report No EUR 25 299–2012, ISBN 978-92-79- 23122-0, ISSN 1831-9424, European Commission Publications Office, Ispra (Italy), 2012.

Jaross, G., Bhartia, P.K., Chen, G., Kowitt, M., Haken, M., Chen, Z., Xu, Ph., Warner, J., Kelly, T. : OMPS Limb Profiler instrument performance assessment, J. Geophys. Res. Atmos 119, 2169-8996, 2014.

Kaiser, J. W., Heil, A., Andreae, M. O., Benedetti, A., Chubarova, N., Jones, L., Morcrette, J.-J., Razinger, M., Schultz, M. G., Suttie, M., and van der Werf, G. R.: Biomass burning emissions estimated with a global fire assimilation system based on observed fire radiative power, Biogeosciences, 9, 527-554, doi:10.5194/bg-9-527-2012, 2012.

Kramarova, N. A., Nash, E. R., Newman, P. A., Bhartia, P. K., McPeters, R. D., Rault, D. F., Seftor, C. J., Xu, P. Q., and Labow, G. J.: Measuring the Antarctic ozone hole with the new Ozone Mapping and Profiler Suite (OMPS), Atmos. Chem. Phys., 14, 2353-2361, doi:10.5194/acp-14-2353-2014, 2014.

Lahoz, W. A., Errera, Q., Viscardy, S., and Manney G. L., The 2009 stratospheric major warming described from synergistic use of BASCOE water vapour analyses and MLS observations, Atmos. Chem. Phys. 11, 4689-4703, 2011

Lambert, A, et al., Aura Microwave Limb Sounder Version 3.4 Level-2 near real-time data user guide, http://disc.sci.gsfc.nasa.gov/Aura/data-holdings/MLS/documents/NRT-user-guide-v34.pdf

Langerock, B., De Mazière, M., Hendrick, F., Vigouroux, C., Desmet, F., Dils, B., and Niemeijer, S.: Description of algorithms for co-locating and comparing gridded model data with remote-sensing observations, Geosci. Model Dev., 8, 911-921, doi:10.5194/gmd-8-911-2015, 2015.

Lefever, K., van der A, R., Baier, F., Christophe, Y., Errera, Q., Eskes, H., Flemming, J., Inness, A., Jones, L., Lambert, J.-C., Langerock, B., Schultz, M. G., Stein, O., Wagner, A., and Chabrillat, S.: Copernicus stratospheric ozone service, 2009–2012: validation, system intercomparison and roles of input data sets, Atmos. Chem. Phys., 15, 2269-2293, doi:10.5194/acp-15-2269-2015, 2015.

Liu, Z., et al., Exploring the missing source of glyoxal (CHOCHO) over China, Geophys. Res. Lett., 39, L10812, doi: 10.1029/2012GL051645, 2012

Massart, S., Flemming, J., Cariolle, D., Jones, L., High resolution CO tracer forecasts, MACC-III Deliverable D22.04, May 2015, available from http://www.gmes-atmosphere.eu/documents/macciii/deliverables/grg

Morcrette, J.-J., O. Boucher, L. Jones, D. Salmond, P. Bechtold, A. Beljaars, A. Benedetti, A. Bonet, J. W. Kaiser, M. Razinger, M. Schulz, S. Serrar, A. J. Simmons, M. Sofiev, M. Suttie, A. M. Tompkins, and A. Untch: Aerosol analysis and forecast in the ECMWF Integrated Forecast System. Part I: Forward modelling, J. Geophys. Res., 114, D06206, doi:10.1029/2008JD011235, 2009.

Rémy, S., Kipling, Z., Flemming, J., Boucher, O., Nabat, P., Michou, M., Bozzo, A., Ades, M., Huijnen, V., Benedetti, A., Engelen, R., Peuch, V.-H., and Morcrette, J.-J.: Description and evaluation of the tropospheric aerosol scheme in the European Centre for Medium-Range Weather Forecasts (ECMWF) Integrated Forecasting System (IFS-AER, cycle 45R1), Geosci. Model Dev., 12, 4627–4659, https://doi.org/10.5194/gmd-12-4627-2019, 2019.

Richter, A., Burrows, J. P., Nüß, H., Granier, C, Niemeier, U.: Increase in tropospheric nitrogen dioxide over China observed from space, Nature, 437, 129-132, doi: 10.1038/nature04092, 2005

*Richter, A., Begoin, M., Hilboll, A., and Burrows, J. P.: An improved NO2 retrieval for the GOME-2 satellite instrument, Atmos. Meas. Tech. , **4**, 1147-1159, doi:10.5194/amt-4-1147-2011, 2011*

Schulz, M., Y. Christophe, M. Ramonet, Wagner, A., H.J. Eskes, S. Basart, A. Benedictow, Y. Bennouna, A.-M. Blechschmidt, S. Chabrillat, E. Cuevas, A. El- Yazidi, H. Flentje, K.M. Hansen, U. Im, J. Kapsomenakis, B. Langerock, A. Richter, N. Sudarchikova, V. Thouret, T. Warneke, C. Zerefos, Validation report of the CAMS near-real-time global atmospheric composition service: Period December 2018 -February 2019, Copernicus Atmosphere Monitoring Service (CAMS) report, CAMS84_2018SC1_D1.1.1_DJF2019_v1.pdf, June 2019, doi:10.24380/7th6-tk72.

Sindelarova, K., Granier, C., Bouarar, I., Guenther, A., Tilmes, S., Stavrakou, T., Müller, J.-F., Kuhn, U., Stefani, P., and Knorr, W.: Global data set of biogenic VOC emissions calculated by the MEGAN model over the last 30 years, Atmos. Chem. Phys., 14, 9317-9341, doi:10.5194/acp-14-9317-2014, 2014.

Smit, H.G.J., W. Straeter, B.J. Johnson, S.J. Oltmans, J. Davies, D.W. Tarasick, B. Hoegger, R. Stubi, F.J. Schmidlin, T. Northam, A.M. Thompson, J.C. Witte, I. Boyd: Assessment of the performance of ECC-ozonesondes under quasi-flight conditions in the environmental simulation chamber: Insights from the Juelich Ozone Sonde Intercomparison Experiment (JOSIE), J. Geophys. Res. 112, D19306, doi:10.1029/2006JD007308, 2007.

Solomon, S., Haskins, J., Ivy, D. J. and Min, F.: Fundamental differences between Arctic and Antarctic ozone depletion, PNAS 2014 111 (17) 6220-6225, doi:10.1073/pnas.1319307111, 2014.

Stavrakou,T., First space-based derivation of the global atmospheric methanol fluxes, Atm. Chem. Phys., 11, 4873-4898, 2013.

Strahan, S.E., A.R. Douglass, and P.A. Newman, The contributions of chemistry and transport to low arctic ozone in March 2011 derived from Aura MLS observations, J. Geophys. Res. Atmos., 118, 1563–1576, doi:10.1002/jgrd.50181, 2013.

Taha, G.; Jaross, G. R.; Bhartia, P. K.: Validation of OMPS LP Ozone Profiles Version 2.0 with MLS, Ozone Sondes and Lidar Measurements, American Geophysical Union, Fall Meeting 2014, abstract #A33J-3322, 2014.

Taylor, K.E.: Summarizing multiple aspects of model performance in a single diagram. J.Geophys. Res., 106, 7183-7192, 2001.

van der A, R. J. , M. A. F. Allaart, and H. J. Eskes, Multi sensor reanalysis of total ozone, Atmos. Chem. Phys., 10, 11277–11294, doi:10.5194/acp-10-11277-2010, www.atmos- chem-phys.net/10/11277/2010/, 2010

van der A, R., M. Allaart, H. Eskes, K. Lefever, Validation report of the MACC 30-year multi-sensor reanalysis of ozone columns Period 1979-2008, MACC-II report, Jan 2013, MACCII_VAL_DEL_D_83.3_OzoneMSRv1_20130130.docx/pdf.

van der A, R. J., Allaart, M. A. F., and Eskes, H. J.: Extended and refined multi sensor reanalysis of total ozone for the period 1970–2012, Atmos. Meas. Tech., 8, 3021-3035, doi:10.5194/amt-8-3021-2015, 2015.

*Vrekoussis, M., Wittrock, F., Richter, A., and Burrows, J. P.: GOME-2 observations of oxygenated VOCs: what can we learn from the ratio glyoxal to formaldehyde on a global scale?, Atmos. Chem. Phys., **10**, 10145-10160, doi:10.5194/acp-10-10145-2010, 2010*

Wagner, A., M. Schulz, Y. Christophe, M. Ramonet, H. J. Eskes, S. Basart, A. Benedictow, Y. Bennouna, A.-M. Blechschmidt, S. Chabrillat, E. Cuevas, A. El-Yazidi, H. Flentje, K.M. Hansen, U. Im, J. Kapsomenakis, B. Langerock, A. Richter, N. Sudarchikova, V. Thouret, T. Warneke, C. Zerefos, Validation report of the CAMS near-real-time global atmospheric composition service: Period September - November 2019, Copernicus Atmosphere Monitoring Service (CAMS) report, CAMS84_2018SC2_D1.1.1_SON2019_v1.pdf, February 2020.

Wennberg, P. O., Mui, W., Wunch, D., Kort, E. A., Blake, D. R., Atlas, E. L., Santoni, G. W., Wofsy, S. C., Diskin, G. S., Jeong, S., and Fischer, M. L.: On the sources of methane to the Los Angeles atmosphere, Environ. Sci. Technol., 46, 9282–9289, https://doi.org/10.1021/es301138y, 2012

Wittrock, F., A. Richter, H. Oetjen, J. P. Burrows, M. Kanakidou, S. Myriokefalitakis, R. Volkamer, S. Beirle, U. Platt, and T. Wagner, Simultaneous global observations of glyoxal and formaldehyde from space, Geophys. Res. Lett., 33, L16804, doi:10.1029/2006GL026310, 2006

WMO (2010), Guidelines for the Measurement of Atmospheric Carbon Monoxide, GAW Report No. 192, World Meteorological Organization, Geneva, Switzerland, 2010.

WMO (2013), Guidelines for the Continuous Measurements of Ozone in the Troposphere, GAW Report No. 209, World Meteorological Organization, Geneva, Switzerland, 2013.

Wunch, D., Wennberg, P. O., Toon, G. C., Keppel-Aleks, G., and Yavin, Y. G.: Emissions of greenhouse gases from a North American megacity, Geophys. Res. Lett., 36, 1–5, https://doi.org/10.1029/2009GL039825, 2009.

Annex 1: Acknowledgements

Listed below are the authors contributing to the sections in this report. The authors contributing to the model description are also provided, as well as acknowledgements to the validation datasets.

Tropospheric reactive gases reactive gases

Annette Wagner, MPG (editor, O3 sondes, GAW data)
Yasmine Bennouna, Valerie Thouret, CNRS-LA (IAGOS)
Harald Flentje, DWD (O3 sondes, GAW data)
Anne Blechschmidt and Andreas Richter, IUB Bremen (GOME-2 NO2, HCHO)
John Kapsomenakis, Christos Zerefos, AA (ESRL)
Natalia Sudarchikova, satellite IR observations (MPG)
Kaj Hansen, Ulas Im, AU (Arctic theme)
Bavo Langerock, BIRA (NDACC)

Tropospheric aerosol

Michael Schulz, MetNo (editor, Aerocom, Aeronet)
Anna Benedictow, Jan Griesfeller, MetNo (Aerocom, Aeronet)
Sara Basart, MTeresa Pay, Oriol Jorba, BSC-CNS (Aeronet, MODIS, AirBase, SDS-WAS NAMEE RC)
Emilio Cuevas, AEMET (Aeronet, MODIS, AirBase, SDS-WAS NAMEE RC)
Harald Flentje, DWD (Backscatter profiles)

Stratospheric reactive gases

Yves Christophe, BIRA (editor, model-satellite intercomparisons)
Simon Chabrillat, BIRA (model intercomparisons)
Annette Wagner, MPI-M (O_3 sondes)
Bavo Langerock, BIRA (NDACC FTIR, MWR, UVVIS DOAS, LIDAR)
Anne Blechschmidt and Andreas Richter, IUB-UB Bremen (SCIAMACHY/GOME-2 NO_2)

Greenhouse gases

Michel Ramonet, IPSL (ICOS)
Abdelhadi El-Yazidi and Leonard Rivier, LSCE (ICOS)
Thorsten Warneke, UBC (TCCON)
Bavo Langerock, BIRA (TCCON)

Reactive gases and aerosol modeling

Johannes Flemming (ECMWF), Antje Inness (ECMWF), Angela Benedetti (ECMWF), Sebastien Massart (ECMWF), Anna Agusti-Panareda (ECMWF), Johannes Kaiser (KCL/MPIC/ECMWF), Samuel Remy (LMD), Olivier Boucher (LMD), Vincent Huijnen (KNMI), Richard Engelen (ECMWF)

Acknowledgements for the validation datasets used

We wish to acknowledge the provision of NRT GAW observational data by: Institute of Atmospheric Sciences and Climate (ISAC) of the Italian National Research Council (CNR), South African Weather Service, National Centre for Atmospheric Science (NCAS, Cape Verde), National Air Pollution Monitoring Network (NABEL) (Federal Office for the Environment FOEN and Swiss Federal Laboratories for Materials Testing and Research EMPA), Atmospheric Environment Division Global Environment and Marine Department Japan Meteorological Agency, Chinese Academy of Meteorological Sciences (CAMS), Alfred Wegener Institut, Umweltbundesamt (Austria), National Meteorological Service (Argentina), Umweltbundesamt (UBA, Germany)

We are grateful to the numerous operators of the Aeronet network and to the central data processing facility at NASA Goddard Space Flight Center for providing the NRT sun photometer data, especially Ilya Slutker and Brent Holben for sending the data.

The authors thank to all researchers, data providers and collaborators of the World Meteorological Organization's Sand and Dust Storm Warning Advisory and Assessment System (WMO SDS-WAS) for Northern Africa, Middle East and Europe (NAMEE) Regional Node. Also special thank to Canary Government as well as AERONET, MODIS, U.K. Met Office MSG, MSG Eumetsat and EOSDIS World Viewer principal investigators and scientists for establishing and maintaining data used in the activities of the WMO SDS-WAS NAMEE Regional Center (http://sds-was.aemet.es/).

We wish to acknowledge the provision of ozone sonde data by the World Ozone and Ultraviolet Radiation Data Centre established at EC in Toronto (http://woudc.org), by the Data Host Facility of the Network for the Detection of Atmospheric Composition Change established at NOAA (http://ndacc.org), by the Norwegian Institute for Air Research and by the National Aeronautics and Space Administration (NASA).

We wish to thank the NDACC investigators for the provision of observations at Ny Alesund, Bern, Jungfraujoch, Izaña, Xianghe, Harestua, Reunion Maido, Uccle, Hohenpeissen, Mauna Loa, Lauder and Haute Provence.

The authors acknowledge the NOAA Earth System Research Laboratory (ESRL) Global Monitoring Division (GMD) for the provision of ground-based ozone concentrations.

The MOPITT CO data were obtained from the NASA Langley Research Center ASDC. We acknowledge the LATMOS IASI group for providing IASI CO data.

SCIAMACHY lv1 radiances were provided to IUP-UB by ESA through DLR/DFD.

GOME-2 lv1 radiances were provided to IUP-UB by EUMETSAT.

The authors acknowledge Environment and Climate Change Canada for the provision of Alert ozone data and Sara Crepinsek – NOAA for the provision of Tiksi ozone data. Surface ozone data from the Zeppelin Mountain, Svalbard are from www.luftkvalitet.info. Surface ozone data from the Villum Research Station, Station Nord (VRS) were financially supported by "The Danish Environmental Protection Agency" with means from the MIKA/DANCEA funds for Environmental Support to the Arctic Region. The Villum Foundation is acknowledged for the large grant making it possible to build VRS in North Greenland.

We acknowledge the National Aeronautics and Space Administration (NASA), USA for providing the OMPS limb sounder data (http://npp.gsfc.nasa.gov/omps.html), the SAGE III-ISS ozone data https://eosweb.larc.nasa.gov/project/sageiii-iss/sageiii-iss_table and the Aura-MLS offline data (http://mls.jpl.nasa.gov/index-eos-mls.php).

We thank the Canadian Space Agency and ACE science team for providing level 2 data retrieved from ACE-FTS on the Canadian satellite SCISAT-1.

The European Environment Information and Observation Network (Eionet) Air Quality portal provides details relevant for the reporting of air quality information from EU Member States and other EEA member and co-operating countries. This information is submitted according to Directives 2004/107/EC and 2008/50/EC of the European Parliament and of the Council.

We are grateful to the IAGOS operators from the various institutes which are members of IAGOS-AISBL (http://www.iagos.org). The authors also acknowledge the strong support of the European Commission, Airbus, and the airlines (Lufthansa, Air France, Austrian, Air Namibia, Cathay Pacific, Iberia, China Airlines and Hawaiian Airlines so far) which have carried the MOZAIC or IAGOS equipment and undertaken maintenance since 1994. In the last 10 years of operation, MOZAIC has been funded by INSU-CNRS (France), Météo-France, Université Paul Sabatier (Toulouse, France) and Research Center Jülich (FZJ, Jülich, Germany). IAGOS has been additionally funded by the EU projects IAGOS-DS and IAGOS-ERI. The MOZAIC–IAGOS database (http://www.iagos-data.fr) is supported by AERIS (CNES and INSU-CNRS). Data are also available via AERIS web site www.aeris-data.fr.

We acknowledge the contribution of the ICOS Atmospheric Thematic Center (Lynn Hazan, Amara Abbaris, and Leonard Rivier) for the near real time data processing of surface CO_2 and CH_4 concentrations. The ICOS monitoring sites are maintained by the national networks: ICOS-Czech Rep. (Michal Marek, Katerina Komínková, Gabriela Vítková), ICOS-Finland (Olli Peltola, Janne Levula, Tuomas Laurila), ICOS-France (Michel Ramonet, Marc Delmotte, Sebastien Conil, Morgan Lopez, Victor Kazan, Aurélie Colomb, Jean Marc Pichon, Roxanne Jacob, Julie Helle, Olivier Laurent), ICOS-Germany (Matthias Lindauer, Dagmar Kubistin, Christian Plass-Duelmer, Dietmar Weyrauch, Marcus Schumacher), ICOS-Italy (Paolo Cristofanelli, Michela Maione, Francesco Apadula), ICOS-Norway (Cathrine Lund Myhre, Ove Hermansen), ICOS-Sweden (Jutta Holst, Michal Heliasz, Meelis Molder, Mikaell Ottosson Lofvenius, Anders Lindroth, Per Marklund), ICOS-Switzerland (Martin Steinbacher, Simon Wyss), European Commission, Joint Research Centre, Directorate for Energy, Transport and Climate (Peter Bergamaschi, Giovanni Manca).

The TCCON site at Orleans is operated by the University of Bremen and the RAMCES team at LSCE (Gif-sur-Yvette, France). The TCCON site at Bialystok is operated by the University of Bremen. Funding for the two sites was provided by the EU-project ICOS-INWIRE and the University of Bremen. The TCCON site at Réunion is operated by BIRA-IASB, in cooperation with UReunion and is funded by BELSPO in the framework of the Belgian ICOS program.

TCCON references:

Hazan, L., J. Tarniewicz, M. Ramonet, O. Laurent and A. Abbaris **(2016)**. *Automatic processing of atmospheric CO_2 and CH_4 mole fractions at the ICOS Atmosphere Thematic Centre*. Atmospheric Measurement Techniques 9(9): 4719-4736.

Blumenstock, T., F. Hase, M. Schneider, O. E. García, and E. Sepúlveda. 2017. "TCCON data from Izana (ES), Release GGG2014.R1." CaltechDATA. doi:10.14291/tccon.ggg2014.izana01.r1.

De Mazière, M., M. K. Sha, F. Desmet, C. Hermans, F. Scolas, N. Kumps, J.-M. Metzger, V. Duflot, and J.-P. Cammas. 2017. "TCCON data from Réunion Island (RE), Release GGG2014.R1." CaltechDATA. doi:10.14291/tccon.ggg2014.reunion01.r1.

Deutscher, N. M., J. Notholt, J. Messerschmidt, C. Weinzierl, T. Warneke, C. Petri, and P. Grupe. 2017. "TCCON data from Bialystok (PL), Release GGG2014.R1." CaltechDATA. doi:10.14291/tccon.ggg2014.bialystok01.r1/1183984.

Dubey, M. K., B. G. Henderson, D. Green, Z. T. Butterfield, G. Keppel-Aleks, N. T. Allen, J.-F. Blavier, C. M. Roehl, D. Wunch, and R. Lindenmaier. 2017. "TCCON data from Manaus (BR), Release GGG2014.R0." CaltechDATA. doi:10.14291/tccon.ggg2014.manaus01.r0/1149274.

Dubey, M. K., R. Lindenmaier, B. G. Henderson, D. Green, N. T. Allen, C. M. Roehl, J.-F. Blavier, et al. 2017. "TCCON data from Four Corners (US), Release GGG2014.R0." CaltechDATA. doi:10.14291/tccon.ggg2014.fourcorners01.r0/1149272.

Feist, D. G., S. G. Arnold, N. John, and M. C. Geibel. 2017. "TCCON data from Ascension Island (SH), Release GGG2014.R0." CaltechDATA. doi:10.14291/tccon.ggg2014.ascension01.r0/1149285.

Goo, T.-Y., Y.-S. Oh, and V. A. Velazco. 2017. "TCCON data from Anmeyondo (KR), Release GGG2014.R0." CaltechDATA. doi:10.14291/tccon.ggg2014.anmeyondo01.r0/1149284.

Griffith, D. W. T., N. M. Deutscher, V. A. Velazco, P. O. Wennberg, Y. Yavin, G. Keppel-Aleks, R. A. Washenfelder, et al. 2017. "TCCON data from Darwin (AU), Release GGG2014.R0." CaltechDATA. doi:10.14291/tccon.ggg2014.darwin01.r0/1149290.

Griffith, D. W. T., V. A. Velazco, N. M. Deutscher, C. Paton-Walsh, N. B. Jones, S. R. Wilson, R. C. Macatangay, G. C. Kettlewell, R. R. Buchholz, and M. O. Riggenbach. 2017. "TCCON data from Wollongong (AU), Release GGG2014.R0." CaltechDATA. doi:10.14291/tccon.ggg2014.wollongong01.r0/1149291.

Hase, F., T. Blumenstock, S. Dohe, J. Groß, and M.ä. Kiel. 2017. "TCCON data from Karlsruhe (DE), Release GGG2014.R1." CaltechDATA. doi:10.14291/tccon.ggg2014.karlsruhe01.r1/1182416.

Iraci, L. T., J. R. Podolske, P. W. Hillyard, C. Roehl, P. O. Wennberg, J.-F. Blavier, J. Landeros, et al. 2017. "TCCON data from Edwards (US), Release GGG2014.R1." CaltechDATA. doi:10.14291/tccon.ggg2014.edwards01.r1/1255068.

—. 2017. "TCCON data from Indianapolis (US), Release GGG2014.R1." CaltechDATA. doi:10.14291/tccon.ggg2014.indianapolis01.r1/1330094.

Kawakami, S., H. Ohyama, K. Arai, H. Okumura, C. Taura, T. Fukamachi, and M. Sakashita. 2017. "TCCON data from Saga (JP), Release GGG2014.R0." CaltechDATA. doi:10.14291/tccon.ggg2014.saga01.r0/1149283.

Kivi, R., P. Heikkinen, and E. Kyrö. 2017. "TCCON data from Sodankylä (FI), Release GGG2014.R0." CaltechDATA. doi:10.14291/tccon.ggg2014.sodankyla01.r0/1149280.

Liu, Cheng, Wei Wang, and Youwen Sun. 2018. "TCCON data from Hefei (PRC), Release GGG2014.R0." CaltechDATA. doi:10.14291/tccon.ggg2014.hefei01.r0.

Morino, I., N. Yokozeki, T. Matsuzaki, and M. Horikawa. 2017. "TCCON data from Rikubetsu (JP), Release GGG2014.R2." CaltechDATA. doi:10.14291/tccon.ggg2014.rikubetsu01.r2.

Morino, I., T. Matsuzaki, and M. Horikawa. 2017. "TCCON data from Tsukuba (JP), 125HR, Release GGG2014.R2." CaltechDATA. doi:10.14291/tccon.ggg2014.tsukuba02.r2.

Morino, Isamu, Voltaire A. Velazco, Akihiro Hori, Osamu Uchino, and David W. T. Griffith. 2018. "TCCON data from Burgos, Ilocos Norte (PH), Release GGG2014.R0." CaltechDATA. doi:10.14291/tccon.ggg2014.burgos01.r0.

Notholt, J., C. Petri, T. Warneke, N. M. Deutscher, M. Palm, M. Buschmann, C. Weinzierl, R. C. Macatangay, and P. Grupe. 2017. "TCCON data from Bremen (DE), Release GGG2014.R0." CaltechDATA. doi:10.14291/tccon.ggg2014.bremen01.r0/1149275.

Notholt, J., T. Warneke, C. Petri, N. M. Deutscher, C. Weinzierl, M. Palm, and M. Buschmann. 2017. "TCCON data from Ny Ålesund, Spitsbergen (NO), Release GGG2014.R0." CaltechDATA. doi:10.14291/tccon.ggg2014.nyalesund01.r0/1149278.

Pollard, David Frank, John Robinson, and Hisako Shiona. 2019. "TCCON data from Lauder (NZ), Release GGG2014.R0." CaltechDATA. doi:10.14291/tccon.ggg2014.lauder03.r0.

Sherlock, V., B. Connor, J. Robinson, H. Shiona, D. Smale, and D. F. Pollard. 2017. "TCCON data from Lauder (NZ), 120HR, Release GGG2014.R0." CaltechDATA. doi:10.14291/tccon.ggg2014.lauder01.r0/1149293.

—. 2017. "TCCON data from Lauder (NZ), 125HR, Release GGG2014.R0." CaltechDATA. doi:10.14291/tccon.ggg2014.lauder02.r0/1149298.

Strong, K., S. Roche, J. E. Franklin, J. Mendonca, E. Lutsch, D. Weaver, P. F. Fogal, J. R. Drummond, R. Batchelor, and R. Lindenmaier. 2018. "TCCON data from Eureka (CA), Release GGG2014.R3." CaltechDATA. doi:10.14291/tccon.ggg2014.eureka01.r3.

Sussmann, R., and M. Rettinger. 2017. "TCCON data from Garmisch (DE), Release GGG2014.R2." CaltechDATA. doi:10.14291/tccon.ggg2014.garmisch01.r2.

—. 2018. "TCCON data from Zugspitze (DE), Release GGG2014.R1." CaltechDATA. doi:10.14291/tccon.ggg2014.zugspitze01.r1.

Té, Y., P. Jeseck, and C. Janssen. 2017. "TCCON data from Paris (FR), Release GGG2014.R0." CaltechDATA. doi:10.14291/tccon.ggg2014.paris01.r0/1149279.

Warneke, T., J. Messerschmidt, J. Notholt, C. Weinzierl, N. M. Deutscher, C. Petri, and P. Grupe. 2017. "TCCON data from Orléans (FR), Release GGG2014.R0." CaltechDATA. doi:10.14291/tccon.ggg2014.orleans01.r0/1149276.

Wennberg, P. O., C. M. Roehl, D. Wunch, G. C. Toon, J.-F. Blavier, R. Washenfelder, G. Keppel-Aleks, N. T. Allen, and J. Ayers. 2017. "TCCON data from Park Falls (US), Release GGG2014.R1." CaltechDATA. doi:10.14291/tccon.ggg2014.parkfalls01.r1.

Wennberg, P. O., C. M. Roehl, J.-F. Blavier, D. Wunch, and N. T. Allen. 2017. "TCCON data from Jet Propulsion Laboratory (US), 2011, Release GGG2014.R1." CaltechDATA. doi:10.14291/tccon.ggg2014.jpl02.r1/1330096.

Wennberg, P. O., D. Wunch, C. M. Roehl, J.-F. Blavier, G. C. Toon, and N. T. Allen. 2017. "TCCON data from Caltech (US), Release GGG2014.R1." CaltechDATA. doi:10.14291/tccon.ggg2014.pasadena01.r1/1182415.

—. 2017. "TCCON data from Lamont (US), Release GGG2014.R1." CaltechDATA. doi:10.14291/tccon.ggg2014.lamont01.r1/1255070.

Wennberg, P. O., D. Wunch, Y. Yavin, G. C. Toon, J.-F. Blavier, N. T. Allen, and G. Keppel-Aleks. 2017. "TCCON data from Jet Propulsion Laboratory (US), 2007, Release GGG2014.R0." CaltechDATA. doi:10.14291/tccon.ggg2014.jpl01.r0/1149163.

Wunch, D., J. Mendonca, O. Colebatch, N. T. Allen, J.-F. Blavier, S. Roche, J. Hedelius, et al. 2017. "TCCON data from East Trout Lake, SK (CA), Release GGG2014.R1." CaltechDATA. doi:10.14291/tccon.ggg2014.easttroutlake01.r1.

Wunch, D., Toon, G. C., Sherlock, V., Deutscher, N. M., Liu, C., Feist, D. G., & Wennberg, P. O. (2015). The Total Carbon Column Observing Network's GGG2014 Data Version. Tech. rep., California Institute of Technology, Pasadena. doi:10.14291/tccon.ggg2014.documentation.R0/1221662

Copernicus Atmosphere Monitoring Service

ECMWF - Shinfield Park, Reading RG2 9AX, UK

Contact: info@copernicus-atmosphere.eu

atmosphere.copernicus.eu copernicus.eu ecmwf.int